Novel D-Lak Peptides combinations against mycobacteria: Bioefficacy and mechanistic studies

Dede, Man Dede

Awarding institution:
King's College London

NOVEL D-LAK PEPTIDES COMBINATIONS AGAINST MYCOBACTERIA: BIOEFFICACY AND MECHANISTIC STUDIES

By

DeDe Kwun Wai MAN

A thesis submitted in partial fulfilment of the requirements

for the Degree of Joint Doctor of Philosophy

at the University of Hong Kong and King's College London

February 2019

Abstract of thesis

entitled

Novel D-LAK peptides combinations against Mycobacteria: Bioefficacy and mechanistic studies

Submitted by

DeDe Kwun Wai MAN

for the degree of Doctor of Philosophy

at the University of Hong Kong and King's College London

in February 2019

Emergence of multidrug-resistant tuberculosis (MDR-TB) renders the two most powerful and commonly used TB antibiotics, rifampicin and isoniazid, ineffective. There is an urgent need for the development of safe and effective strategies against drug-resistant TB. Based on previous studies, two novel antimicrobial peptides, namely D-LAK120-A and D-LAK120-HP13, both consist entirely of D-amino acid residues, have demonstrated inhibitory effect on MDR *Mycobacterium tuberculosis* (*Mtb*) strains when cultured in macrophages and potentiated the antimycobacterial activity of isoniazid *in vitro*. Here, the antimycobacterial activity of D-LAK peptides in combination with anti-TB drugs against MDR-TB clinical isolates was investigated. Furthermore, the mechanisms of action of the proline-containing and proline-free D-LAK peptides, anti-TB drugs alone or in combinations were studied using two mycobacterial models *Mycobacterium smegmatis* and the severely attenuated *Mtb* Bleupan. Finally, the applicability of these two microorganisms for mycobacterial studies was discussed.

In vitro and *ex vivo* antimycobacterial assays revealed the synergy between D-LAK peptides and rifampicin or isoniazid against MDR *Mtb* strain. These findings suggested D-LAK peptide can facilitate the re-sensitization of MDR-TB clinical isolates towards rifampicin and isoniazid possibly through their surface activity. To gain further understanding on their mechanisms on mycobacteria, *M. smegmatis* was employed due to its fast-growing nature and widespread usage in TB studies. With confocal and transmission electron microscopy, the surface-active action of D-LAK peptides were observed which led to visible morphological changes in *M. smegmatis*. Using high-resolution magic angle spinning (HR-MAS) nuclear magnetic resonance (NMR) metabolomics, trans-1,6-diphenyl-1,3,5-hexatriene (DPH) and Laurdan fluorescence spectroscopy, it was shown that bacterial

metabolism was substantially altered when challenged with anti-TB agents, specifically by the remodelling of mycobacterial membrane. The proline-containing D-LAK120-HP13 and proline-free D-LAK120-A peptides demonstrated disparate behaviours in the initiation of membrane remodelling which provides possible rationale for their synergistic interaction with anti-TB agents. These techniques were then applied to the study of another potential mycobacterial model *Mtb* Bleupan which was selected for its safer nature as a *Mtb* surrogate. Changes in membrane components triggered by anti-TB agents were observed but the effect was subtler than that observed in *M. s**megmatis*. These findings suggested the potential of using these biophysical techniques to study the action of anti-TB drugs on mycobacteria and to elucidate the underlying mechanism of synergy demonstrated in the combinations of D-LAK peptides with anti-TB agents.

Finally, the applicability of *M. smegmatis* and *Mtb* Bleupan to be exploited as a *Mtb* surrogate was evaluated. Some key differences in response to anti-TB agents were detected between *Mtb* Bleupan and *M. smegmatis* in terms of the changes in metabolism and membrane properties. These findings demonstrated *Mtb* Bleupan as a safe and desirable model for the generation of translatable findings for TB studies. Further optimization of the growth response study using *Mtb* Bleupan is essential for a more comprehensive understanding of anti-TB agent mechanism.

Overall, this thesis concluded that the combinations of D-LAK peptides with rifampicin or isoniazid were effective against MDR clinical isolates and paved the next step to elucidate the mechanisms using a more reliable surrogate, *Mtb* Bleupan.

(499 words)

Novel D-LAK Peptides Combinations against Mycobacteria: Bioefficacy and Mechanistic Studies

By

DeDe Kwun Wai MAN

A thesis submitted in partial fulfilment of the requirements

for the Degree of Doctor of Philosophy

at the University of Hong Kong and King's College London

February 2019

Declaration

I declare that this thesis represents my own work, except where due acknowledgement is made, and that it has not been previously included in a thesis, dissertation or report submitted to this University or to any other institution for a degree, diploma or other qualifications.

Signed _____

DeDe Kwun Wai MAN

Acknowledgements

The last three years have been one of the most challenging yet the best time in my life.

I would like to start by expressing my heartfelt gratitude to my two supervisors, Dr Jenny KW Lam and Dr A James Mason, for their insightful guidance with their great expertise. Their immense patience, continuous encouragement and unwilting enthusiasm were the strongest support that walked me through this PhD journey lain with unexpected challenges. I am sincerely grateful to be given this precious opportunity to study at HKU and KCL. I will always be thankful for the knowledge and experience I have earned in the PhD.

I am deeply obliged to all my friends in London who have given me endless support during my PhD. To my lovely and cheerful labmates at King's, Tokuwa, Min, Phil, Masirah and Caroline, who have welcomed me with big embraces and shared joyful time with me in the lab and outside: You are the most brilliant people with smart brains and thank you for supporting me in every way possible. Especially sending my thank you and love to Dr Giorgia Manzo, Dr Simona Di Blasio, Angie and Dr Kelly Vandera, you are the best friends/labmates I have ever met. Thank you for all the happy memories and riding through the tough times with me! I would also like to thank my friends Priyah, Christian, Eunmi, Adam and Xenia for their support and kindness to accommodate and share my ups and downs during my stay in London. I am very fortunate to have experienced this memorable time in London and have met such amazing friends who I did not want to say goodbye to at all. Thank you all of you and I will come back to see you again soon!

I would also like to thank my HKU labmates, especially Dr Yolanda Lan and Dr Sophia Liang for their kindness and generous help with my research. And a big thank you to Dr Philip Kwok who has been so kind and have been supporting me since my MPhil studies.

I would like to extend my gratefulness to our collaborator, Dr Brian Roberson of Imperial College London, for his generous support and helpful ideas in the mycobacterial experiments. Thanks also to his research group, Miles, Nitya and Iria for their help in conducting different assays. A special thanks also to Dr Andrew Atkinson of NMR facilities, KCL, and Dr Tom Frenkiel and Dr Alain Oregioni of MRC Biomedical NMR Centre, Francis Crick Institute, for always giving constructive advice and technical support to ensure stability of the NMR spectrometer for data acquisition.

I would like to express my sincere gratitude to Dr Yam Wing Cheong of Department of Microbiology, HKU, for providing us with MDR clinical isolate and facilitating my studies in the BSL 3 laboratory at Queen Mary Hospital. Thanks must also go to his group including Dr Sabrina To and Kenneth for their help in culturing the *Mtb* strains. I would also like to thank the Faculty Core Facility of Faculty of Medicine and Electron Microscope Unit at HKU for their technical support in confocal and TEM experiments. Many thanks to all the technicians and staff in the department for their help in facilitating my studies.

I would also like to express my love and thanks to all my friends for their encouragement and support throughout my PhD studies. I feel very lucky to have all of them by my side and share the happiness and laughter together. Especially my dearest Charmaine, who has been supporting me all the way and thinking about me even when we were separated by an entire continent. Thank you for your love and support expressed in your creative and caring ways till the very last second of my PhD. I am thrilled that we are achieving this milestone together!

I am also most thankful to the Enz's family, for their sweetness and forever warm welcome. And Stefan, for your unfailing patience and support in these difficult times, I am looking forward to starting the next part of our journey together. Lastly, I would like to say a huge thank you to my parents and my family for always supporting my decisions and choices in life. I am grateful for their unconditional love no matter where I am in the world.

DeDe Man Kwun Wai

February 2019

Publications

Articles in scientific journals

Man DKW, Kanno, T., Manzo, G., Robertson, B.D., Lam, JKW., Mason, A.J. Rifampicin or capreomycin induced remodelling of the Mycobacterium smegmatis mycolic acid layer is mitigated in synergistic combinations with cationic antimicrobial peptides. mSphere. 2018;3(4). DOI: 10.1128/mSphere.00218-18

Conference abstracts

Man DKW, Robertson, B.D., Lam, JKW, Mason, A.J. Development of antimicrobial peptides to re-sensitize multidrug-resistant tuberculosis to isoniazid and rifampicin, Antibiotic resistance and mechanisms Workshop 2017. British Society for Antimicrobial Chemotherapy. Birmingham, U.K.

Man DKW, Robertson, B.D., Lam, JKW, Mason, A.J. Combination of D-LAK antimicrobial peptides and isoniazid/rifampicin against multidrug-resistant tuberculosis. Institute of Pharmaceutical Science Symposium 2017. King's College London. London, U. K.

Man DKW, Robertson, B.D., Lam, JKW, Mason, A.J. Combination of D-LAK antimicrobial peptides and isoniazid/rifampicin against multidrug-resistant tuberculosis. European Society of Microbiology Congress 2017. Sibenik, Croatia.

Table of Contents

List of Tables

List of Figures

List of Abbreviations

7H9	Middlebrook 7H9 broth medium
7H9 w Tyloxapol	Middlebrook 7H9 broth medium with 0.025% tyloxapol
7H9O	Middlebrook 7H9 broth medium supplemented with 10% OADC
7H9O w Tyloxapol	Middlebrook 7H9 broth medium supplemented with 10% OADC and 0.025% tyloxapol
A	Alanine
ACC2'	N-acetyltransferase
AG	Arabinogalactan
AMPs	Antimicrobial peptides
ANOVA	Analysis of variance
ATCC	American Type Culture Collection
ATP	Adenosine triphosphate
BSL	Biosafety level
CAP	Capreomycin
CFU	Colony forming unit
COSY	Correlation Spectroscopy
CPMG	Carr-Purcell-Meiboom-Gill
CST	Colistin
CV	Cross Validation
DIM	Phthiocerol dimycocerosate
DLM	Delamanid
DMEM	Dulbecco's modified eagle medium
DMSO	Dimethyl Sulfoxide
DNA	Deoxyribonucleic acid
DOTS	Directly Observed Therapy Short-course
DPH	Trans-1,6-diphenyl-1,3,5-hexatriene
EMB	Ethambutol
FBS	Foetal bovine serum
FDA	Food and Drug Administration
FIC	Fractional Inhibitory Concentration
FICI	Fractional Inhibitory Concentration Index
FID	Free Induction Decay
FITC	Fluorescein isothiocyanate
$FMNH_2$	Flavin mononucleotide
GC-MS	Gas Chromatography Mass Spectrometry
GP	General polarization
H	Histidine
HBDs	Human ß-defensins
HIV	Human immunodeficiency virus
HMDB	Human Metabolome Database
HNP-1	human neutrophil peptide
HR-MAS	High-resolution magic angle spinning
HSQC	Heteronuclear single quantum coherence
INH	Isoniazid
IDRs	innate defense regulators
K	Lysine
L	Leucine

LAM	Lipoarabinomannan
LC-MS	Liquid chromatography mass spectrometry
LDH	Lactate dehydrogenase
LM	Lipomannans
LOS	Lipooligosaccharides
LPS	Lipopolysaccharides
LTBI	Latent TB infection
MA	Mycolic acids
Man-LAM	Mannose-capped lipoarabinomannan
MAP	*Mycobacterium avium* subsp. *paratuberculosis*
MDR-TB	Multidrug-resistant tuberculosis
MFS	Major facilitator superfamily
MIC	Minimum inhibitory concentration
MOI	Multiplicity of infection
MR	Mannose receptors
Mtb	*Mycobacterium tuberculosis*
*MTB*C	*Mycobacterium tuberculosis* complex
MTT	Methylthiazol tetrazolium
NMR	Nuclear magnetic resonance
OADC	Oleic acid-albumin-dextrose-catalase
OD	Optical density
OM	Outer membrane
OPLS	Orthogonal projection to latent structure
OPLS-DA	Orthogonal projections to latent structures discriminant analysis
P	Proline
PAS	Para-aminosalicyclic acid
PBS	Phosphate-buffered saline
PC	Principal component
PCA	Principal component analysis
PCR	Polymerase chain reaction
PG	Peptidoglycan
PGLs	Phenolic glycolipids
PIM	Phosphatidyl insitol mannoside
PLS	Partial least squares
PM	Plasma membrane
PMA	Phorbol 12-myristate 13-acetate
ppm	Parts per million
PZA	Pyrazinamide
QRDR	Quinolone resistance-determining region
RD1	Region of difference 1
REMA	Resazurin microtiter assays
RIF	Rifampicin
RLU	Relative light unit
RNA	Ribonucleic acid
ROS	Reactive oxygen species
SDS	Sodium dodecyl sulfonate
TB	Tuberculosis
TBSA	Tuberculostearic acid
TCA	Tricarboxylic acid

TDM	Trehalose dimycolate
TDR-TB	Totally drug-resistant strains
TEM	Transmission electron microscope
TMM	Trehalose monomycolate
TSP	Trimethylsilylpropanoic acid
WHO	World Health Organization
XDR-TB	Extensively drug-resistant tuberculosis

Chapter 1 Introduction

1.1 TUBERCULOSIS AND THERAPY

1.1.1 TB Etiology and Global TB Crisis

Tuberculosis (TB) is an ancient infectious disease that can be dated back thousands of years. The evidence of TB has been found in the remnant of a bison which lived in Wyoming, US 17,000 years ago[1]. Tubercular decay has also been detected in the spines of Egyptian mummies, which date back to 3000-2400 BC[2], whilst genome-based studies have also suggested the presence of TB in America since AD 100[3]. Tuberculosis, which was also known as the great white plague or phthisis, has claimed countless human lives ever since and still represents the second most life-threatening infectious disease worldwide in our era, after human immunodeficiency virus (HIV) infection. TB was demonstrated to be infectious by a French specialist Jean-Antoine Villemin in 1865[4]. On 24th March 1882, the causative agent of the disease was identified as an eubacterium, named as *Mycobacterium tuberculosis* (*Mtb*) by a German researcher, Robert Koch who was later honoured with the Nobel Prize in 1905 for his contribution in TB research. The World TB day was established then to commemorate his discovery[5].

Mycobacterium tuberculosis is a member of the *Mycobacterium tuberculosis* complex (*MTB*C), a group of closely related strains comprising another human-adapted species *Mycobacterium africanum*, as well as the animal-adapted *Mycobacterium bovis*, *Mycobacterium microti* and *Mycobacterium caprae*. Despite the wide spectrum of mammalian hosts, *MTB*C species possess over 99% of genomic homogeneity; this gives proof to their evolution from a single African origin that resembled *Mycobacterium canetti* strains[6, 7]. TB can infect any part of the body although disease manifestation is generally observed in the lungs. Apart from pulmonary TB, extra-pulmonary TB is mainly found in immunocompromised individuals which includes osseous tuberculosis found in the bones and tuberculous ulcer occurring on the skin[8].

Causing over a billion deaths in the past 200 years, TB has continued to present a grave challenge globally. The World Health Organization declared TB as a global health emergency in 1993. Effort has been concerted worldwide to tackle the disease, as a result of which, the global incident rate has dropped by 3% every year since 2000[9]. Furthermore, the global mortality rate has declined significantly by 37% between 2000 and 2016 as reported by WHO in 2017. The decrease is mainly observed in developed countries in the Western Pacific Region and European Region. Despite the gains in tuberculosis control by the

implementation of effective strategies, TB remains acknowledged as a global emergency accounting for 10.4 million of new cases and 1.3 million of deaths in 2016. About 60% of the TB cases are found in India, Russian Federation, South Africa and China, where poverty, overcrowding, malnutrition and deficient healthcare systems are common[9, 10]. The problem of TB is exacerbated by the emergence of various drug-resistant strains. Those *Mtb* strains that have acquired different level of resistance are categorized as multidrug-resistant tuberculosis (MDR-TB), possessing resistance towards both of the first-line anti-TB agents: rifampicin (RIF) and isoniazid (INH); extensively drug-resistant tuberculosis (XDR-TB), defined as MDR-TB strains that display an added resistance to any fluoroquinolone and at least one of the second-line injectable aminoglycosides such as amikacin, kanamycin or capreomycin[11]; and totally drug-resistant tuberculosis (TDR-TB), known to be resistant to all available drugs[12]. It is reported that there were approximately 0.49 million new MDR-TB cases worldwide in 2016. The prevalence is especially high in Eastern Europe and Central Asia, where an estimated 190,000 people died from MDR-TB, accounting for 48% of the cases worldwide[9]. XDR-TB is calculated to make up 0.5% of global TB cases and has been reported in 91 countries throughout the world. New anti-TB drugs such as delamanid and bedaquiline, as well as shorter regimens, have been introduced to combat the problem of drug-resistant TB. Unfortunately, the treatment success rates were only 54% for MDR-TB and 30% for XDR-TB[9]. In addition to the emergence of drug-resistant strains, HIV co-infection occurs in 10% of all TB-cases and caused 374,000 deaths in 2016. Co-infection with HIV is a major problem in African countries and presents an enormous pressure for TB treatment due to drug interactions. On the other hand, immunological tests have suggested that about 2 billion of the world population might be infected with latent TB, an asymptomatic infection by dormant *Mtb*, with 5-10% of the individuals going on to develop active TB during old age[13], or when their immune systems are comprised. The existence of all these manifestations of *Mtb* complicates the treatment process, and therefore increases the challenge to combat this noxious disease.

Since the discovery of *Mtb* being the primary causative agent of tuberculosis, huge efforts have been made towards to the development of antibacterial and antimicrobial compounds to eradicate this bacterium. In 1945, the first anti-TB therapeutic, streptomycin, was introduced[14]. Unfortunately, the overuse of streptomycin quickly led to the development of drug resistance, resulting in therapy failure. The most effective and affordable anti-TB four-drug regimen [rifampicin, isoniazid, ethambutol (EMB) and pyrazinamide (PZN)] currently in use globally was introduced four decades ago. All these factors combined reflect the

challenges of TB treatment and anti-TB drug development, which in turn reveal the unique nature and behaviour of the bacteria.

The exclusive abundance of lipids is recognized as the hallmark of *Mtb*, accounting for up to 40% of the bacillus dry weight[15, 16]. Approximately 60% of these lipids are primarily long chain fatty acid (mycolic acids, MA) located on the outer layer of the mycomembrane. Compared with the Gram-negative cell wall with only 20% lipid content, the mycobacterial cell envelope is well known to have low porosity and therefore is impermeable to a wide range of antibiotics[17]. This lipid-rich, hydrophobic barrier not only hinders the entry of drugs but also accounts for greater resistance of *Mtb* to antibiotics[18]. The unusual structure and chemical composition of *Mtb* has also given rise to several intrinsic resistance mechanisms[17]. These mechanisms help *Mtb* to reduce their exposure to hostile host cell environment, neutralize drug compounds, adapt to the immoderately radical environment, and therefore increase the chance of survival. The extremely slow metabolism (doubling time 12-24 h) of *Mtb* has also hampered the efficiency of most conventional antibiotics which target specific steps in the metabolic cycle of the bacteria[19]. Moreover, the exceptional mode of pathogenicity of *Mtb* ensures their remarkably well-adapted interaction with the host presents another challenge on TB treatment. They can remain in the host system without being compromised via a vast repertoire of sophisticated pathways[20]. After inhalation, *Mtb* is ingested by alveolar macrophages. Instead of clearing by the first line innate immune system, *Mtb* can resist the degradation by phagosomes and persist or even replicate in the host, leading to the formation of granuloma[21, 22]. Besides, it was reported that *Mtb* can escape into host cytosol by inducing phagosomal rupture and uses the macrophage for its own replication process[23, 24]. In short, *Mtb* arrests the phagosomal maturation and acidification, and impairs the synthesis of lysosome-phagosome complex. Further, it inhibits not only apoptosis of the macrophages but also represses antimicrobial actions leading to death of host cell via necrosis[17]. The capability of *Mtb* to remain in a dormant state deep inside the respiratory tissues makes penetration of drug molecules difficult. Dormant *Mtb* is in a non-replicating state with low-to-absent metabolic activity. They are referred as persisters in the host as they survive through antibiotics treatment by remaining in the dormant state. A subpopulation of the dormant *Mtb* is thought to be accountable for the occurrence of an asymptomatic form of TB referred as latent TB infection (LTBI)[25]. As mentioned previously, almost a quarter of the world population is infected with LTBI[26] while there is still no promising diagnostic tool or therapy developed. This further complicates the TB conundrum with the regular conversion

of LTBI to active infections especially in immunocompromised circumstances such as HIV co-infection.

Another hurdle in combating TB owes to the emergence of drug-resistant strains. Misuse, interrupted and overuse of antibiotics result in the development of resistance in a proportion of bacteria conferring higher tolerance to anti-TB drugs[27]. Resistance is shown to be more likely to develop when patients do not complete the full prescribed therapy and the level of resistant infection is found to be positively correlated with antibiotics consumption[28]. Individuals with fully susceptible TB may progress to drug-resistant TB due to inadequate or low-quality medication[29]. The exposure to suboptimal drug dosage has facilitated *Mtb* strains to evolve into resistant strains through a various of mechanisms including compensatory evolution, decreased cell wall permeability, drug/target alteration and epistasis[30] while horizontal gene transfer is controversial[31, 32]. The rapid emergence of drug-resistant *Mtb* strain has brought us into a rigorous circumstance in anti-TB drug development. Aiming to develop novel drugs to tackle drug-resistant tuberculosis, it is important to understand their resistance mechanisms in order to identify suitable targets. The hardly penetrable mycomembrane and other developed intrinsic as well as acquired resistances of *Mtb* are discussed in detail in section 1.2.

Apart from the challenges in anti-TB drug development, the lack of diagnostic tools for MDR-TB, differences in public health systems, lack of regulation, education and control in using antibiotics especially in developing countries have led to the unequal distribution of MDR-TB incidence rate in the world. With the alarming figures of MDR-TB population and considering the underestimation due to inadequate of surveillance data, global efforts have been initiated by international organizations such as TB Alliance, World Health Organization and Global Health Innovative Technology to take up the leading role to end the TB epidemic[33].

1.1.2 Anti-TB Drug Development and Current Regimens

An all-round anti-TB therapy aims to cure the patient, reduce complication and mortality, decrease reoccurrence and transmission to sensitive individuals, and avoid the emergence of drug-resistant strains. To achieve each of these aims, combination therapy is used for anti-TB treatment following lessons learnt at the very beginning of anti-TB drug development. Streptomycin was the first effective TB antibiotic isolated by Waksman and Schatz from *Streptomyces grieus*[34]. Resistance was quickly developed to this monotherapy, and most patients started to deteriorate after the first month of treatment[35]. To prevent the selection of resistance, the British Medical Council pioneered the first combination therapy of para-aminosalicyclic acid (PAS), an oral agent developed in 1944, with streptomycin for TB treatment[36]. Combination therapy not only reduced the emergence of resistance but also shortened the length of TB treatment. The discovery of rifampicin in the 1960s was a game changer for the development of TB combination therapy[37]. The inclusion of rifampicin to combination enables the shortening of TB therapy from 18 months or more to nine months[38]. A recent multi-stage randomized control trial has also shown the prominence of high-dose rifampicin in combination in treating TB patients[39]. With the addition of pyrazinamide (PZA), treatment length can be further reduced to six months[40].

During the 1990s, the WHO introduced the current standard six-month Directly Observed Therapy Short-course (DOTs) strategy for the treatment of fully drug-susceptible TB[41]. This program consists of two phases in which the first (intensive) phase involves two months with four oral antibiotics: isoniazid, rifampicin, pyrazinamide and ethambutol followed by a second phase (maintenance) of four months comprising isoniazid and rifampicin. The distinct mode of action of each drug in the combination enables the eradication of *Mtb* while minimizing emergence of resistance. Isoniazid is a prodrug which is activated by the bacterial catalase peroxidase enzyme (KatG). Isoniazid is reported to have multiple cellular targets although the most well-known function of isoniazid is its ability to bind to InhA, a NADH-dependent protein reductase and thereby inhibits the synthesis of cell wall mycolic acid[42]. Rifampicin is a semisynthetic compound that belongs to the class of rifamycin initially isolated from *Amycolatopsis mediterranei*[34]. Rifampicin binds to the ß-unit of ribonucleic acid (RNA) polymerase and blocks the elongation of RNA at the length of two to three nucleotides[43]. Pyrazinamide, another prodrug, is derived from the same compound as isoniazid. The mechanism of pyrazinamide was suggested to be the disruption of proton motive force and membrane energetics of the bacteria[44]. Ethambutol, works by inhibiting the

arabinosyl transferase affecting cell wall synthesis[43], also acts as a safeguard towards unidentified resistance towards to other three drugs[45]. This golden combination is highly effective for drug-susceptible TB and has brought a revolutionary decline in TB population since the 1990s.

The emergence of drug-resistant TB has led to increased mortality and longer treatment involving more expensive drugs and injectables. The DOTs plus program is currently recommended in the WHO guidelines for the treatment of MDR-TB[46]. This standardized program extended the treatment duration to at least 20 months consisting pyrazinamide plus four core second-line drugs including one from group A and group B, and at least two from group C (Table 1.1)[5, 43, 47].

Table 1.1 Current medicines recommended for treatment of drug-susceptible and multidrug-resistant TB and their mechanisms of action.

Types	**Group**	**Drug**	**Mechanism**
drug-susceptible TB	First-line oral drugs	Isoniazid	Inhibits cell wall mycolic acid synthesis
		Rifampicin	Inhibits RNA polymerase/ RNA synthesis
		Ethambutol	Inhibits arabinosyl transferase/cell wall synthesis
		Pyrazinamide	Inhibits proton motive force and/or cell wall synthesis
MDR-TB	A. Fluoroquinolones	Levofloxacin	Inhibits DNA gyrase/translation and transcription
		Moxifloxacin	
		Gatifloxacin	
	B. Second-line injectable agents	Streptomycin	Inhibits ribosome/ protein synthesis
		Kanamycin	
		Amikacin	
		Capreomycin	
	C. Other core second-line agents	Cycloserine	Inhibit peptidoglycan synthesis
		Ethionamide	Inhibits InhA/ mycolic acid synthesis
		Linezolid	Inhibits ribosome/ protein synthesis

The protracted nature of treatment and daily injection of highly toxic second-line drugs reduces patient compliance and often serves as the major barrier to therapy nonadherence[48]. Peripheral neuropathy was reported in 31% of patients receiving linezolid[49] whilst lengthy

and high dosage of amikacin therapy was associated with hearing loss in 62% of patients[50]. Other adverse effects, including hepatoxicity, hypoglycaemia, myocardial damage, respiratory complications and jaundice, were demonstrated to account for 30% of all TB treatment failure[51]. This trend of nonadherence not only increases the number of lost to follow-up patients but also heightens the chance for them to develop more severe and resistant forms of TB exacerbating the global TB burden. Attempts have been made to address this issue by shortening the length of treatment[52, 53]. Among them, the Bangladesh regimen involving seven drugs for a nine-month period has displayed promising treatment outcomes in the first observation cohort of 427 patients[54]. This regimen encompasses gatifloxacin, clofazimine, ethambutol, and pyrazinamide which was supplemented with high dose of isoniazid, kanamycin and prothionamid during the first four months. It has achieved a remarkable success having 87.9% of relapse-free patients among all who have used the gatifloxacin-based regimen (206 patients). It should be noted that these findings are yet to be generalized and randomized trials are underway. Besides, other issues including interactions with antiviral drugs such as rifampicin with nevirapine and nelfinavir[55], absence of effective vaccine[56], dosage variance and expensive medication pose additional challenges for an effective drug-resistant tuberculosis management[57]. Furthermore, it was demonstrated that the current TB treatment regimen has failed to generate minimal mycobactericidal concentration in all patients leaving the chance for the development of drug-resistant strain[58]. This suggested the influence of pathogen and host determinants on the bioavailability of drug in TB lesions renders the exposure of bacteria to sub-inhibitory drug concentration[59] and thereby facilitating resistance evolution. Rates and spectrum of antibiotic resistance to existing second-line drugs are continuously growing[60]. Thus, the research and development of novel anti-TB agents with higher potency toward drug-resistant *Mtb*, adequate safety profile, minimal interactions with antimicrobial agent as well as a short treatment duration is an immediate priority for clinical and public health.

1.2 MYCOBACTERIUM TUBERCULOSIS AND ITS RESISTANCE

1.2.1 Mycobacterial Cell Envelope

Mtb belongs to the phylum Actinobacteria and possesses a unique cell envelope conferring to unusually high antimicrobial resistance[18]. The acid-fast bacteria are impervious to Gram stain marking their extraordinary cell wall architecture compared with Gram-positive and Gram-negative bacteria (Fig. 1.1). The complexity of this cell wall offers mycobacteria a remarkably impermeable and hydrophobic armour. This complex network is composed of a capsule, a mycomembrane, an arabinogalactan layer, a peptidoglycan layer, followed by the innermost plasma membrane. Conglomerated with other proteins and polysaccharides, this sophisticated scaffolding becomes a highly difficult barrier for anti-TB agents to cross[61]. The mycomembrane coating is of particular interest as it is rich in mycolic acids (MAs) as well as those covalently-linked to arabinogalactan bestowing the adaption of *Mtb* to intracellular survival against the host immune responses. In essence, mycolic acid constituents have been associated with numerous physiological and biological properties in mycobacteria. Therefore, the related metabolic pathways represent valuable sources for drug target discovery.

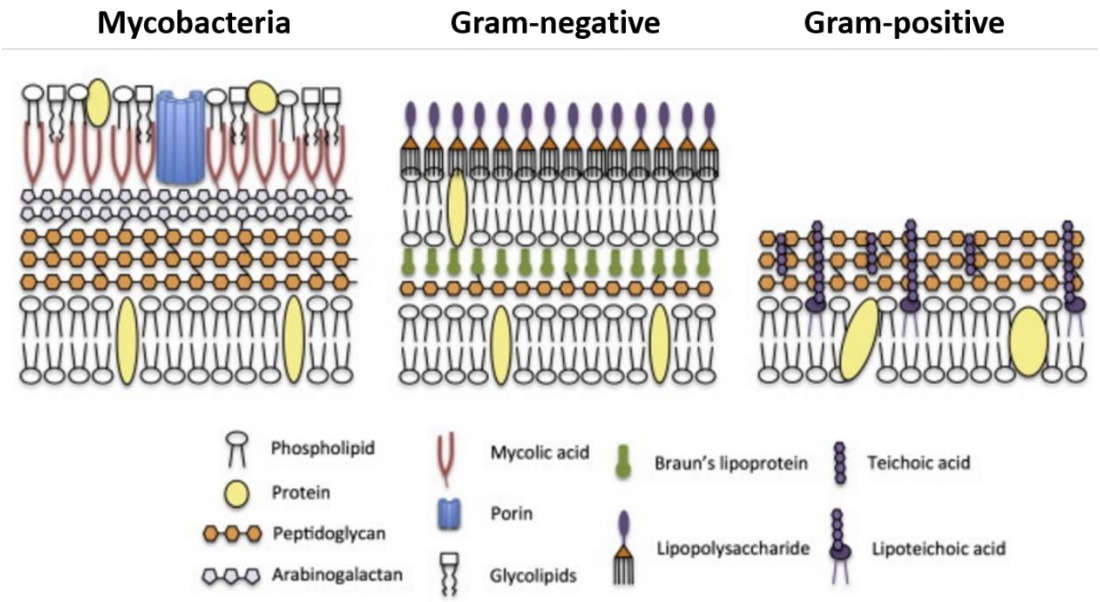

Figure 1.1 Comparison between mycobacterial cell envelope with Gram-positive and Gram-negative bacteria. Unlike Gram-positive and Gram-negative bacteria, the peptidoglycan layer of mycobacteria is covalently linked to a layer of arabinogalactan and further externally to a layer of mycolic acids. (Adapted from Silva et al. [62]).

Evidence of the multi-layered cell envelope organization of mycobacteria has been provided by cryo-transmission electron microscopy[63-65]. Although a clear structural model for mycobacterial cell wall is still yet to develop, the principle components of mycobacterial cell envelope have been rationalized based on the structural model originally proposed by Minnikin *et al.*[66]. The mycobacterial cell envelope has a complex structure comprising multiple layers (Fig. 1.2). The innermost layer is a typical phospholipid bilayer plasma membrane (PM), then a peptidoglycan (PG) layer provides a sacculus support to the plasma membrane and it is linked externally to a layer of arabinoglactan (AG). Via the mycoloyl residues (mycolic acids), this covalent PG-AG complex is linked to the outer membrane (OM), also called the mycomembrane. This mycomembrane is presumably composed of some free extractable lipids including phthiocerol dimycocerosate (DIM), trehalose monomycolate (TMM), trehalose dimycolate (TDM), phosphatidyl insitol mannoside (PIM), sulfolipids and phenolic glycolipids. The outermost layer surrounding the mycobacteria is known as the capsule, consisting of glucan, proteins and glycolipids including lipomannans (LM), lipoarabinomannan (LAM) as well as mannose-capped lipoarabinomannan (Man-LAM)[63, 67].

Synthesis of cell wall is mediated by the mycolyl transferases, namely the antigen-85 protein complexes[8]. These transferases catalyse the transfer of mycolic acid in the cytosolic compartment from TMM to form TDM and a free trehalose. Chiaradia *et al.*[64] has reported the presence of TMM in plasma membrane suggesting the transport of molecules for mycomembrane biosynthesis. It is noteworthy that *Mtb* has a rough colony morphology which is due to the loss of trehalose-based lipooligosaccharides (LOS) production despite the presence of LOS synthesis gene remaining in the genome[68]. Boritsch *et al.* has shown this trait resulted through evolution of *Mtb* to be essential to its superior virulence. Increased level of virulence on *M. canetti* mutants without LOS production ability has been demonstrated in the guinea pig model. Respective essential roles played by each of the components in ensuring the manifestation of *Mtb* are discussed more in detail.

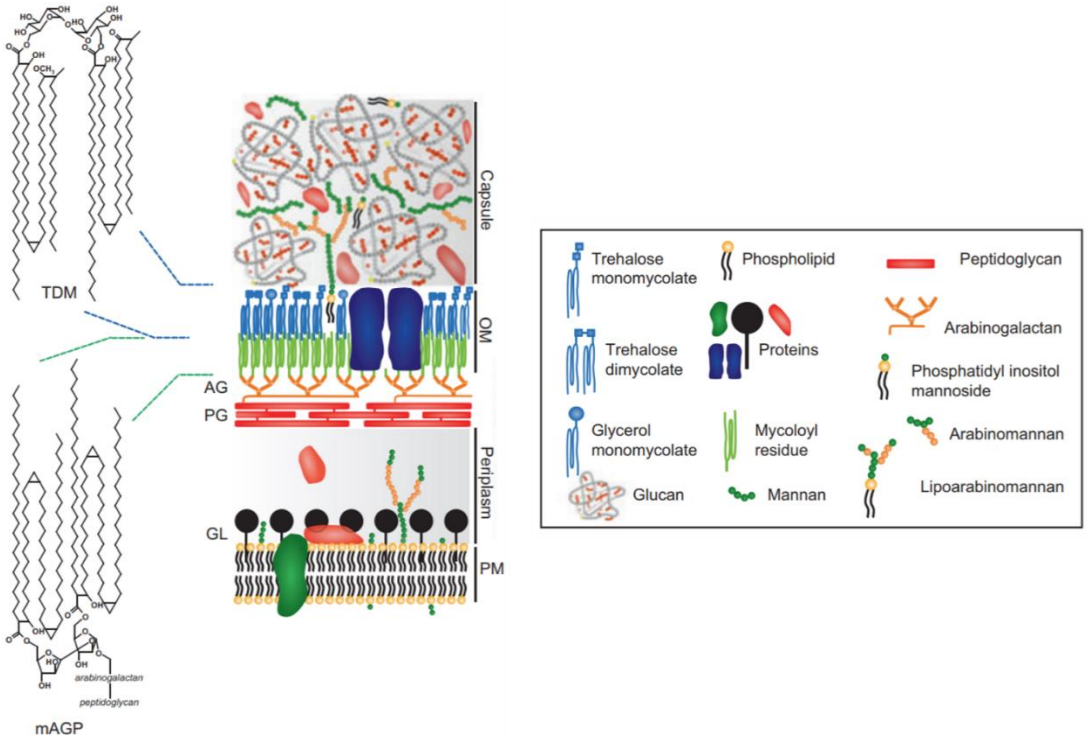

Figure 1.2 Schematic model of mycobacterial cell envelope. The outermost layer of cell envelope known as the capsule contains mainly polysaccharides (glucan and mannan) and proteins. Outer leaflet of the mycomembrane (Outer membrane, OM) consists of free glycolipids noncovalently linked to the mycolic acids such as TMM and TDM (in blue). Mycolic acid residues (in green) link to arabinogalactan and further to peptidoglycan layer forming a robust inner leaflet as mycolyl arabinogalactan-peptidoglycan (mAGP) complex. Chemical representation of TDM and mAGP express the "W-shape" folding mostly found in Mycobacterium tuberculosis species. [69]

The mycobacterial capsule was first described by Chapman *et al.* who observed the existence of a space between the phagosomal membrane of the infected macrophages and the outside of the *Mycobacterium lepraemurium* cell wall[70]. Conventional electron microscopy studies were further carried out to identify this layer as an electron transparent zone made up of a mixture of α-glucan, arabinomannan, proteins and 2-5% lipids in various mycobacterial species[71]. Recently, clear coatings of capsule (thickness ~30 nm) surrounding *M. smegmatis* and *Mtb* cell envelopes have been observed by Sani et al[63] using plunge freezing cryo-electron microscopy. This capsule layer, is considered to have different composition in pathogenic and non-pathogenic bacteria, in turn plays a crucial role in the virulence of pathogenic mycobacteria with the presence of a variety of molecular components such as mannose-capped glycolipids, ß-lactamase, hemagglutinin and catalase/peroxidase[63, 72]. To prevent clumping in mycobacteria cultures, detergents (tyloxapol or tween 80) and agitation are often involved. However, it is important to note that the capsular layer can be shed with treatment involving glass beads, the use of detergent and mechanical agitation [63, 73, 74] therefore affecting both the virulence and morphology of mycobacteria.

Mycolic acids (MAs) are α-alkyl ß-hydroxyl long chain fatty acids which generally consist of two parts: the non-functionalized "mycolic motif" and the "meromycolate chain" containing up to two functional groups at the distal and proximal positions[75] (Fig. 1.3). Unlike the other members under the suborder of *Corynebacteriales*, which usually possess short chains mycolic acids (C_{28}-C_{40}), *Mycobacterium* species depend fully on the long chain mycolic acids (C_{60}-C_{90}) for their growth and survival *in vitro* and *in vivo*[76, 77]. The occurrence of cis- or trans-double bonds, cyclopropyl functional groups or the supplementary oxygen functions located at the distal positions of the mero-chains classifies α-, keto-, methoxy-, hydroxy-, epoxy- and wax-ester-types of mycolic acids[75]. Interestingly, different mycobacteria contain different types of mycolic acids and these can act as a fingerprint. For instance, *M. smegmatis* contains mostly a homologous, α-series mycolic acids cyclopropane and/or alkene functional groups in the mero-chain and also epoxy- in trans configuration whereas α-, methoxy-, keto- and hydroxy-mycolic acids are found in *Mtb*[78] (Fig. 1.4). The conformation of α-mycolic acids might relate to the mycobacterial resistance towards certain anti-TB agent. Strains containing higher percentage of trans double bond or cyclopropane at the proximal position including *Mycobacterium chelonae, Mycobacterium fortinum* and *M. smegmatis* tend to have higher tolerance towards lipophilic antibiotics such as rifampicin[18]. This has been explained by the decrease in cell wall fluidity and therefore permeability resulting from the crystalline arrangement of the trans-functionalized mycolic acids. On the contrary, trans-

cyclopropanation of mycolic acids in *Mtb* was shown to suppress their virulence[79]. This has reflected the structural-functional complexity of mycobacterial mycolic acids and the necessity of deeper understanding.

Mycolic acids are usually existed in mycobacteria in three different ways, (i) bound to AG in mAGP complex; (ii) in cell wall extractable ester as TDM and TMM; or (iii) as free mycolic acids. mAGP complex is the major structural material linking the mycomembrane and plasma membrane. Alterations in the proportion of different types of structural mycolic acids affects fundamentally the fluidity and therefore its permeability towards external agents[80, 81]. Yuan *et al.*[82] demonstrated that the proportion of trans-substituted cyclopropane at the proximal position influenced the cell wall fluidity. Downregulation of *hma* gene in *Mtb* was shown to impair methoxy- and keto-mycolic acids production resulting in a reduced permeability for specific nutrients such as glycerol, leading to the attenuation of the mutant strain in mouse model[83]. Topping the mAGP complex are the TMM and TDM in which the latter, also known as the "cord factor", is likely to be the most abundant glycolipid in mycobacterial cell wall[84], and has been reported to have a define role in bacterial virulence[75]. This important role of TDM was established early in 1950s when reduced virulence was seen after washing the cord factor off drug-susceptible *Mycobacterium tuberculosis* H37Rv with petroleum ether[85]. TDM was described to be critical for intracellular survival of *Mtb* via inhibiting phagosome-lysosome fusion and phagosomal acidification but the exact mechanism is still not fully understood. It was suggested recently the interaction of TDM with macrophage inducible C-type lectin receptor induces signals modulating phagosomal maturation[86]. TDM was also proposed to cause the secretion of high level of proinflammatory cytokines such as TNF-α and IL-6 leading to tissue damage and necrosis[87].

Phthiocerol dimycocerosate (DIM) represents another cell wall lipid attributed to intracellular host-cell modulation. Astarie-Dequeker *et al.*[88] reported, that in contrast to the wild type *Mtb* which mainly reside in non-acidic phagosomes, the majority of DIM knocked-down mutants were found in the acidic phagosome. The delayed acidification in mycobacteria was suggested to be via the inhibition of fusion between vacuolar proton-translocating ATPase and the phagosome[89]. This revealed the contribution of DIM in arresting phagosomal maturation and thereby facilitating intracellular replication. Moreover, the increased production of DIM exhibited a correlation not only with the increased access of *Mtb* into cytosol but also induced host cell death through necrosis[90]. Indeed, DIM was shown to act in concert with the ESX-1 secretion system to facilitate phagosomal rupture and cytosolic

access of *Mtb*[24]. ESX-1 is the most studied system among the five *esx loci* of ESX secretion systems in *Mtb*. It is responsible for the encoding of the 6 kDa Early Secretory Antigenic Target (ESAT-6) as well as the 10 kDa Culture Filtrate Protein (CFP-10) that are regarded as key virulence factors of *Mtb*[91]. The ESX-1 system was demonstrated to be essential for phagosomal rupture as the absence of ESX-1 (due to deletion of the RD-1 region) in *M. bovis* BCG resulted in the absence of cytosolic bacteria in differentiated THP-1 human monocytic cell line[92]. Furthermore, it was recently demonstrated that the production and export of intact DIM is required to ensure *Mtb* getting into cytosol and eventually led to the death of macrophages[93]. This further supported the hypothesis that blockade of acidification process by functional DIM is a pre-requisite for phagosomal rupture mediated by ESX-1 system.

Likewise, PIM, Man-LAM and LAM are important glycolipids to regulate immunobiological processes during phagocytosis to enhance *Mtb* survival. Man-LAM was reported to be recognized by mannose receptors (MR), limiting the phagolysosome fusion while MR blockade reversed the inhibition of fusion during phagocytosis of both H37Rv and live *Mtb* Erdman strains[94]. Understanding of the exact role of free mycolic acids during natural infection is still awaited. In addition to the suggestion of free mycolic acids attracting cholesterol for the formation of biofilm, this was also used to explain the gathering of sufficient carbon source by intracellular *Mtb* to develop into slow growing, persistent strain[95]. Finally, sulfoglycolipids have a role in *Mtb* virulence by hampering the human innate response, appearing as competitive antagonists of TLR2 receptors[96].

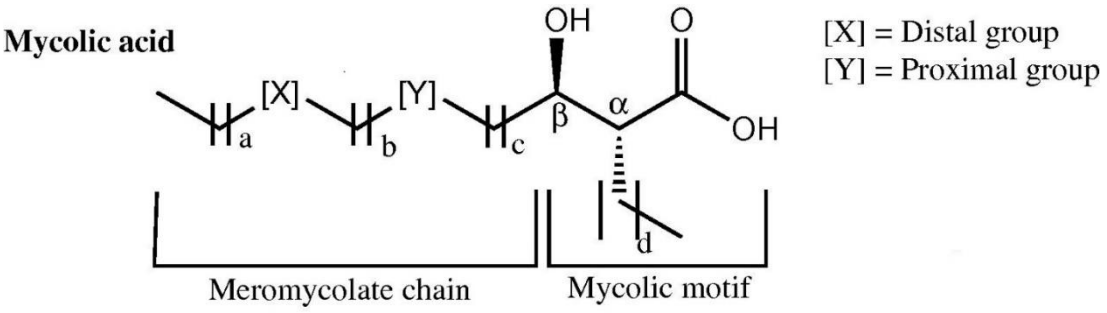

Figure 1.3 General formula of mycolic acid. a-d represents the varying length of methylene chains.[75]

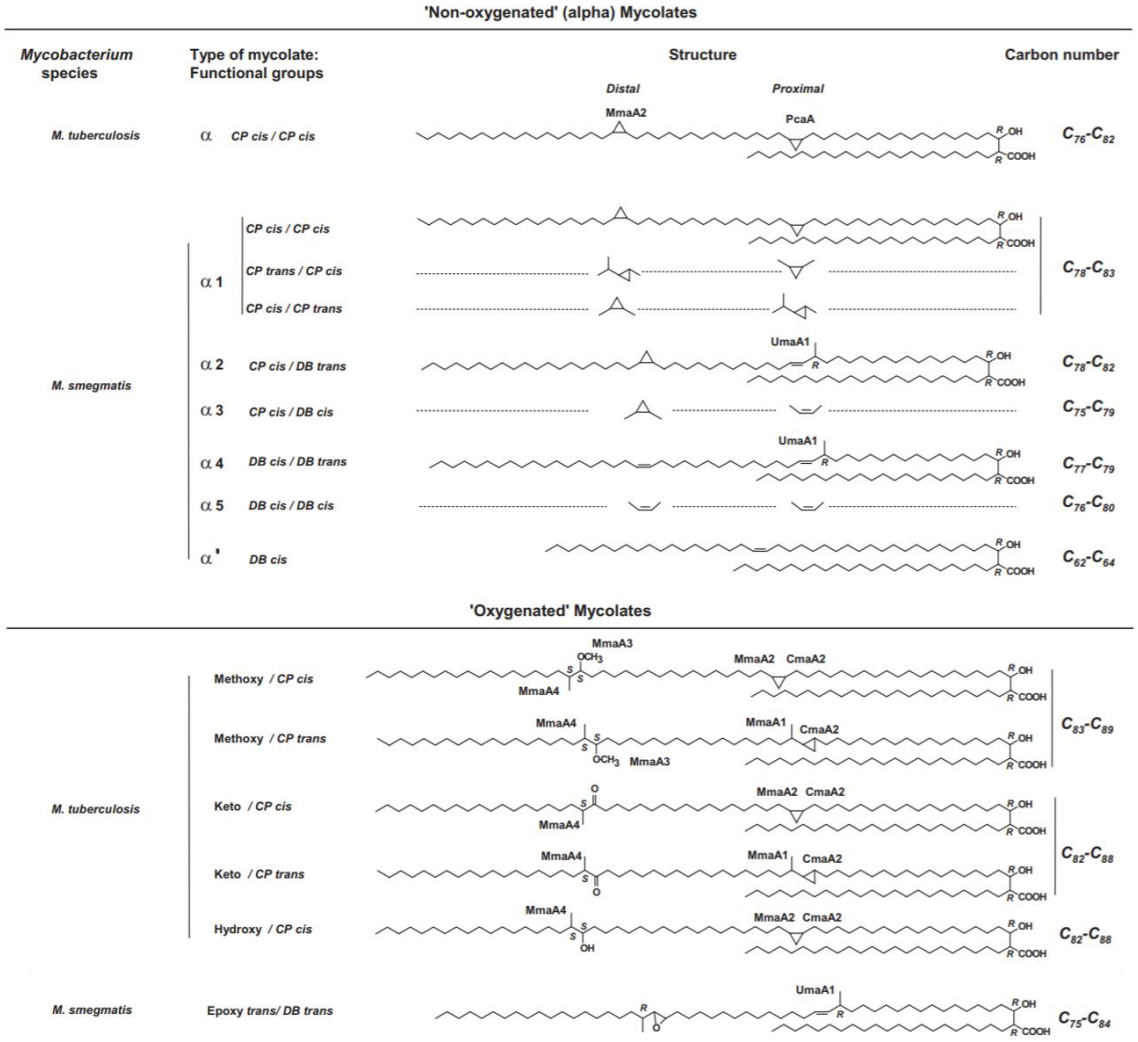

Figure 1.4 Structural characteristics of mycolic acids in Mycobacterium tuberculosis and Mycobacterium smegmatis.[78]

1.2.2 Drug Resistance Mechanisms in Mycobacterium tuberculosis

To tackle the global tuberculosis crisis and develop effective intervention strategies, it is necessary to gain better knowledge of the underlying mechanisms and driving forces behind antibiotic resistance in *Mtb*. Resistance is practically defined as the reduction in sensitivity of a particular strain to a significant degree that it is different from its wild type strain that has never been exposed to the drug[10]. *Mycobacterium tuberculosis* undergoes structural and functional modifications in response to changing environment resulting in the possession of various intrinsic resistances, limiting the number of anti-TB compounds available for treatment[97]. The exposure of *Mtb* to suboptimal drug concentration enables the bacteria to acquire further resistances through chromosomal mutations[17]. Distinctive intrinsic and acquired resistance mechanisms of mycobacteria towards first- and second-line drugs are described in Fig. 1.5. This part of the thesis summarizes these mechanisms with examples of drug resistance.

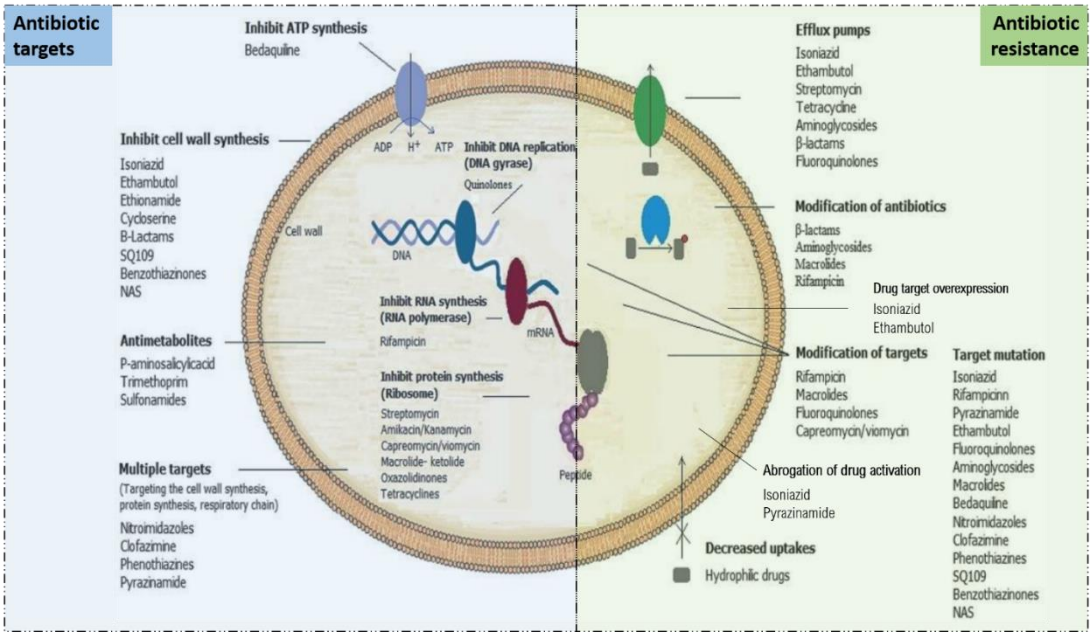

Figure 1.5 Summary of anti-TB drug mechanisms and respective resistance mechanisms in mycobacteria. (Adapted from Nasiri et al.[97]).

Intrinsic resistance

Several intrinsic resistance mechanisms towards antibiotics have been described in mycobacteria. Examples of these mechanisms involving cell wall permeability, drug or target modification and putative efflux pump are listed in Table 1.2. The multiple layer lipid-rich mycomembrane as described in the previous section is a natural armour of *Mtb* that protects it from environmental stress and antibiotic attacks. This dense and thick hydrophobic layer also limits the entry of antibiotics[98]. It has been demonstrated that defects in the lipid barrier increased sensitivity of *Mtb* towards anti-TB drugs[99]. The inactivation of the renowned proteins of antigen 85 (Ag85) complex, responsible for the biogenesis of trehalose dimycolates, affected the integrity of mycomembrane in a pronounced manner resulting in increased permeability of *Mtb* cell envelope[100]. *virS* regulates the expression of monooxygenase operon which controls mycolic acid composition and cell wall integrity[101]. *virS* mutant was found to be more susceptible to rifampicin, isoniazid and ciprofloxacin due to the increased diffusion through more the permeable cell wall. Upregulation of proline-glutamic acid (PE11) protein, a putative lipase involved in cell wall remodelling, modulated cell wall morphology and lipid composition reduced the diffusion of antibiotics in *ex vivo* and *in vivo* models[102]. Hydrophilic drugs are believed to traverse through the mycomembrane via water-filled porins. The presence of very few porin channels represents another intrinsic resistance mechanism of *Mtb* towards hydrophilic compounds[44].

Enzymatic degradation and modification by methylation or acetylation of drugs render them ineffective[17]. Intrinsic resistance of *Mtb* towards ß-lactam antibiotics mediated through the *blaC* gene was established in early studies[103]. On the other hand, acetyltransferase and phosphotransferase are two main classes of aminoglycoside-modifying enzymes with well-described mechanism to protect *Mtb* against capreomycin and kanamycin[104]. Among them, the best characterized N-acetyltransferase (ACC2') can acetylate all the aminoglycosides bearing 2' amino group such as tobramycin, kanamycin, gentamycin and neomycin[105]. *M. smegmatis* was reported to be resistant to rifampicin due to the presence of an ADP-ribosyltransferase[106]. Besides, drug target alteration plays an important role in reducing mycobacteria susceptibility. Methyltransferase erm37 encoded by the erythromycin resistance methylase gene in *Mtb* and *M. bovis* confers their resistance to various macrolides[107]. Binding of fluoroquinolones to DNA gyrase in *Mtb* was hampered by the mycobacteria fluoroquinolone resistance protein A (MfpA) encoded by *mfpA* gene[108]. Three-dimensional structure analysis has revealed MfpA proteins resembles *Mtb* DNA in terms of

shape, size, conformation and overall surface charge suggesting the intervention operates via target mimicry[109]. Resistance to capreomycin and viomycin occurs through the loss of methylation on bacterial ribosome[110]. *Mtb* modulates the deactivation of methyltransferase TlyA resulting in the production of unmethylated ribosome making binding of aminoglycoside becomes impossible. RbpA in *Mtb* and *M. smegmatis* has been found to preferably bind to the RNA polymerase impeding the action of rifampicin[111]. Notably, only recently was relevant clinical significance observed of efflux pump of mono-resistant isolates that increased the attention to this machinery. The upregulation of major facilitator superfamily (MFS) pumps in *Mtb* resulted in increased resistance towards streptomycin, isoniazid and ethambutol[112]. Other identified putative efflux systems such as the resistance-nodulation-cell division superfamily (MmpL5, MmpL7) and the small multidrug resistance family (Rv3065) are also associated with intrinsic resistance in *Mtb*. Furthermore, the low metabolic activities of dormant *Mtb* is implicated with decrease production of antibiotic targets and related machineries. *Mtb* tends to adopt dormancy when it is under a specific environmental cue such as antibiotics exposure or inside macrophages. Oxygen deprivation or heat shock induced *Mtb* dormancy was found to be associated with cessation of nucleic acids and proteins synthesis which subsequently reduced their sensitivity towards rifampicin and isoniazid[113]. Studies have demonstrated the re-sensitization of dormant *Mtb* towards antibiotics due to the resumption of cellular target production[114].

Table 1.2 Intrinsic resistance mechanisms and the associated gene/protein in mycobacteria.

Resistance Mechanism	Gene/protein associated	Resistance to	Mycobacterial strain	References
Cell wall permeability	Ag85 complex	RIF	*M. smegmatis*	[115]
	virS	RIF, INH and ciprofloxacin		[101]
	PE11 protein			[102]
	MspA porin	INH, EMB	*Mtb*	[44]
Drug/ target modification	*blaC*	ß-lactam	*Mtb*	[103]
	N-acetyltransferase	Tobramycin, kanamycin, gentamycin and neomycin	*Mtb, M. smegmatis*	[104, 105]
	Rv0560c	Pyrido-benzimidazole compound '14'	*Mtb*	[116]
	ADP-ribosyltransferase	RIF	*M. smegmatis*	[106]
	erm37	Macrolides	*Mtb, M. bovis*	[107]
	MfpA	Fluoroquinolones	*Mtb*	[108]
	tlyA	Capreomycin and viomycin	*Mtb*	[110]
	RbpA	RIF	*Mtb, M. smegmatis*	[111]
Efflux pump	MmpL7	INH	*Mtb*	[117]
	MmpL5	Azole compounds	*Mtb*	[118]
	Rv2459 (*jefA*)	INH, EMB, streptomycin	*Mtb*	[112]
	Rv3065 (*mmr*)	INH	*Mtb., M. smegmatis*	[119, 120]
	Rv2846(*efpA*)	INH, ETH	*Mtb., M. smegmatis*	[119, 120]

Acquired resistance

Mtb strains generally acquired resistance towards existing anti-TB agents through spontaneous mutation in chromosomal genes. Table 1.3 summarizes the drug targets and possible corresponding resistance mechanism in mycobacteria. Mutation attributing to drug target mutation is frequently observed in *Mtb* against a wide range of antibiotics including first-line anti-TB drugs, fluoroquinolones and aminoglycosides. Over 95% of rifampicin-resistant strains have a mutation within the 81-bp hotspot region at codon 507-533[121]. Mutation in *inhA*, which plays a key role in the fatty acid synthase II system involving in mycolic acid synthesis, hinders the binding of active drugs to their targets[78]. The most common high-level fluoroquinolone resistance usually occurs within a short sequence known as the quinolone resistance-determining region (QRDR) leading to protein structure alteration affecting fluoroquinolone binding affinity[122]. Apart from intrinsic resistance mentioned earlier, acquired resistance through the inactivation of the *tlyA* gene has also presented in *Mtb* clinical isolates[123]. Prodrugs like isoniazid, pyrazinamide and delamanid require the conversion by bacterial enzymes into their active forms. Abrogation of prodrug activation renders them ineffective leading to resistance towards these powerful anti-TB agents. Isoniazid requires the activation by the catalase/peroxidase enzyme encoded by *katG*. Mutation, insertion, deletion and truncation of *katG* are the most common genetic alteration associated with high-level isoniazid resistance[124]. Gu *et al.*[125] demonstrated that *pncA* mutation is highly associated with pyrazinamide resistance trait while resistance rate of XDR-TB was higher than MDR strains. Mutation in the promotor of drug target may cause inhibition of the drug due to the overabundance of the target[17]. *InhA* promotor mutation induces overexpression of *inhA* resulting in low-level resistance of *Mtb* towards isoniazid[42]. EMB has been reported to inhibit the activity of arabinosyl acid transferases, disrupting the formation of mycolyl-arabinogalactan-peptidoglycan complex thereby increasing the cell wall permeability[126]. *AftA* and *ubiA* are two cell wall-associated genes which were shown in several studies to acquire resistance through genetic mutation leading to the overexpression of EmbCAB proteins, contributing to high-level ethambutol resistance in *Mtb*[127]. Resistance developed through increased activity of efflux pumps is usually based on their basal expression, drug-induced expression or the overexpression due to chromosomal mutations[128]. Li *et al.*[119] investigated the expression of efflux pump in MDR clinical isolates and found that eight out of nine strains possess at least one overexpressed efflux pump gene. This finding suggested the link between efflux pump and acquired resistance in *Mtb* and the possibility of

unknown mutations responsible for the phenomenon. More importantly, evidence of mutation in transcription regulator (Rv0678) has been identified in bedaquline-resistant *Mtb* isolates[129]. This brought about the upregulation of MmpL5 expression promoting drug efflux and increased cross-resistance to clofazimine, a second-line anti-TB agent.

Table 1.3 Summary of the first- and second-line anti-TB drug targets and corresponding resistance mechanisms in drug-resistant Mycobacterium tuberculosis.

Agent	Target gene	Gene function	Resistance mechanism	References
Rifampicin	*rpoB*	ß-subunit of RNA polymerase	Drug target mutation	121, 130
Isoniazid	*katG*	Catalase-peroxidase	Abrogation of drug activation	121, 124
	inhA	Enoyl-acyl carrier protein reductase	Drug target mutation	124
	inhA promotor		Drug target overexpression	42
Pyrazinamide	*pncA*	Pyrazinamidase	Abrogation of drug activation	125
Ethambutol	*embB*	Arabinosyl transferase	Drug target mutation	126, 127
Capreomycin	*rrs*	16S ribosomal RNA	Drug target mutation	131
	tylA	rRNA methyltransferase	Abrogation of drug target methylation	123
Amikacin/ Kanamycin	*rrs*	16S ribosomal RNA	Drug target mutation	131
	eis promotor		Drug inactivating enzyme overexpression	132
Streptomycin	*rrs*	16S ribosomal RNA	Drug target mutation	131, 133
	rpsL	S12 ribosomal protein	Drug target mutation	133
Fluoroquinolones	*gyrA*	DNA gyrase subunit A	Drug target mutation	122
	gyrB	DNA gyrase subunit B	Drug target mutation	122
Ethionamide	*ethA*	Monooxygenase	Abrogation of drug activation	134
	inhA	Enoyl-acyl carrier protein reductase	Drug target mutation	124, 134
Cycloserine	*ald*	D-alanine/ glycine/ D-cycloserine proton symporter	Overabundance of drug target substrate	32
	alr	Alanine racemase	Drug target mutation	32, 135
Para-aminosalicylic acid	*thyA*	Thymidylate synthase	Drug target bypassing	136
	folC	Dihydrofolate synthase	Abrogation of drug activation	136
Linezolid	*rrl*	23S ribosomal RNA	Drug target mutation	137
	rplC	50S ribosomal protein	Drug target mutation	138
Delamanid	*ddn*	deazaflavin dependent nitroreductase	Abrogation of drug activation	139
Bedaquiline	*Rv0678*	Transcription regulator	Overexpression of efflux pump	129
	atpE	ATP synthase	Drug target mutation	140

1.2.3 New Treatment Strategies against MDR-TB

TB is a global pandemic compounded by the emergence of MDR- and XDR-TB strains and demands a concerted response. Great endeavours have been put in developing and advancement of new anti-TB agents. At present, there are a number of new drug candidates at various stages of discovery, preclinical and clinical evaluations[8]. Focusing on new developments against drug-resistant *Mtb* strains, this section reviews promising anti-TB agents at different phases of clinical trial, including their background, chemical structures (Fig. 1.6), corresponding efficacy as well as mechanism of action. Recent studies on repurposing of existing FDA-approved drugs for MDR- or XDR-TB treatment are also discussed. Finally, the introduction of adjuvant and novel combinations of currently available drugs are described.

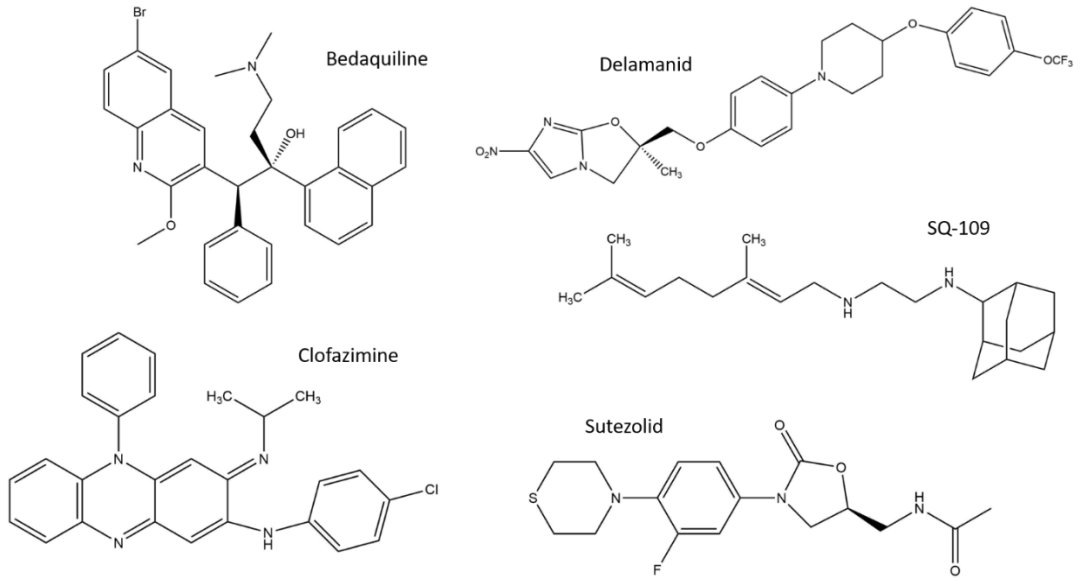

Figure 1.6 Chemical structures of new promising anti-TB drug.

Newly-marketed Drugs

Delamanid (DLM) and bedaquiline are two oral anti-TB medications that first gained FDA-approval since rifampicin in 1967. These two small molecule drugs were identified through drug screening for the treatment of MDR-TB without other indications[141]. This sole indication might be clinically advantageous as the restriction on mycobacterial use could reduce the chance for development of resistance.

Delamanid is the first member of the nitroimidazole class to enter clinical practice. Nitroimidazoles are derived from azomycin, which was a metabolite isolated from *Streptomyces eurocidius* in 1953[33]. It is known to inhibit the production of methoxy- and keto-mycolic acid thereby disrupting the biosynthesis of mycobacterial cell wall with potent *in vitro* and *in vivo* efficacy against *Mtb*[142]. Delamanid is a prodrug that requires the activation mediated by the enzyme deaflavin dependent nitroreductase. This drug has physiochemical properties similar to another new drug candidate pretomanid while possesses an anti-TB activity that well surpasses the latter[142]. Strong activity of delamanid has been reported against MDR *Mtb* clinical isolates[143]. Notably, the bactericidal action of delamanid is found to be similar to that of rifampicin[142]. The fact that delamanid does not induce the expression of P450 enzymes encourages studies of its use in combination with anti-HIV drugs against TB/HIV co-infections[144]. Phase III clinical trials of delamanid for its safety and efficacy in TB/HIV co-infections and pediatric MDR-TB are on-going.

Bedaquiline is a novel, chemically synthesized, diarylquinoline demonstrating potent activities against MDR/XDR-TB. Its action is highly selective, targeting energy generation pathway in mycobacteria, while eukaryotic cells are unaffected[145], and it is ineffective to neither Gram-positive nor Gram-negative bacteria[146]. Hards *et al.*[147] described its mode of action through binding to the subunit c of the bacterial adenosine triphosphate (ATP) synthase, resulting in a futile proton cycle. Bedaquiline has demonstrated superior activity against drug-resistant strains *in vitro*[148]. Moreover, a remarkable synergistic effect has also been displayed when it was used in combinations with pyrazinamide[149]. Although bedaquiline has been approved for the treatment of MDR-TB based on phase IIb results, phase III trials are still in progress as the occurrence of side effects including QT prolongation and the unexplained high mortality rate.

Drugs under clinical trial

Apart from the above mentioned newly-marketed anti-TB drugs, several other promising anti-TB agents are also in early clinical trial status. Sutezolid and SQ-109 are two new drug candidates currently under phase II trial. Sutezolid is a structural analogue of Group C anti-TB agent linezolid. Its bactericidal action of limiting protein synthesis in *Mtb* was demonstrated both *in vitro* and *in vivo*[150]. Unlike linezolid which is associated with high bone marrow toxicity, this new analogue has been established to have a better safety profile as well

as a greater antimicrobial action[151]. SQ-109, identified from screening ethambutol analogues, is considered to be the next-generation drug replacing ethambutol as it displays potent actions in both *in vitro* and *in vivo* settings against drug-susceptible, MDR- and XDR-TB clinical strains[152]. SQ-109 exerts antimycobacterial action through targeting the transmembrane reporter for trehalose monomycolate (MmpL3), intruding the formation of intact outer-membrane of the mycobacterial cell envelope. It was also reported to act as an uncoupler, collapsing the inner mitochondrial membrane potential thereby blocking respiration and ATP synthesis[153]. It is also shown to be safe and well-tolerated by smear-positive TB patients, making the drug a prospective candidate to proceed in further trials. Other phase I registered anti-TB agents include Q203[154] and PBTZ-169[155] which have shown high efficacy against *Mtb* in murine models, and OPS-167832 is suggested to have a different mechanism as the existing anti-TB has promising action with a chemical structure that is yet to be revealed.

Repurposing old drugs

Commercially available medications, currently used for indications other than TB, might be applicable for fighting MDR-TB crisis. This can be facilitated by repurposing approved antimicrobial agents for TB therapy or repositioning neglected anti-TB agents that were once pursued[156]. Since this approach can shorten the process of drug development and clinical trials with the existence of ample human safety and pharmacokinetics data, it is especially essential for low-income high prevalence countries.

Clofazimine is a lipophilic anti-TB compound developed in 1954. Its poor *in vivo* performance in a primate model discouraged its development and it was later repurposed to fight *Mycobacterium leprae* resistant to sulfones[157]. Its notable advantage of inhibiting resistance development to isoniazid in *Mtb* has attracted reinvestigation of its use in MDR-TB treatment. Encouraging cure rates of MDR- and XDR-TB have been shown in corresponding studies in Bangladesh and Korea using clofazimine-containing regimens[158]. The regimen was demonstrated to have low-to-mild adverse effects such that only 0.1% of patients required discontinuation which is comparable to that of first-line TB regimen[159, 160]. However, high cost and low market availability are the biggest obstacles at present for its global use. Sulfonamides were developed between 1930 and early 1950s as monotherapy for anti-TB treatment[161]. Their use was then terminated due to the emergence of better options including isoniazid. Sulphamethoxazole (SMX) was later used in combination with

trimethoprim (TMP) for the prevention of *Pneumocystis jirovecii* infection in TB/HIV co-infected patients[162]. This combination brought about its revival to be used in MDR-TB patients and demonstrated shorter sputum conversion time in two cohorts in Nigeria[163]. Clinical evidence of the potency of SMX/TMP regimens on MDR-TB treatment is still underway. Alsaad *et al.*[164] reported eight out of 10 MDR-TB patients had successfully completed the combination therapy with good tolerance and no sign of reoccurrence in a median treatment period of 381 days. SMX has also shown efficacy on its own against *Mtb* and preliminary success on drug-resistant strains. On the other hand, Minocycline, a leprosy drug, has shown anti-TB action in 1980[165]. Its activities on clinical isolates including MDR-TB was demonstrated and suggested to be bacteriostatic, suitable to be used as adjuvant in TB-chemotherapy[166]. Despite the need of more validation studies and clinical trials of these drugs for the indications on TB, the amiable features such as low rates of adverse events, developed drug profile and relatively higher accessibility suggesting them as good candidates as MDR-TB medication.

1.3 ANTIMICROBIAL PEPTIDES

1.3.1 Nature and Properties of Antimicrobial Peptides

The therapeutic effect of antimicrobial peptides (AMPs) was first discovered by Rene J. Dubois who isolated gramicidin from the soil bacterium *Bacillus brevis* during World War II. Gramicidin was found to be useful against infections caused by Gram-positive bacteria and therefore widely applied for wounds and ulcers on soldiers[167]. In the 1980s, two well-known mammalian AMPs, defensin and cathelicidins were identified and demonstrated the production of these endogenous protective compounds by the innate immune defence systems in animals[168]. This has initiated an increasing number of in-depth studies on the isolation and the synthesis of new AMPs as well as the understanding of their corresponding mechanisms for therapeutics development. To date, over 5000 AMPs have been discovered either from natural prokaryotes and eukaryotes or by chemical synthesis. The majority of these have been shown to possess antimicrobial activities towards both Gram-positive and Gram-negative bacteria, fungi, viruses or mycobacteria with ample potential to be developed into therapeutics[169-172].

AMPs are generally positively-charged amphipathic small peptides, composed of 12-50 amino acid residues. They can be classified into four forms according to their secondary structures: α-helix, ß-sheet, extended and loop (Fig. 1.7)[173]. The possession of cationic amino acids including lysine and arginine confers a net positive charge on AMPs that is important for binding to anionic bacterial membranes. The amphipathic nature of AMPs refers to the availability of both hydrophobic and hydrophilic regions, facilitating partition into membrane interface as well as ensuring sufficient aqueous solubility. Natural occurring AMPs were initially neglected as therapeutic agents due to their vulnerability and instability towards proteolytic enzyme degradation which leads to poor bioavailability. With the continuous exploration and studies, newer technologies such as conjugation, formulation approaches and chemical modification were incorporated to improve the stability of endogenous AMPs whilst the production of synthetic AMPs was also made available[174]. These technological breakthroughs have enormously expanded the exploitability of AMPs in therapeutic applications. This section discusses the physicochemical properties and structural arrangements including length, conformation, hydrophobicity, net charge, charge angle of AMPs which could be further optimized to enhance their specificity, selectivity and maximize their discerning antimicrobial activity while minimizing toxicity.

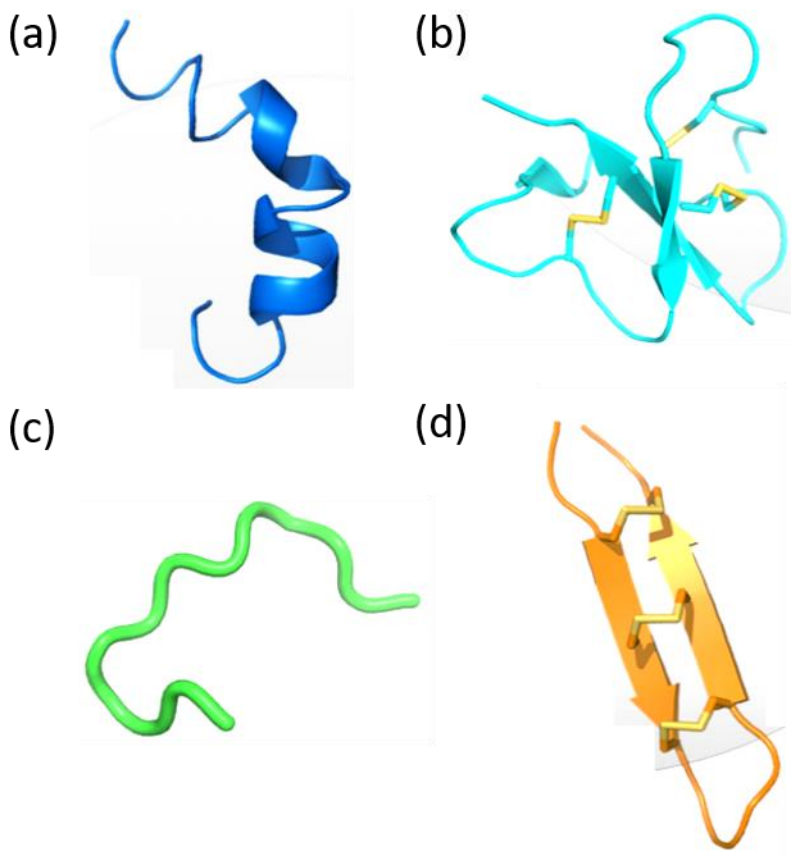

Figure 1.7 Molecular modals of AMPs secondary structures. (a) α-helix, (b) ß-sheet, (c) extended and (d) loop[173].

The length of AMPs has a decisive role in their fundamental nature as a minimum of three to four amino acids are required for the formation of an amphipathic peptide possessing both hydrophobic and hydrophilic units. Besides, length affects the mode of action and secondary structure of AMPs, which consequently influence their ability to permeate through membranes. For instance, at least 22 units for α-helix and eight units for ß-sheet peptides are necessary for the penetration via the barrel-stave model[175]. Shorter AMPs are often shown to have lower toxicity and higher activity. A 15-residue synthetic melittin exhibited significantly lower toxicity (300%) on rat erythrocytes when compared to its original 26-residue form[176]. Moreover, HP-A3 peptide, derived from N-terminus of *Helicobacter pylori* ribosomal protein L1 (RpL1), demonstrated enhanced antibacterial and antifungal action without any hemolytic effect[177]. Juba *et al.*[178] demonstrated the effect of peptide length in relation to respective antimicrobial activity. It was shown that full length 34-residue NA-

CATH eliminated ~5% of *E. coli* and *B. cereus* while the 11-residue truncated peptide L-ATRA-1A achieved 10-20% of growth inhibition on the bacterial species.

A higher net positive charge of peptides can promote their antimicrobial activity. This cationic property is primarily responsible for the interaction with the negatively-charged bacterial membranes, rich in anionic components such as phosphatidylglycerol, lipopolysaccharides and teichoic acid. Studies with magainins and other α-helical peptides have portrayed the direct association between peptide net charge and antimicrobial activities[179, 180]. However, increase in charge beyond +8 induces undesirable effects on mammalian cells due to the higher hemolytic activity[181]. Therefore, it is essential to maintain a balance to obtain an optimal net charge for the high selectivity of AMPs towards microbes with the least toxicity on the host cells. Besides, charge angle subtended by the cationic helix domain is considered to be a measurement of proportion between polar to non-polar content in helical peptides[182].

AMPs may assume different secondary structures which is another extended key to determine their antimicrobial efficacy. The α-helix is the most common conformation adopted by AMPs, comprising around 27% of all AMPs with known secondary structures[183]. Reduction in peptide activity was shown with reduced helicity. This is because the helical structure enables the peptides to permeate bacterial membrane efficiently[184]. Paradoxically, presence or incorporation of proline residue which disrupts the helical conformation thereby altering the selectivity and efficacy of AMPs may affect their potency. Proline was found to be crucial for membrane permeation and intracellular targeting of buforin II. Substitution of proline resulted in the reduction of peptide activity[185, 186]. Proline may also enhance conformation flexibility and enable the formation of C-terminal α-helix, facilitating their translocation across the interior membrane[187]. It is evident that the position of proline influences the antimicrobial activities through altering the peptide conformation. Substitution of proline at central region led to significant increase in activity towards *E. coli* and *P. aeruginosa*[188]. Xie *et al.*[185] also reported the relocation of proline towards either C- or N-terminal resulted in reduced buforin II transposition through membrane.

Overall hydrophobicity affects the bioactivity of AMPs intensively. It represents the percentage of hydrophobic residues in the peptides and thus determining the partition ability into membrane. An increase in hydrophobicity generally increases the antimicrobial activity of α-helical AMPs[189]. Nevertheless, increase of hydrophobicity over a certain threshold often induces complications and reduces peptides bioactivity. Chen *et al.*[190] analysed the impact of

hydrophobicity on α-helical AMPs and reported that an optimal hydrophobic window is critical to achieve high antimicrobial activity. Peptides with high hydrophobicity tend to self-associate, forming dimers/oligomers, hindering their penetration into the bacterial cell wall[19]. However, aggregated peptides could still enter eukaryotic membranes leading to higher toxicity profile towards mammalian cells. Cytotoxicity towards murine macrophage RAW 264.7 cells was significantly higher when exposed to peptides with higher hydrophobicity[191]. Moreover, optimization of hydrophobicity is important as it also influences other properties of the peptide. Several studies have suggested that there is a positive correlation between hydrophobicity and α-helicity[190, 192]. To tackle the hydrophobic scaffolding of mycobacteria, AMPs with increased proportion of hydrophobicity and helicity has been engineered to improve their mycobactericidal effect. Flow cytometry data revealed the enhanced rate and extent of membrane permeability by peptides displaying higher hydrophobicity and helicity[193]. Taken together, rational design of peptides involves not only a single element, but a good combination of various structural parameters. It is also obligatory to determine the full toxicity profile towards the host cells, ideally by *in vivo* experiments.

Due to their promising antimicrobial activity, the investigation of AMPs for therapeutic applications is becoming popular with their superior advantages over other small molecule drugs. These include their broad-spectrum activity and direct killing mechanism, high specificity and selectivity, high affinity to bacterial membrane as well as the low rate of bacterial resistance emergence. However, AMPs also possess certain limitations such as tendency to aggregation and poor bioavailability through oral route, susceptible to enzymatic degradation, temperature and pH fluctuation, high hepatic clearance, difficulty in crossing physiological barriers and high production costs. Fortunately, extensive research has been undertaken to improve the formulations by rational design[194]. Different predictive software is available to evaluate physiochemical properties[195]. Incorporation with non-natural amino acids, conjugation with fatty acids and terminal modifications could improve bioavailability and stability. Also, performance of AMPs can be enhanced by delivery through inhalation and encapsulation into nanoparticle formulations. The production costs can potentially be reduced by commercial-scale platform using fungi and plants to produce recombinant AMPs at high yield[196].

Although the rate of development of resistance towards AMPs is lower when compared to small molecule drugs, pathogens exposed to externally administered or endogenous overexpressed AMPs may lead to the development of resistance eventually. It has already

been suggested that bacteria tend to alter their surface charge to reduce their susceptibility upon peptide challenges[197]. This can be modulated by a single gene which controls the level of dephosphorylation of LPS, therefore reducing the surface negative charge. Thus, continuous innovation in AMPs design, targeting strategies as well as combination therapeutics are of immediate priority in fighting against tuberculosis.

1.3.2 Mechanism of Action

Apart from the study of AMP design, better understanding of the mode of peptide action is also important to ensure successful development of therapeutics. Despite the little resemblance of amino acid sequence, AMPs adopt similar structural conformation and folding, suggesting the AMPs interact with bacterial membrane in a parallel orientation[198]. The interactions of AMPs and bacterial components are commonly based on electrostatic attraction and receptor-based interaction. In this section, two major mechanisms depicted in Fig. 1.8: (i) direct antimicrobial action involving cell envelope and intracellular targets and (ii) immunomodulatory effect, exerted by AMPs are discussed.

Direct antimicrobial actions

Disruption or pore formation of the bacterial cell wall is the most well-known activity of AMPs. This activity is caused by their mostly α-helical or ß-sheet conformation which enhance their cationic and secondary amphipathic properties. Integration of a non-polar region of AMPs brings about the accumulation of peptide into the membrane, promoting its permeability, leading to the loss of barrier functions, leakage of cellular components, resulting in cell death[199]. This direct killing effect of AMPs targeting cell membrane was mostly postulated by three different models (Fig. 1.9): (i) barrel-stave model; (ii) carpet model; and (iii) toroidal model. Barrel-stave model describes the accumulation of peptides up to a threshold at the membrane surface, thereby initiating the penetration by arranging the hydrophobic region of AMPs in line with the lipid core and hydrophilic regions towards the interior of the membrane creating transmembrane channels. In the carpet model, strong interactions of peptides and the outer leaflet of bacterial membrane takes place. The peptide carpet damages the curvature of bilayer and causes complete degeneration of membrane. In toroidal model, peptides are inserted into the membrane causing the lipids to tilt from the usual lamellar structure; the inner and outer leaflets are forced to connect forming a toroidal hole.

AMPs can induce cell wall permeability not only by mechanical disturbance but also by targeting cell surface elements. Through binding to cell-wall proteins such as ATPase, AMPs could interfere with cell ion exchange and lead to imbalanced cell pH homeostasis, thereby impairing mycobacterial growth[200, 201]. Antimicrobial peptide LLAP was shown to inhibit 50% of *Mtb* growth through targeting basal ATPase activity of the mycobacterial

membrane[202]. It is also reported that AMPs can exhibit more than one mode of action against *Mtb*. The dual mode of action of lantibiotics such as nisin was characterized by Carroll's group and reported to involve membrane pore formation as well as cell wall synthesis disruption after binding to peptidoglycan precursor[203].

After translocating across the bacterial membrane, some AMPs also play a role in manipulating intracellular processes via targeting proteins or nucleic acids. Human neutrophil peptide-1 achieved *in vitro* and *ex vivo* killing of *Mtb* H37Rv by binding to the unprotected genomic DNA without causing significant damage to the membrane[204]. The same group also reported mycobactericidal action of a series of synthetic antimicrobial peptides, targeting mycobacterial nucleic acids and thereby impeding replication and transcription processes, leading to cell death[205]. Heat shock protein, which is essential for chromosomal replication in bacteria, might also be a potential target for AMPs such as pyrrhocoricin and drosocin[206].

Immunomodulatory effect

The other advantage of employing AMPs as anti-TB therapeutic is their multifunctional characteristics. In addition to their direct killing abilities, some AMPs can also regulate the immune defence system to eliminate invaded bacteria. Release of pro- and anti-inflammatory cytokines can be triggered by AMPs during the infection. LL-37 promoted the secretion of anti-inflammatory cytokines IL-10 and TGF-β in *Mtb*-infected macrophages which was shown to be triggered by the mycobacterial antigens[207]. Recently, recombinant human and mouse lactoferrin was found to reduce the production of inflammatory cytokine IL-12p40 *in vivo*, which in turn, effectively reduced *Mtb* TDM-induced pathological granulomas and therefore critical to lessen disease progression[208]. Endogenous cathelicidins, mostly expressed in leukocytes and epithelial cells, were also shown to modulate induced autophagy as another mechanism to clear intracellular *Mtb* in various studies[209, 210]. Further, innate defense regulators (IDRs) have attracted immense interest of researchers with their high efficacy at low and non-toxic concentration[211]. Their ability to trigger proper endogenous expression of chemokines and downregulate inflammatory signals gives rise to the promising role in the treatment of immunocompromised patients.

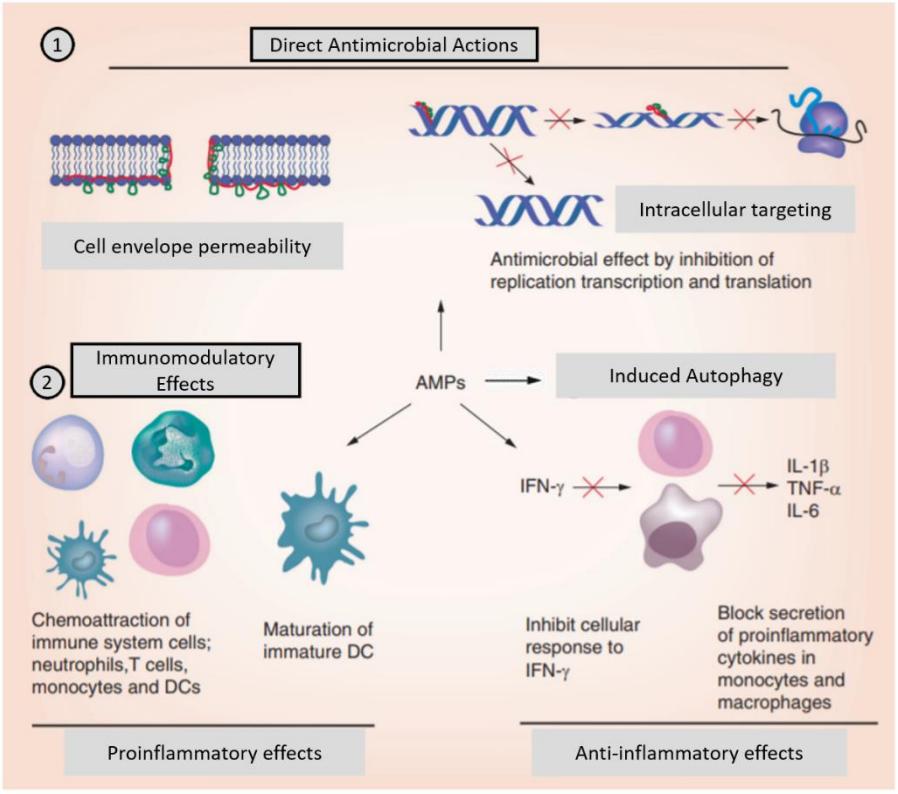

Figure 1.8 Diverse mode of action of AMPs against mycobacteria. Two major mechanisms of AMPs (1) direct antimicrobial action involving disturbing cell envelope permeability and intracellular targets and (2) immunomodulatory effects which can induce downstream proinflammatory or anti-inflammatory responses as well as autophagy leading to cell death. (Adapted from Rivas-Santiago et al.[212]).

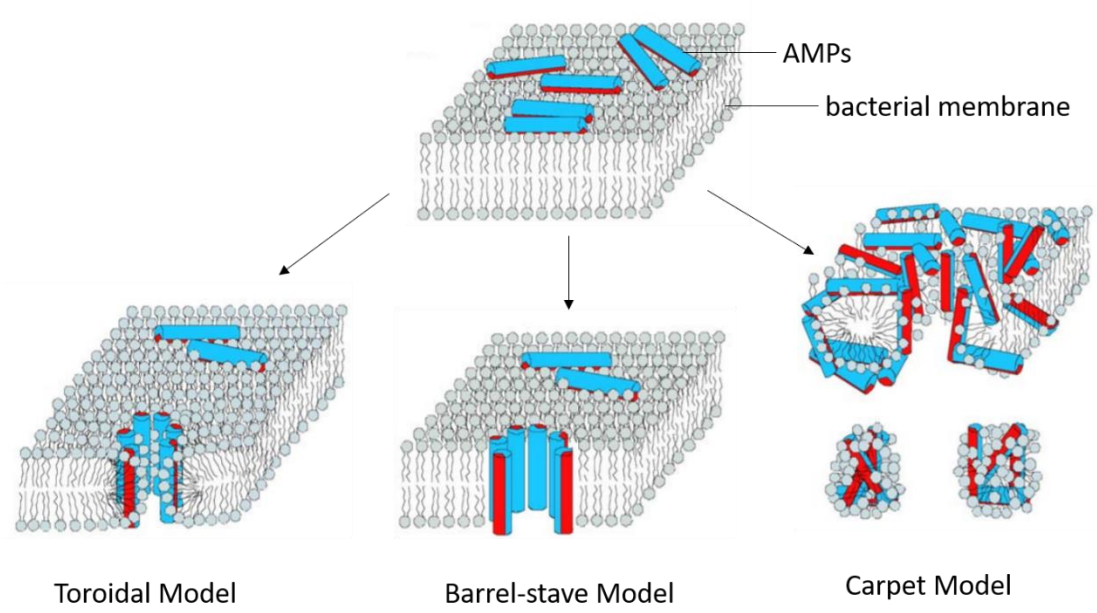

Figure 1.9 Schematic illustration of models describing underlying membrane active mechanism of AMPs. Three models demonstrating the membrane disruption action mediated by AMPs. Barrel-stave model initiates the penetration by the accumulation of AMPs, carpet model damages the membrane by the arrangement of AMPs in a carpet fashion, toroidal model inserts the AMPs into the membrane and initiates the formation of a toroidal hole. (Adapted from Salditt et al.[213]).

1.3.3 AMPs and Combination Strategy as Anti-TB Therapeutics

Despite the underestimation of the AMPs' potential in early years and various difficulties encountered for their clinical applications, peptide-based drugs have successfully entered the market as treatment of different diseases including infectious diseases, cancers, diabetes and cardiovascular diseases. Currently, there are over 160 peptides and proteins drugs approved by the FDA[194]. The emergence of drug-resistant *Mtb* strains demands novel strategies which could be an appropriate role that AMPs fit in. For example, *Mtb* acquired resistance towards isoniazid and ethambutol targeting mycolic acid synthesis. Subsequently, dermcidin, a human sweat glands peptide, which was suggested to inhibit mycolyl transferase, was shown to be a potential adjuvant or replacement therapeutic[214]. Khara *et al.*[215] studied a range of unnatural amino acid analogues of the $I(LLKK)_2I$ peptide and showed their good safety profile with potent antimycobacterial activity against MDR clinical isolates. Pin 2 variants, derived from pandinin 2, displayed high efficacy against MDR *Mtb* strains through membrane disruption[216]. Another α-helical peptide with 26 amino acid residue, D-V13K, was also demonstrated to be active against MDR strains due to the determining substitutions of valine and lysine promoting hydrophilicity and positive charge of the peptide[199]. Human ß-defensins (HBDs), a family of endogenous AMPs with a broad spectrum of bactericidal action, have been studied using computational approaches. Among the discoveries, HBD3-M-HBD2 was shown to act effectively against MDR-TB strains at a non-hemolytic concentration, signifying the anti-TB potential of this peptide[217]. Efficacy studies of MDR-infected murine model was also performed using peptide candidates with proved efficacy in *in vitro* and intracellular settings. Semisynthetic peptides E2 and E6 displayed stronger inhibitory effect on *Mtb* H37Rv than LL-37 and mouse CRAMP *in vitro*[169]. More importantly, these two AMPs significantly reduced lung bacillary burden in the MDR-TB infected model whilst the activities of the parent cathelicidins were not significant. IDR-1018, with its profound immunomodulatory functions without apparent cytotoxic effect suppressed MDR-TB bacilli growth *in vivo* and simultaneously reduced pneumonic region of infected mice[211]. L-isoleucine was reported to be a highly specific ß-defensin inducer and this effect was shown to be therapeutically applicable against *Mtb*[218]. Administration of L-isoleucine intratracheally led to significant increased expression of ß-defensins 3 and 4 and lower lung bacillary load in both drug-sensitive and drug-resistant *in vivo* models[219]. Notably, lung histopathology was also improved in L-isoleucine-treated mice as compared with control animals.

Despite the immense potential expressed by these multifunctional AMPs, high dosage is required to attain an adequate antimycobacterial effect. This possibly elevates toxicity, degradation complications as well as formulation difficulties. Therefore, instead of using AMPs as single treatment, combination formulations have been introduced to maximize the capability of anti-TB agents using the concept of synergy.

As described previously, the extreme hydrophobicity of the mycobacterial cell wall contributes to its pathogenicity and is an impediment to the ingress of chemotherapeutic agents. Interestingly, the membrane active characteristics of AMPs can act as an adjuvant to enhance the activity of conventional anti-TB drugs. Using *M. smegmatis* as model, full-length cathelicidins and its shortened version, ATRA-1A with membrane permeable ability, were shown to interact synergistically with rifampicin, killing 75% and 68% of intracellular bacteria as compared with less than 40% when using rifampicin alone[220]. Khara *et al.*[193] observed similar synergistic interaction in synthetic α-helical $(LLKK)_2$ peptide with rifampicin against *M. smegmatis*. Flow cytometry analysis provided further support to the peptide-induced pore formation, thereby potentiating the action of rifampicin. Kalita *et al.*[221] tested human neutrophil peptide (HNP-1) as an adjunct to isoniazid and rifampicin *in vitro*, *ex vivo* and *in vivo*. They reported synergism between the combinations and reduction of efficient concentration down to 1/8 MIC against intracellular *Mtb* H37Rv. A remarkably significant reduction in bacillary load in infected mice was also resulted. This was explained by the increase in permeability of mycobacterial cell envelope by HNP-1, facilitating the access of anti-TB drugs to intracellular targets. HBD-1 was shown to have an enhanced effect against MDR-TB clinical isolate when treated in conjunction with isoniazid[222]. The bactericidal efficacy of the combination was significantly higher than when isoniazid was used alone.

1.4 METABOLOMICS

In this thesis, one of the techniques employed to study the mechanism of various anti-TB agents and their combinations is nuclear magnetic resonance (NMR) metabolomics. This section will give a brief introduction on metabolomics and discuss more in detail the principle of NMR metabolomics as well as its use in TB studies.

Metabolomics represents a means of comprehensive identification and quantification of low molecular weight metabolites (< 1 kDa) present in biological systems such as a cell, tissue, organism, or culture media[223]. It records the unique set of physiological, biochemical and pathophysiological processes occurring in a life form at a specific time point, with the employment of highly sensitive analytical methods together with bioinformatics. As an extension of genomics, proteomics, and transcriptomics, metabolomics allows the examination of a variety of metabolome containing substances including amino acids, lipids, sugars, cofactors, nucleotides and xenobiotics, in an unbiased analytical systems-based approach. In contrast to other "omics" techniques, metabolomics is commonly exploited to define phenotypes[224]. This is attributed to the capability of this technique to measure the direct result of changes in the activity of a protein or enzyme while such biological activity does not necessarily correlate to the level of certain gene expression[225]. Thus, metabolomics can provide an objective picture of how the system responds to the environment stressor or disease state.

Metabolomics offers biological and technical advantages over other "omics" sciences in providing fundamental knowledge in investigating biochemical networks. The full metabolic profile associated with all biological processes can provide a more complete understanding of cellular dysfunction caused by various disorders and environmental challenges. Instead of disease predisposition, metabolomics can clarify the disease development, progression and adaptation by tracking the changes of metabolites with time[226]. Furthermore, it can help to identify early perturbation in cellular metabolism through their responses to internal or external stress factors. Due to its simplicity, high information content and universal application, metabolomics is an appealing tool in disease-related and medicinal research.

The investigation of a given metabolome can follow two different approaches: targeted and non-targeted. A targeted approach is effectively used to observe changes of specific metabolites based on prior studies or hypothesis, whereas non-targeted metabolomics discovers unknown metabolites or metabolic pathways that are triggered by external stimuli

or genetic variation[227]. In other words, untargeted approach aims to monitor the entire collection of metabolites and obtain a comprehensive depiction of the treatment effect or disease progression. Several analytical techniques are routinely used for metabolomics studies. Notably, each of the techniques possesses advantages, limitations and differing predictive power which are summarized in Table 1.4. Liquid chromatography mass spectrometry (LC-MS) and gas chromatography mass spectrometry (GC-MS) have high sensitivity that can produce data with better spectral resolution, mass accuracy and separation efficiency. On the other hand, non-destructive NMR assay offers high selectivity and reproducibility as well as more quantifiable data renders it preferable for intact organism analysis[228]. High-resolution magic angle spinning (HR-MAS) is the NMR assay for semi-solid state sample such as whole cells and soft tissue which will be discussed in detail in the next section.

Table 1.4 Comparison of NMR, HR-MAS, Liquid Chromatography (LC-MS) and Gas Chromatography (GC-MS) Mass spectrometry for metabolomics studies.

Technique	Strengths	Weaknesses
NMR	• Nondestructive technique • Versatility for analyzing metabolites in biofluids, tissues, or *in vivo* • Reproducibility and repeatability • Rapid analysis	• Low sensitivity (only metabolites with relatively high concentration [micrograms] can be detected) • Overlap in peaks and high chemical degeneracy (different metabolites have resonances in the same spectral region)
HR-MAS	• Whole-cell experiment possible	• Lower sensitivity • Less resolution than liquid-state NMR
LC-MS/ GC-MS	• High-resolution capacity • Very sensitive (picogram quantities)	• Lower reproducibility (within and across laboratories) • Slow analysis • Destructive to sample

For more than 100 years, the study, diagnosis and treatment of TB was limited to culture-based technology. Owing to the slow growth and complex culture procedures of different TB species, extensive time and specialized laboratories are required. Entering the genomic era, the emergence of new and powerful instrumentations has brought about enormous improvement in developing TB treatment and diagnostic strategies. The unprecedented investigation of drug mechanisms and their side effects is made possible by the identification

of metabolic biomarkers. Although the drug-susceptible TB regimen has been standardized, the exact mode of action and xenobiotic mechanism of the drugs remain poorly understood. Applying an ultra-performance liquid chromatography/time-of-flight mass spectrometry metabolomics approach, Li *et al.*[229] characterized the metabolism of isoniazid in human and suggested that isoniazid inhibited growth of *Mtb* by an additional mechanism of disrupting essential amino acid metabolism. Using a similar approach, Loots *et al.*[230] investigated the toxicity of combined anti-TB drugs (rifampicin, isoniazid and pyrazinamide), Rifater. They reported an increase of oxidative stress in treated-rats which was relieved with the application of an antioxidant, melatonin. Their findings provided reasonable explanations for the side effects such as hepatotoxicity reported for Rifater which can be caused by an extensive oxidative stress. Metabolomics can also be used to elucidate molecular mechanisms associating with the resistance phenotype in *Mtb* strains. Du Preez *et al*.[231] pioneered the characterization of rifampicin resistance with fatty acid metabolism in *rpoB* mutants and wild type *Mtb* strains using GC-MS metabolomics. Their study indicated the reduced production of various types of cell wall lipids in drug-resistant strains and the switching of metabolism to the consumption short-chain fatty acid as an alternative carbon source. Another application of metabolomics is the monitor of anti-TB treatment efficiency and outcome. By comparing the metabolic profiles of biofluid samples at different times, it is possible to decide whether the treatment is suitable for certain patients, therefore shortening the time for trial-and-error therapy and reduces the chance for resistance development. Lastly, metabolomic biomarker is useful for the evaluation of new anti-TB drugs. Tuberculostearic acid (TBSA) in sputum sample was demonstrated to be a potential quantitative biomarker for *Mtb* growth[232]. TBSA was found to correlate positively with the number of colony and persistent in the culture but is not accumulating when bacteria stopped replicating. However, due to its low stability in nonviable bacteria, the need of a secondary biomarker was suggested. With the great capacity of *Mtb* to synthesize lipids, lipidomics, which seeks to scrutinise lipid metabolites, is also a popular subfield in mycobacterial metabolomics research[233]. Thanks to the continuous rapid development in mycobacterial metabolomics, more evidences have shown the capability of this technology to play a crucial role in the understanding and management of TB.

1.5 NUCLEAR MAGNETIC RESONANCE SPECTROSCOPY

NMR spectroscopy is a powerful, interdisciplinary analytical technique discovered in 1940s. Since then, the application of this technology has largely expanded, including spectroscopy and magnetic resonance imaging. NMR spectroscopy has been applied to metabolite studies of liquid-state, solid-state systems and intact organisms. As a result of the unique sample properties of different systems, especially induced by their particular spin interactions that greatly affect the NMR spectrum, disparate techniques are used in corresponding experiment[234]. The principle of NMR technique is briefly discussed, with the emphasis on HR-MAS, followed by their application to TB studies.

1.5.1 Principle

The theory of NMR and the nuclear-spin dynamics is fully established and can generally be interpreted by classical models. An in-depth explanation requires the knowledge in quantum mechanics which is beyond the scope of this thesis. Classical vector models are used here to introduce the fundamental concepts of NMR.

Magnetism: Matter is composed of atoms which possess nuclei with a characteristic proton/neutron composition. The atomic nuclei are positively charged and carry magnetic properties. This property arises from the angular momentum which is known as 'spin' of the nuclei. In essence, nuclear spins are of discrete values owing to the quantum nature of atoms. The total nuclear spin depends on the nucleon content thereby the number of protons and neutrons. Possession of even number of protons and neutrons results in a total spin of zero (^{12}C, ^{14}C, ^{16}O…) while odd number of either or both results in non-zero total spin (^{1}H, ^{13}C, ^{15}N, ^{19}F…) which creates a magnetic moment. NMR spectroscopy takes advantage of this magnetic moment of atomic nuclei.

When exposed to an external static, homogenous magnetic field B_0, the magnetic moment aligns along B_0 according to Boltzmann distribution, with the ones aligning parallel to the field in the lower energy level. At the same time, the nuclei precess in the magnetic field with a resonance frequency named as the Larmor Precession frequency f_o (Fig. 1.10a). This frequency uses to classify NMR spectrometers is denoted in equation 1.

Equation 1

$$f_0 = \frac{\gamma}{2\pi} \times B_0$$

where γ is the gyromagnetic ratio of atom (^{1}H = 26.7522128x10^7 radT^{-1}s^{-1}). In reality, there are many nuclei in the sample so due to the static averaging of all magnetic moments, the effect on a net magnetisation M_0 is visualized. For the generation of NMR signals, an electromagnetic radiation, B_1-pulse, equals to the Larmor frequency is applied and this is when resonance occurs. Consequently, the net magnetisation absorbs the energy from the wave and is tilted orthogonal to B_0 to the x-axis and reaches a higher energy state. The energy required to bring about the flipping between the two energy states depends on the external B_0 (Fig. 1.10b) and is described as

Equation 2

$$\Delta E = \gamma h \mathrm{B}_0 / 2\pi$$

where h is the Planck's constant = 6.63x10^{-27} Js. According to Bohr condition, the resonant frequency f_A can then be written as

Equation 3

$$\mathrm{f}_A = \gamma \, \mathrm{B}_0 / 2\pi$$

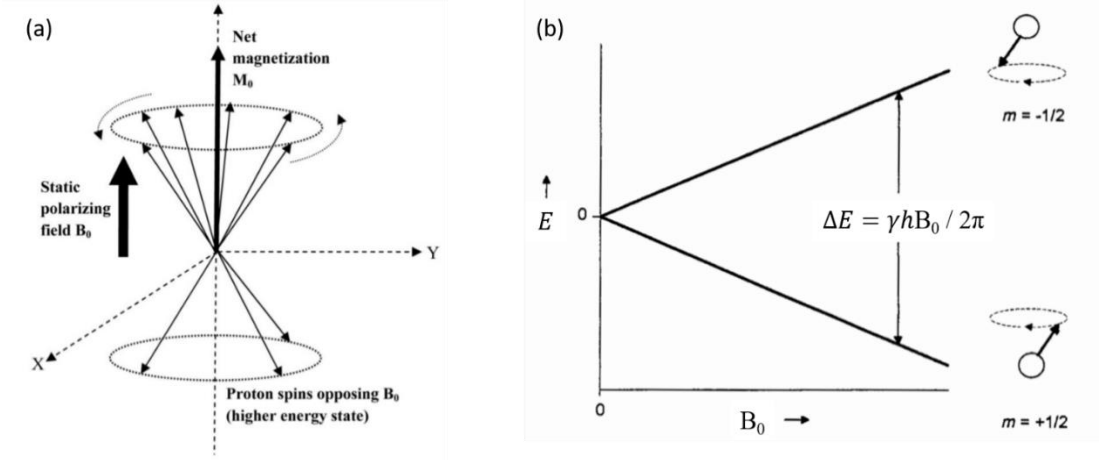

Figure 1.10 Nuclear spin precession and energy difference between spin states. (a)Precession of the magnetic moment in two possible spin states of +1/2 and -1/2 (also denoted by nuclear spin quantum number, m) around external magnetic field B_0. M_0 represents the net nuclear magnetization resulting from the vector sum of all individual magnetic moments. (b) Relative energy of both spin states as a function of the strength of B_0.[235, 236].

Signal Detection: When the B_1-pulse is removed, M_0 relaxes and precesses back to their lower energy state. As such, this relaxation releases energy as a radio waves which induces a voltage in the receiver coil of the magnet. The voltage is directly proportional to the number of spins precessing with f_0. This signal generated as a decaying wave function over time is known as Free Induction Decay (FID). Through Fourier transform, the wave function is mathematically transformed into a function of frequency appearing as peaks in NMR spectra (Fig. 1.11).

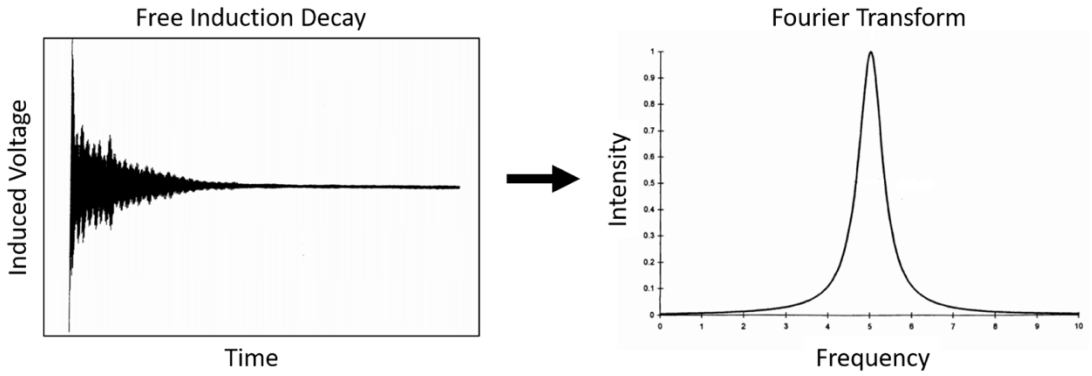

Figure 1.11 NMR signal generation by Fourier transformation of Free Induction Decay curve. Relaxation of M_0 recorded as a wave function of time known as Free Induction Decay. FID curve is then Fourier transformed into a function of frequency[236].

Chemical Shift: Due to the diamagnetism of electron clouds surrounding the nuclei, a small magnetic field is induced which opposes the external B_0. The nuclei, therefore experience a small change in local magnetic field as compared to the B_0 field; this phenomenon is referred as electron shielding of the nuclei. As a result, the f_A of a nucleus is determined by the effective magnetic field it experiences and in turn its surrounding chemical environment. This information is represented by the value $(f_A - f_0)/ f_0 \times 10^6$, measuring in parts per million (ppm) with respect to B_0, is called chemical shift. Any factor changing the electron density around the nucleus will induce shielding or deshielding effect, leading to up-field or down-field shifting of the peaks in NMR spectra. For example, presence of electronegative species draws electrons away from the protons, this deshields the protons and therefore, their chemical shifts increase and appear at higher ppm in the NMR spectrum. Definition of f_0 is usually by means of a reference compound such as Trimethylsilylpropanoic acid (TSP). Noteworthily,

chemical shift is independent of the external B_0, so comparison of data is possible from spectrometers of different field strength.

Despite its high reproducibility, NMR has the major limitation of low sensitivity. This is inherited from the small difference between spin population in the higher and lower energy levels[236]. According to Boltzmann's law, this difference has a linear relationship with external B_0. As stated in Eq. 3, resonant frequency increases with increasing B_0, thus peaks become narrower at higher field strength and less overlapping occurs rendering higher resolution. Besides employing a more powerful magnet, sensitivity can be enhanced by the number of nuclei (e.g. sample concentration or volume) or the configuration of the detection devices[237]. NMR experiments described in this thesis were performed at ^{1}H frequencies of 600 and 700 MHz.

1.5.2 High-Resolution Magic Angle Spinning (HR-MAS)

The most obvious difference between solid-state and liquid-state NMR spectrum is the multiple line broadening effect in solid-state systems. This is attributed to the unaveraged anisotropic interaction of the molecules primarily through dipolar coupling, the interaction between the dipolar magnetic fields induced by each magnetic moment or spin. This issue is not seen in liquid state samples as fast tumbling action of molecules effectively averages the dipolar coupling to zero[234]. Line broadening in solid-state NMR causes a loss of spectral resolution, limiting the usage of the technique in tissues and cells. Thanks to the work of Andrew and Lowe, who discovered that spinning the sample at an angle of 54.74° could largely remove the dipolar coupling, high-resolution magic angle spinning (HR-MAS) NMR technique was then developed (Fig. 1.12). This magic angle is the angle of the cross diagonal of a cube. Any point on this diagonal has identical x, y and z coordinates and therefore the anisotropic information is lost. Further, spectral resolution can be improved by increasing the spinning rate[238]. Another merit of HR-MAS is the visibility of both lipid components as well as small polar molecules. With the high versatility and much improved resolution, HR-MAS has become a popular tool for the study of complex biological tissues and whole cell samples[239, 240]. Nonetheless, the experiment of whole cell sample may result in the overlapping of polar and non-polar metabolite which accounts for one of the major practical drawbacks of the technique. Hence, careful experimental design should be done according to the properties of the sample, other analytical options like lipid extraction for lipidomics studies might be used to increase the number of identifiable metabolites.

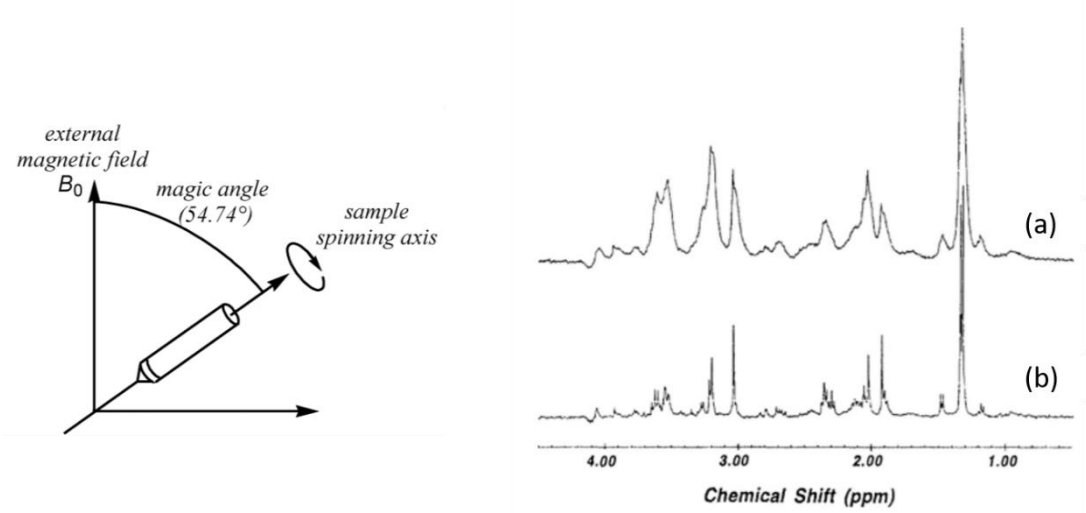

Figure 1.12 Schematic diagram of magic angle spinning (MAS) and static NMR spectra comparison. (Left) Sample spinning along the axis tilted at the magic angle of 54.74° with respect to the external magnetic field B_0. (Right) Comparison of human brain proton NMR spectra acquired with (a) static state and (b) MAS[241, 242].

1.5.3 Data Processing

Data pre-processing: As an intermediate step prior to data analysis, pre-processing is necessary to reduce noise and transform the data to facilitate subsequent analyses and modelling. It includes baseline adjustment, phasing, alignment and binning as well as normalization and scaling.

Baseline distortion arising from the non-linearities of the electronic detection process is usually corrected by subtracting a tailored polynomial from the raw spectrum. Phasing aims to correct the imperfections in the consequence of frequency-dependent factors[237]. Automatic as well as manual correction of processes are required to ensure reliability as artefacts in spectra can only be identified visually. Alignment of spectra avoids the misinterpretation of results because of peak shifting arises from changes of pH, salt concentration, temperature, overall dilution of samples and many more. The icoshift algorithm was chosen in experiment described in this thesis for its faster processing speed. In addition to alignment, binning or bucketing is another method applied to lessen peak shifting (Fig. 1.13). Equidistant binning is used by vast majority of 1D ^{1}H-NMR studies in which the spectra are split into evenly spaced integral region with defined spectral width[237]. This produces smaller sets of variables which also reduces the data size for quicker subsequent processing procedures. Furthermore, normalization generates data that allows direct comparison and accounts for variations of the overall concentration of samples attributable to the difference number of cells, biofluid volume and size of tissue. Finally, scaling methods can be used to avoid the domination of signal with the highest intensity during data analysis[243]. Feature selection for pre-processing is critical and should be done appropriately in order to improve the reliability of models generated in supervised analyses.

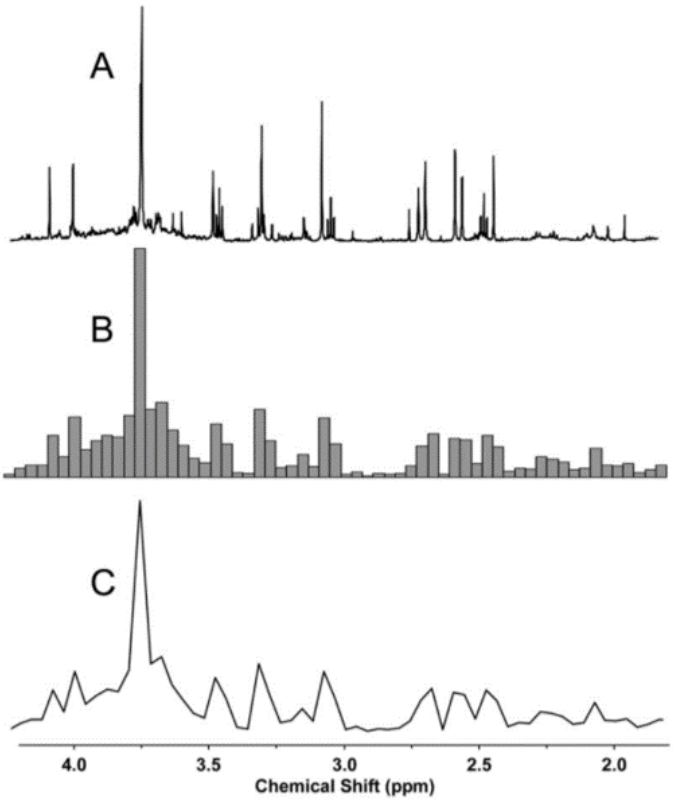

eee

Figure 1.13 Illustration of binning on a ^{1}H NMR spectrum of a rat urine sample. Using a bin spectral width of 0.04ppm, the number of data variables reduced from 65,536 to 312, facilitating further multivariate analysis. (A) original spectrum, (B) 0.04ppm binning, (C) resulting spectrum[244].

Multivariate analysis: Each 1D NMR spectrum contains thousands to tens of thousands of data points. The analysis of this staggeringly high information content is of high complexity; the challenge of generating relevant biological conclusions from such variable datasets indeed requires specialized and robust methods of statistical analysis. For this purpose, multiple methodologies have been developed and extensively reviewed[244, 245]. The hallmark of analysing metabolomic data is the use of multivariate analysis methods. Among all, principal component analysis (PCA), partial least squares (PLS) and orthogonal projection to latent structure (OPLS) are the most popular methods.

The primary goal of all these methods is to identify differences between classes, despite class variability. PCA is an unsupervised algorithm for exploratory analysis to find pattern in the multivariate dataset. It aims to reduce the number of dimensions and achieve a linear transformation that preserves the most variance in the original data[246]. This unbiased method reveals differences only when within-group variation is sufficiently less than that of between-

group. The transformed variables are uncorrelated called the principal components which explain the largest possible variability in the data. The data can be plotted into 'score plot' in two or three dimensions orthogonal to each other, thus, each principal component denotes independent variations in the data. The contribution of each variable to the principal component can also be visualized in the 'loading plot'. In this way, identification of certain variable/NMR resonance contributing to the variations can be primarily determined. Meanwhile, variables that are co-located away from the origin in the loading plots might infer correlations. This gives initial clue of the metabolites exerting an effect in the data.

PLS and the extension version OPLS are supervised form of discriminant analysis that allows identification of significant spectral features by making an explicit use of class membership. The creation of a linear regression model allows more apparent separations between classes in scores space. However, both methods have an innate tendency of over-fitting the models, even in the scenario of totally random variables[247]. Over-fitting is a general issue in "omics" studies as the number of variables almost always immensely out-scale the number of biological samples. This increases the risk of inclusion of random noise as true signals. Hence, it is important to perform validation for the assurance of model reliability. Cross validation is a standard method which partitions the data into a training set, to generate a model to make prediction of the remaining data, known as the test set. Double cross validation is used in the analysis preformed in this thesis, in which the samples are randomly assigned to be training, test and validation sets. Merit of this method is the fact that models constructed is in absolute absence of test set[248]. The training set creates a preliminary model that is tested on the validation set to determine the optimal number of components for model construction. Afterwards, the test set assesses the predictive ability of the model generated by training and validation sets combination. This process is repeated at least a thousand times to ensure reliability of the model.

1.5.4 Applications of NMR Metabolomics on TB Treatment Research

With regards to the application of metabolomics on TB, NMR, being a non-destructive technique, is widely applied to study various aspects relating to the disease. Studies of anti-TB drug toxicity with biological matrix such as urine, plasma and serum reduce the complication of sample preparation and produce comprehensive profile. Halouska *et al.*[135] applied ^{1}H-^{13}C NMR to determine the minimum inhibitory concentration of anti-TB drug D-

cycloserine and its effect on peptidoglycan biosynthetic pathway. Cycloserine was shown to inhibit several cell wall enzymes in *M. smegmatis*, particularly D-alanine-D-alanine ligase (Ddl), the main enzyme for peptidoglycan synthesis. The same group conducted a follow-up study which demonstrated that cell growth was inhibited when the production of Ddl is halted, indicating Ddl is a promising target for anti-TB drug development[249]. Stress response mechanism can also be determined using NMR. Behrends *et al.*[250] demonstrated that *M. smegmatis* produces free glucosylglycerate under nitrogen depletion. This revealed an alternative mechanism adopted by mycobacteria to sustain their viability by reducing rate of growth and intake of ammonium. Biomarkers might also be identified by means of ^{1}H NMR for mycobacterial infection diagnosis. Sera of calves infected by *Mycobacterium avium* subsp. *paratuberculosis* (MAP) was found to be distinctly separated from non-infected samples using discriminant analysis. Increased isobutyrate and fat metabolism were observed in infected cattle regardless infectious burden[251]. For pathological significance of lipid components in *Mtb*, different functional modes of NMR can rapidly generate qualitative and quantitative profile of clinically relevant lipids found in mycobacteria. Engy *et al.*[252] pioneered the usage of 2D ^{1}H-^{13}C heteronuclear single quantum coherence (HSQC) NMR to analyse mycobacterial cell wall lipids of ^{13}C-enriched *Mtb* clinical isolates. The group underscored the utility of this technology to identify specific virulence factors especially non-polar lipids of low abundance for instance, phenolic glycolipids (PGLs). This finding has introduced a powerful usage of NMR on TB lipidomics. Lastly, anti-TB drugs with similar modes of action demonstrated similar metabolomic profile and resulted in distinct clustering pattern which correlates with *in vivo* drug activity[253]. Therefore, NMR metabolomics is also useful in determining drug action, facilitating the discovery of new drugs and targets.

Chapter 2 Aims and Objectives

2. AIMS AND OBJECTIVES

The requirement of highly toxic second-line drugs and long duration of treatment of MDR-TB leads to a serious concern in anti-tuberculosis therapy. While enormous effort has been put to develop new drugs in the pipeline[52, 156], efficacy and toxicity studies are still ongoing whereas resistance towards certain new drugs has already been reported[139, 140]. This renders an urgent need to improve current treatment. One of the strategies is to enhance the efficacy of existing antibiotics against MDR-TB.

Novel D-LAK peptides have demonstrated synergistic mycobactericidal activity with isoniazid, re-sensitizing MDR strain GB2 towards this first-line antibiotics. Therefore, the overall aim of this thesis was to further investigate the strategy of using the novel D-LAK peptides in combination with existing anti-TB agents against mycobacteria, and to understand the basis for such synergy. The thesis is divided into three parts with specific objectives:

Study 1: The bioefficacy of D-LAK120-A and D-LAK120-HP13 peptides in combination with rifampicin and isoniazid was investigated on a series of MDR-TB clinical isolates and the severely attenuated *Mtb* Bleupan strain. The cytotoxicity of the D-LAK peptides and their combinations was also examined on mammalian cell lines.

Study 2: The mechanism of action of D-LAK peptides, existing antibiotics and their combinations was elucidated, using *M. smegmatis* as a surrogate model. In particular, the biophysical and fluorescence techniques for studying the mechanism of anti-TB agents and their membrane activity were established.

Study 3: The mechanism of action of D-LAK peptides, existing anti-TB agents and their combinations was studied on severely attenuated *Mtb* Bleupan strain, using the techniques established in study 2.

Chapter 3 Materials and Methods

3.1 MICROBIOLOGICAL ASSAYS AND CELL CULTURE

3.1.1 Antibiotics and reagents

The following antibiotics and reagents were purchased from Sigma Aldrich: rifampicin (RIF) (Cat.# R3501), isoniazid (INH) (Cat.# I3377), capreomycin sulfate from *Streptomyces capreolus* (CAP) (Cat.# C4142), colistin sulfate salt (CST) (Cat.# C4461), dimethylsulfoxide (DMSO) (Cat.# D8418), phosphate buffered saline (PBS) (Cat.# P4417), formaldehyde solution (Cat.# 252549) and tyloxapol (Cat.# T8761). Delamanid (DLM) (Cat.# ABE5876) was purchased from Source BioScience (Nottingham, UK).

3.1.2 Antimicrobial peptides

Two structurally similar D-LAK peptides (Table 3.1) were custom synthesized by China Peptides Co. Ltd. (Shanghai, China), stored at -20°C in lyophilized form. The purity of synthesized peptides was confirmed to be >85% by reverse-phase high performance liquid chromatography (HPLC) and electrospray-ionization mass spectrometry (ESI-MS). All peptides were amidated at the C-terminus. Consensus hydrophobicity index was used to determine average hydrophobicity of peptides. Peptide stock solutions at 1 mM were prepared in distilled water and stored at -20°C before use.

Table 3.1 The sequence and physiochemical properties of D-LAK peptides studied. (A-alanine, H-histidine, K-lysine, L-leucine, P-proline, W-tryptophan)

D-LAK peptide	Sequence	Nominal charge	Average Hydrophobicity	Charge Angle
D-LAK120-A	KKLALALAKKWLALAKKLALALAKK-NH_2	+9	-0.02	120
D-LAK120-HP13	KKALAHALKKWLPALKKLAHALAKK-NH_2	+9	-1.07	120

3.1.3 Cell Culture

Adenocarcinomic human alveolar basal epithelial A549 cells (ATCC® CCL-185™) were maintained in Dulbecco's modified eagle's medium (DMEM) (Life Technologies, USA) supplemented with 10% (v/v) fetal bovine serum (FBS) (Invitrogen, Cat.# 10270-106) and Antibiotic−Antimycotic solution (containing final concentration of 100 units/ml of penicillin, 100 µg/ml of streptomycin and 0.25 µg/ml of Fungizone®) (Invitrogen, Cat.# 15240-096). Human monocytic THP-1 cells purchased from the American Type Culture Collection (Manassas, Virginia, USA) were used as a macrophage model after they were differentiated into macrophage-like cells by treating with 100 nM phorbol 12-myristate 13-acetate (PMA) (Sigma Aldrich, Cat.# P8139). Roswell Park Memorial Institute medium (RPMI-1640) (Invitrogen, Carlsbad, California, USA, Cat.# 31800-022) supplemented with 10% (v/v) FBS, Antibiotics−Antimycotic solution, and additional supplements as follows: 0.05 mM 2-mercaptoethanol (2-ME) (Invitrogen, Cat.# 21985-023), 2 g sodium hydrogencarbonate ($NaHCO_3$) (Sigma Aldrich, Cat.# S5761), 1 mM sodium pyruvate (Sigma Aldrich, Cat.# P2256) and 10 mM 4-(2-Hydroxyethyl) piperazine-1-ethanesulfonic acid, N-(2-Hydroxyethyl)piperazine-N′-(2-ethanesulfonic acid) (HEPES) (Sigma Aldrich, Cat.# H3375) were used to maintain the THP-1 cells in the *ex vivo* mycobactericidal assay covered in section 3.1.9. All cells were cultured in a humified atmosphere at 37°C and 5% CO_2.

Regarding the additional supplements in RPMI-1640, sodium pyruvate is used by cells as an easily accessible carbohydrate source. Additionally, it is involved with amino acid metabolism and initiates the Kreb's cycle. 2-ME is proposed to enhance uptake of cysteine and consequently the maintenance of intracellular glutathione levels. This protects the cells from oxidative damage, enhances antigen presentation and reduces clumping[254].

3.1.4 Mycobacterial strains and growth conditions

To investigate the antimicrobial capacity and mechanism of action of anti-TB agents, this study used several mycobacterial species and exploited a series of biological, microscopic and biophysical techniques. For the ease of understanding, Table 3.2 summarized the details of corresponding experiment performed on each species.

Table 3.2 Overall summary of mycobacterial species used in corresponding experiment in this study.

Section	Experiment		MDR-TB clinical isolates[a] and drug-susceptible *Mtb* H37Rv	*Mycobacterium smegmatis* mc^2 155	*Mtb* Bleupan[b]
3.1.5	Strain Provenance			x	x
3.1.7	*In vitro* bacterial inhibitory assay (Resazurin)[c]		x	x	
3.1.8	*In vitro* mycobactericidal assay		x		
3.1.9	*Ex vivo* mycobactericidal assay		x		
3.1.10	*In vitro* bacterial inhibitory assay (Bioluminescence)[d]				x
3.1.11	*In vitro* time-kill assay				x
3.2	Transmission electron and Confocal Microscopy			x	
3.3-3.5	Mycobacterial growth response assays	Fluorescence assays		x	x
		Nuclear magnetic resonance (NMR) metabolomics			

[a] MDR- multidrug-resistant *Mycobacterium tuberculosis* clinical isolates.
[b] *Mtb* Bleupan- Severely attenuated *Mycobacterium tuberculosis* Bleupan strain.
[c] Detection performed by Resazurin microtiter assays.
[d] Detection performed by bioluminescence measurement.

Multidrug-resistant Mycobacterium tuberculosis *clinical isolates, drug-susceptible* Mycobacterium tuberculosis *H37Rv and* Mycobacterium smegmatis *mc²155*

Five *Mycobacterium tuberculosis* strains were employed in this study, including four MDR clinical isolates and one standard laboratory strain H37Rv. *Mycobacterium smegmatis* mc^2 155 was the biosafety 1 species used in the mechanistic study (section 3.2). All the bacterial strains were kindly provided by Dr WC Yam from Department of Microbiology, The University of Hong Kong, Hong Kong. Antibiograms (Table 3.3) of the *Mtb* strains used in the study were previously determined using the agar proportion method according to Clinical Laboratory Standard Institute (CLSI) recommendations. The cultures were routinely maintained on Lowenstein-Jensen (LJ) solid medium (bioMérieux, Craponne, France) at room temperature with continuous aeration. *In vitro* assays were performed either in Middlebrook 7H9 broth (Difco, Detriot, Michigan, USA, Cat.# 271310) supplemented with 10% (v/v) oleic acid-albumin-dextrose-catalase (OADC) enrichment (Becton Dickinson, Franklin Lakes, New Jersey, USA, Cat.# 212240) and 0.2% (v/v) glycerol (Sigma Aldrich, Cat.#G-5516) or on 7H10 agar (Difco, Cat.#271310) supplemented with 10% (v/v) OADC enrichment and 0.5% (v/v) glycerol. All the *Mtb* experiments were conducted in the University Pathology Building P3 Laboratory, The University of Hong Kong.

Severely attenuated Mtb *Bleupan and* Mycobacterium smegmatis *mc²155*

Mycobacterial strains were provided by Dr Robertson group from Imperial College London (ICL), United Kingdom. Frozen stocks in 10% (v/v) glycerol were prepared in ICL and transported to store in King's College London for bacterial assays. Mycobacteria were maintained either in Middlebrook 7H9 broth (Sigma Aldrich, Cat.# MO178) supplemented with 10% (v/v) oleic acid-albumin-dextrose-catalase (OADC) enrichment (US Biological Life Sciences, Cat.# M3895-01) and 0.2% (v/v) glycerol (Sigma Aldrich, Cat.# G-5516) or on 7H10 agar (Sigma Aldrich, Cat.# MO 303) supplemented with 10% (v/v) OADC enrichment and 0.5% (v/v) glycerol. Additional supplement of 10 mg/ml L-Leucine (Sigma Aldrich, Cat.# L8912), 24 mg/ml calcium pantothenate (Sigma Aldrich, Cat.# C8731), 25 µg/ml kanamycin sulfate from *Streptomyces kanamyceticus* (Sigma Aldrich, Cat.# K1377) and 50 µg/ml hygromycin B (FluoroChem,U.K. Cat.# M01839) were used to maintain the bioluminescent *Mtb* Bleupan. *M. smegmatis mc²155* and *Mtb* Bleupan were grown to mid-log phase in supplemented 7H9 broth in falcon tubes. The cultures were incubated at 37℃ for 48 h for *M. smegmatis* or six weeks for *Mtb* without agitation or detergent to minimize the

external manipulation on the structure of the bacteria such as their cord-forming ability[255]. Aeration, vortexing and 1 ml of fresh medium replenishment were done twice-weekly to maintain the growth of *Mtb* Bleupan. Subcultures were performed at initial Optical Density (O.D.) = 0.05 for both strains. This *M. smegmatis* mc^2 155 from KCL was used in bacterial inhibitory assay (section 3.1.7) and growth response assay (section 3.3-3.5).

Table 3.3 Antibiogram of mycobacterial strains. Information provided by Department of Microbiology, The University of Hong Kong, boxes marked with "--" indicate details not available. (R- resistant, S-susceptible; INH-isoniazid, RIF-rifampicin, EMB-ethambutol, STR-streptomycin, PZA-pyrazinamide, OFX-ofloxacin, AMI-amikacin, CAM-chloramphenicol, CYC-cycloserine, ETH-ethionamide, KAN-kanamycin)

Sample ID	**H37Rv**	**GB2**	**08M**	**03M**	**08MB**
Strain type	Laboratory strain	Clinical isolate	Clinical isolate	Clinical isolate	Clinical isolate
Sex	--	M	M	--	--
Age	60	38	--	--	--
Isolation date	--	2005	2008	2003	2008
INH	S	R	R	R	R
RIF	S	R	R	R	R
EMB	S	S	S	S	S
STR	S	S	S	R	R
PZA	S	S	S	--	--
OFX	--	S	S	S	--
AMI	--	S	S	--	--
CAM	--	S	S	--	--
CYC	--	S	S	--	--
ETH	--	S	S	S	--
KAN	--	S	S	S	--

3.1.5 Strain Provenance

Before conducting experiment at King's College London, the provenance of severely attenuated *Mtb* Bleupan and *M. smegmatis* mc^2 155 was verified at Imperial College London by the following methods.

DNA extraction

Mtb Bleupan: Bacterial cells were harvested from suspension culture by centrifugation. Supernatant was discarded into detergent vesphene (STERIS Solutions Limited, U.K.) and the pellet was resuspended in Tris-EDTA (TE)[a]. An equal volume of chloroform:methanol (2:1 by volume) was added, followed by rocking for 5 min. The suspension was centrifuged at 4200 rpm for 10 min at room temperature. Both the aqueous and organic phases were removed. The remaining solid bacterial mass was air-dried inside the cabinet for 2 h. After drying, the pellet was resuspended in 5 ml TE containing 0.1 M Tris (pH9). Lysozyme was added to the final concentration of 100 µg/ml. The tube was then placed in a metal canister and incubate at 37℃ for 1 h. Followed by adding 0.1 volume of 10% (w/v) SDS and 100 µg/ml proteinase K[b], the mixture was left heated for 3 h at 50℃. This viscous solution was transferred to mix thoroughly with an equal volume of phenol:chloroform (1:1 by volume). The mixture was left for 30 min and then subjected to rocking for another 30 min at room temperature. The pellet was collected by centrifugation at 13,000 rpm for 15 min. The aqueous phase was transferred to a new tube and mixed again with an equal volume of chloroform. The aqueous phase was retrieved after centrifugation, and the DNA was precipitated with 0.1 volume of 3 M sodium acetate and an equal volume of isopropanol. The DNA was washed by 70% (v/v) ethanol and resuspended in 40–100 µl of TE.

M. smegmatis: The culture was harvested and centrifuged; the bacterial pellet was resuspended in 400 µl of TE and incubated for 20 min at 80°C. After cooling at room temperature, 50 µl of 10 mg/ml. lysozyme was added and the mixture was vortexed and incubated for 1 h at 37°C. Followed by adding 75 µl of SDS/Proteinase K MIX[c], the mixture was incubated for 10 min at 65°C. NaCl (5 M) and CTAB/NaCl solution[d] (100 µl each)

[a] TE: 10mM Tris/HCl, pH 8, 1mM EDTA. Dissolve in distilled water. Autoclaved and store at room temperature.
[b] Proteinase K: 10mg proteinase K/mL in distilled water. Store at-20°C.
[c] SDS/Proteinase K MIX: 5 µL proteinase K 10 mg/mL in 70 µl of 10% (w/v) SDS per sample.
[d] CTAB/NaCl solution: Dissolve 4.1 g NaCl in 80 mL distilled water. Add 10 g CTAB (Cetyl trimethylammonium bromide) while stirring. If necessary, heat at 65ºC for complete dissolution. Adjust volume to 100mL. Store at room temperature.

preheated at 65°C were added, followed by vortexing and 10 min incubation at 65°C. Chloroform:isoamilic alcohol (24:1 by volume) (750 µl) were added, the mixture was vortexed and centrifuged 5 min at 13,000 rpm. The aqueous phase was transferred to a new tube and the previous step was repeated once again. The aqueous phase is transferred to a new tube and the DNA was precipitated with a 0.6 volume of isopropanol. The DNA was then centrifuged for 15 min at 13,000 rpm at 4°C, washed with 70% (v/v) ethanol, centrifuged again for 2 min and air-dried or dried using a DNA concentrator (miVac, Fisher Scientific, U.S.A.). Finally, the DNA is resuspended in TE.

Polymerase chain reaction (PCR)

In each independent PCR assay, test results were compared with the results of one positive and one negative control. The positive controls included the DNA of H37Rv strain provided by Colorado State University, Fort Collins, USA, (Contract No 1-A1-40091). The negative control included PCR grade water.

Identification of strain provenance was done using specific pair of primers designed to amplify *MSMEG 3582*, *Leu D* and *RpfC* sequences in the mycobacterial DNA and the primer sequences and amplicon size are described in Table 3.4. A 50 µl reaction buffer contained 10 × assay buffer (Bangalore Genei, Bangalore, India), 10 mM dNTP's (Bangalore Genei), 10 pmol of each primer (SIGMA-GENOSYS, USA), 2.5 units Taq DNA Polymerase (Bangalore Genei) and 5 µl of extracted DNA. Amplification was carried out in a thermal minicycler (peqlab Biotechnologie GmbH, Erlangen, Germany), which involved 40 cycles of denaturation at 94°C for 2 min, annealing of primers at 68°C for 2 min, and primer extension at 72°C for 1 min. The amplification products were separated on 2% (w/v) agarose gels, visualized on a UV-light transilluminator (Biotech R & D Laboratories, Salem, India) and photographed.

Table 3.4 Respective amplicon size (bp) of primers used to identify gene expression in corresponding mycobacterial strains.

Gene	Gene function	Primer sequence (5' →3')[a]	*M. smegmatis mc² 155*	*Mtb* H37Rv	*Mtb* Bleupan
MSMEG 3582	ATP-dependent protease La	F: ATGGCTGAAGCCAAGACAGTGCC R: CGCCCCAAACCGCTCGG	2340 bp	--	--
Leu D	Leucine Biosynthase	F: CTTCGAAGGGCGGCAGGGC R: GAGCACGTCAATGAGCTCTGC	971 bp	971 bp	749 bp
RpfC	Resuscitation promoting factor	F: GTGCATCCTTTGCCGGCCGAC R: GCGCGGAATACTTGCCTGAATG	--	528 bp	528 bp

[a]R, reverse primer; F, forward primer.

The examination of *Mtb* Bleupan DNA through polymerase chain reaction amplification concluded its possession of a shortened leucine D and a signature *Mtb RpfC* gene with the absence of a signature *M. smegmatis* sequence MSMEG 3582 (Fig. 3.1). This confirms the identity of the bacteria as *Mtb* while bearing a characteristic deletion of *Mtb* Bleupan. In addition to the deletion in leucine D sequence, *Mtb* Bleupan was characterized by another deletion in the pantothenate sequence rendering it a double auxotroph. Therefore, a phenotypic growth assay was further performed for validation. Bacteria were incubated in the conditions with or without the two additional nutrient supplements: leucine and pantothenate for a week. Obvious growth was observed in the medium with additional supplement whereas a clear medium showing limited growth was resulted in the condition without supplements (Fig. 3.2). This matches the phenotype of *Mtb* Bleupan as a double auxotroph arising from the deletions in leucine D and pantothenate CD sequences[256]. These results confirmed the sample is *Mtb* Bleupan strain. As a result, this validation process enables the proof of identity of *Mtb* Bleupan strain and reassurance of adequate level of biosafety facilities for the performance of further studies.

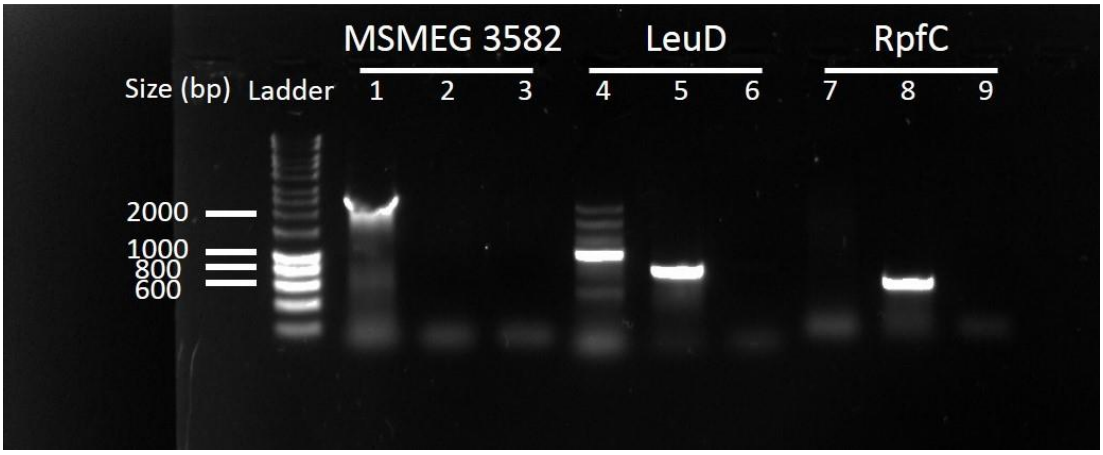

Figure 3.1 Agarose gel electrophoresis on amplified DNA extracted from various mycobacterial strains. DNA extract of M. smegmatis (lane 1,4,7), attenuated Mtb Bleupan (lane 2,5,8) and autoclaved water control (lane 3,6,9).

Figure 3.2 Phenotypic growth evaluation of the severely attenuated Mtb Bleupan strain. Growth of Mtb Bleupan strain supplemented with Leucine and Pantothenate (left) or without leucine nor pantothenate as control (right) on day 8.

3.1.6 Cytotoxicity study

D-LAK peptides, rifampicin and isoniazid were assessed for their cytotoxicity on A549 cells. A549 cells were seeded in sterile 96-well culture plates at a density of 1×10^4 cells per well. The cells were incubated for 24 h to allow attachment. Rifampicin, isoniazid or peptides at designated concentrations, prepared in DMEM supplemented with 10% (v/v) FBS, were added to the cells. Their cytotoxic effects were evaluated using the 3- (4,5-cimethylthiazol-2-yl)-2,5-diphenyl tetrazolium bromide (MTT) cell viability assay after 24 h of incubation. Culture medium was discarded from each well and replaced by MTT solution (0.8 mg/ ml in PBS) followed by incubation at 37°C for 2 h. The precipitated formazan crystals were dissolved in absolute isopropanol and kept at 4 °C for 30 min. Absorbance was measured at 595 nm using a microplate reader (Bio-Tek Microplate Reader, Winooski, VT, USA). Percentage of viable cells was calculated based on the equation shown below in which untreated cells were taken as control with 100% cell viability.

$$cell\ viability\ (\%) = \frac{absorbance\ of\ sample\ well}{absorbance\ of\ control\ well} \times 100\%$$

The results were expressed as mean ± SD of three independent measurements in triplicates.

3.1.7 In vitro *bacterial inhibitory assay*

Minimum inhibitory concentrations (MICs) of the anti-TB agents (rifampicin, isoniazid, D-LAK peptides, capreomycin, and colistin) on different mycobacterial strains were determined using broth micro-dilution assay in 96-well plates. Bacterial colonies from LJ slants were scraped and re-suspended in 7H9 broth medium. Homogeneous mycobacterial suspension was prepared in sterile water, vortexed with glass beads (1-5 mm) for 5 min. After 15 min for aerosol settlement, the colony-forming unit (CFU) of the suspension was determined by the measurement of optical density (OD) using the SmartSpec™ Plus spectrophotometer (BIO-RAD, CA, USA) at 620 nm. D-LAK peptides were first prepared by two-fold serial dilutions (1 µM to 128 µM) in Middlebrook 7H9 medium supplemented with OADC and glycerol as aforementioned. Anti-TB drugs were serially diluted to a range of concentrations: RIF from 0.4 µM to 24 µM, INH from 5.5 µM to 730 µM, CAP from 1.1 µM to 150 µM and CST from 0.65 µM to 87 µM. The prepared D-LAK peptides or drug stock solutions were added to an equal volume (100 µl) of mycobacterial suspension to obtain the final concentration of 1×10^7 CFU/ml for *Mtb* strains or 5×10^4 CFU/ml for *M. smegmatis*.

The untreated bacterial suspension and sterile medium were used as positive and negative growth controls. The plates were then incubated at 37°C (in 5% CO_2 for *Mtb* strains) for 7 days for *Mtb* strains or 24 h for *M. smegmatis*. A volume of 30 µl of 0.02% (w/v) resazurin dye was added to each well at the end of the incubation period. The color change was evaluated after 48 h for *Mtb* strains or 24 h for *M. smegmatis*. Resazurin assay is a colorimetric assay in which the viable cells reduce blue resazurin into fluorescent pink resorufin. MIC of each anti-agent on H37Rv and clinical isolates was determined visually and defined as the lowest concentration remained in blue. For *M. smegmatis* mc^2 155, fluorescence was measured by excitation at 530 nm and emission at 590 nm using the BioTek Synergy HT Multi-Mode Microplate Reader (Vermont, U.S.A.). MIC_{50}, refers to the minimum concentration to inhibit 50% of bacterial growth, was determined using sigmoidal-response (variable slope) in GraphPad Prism 7.04 (GraphPad Software, CA, USA). Experiments were carried out in triplicate on three separate occasions.

Antimicrobial interactions between D-LAK peptides and rifampicin or isoniazid were evaluated via chequerboard assay with modification[193]. The 96-well plate was set into x- and y-axis which were designated for D-LAK peptides and anti-TB drugs, respectively (Fig. 3.3). For *Mtb* strains, each anti-TB agent [x-axis: D-LAK peptides (1 µM to 32 µM); y-axis: RIF (0.8 µM to 48.6 µM) or INH (2.3 µM to 146 µM)] was added into the designated wells to give combination treatments. For *M. smegmatis*, anti-TB agents were prepared as follows, x-axis: D-LAK peptides (0.03 µM to 4 µM); y-axis: RIF (3.8 µM to 122 µM) or INH (23 µM to 730 µM) or CAP (0.2 µM to 7.5 µM) or CST (0.5 µM to 17 µM). Mycobacterial suspension was prepared, seeded in each well and incubated as aforementioned. The untreated bacterial suspension (**B**) and sterile medium (**S**) were used as positive and negative growth controls, respectively. After 7 days for *Mtb* strains or 24 h for *M. smegmatis*, resazurin assay was performed and fractional inhibitory concentration (FIC) of the combination treatment was determined as the lowest combination concentrations remained in blue. Synergistic interactions between anti-TB agents in combination treatment is denoted by the Fractional inhibitory concentration index (FICI). FICI of each combination was calculated by the following formula:

$$\text{FIC index} = FIC_A + FIC_B = [A]_{\text{in combination}} / MIC_A + [B]_{\text{in combination}} / MIC_B$$

Where [A] is the lowest inhibitory concentration of D-LAK peptides in the presence of the anti-TB drug, MIC_A is the MIC of D-LAK peptides treated as single agent and FIC_A is the FIC of D-LAK peptides; [B], MIC_B and FIC_B are the corresponding values for the anti-TB

drug. The interpretation of anti-TB agent interactions according to Caleffi-Ferracioli *et al.* defines synergy to occur when FIC index is < 0.5; additive when values are between 0.5-4.0 and > 4.0 as antagonistic[257]. Experiments were carried out in triplicate on three separate occasions.

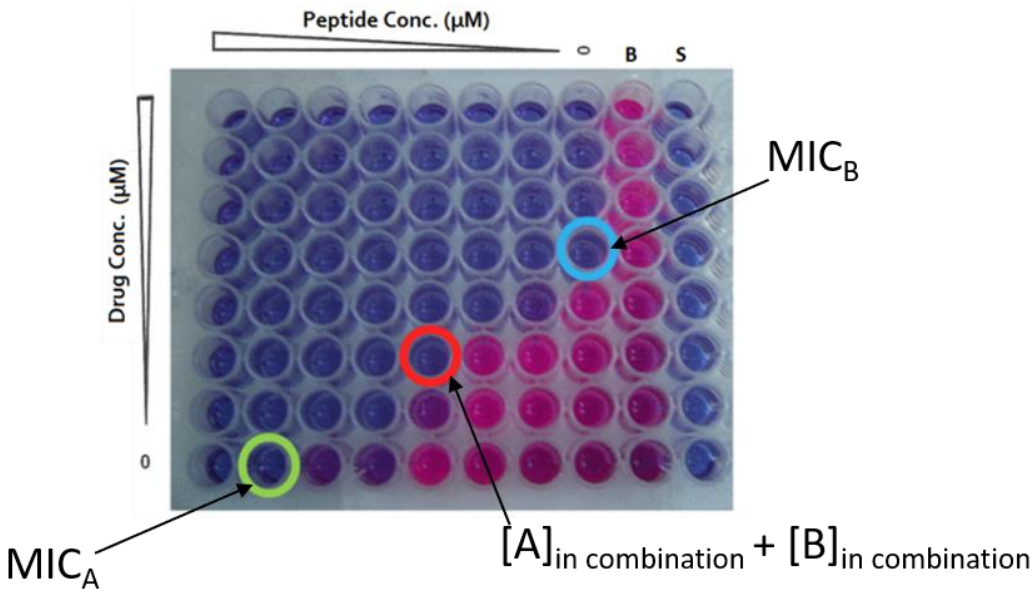

Figure 3.3 Schematic diagram of chequerboard assay on 96-well plate. X-axis and y-axis denote the two-fold decreasing concentration of D-LAK peptide and anti-TB drug respectively, B is the untreated bacterial growth control and S is the sterile negative control.

MIC and FIC experiments were also performed in the presence of 0.025% (v/v) tyloxapol on *M. smegmatis* to evaluate the effect of the surfactant. Tyloxapol, a non-ionic liquid surfactant commonly used to culture mycobacteria to prevent clumping of colonies in broth medium, was chosen instead of Tween 80 since the de-esterification of the later can furnish mycobacteria with oleic acid[258]. This potentially introduces an external factor in the carbon metabolism of the bacteria which interferes with the subsequent metabolomics study, therefore a nonhydrolyzable detergent, tyloxapol was used.

3.1.8 In vitro *mycobactericidal assay on MDR clinical isolates 03M and 08MB*

In vitro mycobactericidal assay of individual anti-TB agent was performed by treating *Mtb* strains with anti-TB agents at their respective ½x, 1x and 2x MIC for seven days. After seven-day incubation of anti-TB agent and mycobacterial inoculum, 50 µl contents from each

well was plated out on a 60 mm Middlebrook 7H10 agar plate enriched with OADC and glycerol. Two dilutions of 1x and 10x or 10x and 100x were made and spread on plates in duplicates. All plates were incubated at 37°C with 5% CO_2 for 3 to 4 weeks before CFUs were counted.

In vitro mycobactericidal assay of D-LAK120-A or D-LAK120-HP13 in combination with RIF or INH against *Mtb* strains was performed in 96-well plate. After day 7 of incubation, four wells of lowest combination concentration showing no apparent bacterial growth visually (remain clear) were plated out on 7H10 agar as mentioned above for CFU counting after 3 to 4 weeks of further incubation at 37°C with 5% CO_2. The percentage growth of *Mtb* of each treatment group compared to the control group was calculated.

3.1.9 Ex vivo *mycobactericidal assay on MDR clinical isolates 03M and 08MB*

Anti-TB agents and their combinations were studied in the intracellular mycobactericidal assay. The method was described in the previous study with modification[259]. THP-1 cells at a density of 1 x 10^5/well were differentiated by treating with 100 nM PMA in RPMI-1640 with 10% (v/v) FBS in 24-well plates for 24h without the presence of Antibiotic-Antimycotic solution. Afterwards, the cells were washed with PBS and incubated with RPMI-1640 with 10% (v/v) FBS overnight. Differentiated THP-1 cells were challenged overnight with MDR *Mtb* strains 03M and 08MB (Day 1) suspended in RPMI-1640 Antibiotic-Antimycotic-free medium at a multiplicity of infection (MOI) of 1 (bacterium-to-cell ratio 1:1). On the day of experiment (Day 0), infection medium was discarded and the cells were washed with phosphate buffered saline (PBS) thrice to remove the extracellular mycobacteria. Individual anti-TB agent or combination treatment at designated concentrations were prepared in RPMI-1640 Antibiotic-Antimycotic-free medium and added into respective wells. Infected cells treated with RPMI-1640 antibiotic-free medium alone served as growth control. On day 7, cells were lysed with 1 ml of 0.1% (w/v) sodium dodecyl sulfate (SDS). Two dilutions of 1x and 10x or 10x and 100x were plated out on Middlebrook 7H10 agar plates in duplicates. Following incubation at 37°C and 5% CO_2 for four to six weeks, bacterial colonies were enumerated and data were expressed as the percentage growth of *Mtb* in each treatment group compared to the control group. Experiments were performed in triplicates on two independent occasions.

3.1.10 In vitro *bacterial inhibitory assay on bioluminescent Mtb Bleupan*

MIC of the anti-TB agents (rifampicin, isoniazid, D-LAK peptides and capreomycin, colistin and delamanid on bioluminescent *Mtb* Bleupan was determined by the measurement of luminescence in 96-well plates. D-LAK peptides were first prepared by two-fold serial dilutions (1 µM to 128 µM) in Middlebrook 7H9 medium supplemented with OADC and glycerol as aforementioned. Each anti-TB agent was serially diluted as follows, RIF (0.01 µM to 12 µM), INH (0.07 µM to 73 µM), CAP (0.01 µM to 15 µM), CST (1.7 µM to 1730 µM) and DLM (0.01 µM to 9 µM). Mycobacterial suspension was prepared in 7H9 broth supplemented with OADC. Diluted mycobacterial culture, with an inoculum size of 1×10^7 CFU/ml, was added to an equal volume (100 µl) of each anti-TB agent solution. Untreated bacterial suspension and sterile medium were treated as growth controls. The plates were then incubated at 37°C and 5% CO_2 for 7 days. Viability of bacteria was assessed by bioluminescence measurement. Bioluminescence of *Mtb* Bleupan expressing the *lux* operon was measured for 1s using the Envision 2105 Multimode Plate reader (Perkin Elmer, MA, USA). Bioluminescence was expressed as relative light units (RLU). MIC was defined as the lowest drug concentration resulted in 1-log reduction in bioluminescence compared with the untreated control[260]. MIC_{50} was determined using sigmoidal-response (variable slope) in GraphPad Prism 7.04 (GraphPad Software, CA, USA). Experiments were carried out in triplicate on three separate occasions.

FICs of the combination treatment of rifampicin, isoniazid or capreomycin and D-LAK peptides were determined using chequerboard assay. Synergistic interactions between anti-TB agents in combination treatment was determined as mentioned above. Two-fold serial dilutions of each anti-TB stock solution [x-axis: D-LAK peptides (1 µM to 32 µM); y-axis: RIF (0.02 µM to 1.2 µM), INH (0.6 µM to 36.5 µM) or CAP (0.19 µM to 12 µM] was added into the designated wells to give six different combination treatments as follows: D-LAK120-A + RIF, D-LAK120-A + INH, D-LAK120-A + CAP, D-LAK120-HP13 + RIF, D-LAK120-HP13 + INH and D-LAK120-HP13 + CAP. Mycobacterial suspension was prepared as forth mentioned and 1×10^7 CFU/ml was seeded in each well. After seven days, measurement of bioluminescence was performed and FICI of each combination was calculated. Experiments were performed in triplicates on three independent occasions.

3.1.11 Time-kill assay

Mtb Bleupan were seeded in 96-well plates at O.D. = 0.02. The bacteria were incubated at 37°C until RLU > 10,000 in all wells (Day 0). Antimycobacterial agent (100 µl) alone or in combination at ½x, 1x, 2x, 4x MIC was added in the designated wells. Luminescent measurements were taken daily for 7 days with the Envision 2105 Multimode Plate reader. Data were plotted by Log RLU over time. All experiments were performed in triplicates on three independent occasions.

3.2 MICROSCOPIC TECHNIQUES

3.2.1 Transmission electron microscopy study

M. smegmatis mc^2 155 was treated with D-LAK peptides at 1x MIC for 5, 15 and 30 min. Samples were then washed thrice with PBS and cell pellets were collected by centrifugation. Cell pellets were fixed in 2.5% (v/v) glutaraldehyde until further processing. Samples were rinsed thrice with piperazine-N,N'-bis(ethanesulfonic acid); 1,4-piperazinediethanesulfonic acid (PIPES buffer) (Sigma Aldrich Cat.# P6757) followed by second fixation in 1% (v/v) osmium tetroxide (OsO_4) (Sigma Aldrich Cat.# 75632) for 1 h at room temperature. The first embedding into agar was done to reduce sample loss. Pellets were then dehydrated using ethanol (EtOH) [50, 70, 90% (v/v) for 10 min each and then 100% thrice for 20 min]. After dehydration, samples were infiltrated using 1:1 epoxy resin/ propylene oxide mixture overnight at 37 °C. The next day, pellets were infiltrated with fresh epoxy resin for 1 h at 37 °C followed by polymerization at 60 °C overnight. Samples were viewed using CM100 TEM (Philips, U.S.A) equipped with a TENGRA 2.3K X 2.3K camera.

3.2.2 Confocal microscopy study

Effect on membrane permeability of peptides using confocal microscopy was studied previously[261] with modification. *M. smegmatis mc^2 155* cultures grown up to mid-log phase was treated with 250 µg/ml 150 kDa FITC-labelled dextran (Sigma Aldrich, Cat. #46946) and D-LAK peptides or first-line drugs (RIF or INH) at ½x, 1x and 2x MIC for 20 min. Bacterial cells treated only with FITC-dextran was used as control. Following the treatment, the bacterial cells were centrifuged at 7500 rpm for 10 min and washed thrice with PBS to remove the unassociated dextran. Cells were then fixed in 2% (v/v) formaldehyde at room

temperature for 20 min. After fixation, cells were washed twice and re-suspended in PBS. A volume of 20 µl sample was then allowed to air-dry on microscope slides overnight. FITC was excited with a 488 nm laser and detected with a 505 nm long-pass filter. Samples were imaged with a 65x oil-immersion objective lens using a Zeiss LSM-510 inverted confocal microscope (Carl Zeiss Inc., Germany).

3.3 MYCOBACTERIAL GROWTH RESPONSE ASSAY

3.3.1 Mycobacterial growth response study

To elucidate the mechanism of action of anti-TB agents on mycobacterial growth, sub-MIC challenge assays were conducted to observe the growth response of *M. smegmatis* mc^2 155 and *Mtb* Bleupan. For *M. smegmatis*, 1% inoculum in the presence of 0.025% (v/v) tyloxapol or ¾ MIC of each anti-TB agent, alone or in combination, was cultured in 10 ml supplemented 7H9 broth medium at 37°C for 5 days. For *Mtb* Bleupan, two challenge conditions by each anti-TB agent, alone or in combination were studied: i) six weeks challenge of 1% inoculum with ¼ MIC of anti-TB agents and ii) 72 hours challenge of six-week cultured bacteria with ½ MIC of anti-TB agents. The bacteria were processed and subjected to trans-1,6-diphenyl-1,3,5-hexatriene (DPH) fluorescence assay, Laurdan fluorescence assay and nuclear magnetic resonance (NMR) metabolomics analysis.

3.4 FLUORESCENCE ASSAYS

3.4.1 Laurdan fluorescence assay

At the end point of the growth response assay mentioned above in section 3.3.1, tubes with mycobacteria were vortexed to break down the biofilms and de-clump the bacterial lumps. O.D. of the bacteria suspension was measured at 600 nm. The average of triplicate measurements was taken. Bacterial suspension (3 ml) at OD = 0.6 was made by diluting with PBS. The remaining suspension was kept for metabolomics studies. The 3 ml bacterial suspension was then fixed by 0.25% (v/v) formaldehyde [4% (v/v) for *Mtb* Bleupan] for 1 h at room temperature. After fixing, the bacterial cells were pelleted by centrifugation at 5, 000 rpm, 4℃ for 8 min and washed by PBS once (thrice for *Mtb* Bleupan samples). The samples were kept at -20℃ until further studies. Laurdan (6-dodecanolyl—N,N-dimethyl-2-

napthtylamine) was prepared by dissolving in complete methanol. Bacteria were re-suspended in PBS and stained by 2.5 µM Laurdan fluorescent probe. All tubes were wrapped with foil to prevent photodegradation of the dye and incubated at 37℃ for 1 h. Samples were added into the cuvette and excited at 350 nm using fluorescence spectrophotometer (Varian Cary Eclipse, Mulgrave, Victoria, Australia). Measurements were performed at 37℃ and signals were collected at emission wavelength range of 400-600 nm (no. of scans = 20). General polarization (GP) value corresponding to the order of membrane was calculated as below where I_{440} and I_{490} are the emission intensities at corresponding wavelengths:

$$GP\ value = \frac{I_{440} - I_{490}}{I_{440} + I_{490}}$$

3.4.2 Trans-1,6-diphenyl-1,3,5-hexatriene (DPH) fluorescence assay

Mycobacterial cells were harvested, fixed and washed with the same procedure as for Laurdan assay. Bacteria cells were re-suspended in PBS and stained by 2.5 µM DPH fluorescent probe. All tubes were wrapped with foil and incubated at 37℃ for 30 min. Samples were added into the cuvette and excited at 358 nm using the fluorescence spectrophotometer (Varian Cary Eclipse, Mulgrave, Victoria, Australia). Signals were collected by single wavelength scanning at emission wavelength 430 nm. The spectral bandwidth of the emission monochromator and the measurement of emission spectra were set at 10 nm. Steady-state fluorescence anisotropy, r, was calculated as

$$r = \frac{I_{VV} - GI_{VH}}{I_{VV} - 2GI_{VH}}$$

where I_{VV} and I_{VH} are the parallel and perpendicular polarized fluorescence intensities measured with the vertically polarized excitation light, I_{HV} and I_{HH} are the same fluorescence intensities measured with the excitation light horizontally polarized, and G is the monochromator grating correction factor given by $G = I_{HV}/I_{HH}$.

3.5 NUCLEAR MAGNETIC RESONANCE (NMR) METABOLOMICS

3.5.1 NMR sample preparation

After the end of the designated challenge period, mycobacterial cells were harvested by centrifugation at 5,000 rpm, 4℃ for 8 min. Supernatant was collected and filtered through 0.22 µm membrane filters to remove remaining bacterial cells. Metabolic activities in the supernatant was quenched immediately by freezing at -80℃ and stored until further use. Bacterial cells were washed twice with PBS. PBS was aspirated to obtain a bacteria pellet which was then snap frozen in liquid nitrogen for 3 min. The pellet was lyophilized at -50°C overnight using an Alpha 1-2 LD plus freeze dryer (Martin Christ, Germany). For *Mtb* Bleupan samples, the harvested cells were fixed with 4% (v/v) formaldehyde for 1 h at 4℃. The pellet was washed twice with PBS after fixation. Samples were prepared according to the procedures above. The lyophilized pellets were stored at -20℃.

3.5.2 NMR data acquisition

Prior to NMR acquisition, the lyophilized cell pellet were re-suspended in 40 µl D_2O containing Trimethylsilylpropanoic acid (TSP) for at least 2 hours before data acquisition to provide a deuterium lock signal. This is to ensure the complete rehydration of cells in order to avoid larger spectral linewidths. The re-suspended pellet was placed in Kel-F insert (Bruker, Rheinstetten, Germany) and then in the 4 mm Zirconia Magic Angle Spinning (MAS) rotor and preserved with a Kel-F cap. The filtered supernatant samples were prepared with 10% (v/v) D_2O with TSP and transferred to NMR tubes. Complete D_2O was not used since the 7H9 broth medium contains a considerable amount of ferric ion which interfere with NMR data acquisition.

For HR-MAS NMR, spectrum acquisition was performed on a 600 MHz Bruker Avance III spectrometer equipped with a 4mm $^{1}H/^{13}C$ HR-MAS probe (Bruker UK Limited, Coventry, UK). The temperature was kept at 310 K. The magic angle spinning frequency was 5 kHz. 1D ^{1}H NMR spectra were collected with a pulse-acquire with pre-saturation (zgpr) pulse sequence in order to avoid the water signal. The spectrum width was 12.01 ppm, relaxation delay (d1) was 3 s and ^{1}H 90 pulse length was 5.025 µs. Before recording acquisition data, eight dummy scans were performed. Total acquisition time was 1.14 seconds with a pre-scan delay of 6.5 µs and Tau delay (d20) of 200 µs. The size of raw spectrum was recorded with

131k data points. A total of 128 scans and 10 min were used to obtain each of the NMR spectra. Free induction decay was multiplied by an exponential function with line broadening of 0.3 Hz. For liquid state NMR, data were recorded under automation on a Bruker Avance II 700 NMR spectrometer (Bruker BioSpin, Coventry, United Kingdom) equipped with a 5-mm helium-cooled quadruple resonance cryoprobe and a cooled SampleJet sample changer. The samples were kept at 4℃ before inserting into the magnet. 1D ^{1}H spectrum acquisition was done at 298 K and 700 MHz using a Carr-Purcell-Meiboom-Gill pre-saturation (cpmgpr1) pulse sequence. Spectra were acquired after four dummy scans with 64 transients, a spectrum width of 20.1 ppm, 65 k data points and a relaxation delay of 4 s. Free induction decays were multiplied by an exponential function equivalent to a 0.3-Hz line broadening factor, followed by Fourier transformation and calibration to the methyl peak of TSP-d_4 set to 0.0 ppm. Phase correction of spectra was performed manually using Brucker Topspin 3.5 Software, and automatic baseline correction was applied. Due to the inherit variability in biological samples, nine samples from three experimental replicates were collected for each of the treatment condition to achieve a robust statistical analysis. For assignment purposes, two dimensional (2D) spectra of ^{1}H-^{1}H correlation spectroscopy (COSY) (cosygpprqf) spectra were acquired for selected samples.

3.6 STATISTICAL ANALYSIS

Data analysis was performed using GraphPad Prism version 7.04 (GraphPad Software, La Jolla California USA, www.graphpad.com). ANOVA test followed by Dunnett's or Bonferroni's Multiple Comparisons Test or Tukey's post-hoc test was used to establish statistical significance. Student's t-test was performed for pairwise comparison. Values are expressed as mean ± standard deviation (SD). Differences were determined as statistically significant with probability value $p \leq 0.05$. All experiments were performed in triplicates.

3.6.1 NMR metabolomics data pre-processing and multivariate analysis

NMR metabolomics data processing and analysis were performed using a set of software previously developed in the Mason laboratory, Kings College London by Dr Louic Vermeer together with MVAPACK[262] and an open source Octave library. Python 3, used in the in-house script, is a programming language allows the integration of mathematical Numpy, SciPy extension and Metplotlib for the visualization of principal component analysis (PCA) and Orthogonal Partial Least Squares/Projection onto Latent Structures (OPLS) plots[263].

Proper preprocessing of metabolomics data is vital to attain a meaningful interpretation through the generation of reliable PCA, Orthogonal Partial Least Squares-Discriminant Analysis (OPLS-DA) models. Pre-processing procedures generally includes removal of noise regions, normalization, data scaling, binning and alignment. As a result, the residual water resonances (4.46-4.87 ppm) were excluded. The NMR spectrum regions below 0.2 ppm and above 10 ppm containing the reference TSP peak and noise were also removed to eliminate any undesired variations. The processed NMR data were reduced into spectral regions of 0.005 ppm in the octave environment using the icoshift alignment and optimized binning algorithm. Probabilistic quotient normalization (PQN) was employed to normalize the data set based on the assumption that changes in the concentration of a particular analytes only affect a section of the spectrum while the effect overall concentration dominates the influence of the whole spectrum[264]. PQN was carried out via the calculation of median spectrum thereby the median quotient and finally dividing each data point by the median quotient[264]. Autoscaling was then performed by mean centering the data points and then divide the standard deviation for the variable. This treatment prevents the intense peaks from having a dominating effect in the multivariate analysis.

Louic's Metabolomics Thingy' developed by Dr Louic Vermeer used for metabolomics data processing and analysis was featured in several publications in the past years[263, 265]. This software is equipped with a PyQT front end Graphical User Interface (GUI) which allows the import of raw NMR spectra and transformation into PCA and OPLS-DA plots, facilitating processing and analysis of data for non-experts. All reduced data matrices were initially analyzed by PCA to examine the intrinsic variation of in the data set, identifying general trends and outliers. PCA involves the mathematical procedures that transform the large number of possibly related variables (metabolites) into smaller number of unrelated variables known as Principal Components (PC). PC1 always account for the greatest variance of the data set and the accountability of the variance in the remaining data would be accounted by subsequent PCs[266]. OPLS-DA was employed to further extract useful information by maximizing the separation between control and each treatment condition. Double cross validation was used to provide a robust assessment for the generation of statistical models. Leave-One-Out Cross-Validation (LOOCV) using a 7-fold method in which one sample is left out of the training set and is used to validate the model, therefore, 85% of the samples were used as the training set while the other 15% served as the test set. The quality assessment statistics (Q^2) is typically used to report the result of cross validation. Although there is no standard comparison or critical significant value for Q^2, the normal practice is to

compare to its theoretical maximum of 1 or empirically acceptable value of ≥ 0.4 in biological models[247]. Thus, a higher Q^2 (closer to 1) indicates a better predictability of the model generated. The procedure was repeated for 1000 times with samples randomly chosen in the training sets and test sets, a total of 7 x 1000 models was generated. For further validation, random permutation test of 1000 repeats were exploited to test the null hypothesis for a model's Q^2. This allows another point of comparison of Q^2 in which a more reliable model would yield a significantly larger Q^2 when compared to that generated from the random models (permutated) from the same data set[244]. The processed data were illustrated as plots of back-scaled loadings, Q^2 histogram, the principal components histogram, the prediction per sample and the predicted residual error sum of squares (PRESS)/sample. A representative visual output of cross-validated OLPS-DA is shown in Fig. 3.4.

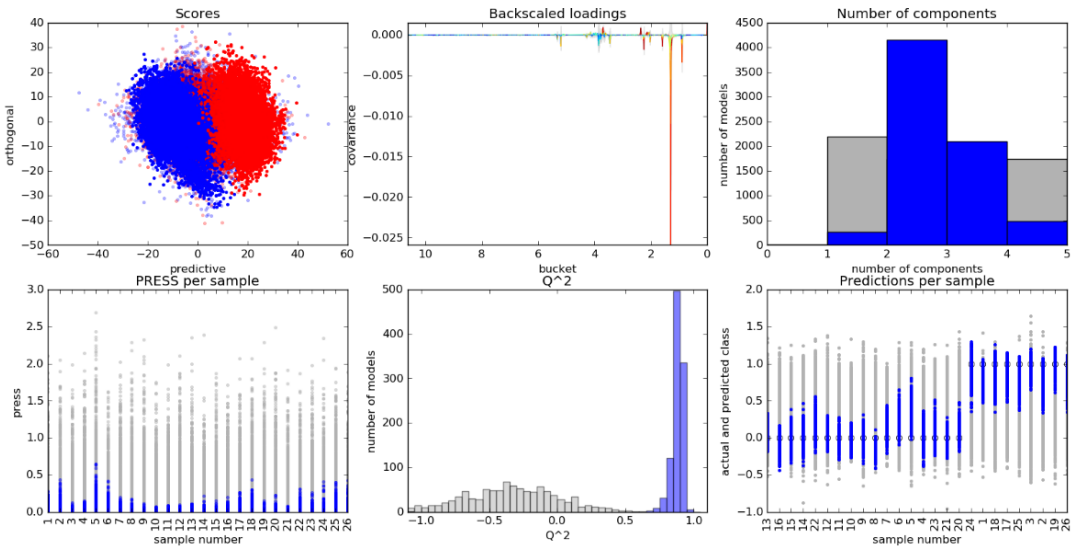

Figure 3.4 Representative visual output of OPLS-DA cross-validation data. The data as shown are taken from the M. smegmatis grown in the presence of 0.025% (v/v) tyloxapol surfactant. Processed results are plotted in which the blue represents the sample data while the grey is the random assignment of classes denoted as the permutated data. Top left: Scores plot from the double cross-validation strategy. Each point represents an individual NMR spectrum of a sample and are plotted according to their score of the predictive and orthogonal components. This plot depicts the separation between control (blue) and treatment (red) classes when using variables that can distinguish between classes. These variables are the metabolic resonances that have the most discriminatory importance in the data which is illustrated in the Back-scaled loadings plot. This plot is generated with the covariance of the metabolic resonance associated with the class; correlation weights are differentiated using color. Top right: Principal components histogram shown the number of components used to create the OPLS-DA models with each iteration of cross-validation. Bottom left: PRESS/sample is a dot-plot of sample and permutated data for the further inspection of extreme outliers in accordance with the Prediction per sample plot (Bottom right). Bottom middle: Q^2 histogram allows the visualization of the model predictability by comparing the values between sample and permutated data. This combination of plots gives an overview of the predictability of the generated OPLS-DA model.

Assignment of metabolic resonances were made with the aid of literature[267-270], the Biological Magnetic Resonance Bank (BMRB)[271], Chenomx software and the ranges of 2D NMR spectra. Representative figures for peak assignment are shown in appendix A. MultiExperiment Viewer (MeV), a part of the TM4 Microarray Software Suite[272] was used to generate heatmaps with the quantified variation in metabolite concentrations. Hierarchical cluster analysis using the Euclidian distance algorithm was employed to evaluate the differences in changes of metabolites and compute the clustering relationship of the treatment conditions.

For volcano plots, significant results from OPLS-DA analysis justified univariate analysis of peaks associated with predictive value in the multivariate models. Therefore, the integrals of assigned NMR peaks were analyzed using non-parametric univariate methods. Volcano plots were used to compare the fold change in metabolite values between each treatment condition and the untreated control. Fold change was calculated as the ratio between the two conditions (Treatment/Control). Mann-Whitney U test was exploited to compare means and associated p-values were False Discovery rate adjusted using the Benjamini-Hochberg method (α = 0.05). Volcano plots were generated using custom scripts in Python with Numpy, Pandas, Matplotlib and Seaborn packages. Partial least-squares (PLS) Regression was performed in Python using the PLS Regression function in the scikit-learn software package. Only one component was necessary for best model performance as determined in the initial model assessment. Increased number of components led to a decrease in Q^2. Monte Carlo cross-validation of models was employed through the random splitting of data into 70/30 training/test set splits. The procedure was repeated 1000 times to avoid bias by sample separation and R^2 and Q^2 values were computed to evaluate model performance. R^2 denotes how well the model describes the training data set while Q^2 demonstrates the predictability of model on the test set. Spearman correlation coefficient was used to measure the strength of the relationship between the changes in selected influential metabolites and the respective DPH anisotropy of the samples.

Chapter 4 Combinations of D-LAK peptides and anti-TB drugs against drug-resistant TB and *Mtb* Bleupan

4.1 INTRODUCTION

Mycobacteria possess the intrinsic resistance to many antibiotics that are effective against other bacteria, and this is deemed possible owing to the superior protection offered by the lipid-rich mycolic acid-containing mycobacterial cell envelope[18]. Anti-TB drug research has been focused on identifying candidates capable of breaching the cell wall of mycobacteria in order to tackle the problem arises from the emergence of resistance to the limited number of existing antibiotics for TB. This approach may provide a means to kill the mycobacteria directly or re-sensitize them to existing first-line anti-TB agents.

To this end, increasing interest has been drawn to the use of AMPs for their rapid antibacterial actions which involve direct membrane disruption and membrane penetration to target important intracellular functional sites[67]. The salient features of net positive charge and amphipathicity possessed by AMPs render them useful to target and kill bacteria. The action of AMPs often leads to rapid cell death which reduces the chance of bacteria to develop resistance towards AMPs, making them a potential candidate for TB treatment[19, 62]. In essence, the anti-TB ability of AMPs have not only been studied in isolation, but also in combination with first-line anti-TB drugs such as rifampicin and isoniazid against both drug-susceptible and drug-resistant MDR-TB strains[222, 261]. Among these peptides, those containing all-D-amino acids demonstrated better stability due to their resistance to proteolytic degradation and therefore improved mycobacterial selectivity and antimicrobial activities *in vitro* and *in vivo* as compared to the L-form[190, 215, 273].

The development of a range of highly cationic D-LAK AMPs has been reported in recent publications for their action against Gram-negative bacteria, attenuated *Mtb* H37Ra and MDR *Mtb* strains[188, 259]. These amphipathic D-LAK peptides consist of 25 amino acids residues including leucine (L), alanine (A) and lysine (K) in their D-conformation. D-LAK peptides were rationally designed to adopt an α-helix conformation when interacting with the bacterial membrane[188]. They possess a charge angle subtended by the positively charged lysine residue (Fig. 4.1) which can be modified to enhance disruption on anionic bacterial membranes[188]. According to the structural-activity studies, D-LAK peptides with a charge angle of 120° demonstrated the highest potency against attenuated *Mtb* strain H37Ra. Furthermore, the effect of conformational flexibility and hydrophobicity were evaluated by substitution of various amino acid residues including histidine (H) and proline (P) in the parent LAK peptide sequence (KKLALLALKKWLLALKKLALLALKK-NH_2). Conformational flexibility is a key property that is associated with better membrane

penetration and intracellular targeting ability of AMPs[188]. The incorporation of proline residue at position 13 was shown to enhance conformation flexibility and displayed efficient killing effect on *Plasmodium falciparum* while mitigating hemolytic toxicity[188]. This is supported by a transcriptomics and NMR metabolomics study which revealed the improved membrane penetration of the proline-containing D-LAK120-HP13 peptide[274].

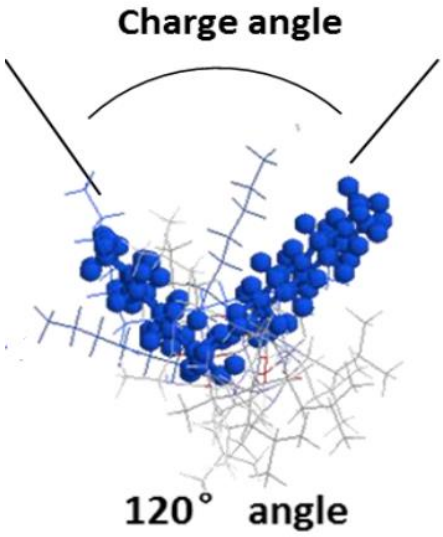

Figure 4.1 Schematic diagram of α-helical peptide with a charge angle of 120° subtended by positively charged lysine residues in blue.

In a previous study, six promising D-LAK peptides possessing the nominal charge of +9 at neutral pH, namely D-LAK120, D-LAK120-H, D-LAK120-A, D-LAK120-P13, D-LAK120-HP13 and D-LAK120-AP13, were selected to evaluate their activity against MDR and XDR *Mtb* strains[259]. These D-LAK peptides demonstrated a de-clumping effect which enabled the disruption of colonies of MDR-TB strains. This resulted in inhibition of mycobacterial growth *in vitro* and in differentiated THP-1 macrophage-like cells. Moreover, the D-LAK peptides were able to potentiate the activity of first-line anti-TB drug isoniazid *in vitro*. Among the six peptide candidates, D-LAK120-A and D-LAK120-HP13 were found to show the highest efficacy in inhibiting the growth of drug-resistant *Mtb* clinical isolates[259]. These findings revealed that D-LAK peptides have the potential to act as an adjuvant in combination with other anti-TB agents to potentiate the antimicrobial effect towards *Mtb*.

Furthermore, due to the lack of a safe and reliable surrogate model for the study of anti-TB drug action to date, a severely attenuated *Mtb* Bleupan strain was included, to evaluate its

potential as an applicable surrogate model. The severely attenuated *Mtb* Bleupan strain is a *Mtb* mutant derived from the virulent drug-susceptible H37Rv strain. This strain was named *Mtb* Bleupan as it was created through the deletions of two loci in *Mtb*, the essential ***leu****D* (*Mtb* H37Rv gene number Rv2987c) and ***pan****CD* (Rv3602c and Rv3601c)[256]. As an early attempt to be developed as vaccine candidate, the combination of these two independent, attenuating and non-revertible mutations render the strain auxotrophic for both leucine and pantothenate and highly attenuated *in vivo*. This double auxotroph therefore provides a safer means for studying *Mtb* biology and drug screening. The attenuation of this strain enables it to be used in biosafety level 2 (BSL 2) containment rather than biosafety level 3 (BSL 3) which increases operator safety and enables the performance of experimental assays which otherwise are difficult under BSL 3 conditions. As a derivative of the H37Rv strain, studies on *Mtb* Bleupan can potentially generate findings in closer resemblance to the virulent parent strain in terms of cell metabolism, membrane remodeling and morphological changes upon stimulation by drug treatment. Recently, Vilchèze *et al.* generated triple auxotrophic MDR *Mtb* mutants with their drug-resistant and persistence characteristics well-retained, providing attractive candidates relevant to most types of MDR *Mtb* studies and circumventing the need for BSL 3 facilities[275].

Another merit of the *Mtb* Bleupan strain is its expression of the full *luxCDABE* operon from *Photorhabdus luminescens*[276], giving rise to autoluminescence of luciferase in the bacteria. The biochemical requirements for light production including reduced flavin mononucleotide ($FMNH_2$) cofactor and oxygen, are generated in the cytosol of mycobacteria growing aerobically[277]. In viable bacteria, the α and ß subunits of the heterodimeric catalase, luciferase, is encoded by *luxA* and *luxB* respectively; *luxC*, *luxD*, and *luxE* are responsible for the encoding of a reductase, transferase and synthase, respectively, to form the reaction substrate[278]. Bioluminescence is produced through the oxidation of $FMNH_2$ using the endogenously generated long-chain fatty acid aldehyde substrate. Other transcriptional reporter strains based on fluorescent proteins, firefly luciferase (FFluc) and bacterial luciferase from *Vibrio harveyi* (luxAB) have been commonly employed in *Mtb* studies[279-281]. However, fluorescent reporters exhibit low signal-to-noise ratio in microtiter plates; luciferase enzymes FFluc and luxAB offer relatively higher signal-to-noise ratio but require the addition luciferin substrate which is time-consuming and destructive, leading to endpoint measurements[282]. Autoluminescent *Mtb* Bleupan precludes the need for substrate addition, it can therefore overcome these limitations and enables real-time *in vitro* and *ex vivo* monitor of antibiotics efficacy with high sensitivity[260, 283]. Furthermore, these *Mtb* Bleupan

characteristics also revealed their advantage over the conventional measurement of bacterial optical density or resazurin fluorescence in the detection of bacterial inhibitory activity of anti-TB agents. Detection of bacterial turbidity is a convenient method but it fails to distinguish dead and live cells, and the clumping nature of *Mtb* poses further issues. Moreover, without the need of resazurin dye addition, assay protocol can be simplified and any interaction between the dye and drug molecules can be avoided[284]. In fact, the changes in bacterial metabolism demonstrated in *M. smegmatis* revealed the ability of some antibiotics to trigger oxidative stress responses. Due to the sensitivity of resazurin dye to redox environment, detection of bioluminescence in *Mtb* Bleupan eliminates the uncertainties and therefore serve as a superior model.

The aim of this chapter was to extend the investigation of bioefficacy of the combinations of existing anti-TB agents with D-LAK peptides to a series of MDR-TB clinical isolates. In this study, cytotoxicity of D-LAK peptides, rifampicin and isoniazid used alone or in combination was determined using 3-(4,5-cimethylthiazol-2-yl)-2,5-diphenyl tetrazolium bromide (MTT) assay. Antimicrobial activity of D-LAK peptides and anti-TB agents, when used alone or in combination, were assessed in MDR-TB clinical isolates and *Mtb* Bleupan. *In vitro* bacterial inhibitory assay was performed on MDR clinical isolates and *Mtb* Bleupan; the inhibitory concentrations were detected by resazurin dye and bioluminescence respectively. *In vitro* and *ex vivo* mycobactericidal assay were also carried out on MDR clinical isolates and the results were determined by colony-forming unit (CFU) counting method. Time-kill assay against *Mtb* Bleupan by anti-TB agents alone and in combination was also performed through monitoring bioluminescence.

4.2 RESULTS

4.2.1 Cytotoxicity assay

In this study, cytotoxicity of anti-TB agents alone and their combinations was assessed using 3-(4,5-cimethylthiazol-2-yl)-2,5-diphenyl tetrazolium bromide (MTT) assay on A549 cells. D-LAK120-A demonstrated higher toxicity than D-LAK120-HP13 (Fig. 4.2). Both D-LAK peptides displayed significant toxicity ($p < 0.0001$) at 16 μM or above. D-LAK120-A displayed significant cytotoxicity at the concentration of 8 μM, resulting in 56.6 ± 7.7 % of viable cells, while the viability of cells treated with D-LAK120-HP13 at the same concentration was not significantly different from the control. Both peptides were not cytotoxic at the concentration of 4 μM or below on A549 cells with cell viability over 90%. In a previous study, the cytotoxicity of D-LAK peptides was assessed on differentiated THP-1 cells and mouse monocytic macrophage cell line RAW 264.7 using the lactate dehydrogenase (LDH) [259] and MTT assay[188] respectively. Significant cytotoxicity was observed at concentrations ≥ 12.5 μM for D-LAK120-A and ≥ 3.13 μM for D-LAK120-HP13. Both studies suggested the peptides have low cytotoxicity on mammalian cells at 4 μM or below. Here, the IC_{50} of D-LAK120-A and D-LAK120-HP13 were found to be 7.89 ± 0.21 μM and 12.2 ± 3.85 μM, respectively, on A549 cells. The cytotoxicity of rifampicin and isoniazid was also measured on A549 cells (Fig. 4.3A-B). No significant cytotoxic effect was demonstrated by the rifampicin and isoniazid up to 91.1 μM and 2190 μM, respectively. Cell viability significantly dropped to below 55% ($p < 0.0001$) when the cells were exposed to rifampicin at 182 μM or higher. In contrast, isoniazid did not induce any significant cytotoxic effect at the highest tested concentration of 2190 μM.

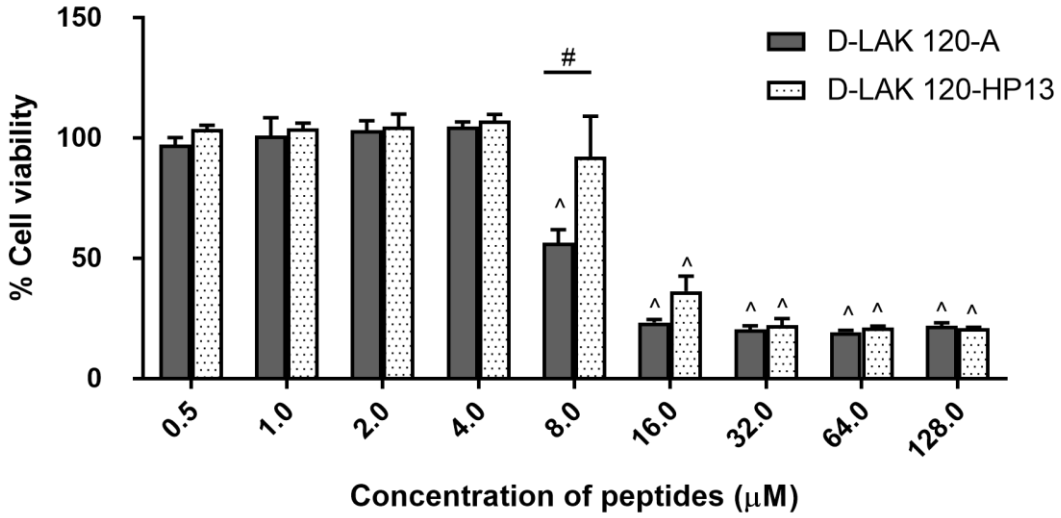

Figure 4.2 Cytotoxicity study of D-LAK peptides on A549 cells. The cells were incubated with D-LAK120-A or D-LAK120-HP13 at various concentrations for 24 h before MTT assay was carried out, data were presented as mean ± SD (n=3). Significant difference was determined by two-way ANOVA analysis followed by Dunnett's or Bonferroni's Multiple Comparisons Test, ^ represents p<0.0001 compared to the untreated control; # represents p<0.0001 compared between peptides.

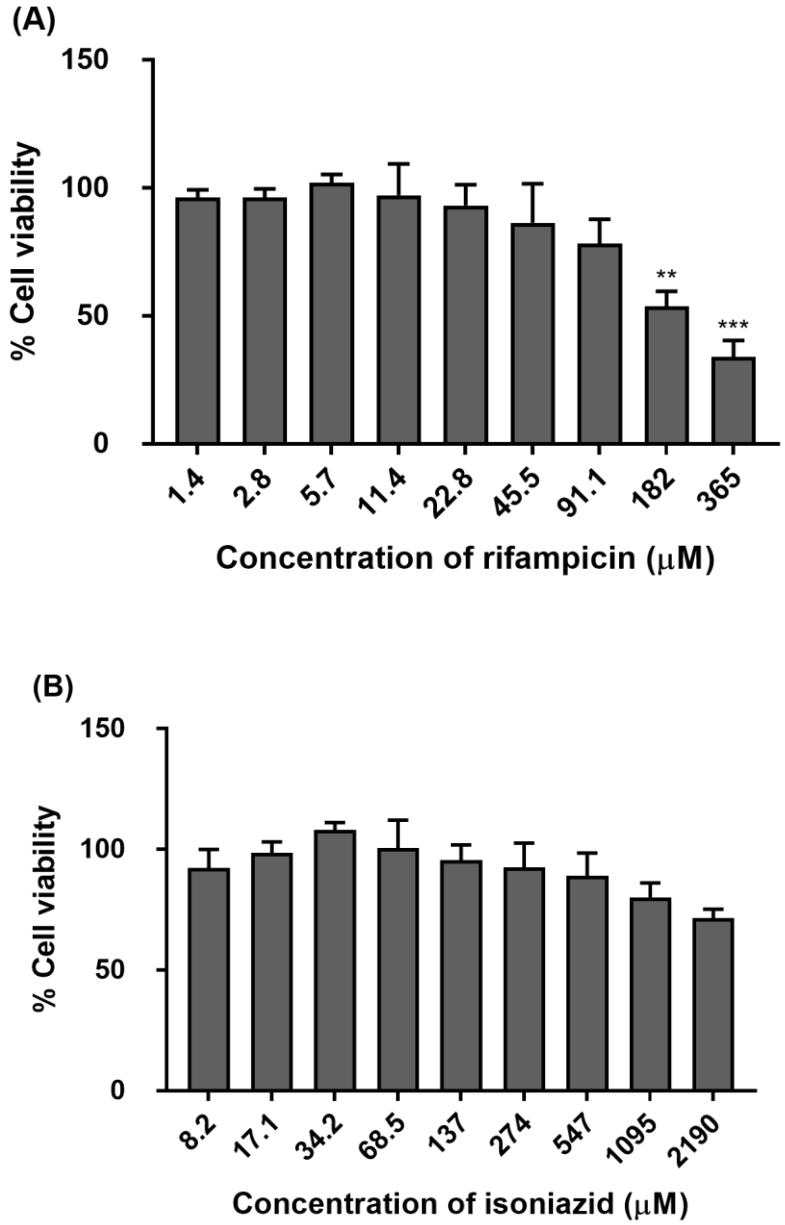

*Figure 4.3 Cytotoxicity study of RIF (A) or INH (B) on A549 cells. The cells were incubated with the drug at various concentrations. MTT assay was carried out after 24 h of incubation. Data were presented as mean ± SD, (n=3). Significant difference was determined by one-way ANOVA followed by Dunnett's Multiple Comparisons Test, ***p<0.001, ****p<0.0001 compared with untreated control.*

As reported in previous studies, the combination of D-LAK peptides with isoniazid reduced the effective concentration of both agents against MDR strain GB2[259], therefore reducing the risk of toxicity. Combinations of D-LAK peptides (up to 8 μM) and rifampicin (up to 12.2 μM) or isoniazid (up to 72.9 μM) were subjected to MTT assay after 24 h of incubation (Fig. 4.4 to 4.7). The studied concentration for the combinations was chosen based on their effective concentrations. For the combination of D-LAK120-A and rifampicin, no significant cytotoxicity was observed when the concentration of the peptide was used at 4 μM or below (Fig. 4.4). Interestingly, when the peptide concentration was increased to 8 μM, the combinations became cytotoxic except the one contained the highest concentration of rifampicin of 12.2 μM. Similar to D-LAK120-A in combination with rifampicin, when the peptide was combined with isoniazid, no significant cytotoxicity was observed when the concentration of the peptide was at 4 μM or below (Fig. 4.5). Significant cytotoxicity was demonstrated in this combination when the concentration of D-LAK120-A was used at 8 μM. No significant cytotoxicity was displayed by the combinations of D-LAK120-HP13 with rifampicin (Fig. 4.6) or isoniazid (Fig. 4.7).

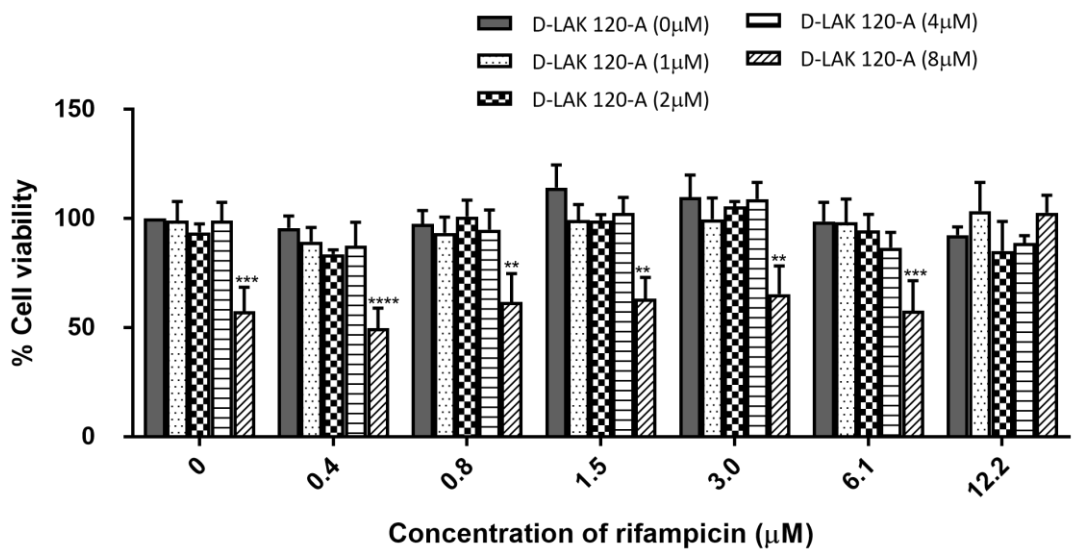

*Figure 4.4 Cytotoxicity study of combinations of D-LAK120-A and RIF on A549 cells. The cells were incubated with the combination of D-LAK120-A and RIF at various concentrations for 24 h before MTT assay was carried out, data were presented as mean ± SD, (n=3). Significant difference was determined by one-way ANOVA analysis Test followed by Dunnett's Multiple Comparisons Test, **p<0.01, ***p<0.001, ****p<0.0001 compared with untreated control.*

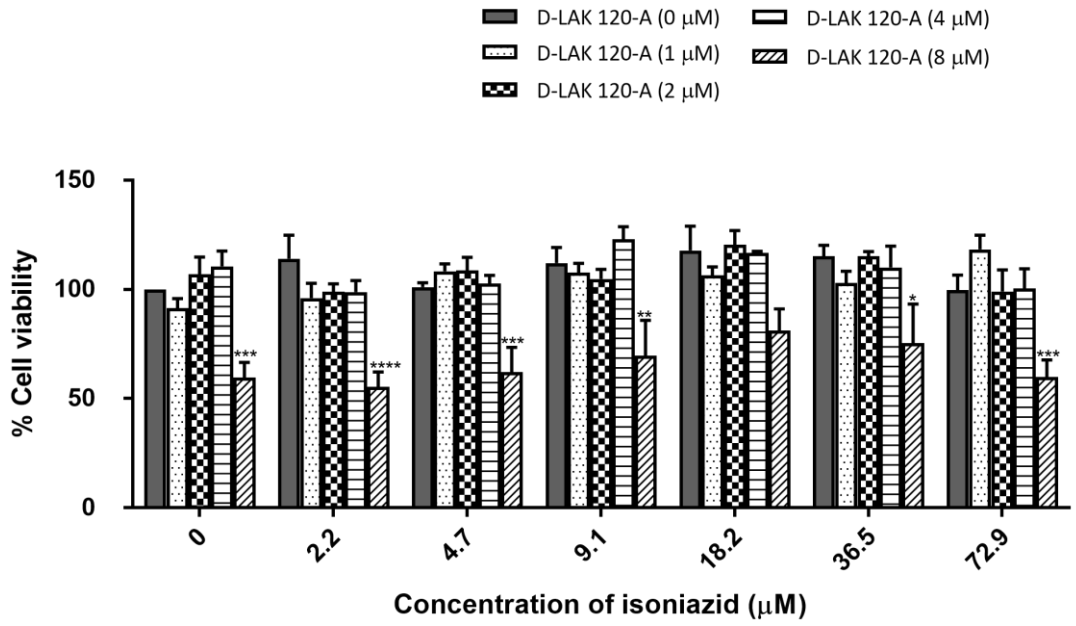

*Figure 4.5 Cytotoxicity study of combinations of D-LAK120-A and INH on A549 cells. The cells were incubated with the combination of D-LAK120-A and INH at various concentrations for 24 h before MTT assay was carried out, data were presented as mean ± SD, (n=3). Significant difference was determined by one-way ANOVA analysis Test followed by Dunnett's Multiple Comparisons Test, **p<0.01, ***p<0.001, ****p<0.0001 compared with untreated control.*

.

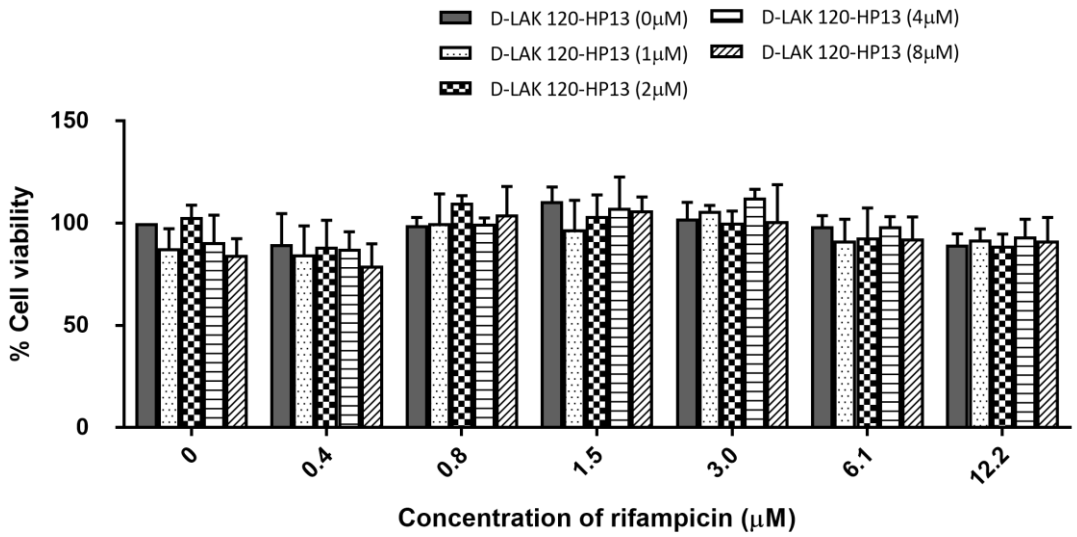

Figure 4.6 Cytotoxicity study of combinations of D-LAK120-HP13 and RIF on A549 cells. The cells were incubated with the combination of D-LAK120-HP13 and RIF at various concentrations for 24 h before MTT assay was carried out, data were presented as mean ± SD, (n=3).

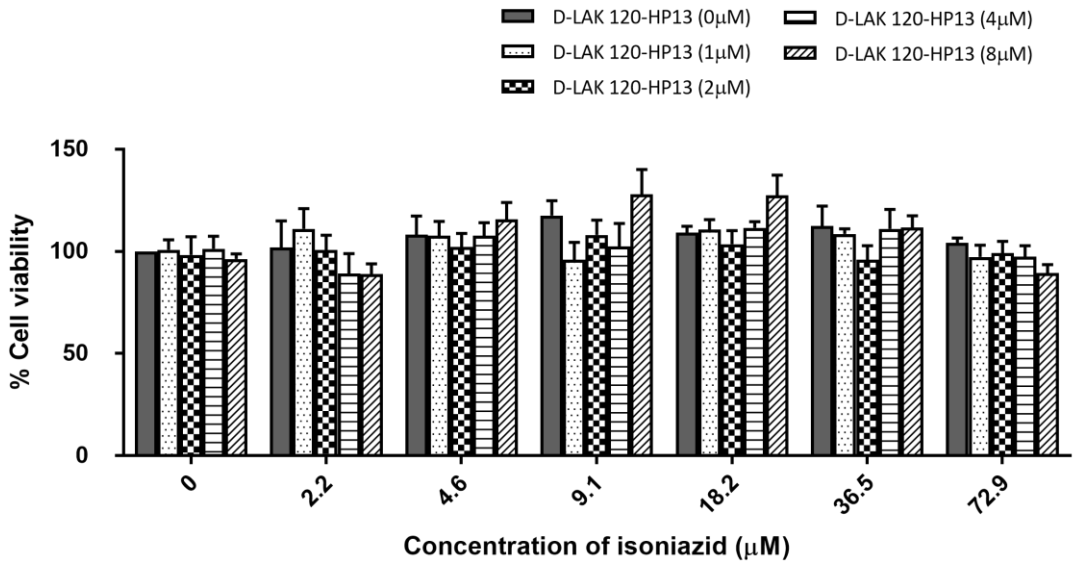

Figure 4.7 Cytotoxicity study of combinations of D-LAK120-HP13 and INH on A549 cells. The cells were incubated with the combination of D-LAK120-HP13 and INH at various concentrations for 24 h before MTT assay was carried out, data were presented as mean ± SD, (n=3).

4.2.2 In vitro bacterial inhibitory *assay of D-LAK peptides and anti-TB agents alone or in combinations against MDR clinical isolates, virulent Mtb H37Rv and Mtb Bleupan*

Resazurin microtiter assays (REMA) were performed to understand the *in vitro* bacterial inhibitory capacity of six different antimicrobial agents (two D-LAK peptides and four existing anti-TB drugs) on five *Mtb* strains (four MDR strains and the drug susceptible H37Rv) (Table 4.1). In addition, bioluminescence measurement was performed to evaluate the activity of these antimicrobial agents and delamanid on *Mtb* Bleupan. The minimum inhibitory concentration (MIC) of each anti-TB agent was defined either by the lowest concentration remained in blue in the REMA or 1-log reduction in bioluminescence as compared with untreated controls. Both D-LAK peptides did not show antimicrobial effect on any of the *Mtb* strain, even at their highest tested concentration of 128 μM. Higher concentration was not used due to the solubility issue in 7H9O medium. As compared with the drug susceptible *Mtb* strain H37Rv, all the four MDR clinical isolates clearly demonstrated resistance towards the two first-line anti-TB drugs, rifampicin and isoniazid, as reflected by their much higher MICs. Potent bacterial inhibitory effect was shown by both first-line anti-TB agents against H37Rv. Their MIC values against H37Rv were found to be at least 25 times lower than that of MDR clinical isolates. Susceptibility of H37Rv towards both first-line drugs was significantly higher than that of *Mtb* Bleupan ($p < 0.01$) by student's t-test.

Capreomycin, a second-line anti-TB agent, demonstrated satisfactory inhibitory effect against all mycobacterial strains tested. The MICs of capreomycin ranged from 2.71 to 4.69 μM on different *Mtb* strains. On the contrary, colistin did not show any inhibitory effect on any of the *Mtb* strains, even at the highest studied concentrations. This observation was reasoned by the absence of lipooligosaccharides (LOS) target in *Mtb* for the action of the drug, therefore it was not studied further. In addition, *Mtb* Bleupan was shown to be susceptible to delamanid, a new FDA-approved MDR-TB drug, which was included as reference for its reported mode of action on keto- and methoxy-mycolic acids synthesis in *Mtb*.

Table 4.1 MIC of anti-TB agents against drug-susceptible Mtb H37Rv and Mtb Bleupan strain and MDR clinical isolates 03M, 08M, 08MB and GB2. MIC is the minimum inhibitory concentration defined by the lowest concentration remained in blue in the Resazurin microtiter assays or 1-log reduction in bioluminescence as compared with untreated controls, expressed as mean ± SD, (n=3).*

Anti-TB agent	MDR clinical isolates				Drug-susceptible strains	
	MIC (μM)					
	03M	**08M**	**08MB**	**GB2**	**H37Rv**	**Bleupan***
D-LAK120-A	>128	>128	>128	>128	>128	>128
D-LAK120-HP13	>128	>128	>128	>128	>128	>128
RIF	>121	>121	14.2 ± 1.5	5.1 ± 2.2	0.190	0.5 ± 0.2
INH	20.1 ± 2.6	>730	>730	>730	0.8 ± 0.3	6.9 ± 2.3
CAP	4.7 ± 2.9	3.1 ± 1.2	3.3 ± 1.3	2.7 ± 1.8	4.1 ± 1.2	2.6 ± 0.9
CST	>86	>86	>86	>86	>86	>1730
DLM	--	--	--	--	--	0.2 ± 0.1

The bacterial inhibitory efficiency of first-line anti-TB drugs and their combinations with D-LAK peptides were evaluated using chequerboard assay. Interactions between anti-TB agents were assessed and represented by the fractional inhibitory concentration index (FICI); it has been well-established that a FICI of < 0.5, indicative of a 4-fold reduction of MIC of each agent in the combination, is considered as synergistic interaction between two agents[257]. When D-LAK peptides were used in combination with rifampicin or isoniazid against MDR-TB strains, the FICIs were all < 1 (Table 4.2). The result suggested that D-LAK peptides exert at least additive effect with the two first-line drugs.

D-LAK peptides in combination with rifampicin was shown to have a broader efficacy as indicated by their antimicrobial activity against all the studied MDR clinical isolates. Except the combination of rifampicin and D-LAK120-HP13 on the 08M strain, FICIs of D-LAK peptide in combination with rifampicin were all < 0.5, demonstrating their synergistic interaction on the MDR strains. This synergy of combinations also resulted in a drastic reduction of effective concentration of rifampicin, which was 2.5 to 40 times lower than when it was used alone. Moreover, being the most impervious strain, 08M strain was not susceptible to any single agent at the highest tested concentrations: D-LAK peptides at 128 μM; rifampicin at 121 μM; or isoniazid at 730 μM. The growth of 08M strain was successfully inhibited by combining D-LAK120-A peptide (32 μM) and rifampicin (12.2 μM), showing the synergistic interaction of the two agents.

D-LAK peptides in combinations with isoniazid were effective against 03M strain and 08MB strain in a synergistic manner, with a more potent effect on 08MB strain. In the combinations with either D-LAK peptides, effective concentration of isoniazid was reduced by 40 times and 4 times against 08MB and 03M respectively when compared with using isoniazid alone. FICI of D-LAK peptides in combination with isoniazid was not determined on 08M and GB2 strains, as an inhibitory effect was not observed at their highest tested concentrations, i.e. D-LAK peptide at 32 μM and isoniazid at 146 μM. Through understanding the nature of interaction of the combinations, this antibacterial assay has clearly demonstrated that combining D-LAK peptides with first-line anti-TB drugs, rifampicin and isoniazid, is a promising strategy in re-sensitising the MDR-TB strains towards exisiting anti-TB drugs.

Table 4.2 Effect of D-LAK peptides in combination with RIF or INH against MDR clinical isolates. MIC is the minimum inhibitory concentration defined by the lowest concentration remained in blue in the resazurin microtiter assays, (n=3).

		MIC in combination (μM)				FICI	Interaction
Combination	**MDR strain**	**D-LAK120-A**	**D-LAK120-HP13**	**RIF**	**INH**		
D-LAK120-A + RIF	03M	32		3.04		**<0.28**	synergistic
	08M	32		12.2		**<0.35**	synergistic
	08MB	32		3.04		**<0.46**	synergistic
	GB2	16		0.76		**<0.28**	synergistic
D-LAK120-HP13 + RIF	03M		32	3.04		**<0.28**	synergistic
	08M		32	48.7		<0.65	additive
	08MB		32	3.04		**<0.46**	synergistic
	GB2		32	0.76		**<0.26**	synergistic
D-LAK120-A + INH	03M	32			4.60	**<0.48**	synergistic
	08M	>32			>146	ND[1]	--
	08MB	16			18.25	**<0.15**	synergistic
	GB2	>32			>146	ND	--
D-LAK120-HP13 + INH	03M		32		4.60	**<0.48**	synergistic
	08M		>32		>146	ND	--
	08MB		8		18.3	**<0.09**	synergistic
	GB2		>32		>146	ND	--

[1]ND stands for not-determined, no inhibitory effect at highest tested concentration: 32 μM for D-LAK peptides and 146 μM for isoniazid.

For *Mtb* Bleupan, bacterial inhibitory activity of combinations of D-LAK peptides with either rifampicin, isoniazid or capreomycin was determined by bioluminescence measurement (Table 4.3). The MIC_{50} of each anti-TB agent was determined using sigmoidal-response (variable slope) algorithm. D-LAK peptides were ineffective against *Mtb* Bleupan when they were used alone. However, combinations of D-LAK peptides with anti-TB agents reduced the MICs of all the agents compared to that when they were used alone. Notably, the concentration of D-LAK peptides used in combination was reduced by 30-fold compared to the highest concentration tested for single peptides. With a small amount of D-LAK peptides, substantial reductions in effective concentration of the first-line anti-TB drugs were achieved; with a four-fold and two-fold reduction for rifampicin and isoniazid, respectively. Conversely, the reduction in capreomycin concentration when used in combinations with the D-LAK peptides was not evident. Combinations of D-LAK peptides with rifampicin displayed a highly synergistic relationship represented by an FICI of < 0.043 with D-LAK120-A, and < 0.087 with D-LAK120-HP13 (Table 4.4). Comparing with the results observed in MDR-TB isolates, this high-level of synergy might be attributed to the intrinsic drug susceptibility of *Mtb* Bleupan. Modest synergy was observed when D-LAK peptides were used in combination with isoniazid, of which D-LAK120-HP13 demonstrated a better effect with a FICI of < 0.5. On the other hand, the interaction of D-LAK peptides with capreomycin was additive, which suggests that the D-LAK peptides were not as useful in assisting the action of capreomycin against *Mtb* Bleupan when compared to that of rifampicin and isoniazid.

Table 4.3 MIC_{50} of anti-TB agents alone and in combination against Mtb Bleupan strain. MIC_{50} was determined using sigmoidal-response (variable slope) algorithm, expressed as mean ± SD, (n=3).

Anti-TB agent	MIC_{50} alone (μM)	MIC_{50} in combination (μM)				
		D-LAK120-A	D-LAK120-HP13	RIF	INH	CAP
D-LAK120-A	>128			0.27 ± 0.11	0.67 ± 0.29	0.31 ± 0.06
D-LAK120-HP13	>128			0.57 ± 0.10	3.91 ± 3.01	0.66 ± 0.34
RIF	0.09 ± 0.01	0.02 ± 0.01	0.02 ± 0.01			
INH	3.72 ± 0.95	1.46 ± 0.58	1.67 ± 0.07			
CAP	0.41 ± 0.09	0.40 ± 0.11	0.38 ± 0.25			
CST	>1730					
DLM	0.09 ± 0.02					

Table 4.4 FIC index of D-LAK peptides in combination with various antibiotics against Mtb Bleupan strain.

Anti-TB agent	RIF	INH	CAP
D-LAK 120-A	**<0.043 ± 0.016**	<0.58 ± 0.04	<0.82 ± 0.03
D-LAK 120-HP13	**<0.087 ± 0.001**	**<0.46 ± 0.10**	<0.60 ± 0.02

4.2.3 In vitro *and* ex vivo *mycobactericidal activity of D-LAK peptides, rifampicin or isoniazid alone or in combinations against Mtb clinical isolates*

In the previous section, combinations of D-LAK peptides with rifampicin and isoniazid demonstrated significant inhibitory effect on the growth of MDR-TB strains *in vitro* using the REMA colorimetric assay. In particular, a potent antimicrobial activity was observed on 03M and 08MB strains, as reflected in their respective FIC indices. As a result, these combinations were subjected to further studies to evaluate their mycobactericidal ability *in vitro* and *ex vivo*. When D-LAK peptides were used in combination with rifampicin or isoniazid, their effective concentration was reduced to 16 to 32 μM. However, at these concentrations, the peptides were cytotoxic in mammalian cells. In order to reduce toxicity, concentration of peptides used in the combination in the mycobactericidal assay was conducted at 8 μM or below.

Both 03M and 08MB strains were incubated with different concentrations of D-LAK peptides, rifampicin or isoniazid, either alone or their combinations, for seven days. Since 03M demonstrated a higher sensitivity towards isoniazid and 08MB demonstrated higher sensitivity towards rifampicin, the mycobactericidal activity of combinations of D-LAK peptides with isoniazid and rifampicin were evaluated on 03M and 08MB, respectively. The growth of challenged bacteria was then evaluated on the agar plates by counting the colony-forming unit (CFU), a test to determine any bactericidal activity of the combination. For 03M strain, both D-LAK peptides and isoniazid demonstrated *in vitro* bactericidal effect in a concentration-dependent manner when they were used alone (Fig. 4.8). Significant reduction of bacterial load was shown in D-LAK120-A at 256 μM, D-LAK120-HP13 at 128 μM or above, and isoniazid at 22 μM (1x MIC) or above. When isoniazid was used alone at 1x MIC, almost 1-log reduction of bacteria load was achieved. At 2x MIC, a complete eradication of the bacteria was almost attained. Bactericidal effect was also seen in the combination of D-LAK peptides and isoniazid, in which both agents were used at a lower concentration than when they were used alone. Prominent killing effect was observed when the combination contained 18 μM of isoniazid, regardless of the concentration of D-LAK peptides. Specifically, the combinations of isoniazid with either D-LAK120-A (at 2 μM) and D-LAK120-HP13 (at 4 μM) were more effective than isoniazid alone at 1x MIC, leading to 1-log reduction in bacterial load comparing with the untreated control. Moreover, the combinations with D-LAK120-HP13 at 4 μM achieved the greatest reduction of bacterial load without exhibiting any cytotoxicity. This supports that D-LAK peptides have an assisting character that enhances the action of isoniazid; when used in combination, they

result in the same synergistic interaction deduced from the chequerboard assay. Nonetheless, the two other combinations where isoniazid concentration was reduced to half and D-LAK peptides concentrations were increased to 32 μM, the killing mechanism was completely ineffective. These findings suggest that isoniazid serves as the active agent in the combination.

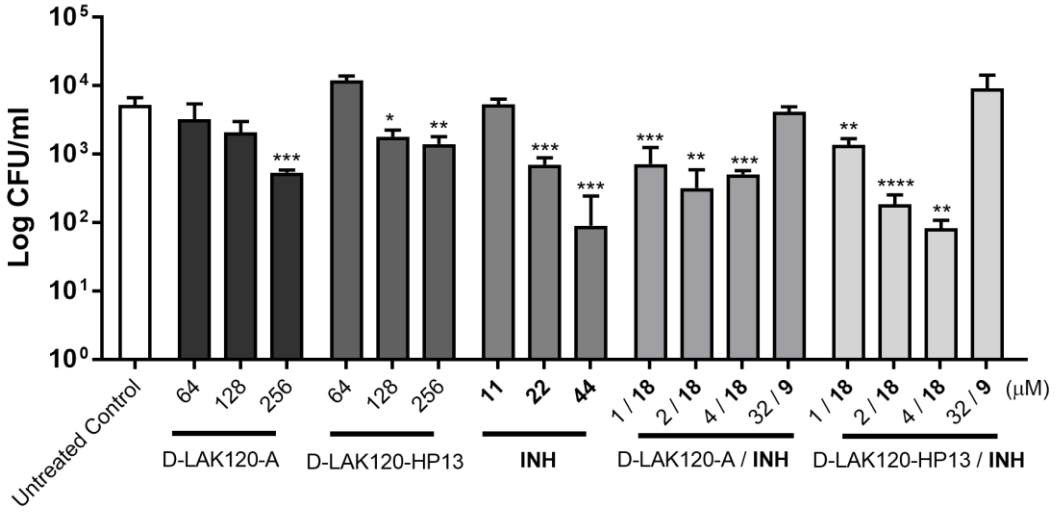

*Figure 4.8 In vitro mycobactericidal study of anti-TB agents against MDR-TB 03M strain. The bacteria were challenged with D-LAK peptides or **INH** alone or their combinations at various concentrations for 7 days before plating was carried out, data were presented as mean ± SD, (n=3). Concentrations for **INH** are shown in **boldface**. Significant difference was determined by one-way ANOVA analysis test followed by Tukey's Comparisons Test, *p<0.05, **p<0.01, compared to the untreated control.*

In vitro mycobactericidal efficiency of D-LAK peptides and rifampicin, either alone or in combination, were studied on MDR-TB strain 08MB (Fig. 4.9). Concentration-dependent killing effect was observed when the anti-TB agents were used alone. Compared with the untreated control, significant reduction ($p < 0.0001$) in bacterial growth resulted at all treatments. Since rifampicin at ½x MIC (7.3 μM) achieved significant mycobactericidal efficiency, lower rifampicin concentrations at 3 μM and 6 μM were employed in combinations with D-LAK peptides.

Amongst all the combinations with D-LAK peptides, those with higher concentration of D-LAK peptides or rifampicin displayed a higher mycobactericidal ability than those with lower concentration of both agents. In particular, D-LAK120-HP13 combined with 6 μM of rifampicin displayed significantly higher *Mtb* killing capacity than when combined with 3

μM of rifampicin ($p < 0.01$), and this also observed when D-LAK120-HP13 was increased to 8 μM. D-LAK120-A at 8 μM with rifampicin at 6 μM achieved the highest mycobactericidal ability, reducing almost 1-log of bacterial load as compared with rifampicin when used alone at ½x MIC, although the difference was not statistically significant. This shows that with the addition of D-LAK peptide, similar or higher *Mtb* killing ability can be achieved with a reduced amount of rifampicin concentration. This indicates the possible assisting role of D-LAK peptides in potentiating mycobactericidal activity of rifampicin.

Overall, the studies of D-LAK peptides in combination with isoniazid against 03M and D-LAK peptides in combination with rifampicin against 08MB, demonstrated the ability of D-LAK peptides to further potentiate the potency of rifampicin and isoniazid against the more sensitive MDR *Mtb* strains.

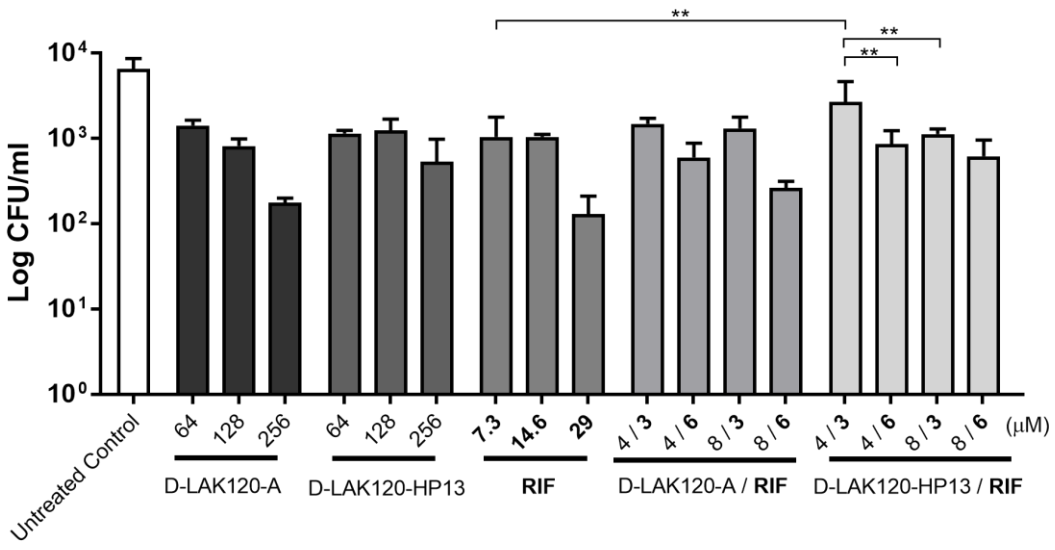

*Figure 4.9 In vitro mycobactericidal study of anti-TB agents against MDR-TB 08MB strain. The cells were challenged with D-LAK peptides or **RIF** in alone or their combinations at various concentrations for 7 days before plating was carried out, data were presented as mean ± SD, (n=3). Concentrations for **RIF** are shown in **boldface**. Significant difference was determined by one-way ANOVA analysis Test followed by Tukey's Comparisons Test, *p<0.05, **p<0.01, ***p<0.001, ****p<0.0001, compared between treatments.*

Ex vivo studies were carried out using combinations of D-LAK peptides with isoniazid against 03M strains (Fig. 4.10). After the infection of differentiated THP-1 cells by 03M strain, the combination was added to the infected cells and incubated for seven days. Mycobactericidal capacity of combinations was then assessed by CFU counting method. D-LAK peptides in combination with isoniazid demonstrated higher mycobactericidal efficiency than when each anti-TB agent was used alone. Treatment with isoniazid alone at 18 μM, or combinations with D-LAK120-A or D-LAK120-HP13 at 1 μM, 2 μM and 4 μM resulted in significant reduction of bacterial load when compared with the untreated control. Albeit modestly, combining 4 μM of D-LAK120-A or D-LAK120-HP13 with isoniazid attained a lower bacterial load in which the latter achieved 1-log bacterial reduction as compared with isoniazid alone at the same concentration. However, the difference was not statistically significant. Furthermore, to understand the role of anti-TB agents in the combination, a high peptide concentration of 32 μM was combined with a low isoniazid concentration at 9 μM. This combination did not demonstrate mycobactericidal activity. Overall, combinations of D-LAK peptide at 4 μM with isoniazid were shown to exhibit the best mycobactericidal capabilities.

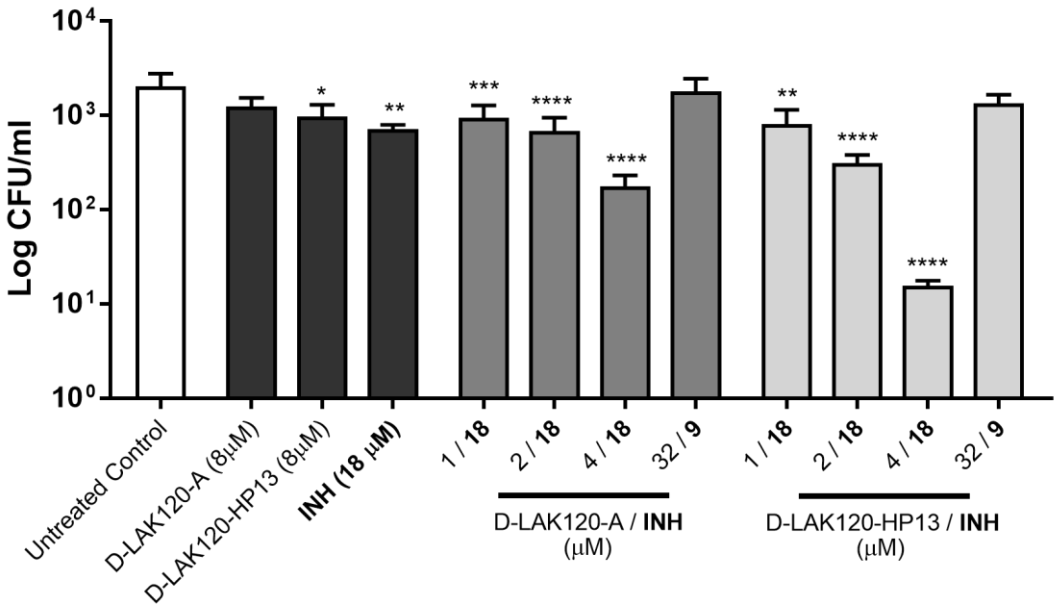

*Figure 4.10 Ex vivo mycobactericidal study of anti-TB agents against MDR strain 03M-infected differentiated THP-1 cells. The infected cells were challenged with D-LAK120-A or its combinations with **INH** or D-LAK120-HP13 or its combinations with **INH** at various concentrations for 7 days before plating was carried out, data were presented as mean ± SD, (n=3). Concentrations for **INH** are shown in **boldface**. Significant difference was determined by one-way ANOVA analysis Test followed by Tukey's Comparisons Test, *p<0.05, **p<0.01, ***p<0.001, ****p<0.0001, compared to the untreated control.*

4.2.4 In vitro *time-kill assay against* Mtb *Bleupan*

To determine the bactericidal activity of each of the anti-TB agents (D-LAK120-A, D-LAK120-HP13, rifampicin, isoniazid, capreomycin, delamanid and colistin), time-kill assays against *Mtb* Bleupan were performed at their respective 0.5x, 1x, 2x or 4x MICs (Fig. 4.11). Rifampicin, isoniazid and capreomycin showed a concentration-dependent effect against *Mtb* Bleupan). The rapid killing effect of capreomycin and rifampicin could already be observed on day 1. More than 1-log reduction in bacterial load (≥ 99% killing) was achieved by 2x and 4x MICs of rifampicin or capreomycin on day 7, which was the end-point of the study. Rifampicin was more effective than isoniazid in killing *Mtb* Blueplan at all tested concentrations. Delamanid had the highest bacterial killing efficacy, reducing 1.5-log of *Mtb* Blueplan on the first day at 1x, 2x and 4x MIC but did not result in eradication of *Mtb* Bleupan at the end point of the study. D-LAK120-A demonstrated a higher killing capacity relative to D-LAK120-HP13 at their highest tested concentrations.

Furthermore, the killing assays were carried out to evaluate the efficiency of the combinations between D-LAK peptides and rifampicin or isoniazid (Fig. 4.12). When used alone at 4x MIC, both rifampicin and isoniazid can effectively eliminate almost 1-log of bacterial population of *Mtb* Bleupan by day 7. Interestingly, the addition of D-LAK peptides could reduce the amount of rifampicin or isoniazid in order to achieve a similar killing efficacy at the end of the study. The concentration of rifampicin required was reduced by two- to four-fold whereas that of isoniazid was reduced by two-fold. The combination of D-LAK peptides and rifampicin was capable of achieving more consistent and rapid killing effect than D-LAK peptides with isoniazid; this combination may also be considered as more beneficial for treatment as both the peptide and rifampicin were used at lower concentrations. The result agrees with the highly synergistic interaction of D-LAK peptides and rifampicin combination as demonstrated in the chequerboard assay.

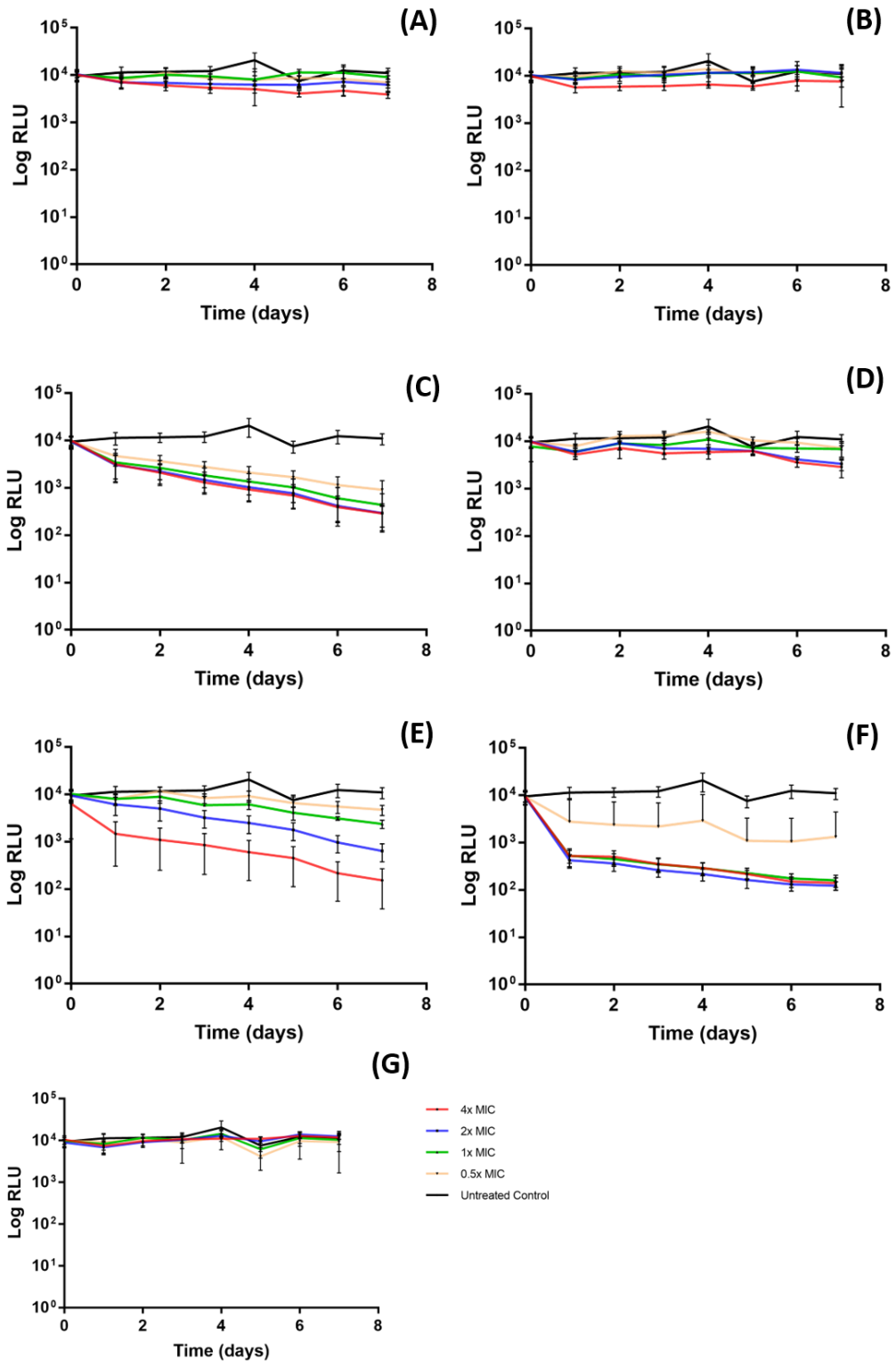

Figure 4.11 Time-kill curves of anti-TB agents when used alone against Mtb Bleupan. (A) D-LAK120-A, (B) D-LAK120-HP13, (C) rifampicin, (D) isoniazid, (E) capreomycin, (F) delamanid and (G) colistin at various concentrations (0.5x, 1x, 2x and 4x MIC) were incubated over 7 days with Mtb Bleupan, Data were presented as mean ± SD, (n=3).

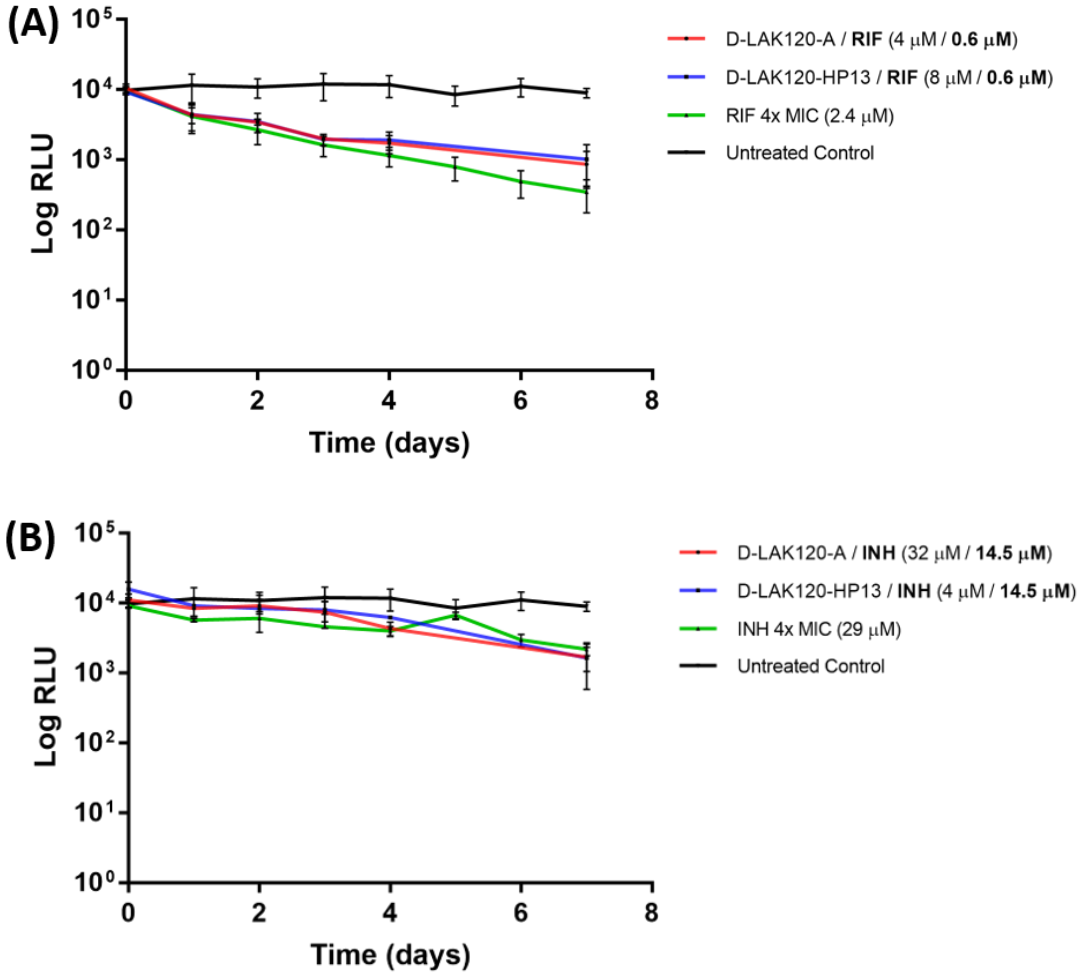

*Figure 4.12 Time-kill curves of combinations between D-LAK peptides and RIF or INH against Mtb Bleupan. D-LAK120-A or D-LAK120-HP13 in combination with **RIF** or 4x MIC RIF alone (A), D-LAK120-A or D-LAK120-HP13 in combination with **INH** or 4x MIC INH alone (B) were incubated over 7 days with Mtb Bleupan. Data were presented as mean ± SD, (n=3).*

4.3 DISCUSSION

Previous studies on D-LAK peptides showed that they possessed a de-clumping effect on mycobacteria. They were also able to inhibit the growth of various *Mtb* strains including drug-susceptible H37Rv strain, MDR clinical isolates GB2 and XDR clinical isolate WYC-11 at a concentration-dependent manner[259]. Other studies using various biophysical techniques such as fluorescence spectroscopy and atomic force microscopy have also shown that high concentration of AMPs is generally required to cause bacterial death via membrane disruption mechanism[285]. D-LAK peptides induced toxicity in mammalian cells at high concentration while the non-toxic concentration was ineffective against *Mtb* clinical isolates[259]. However, D-LAK peptides were able to potentiate the activity of isoniazid against MDR clinical isolate when they were used in combination[259]. The potential synergistic interaction of the combination can reduce the effective concentration of both D-LAK peptides and the first-line anti-TB drug. The aim of this chapter was to investigate the potential of combining D-LAK peptides with first-line anti-TB agents, rifampicin or isoniazid, by evaluating the cytotoxicity of the combinations in mammalian cells, and understanding the nature of interaction of the combinations against a series of MDR-TB clinical isolates and the severely attenuated *Mtb* Bleupan strain.

Here, a number of key findings from the evaluation of antimicrobial activity of anti-TB drugs, D-LAK peptide and their combinations are highlighted. D-LAK peptides alone were not effective in inhibiting the growth of MDR clinical isolates or *Mtb* Bleupan but they were shown to be highly synergistic with rifampicin when used in combinations. Moderate synergy was also shown against *Mtb* Bleupan when D-LAK peptides were used in combinations isoniazid, and additive effect was shown in combination with capreomycin. In the CFU counting assays, the combinations of D-LAK peptides with isoniazid and rifampicin demonstrated mycobactericidal activity against MDR *Mtb* 03M and 08MB strains, respectively. The use of combinations also resulted in a reduced effective concentration of both the peptides and rifampicin or isoniazid *in vitro* and *ex vivo*. Time-kill assay revealed that high killing efficacy on *Mtb* Bleupan was achieved using at least two-fold reduced concentration of rifampicin or isoniazid when they were combined with D-LAK peptides.

MDR-TB clinical isolates exhibit high tolerance towards D-LAK peptides and anti-TB drugs whereas both Mtb *Bleupan and drug-susceptible H37Rv displayed susceptibility towards first-line anti-TB drugs*

Rifampicin and isoniazid are potent antibiotics against *Mtb*. Rifampicin inhibits the activity of the essential DNA-dependent RNA polymerase by binding to the ß-subunit (*rpoB*). This leads to the physical blockage of RNA chain growth, suppressing bacterial protein synthesis[286]. Isoniazid is a prodrug that requires the activation by intracellular catalase-peroxidase which is expressed by *katG*. The catalase-peroxidase plays a critical role in *Mtb* to counteract the oxidative stress experienced by the bacteria. Isoniazid is designed to be oxidized via the action of this peroxidase to produce the active mycobactericidal isonicotinic acid under aerobic conditions. It inhibits the synthesis of mycolic acid through targeting the inhA carrier protein involving in fatty acid synthesis[287]. Therefore, genetic mutation at the *rpoB*, *katG* and *inhA* genes are commonly responsible for the resistance of *Mtb* towards rifampicin and isoniazid. In addition to the genetic mutations reported in resistant *Mtb* strains, alteration in mycobacterial membrane is another way which resistance is developed[288]. This resistance mechanism might also account for the multidrug-resistant phenotype towards first-line anti-TB drugs rifampicin and isoniazid since both drugs act on the intracellular targets of mycobacteria. It is hypothesized that the surface activity of the D-LAK peptides could intervene with the cell wall of drug-resistant *Mtb* strains potentially causing bacterial damage, thereby facilitating drug permeation.

To test this hypothesis, *in vitro* and *ex vivo* mycobactericidal assays were previously performed against *Mtb* clinical isolates using D-LAK120-A, D-LAK120-HP13, rifampicin and isoniazid, either alone or in combinations. By evaluating the growth and morphology of *Mtb* colonies using light microscopy, it was reported that the de-clumping effect of D-LAK peptides was observed at a concentration-dependent manner. However, none of the D-LAK peptides managed to achieve complete eradication of *Mtb* clinical isolates at the highest tested concentration of 100 μM[259]. In the present study, bacterial inhibitory activity determined by a colorimetric resazurin assay also revealed the high tolerance of *Mtb* strains towards D-LAK120-A and D-LAK120-HP13 up to the concentration of 128 μM. This shows that although the action of D-LAK peptides on the mycomembrane has led to the de-clumping effect on *Mtb* strains, the concentration might not be high enough to cause membrane disruption[289] and induce mycobacterial lysis. It was suggested that a threshold concentration is critical for AMPs to exert detrimental actions on bacterial membrane[290]. This threshold concentration is determined by the intrinsic ability of the peptide to induce self-

assembly as well as the extrinsic factors such as bacterial membrane composition and fluidity. The distinct feature of high-mycolic acid content in *Mtb* cell envelope renders its comparatively low membrane fluidity than Gram-positive and Gram-negative bacteria[291]. This may explain the high tolerance of *Mtb* strains towards the D-LAK peptides, unlike the high efficacy of these peptides against *Pseudomonas aeruginosa* and *Escherichia coli*. The membrane permeabilization activities of AMPs have been extensively reported[19, 292]. They typically act on the membrane through mechanisms such as thinning, pore formation or complete disintegration. The binding between cationic AMPs with the negatively charged components on *Mtb* leads to membrane disruption[194]. Besides, AMPs can interact with membrane surface cell-wall protein such as ATPase and inhibit mycobacterial growth[200]. Apart from destabilization of bacterial membrane, AMPs can also adopt different strategies to interact with lipid membrane[293]. Therefore, the mechanism of D-LAK peptide might not be entirely depending on direct disruption but rather to interact with membrane components and alter its permeability.

Notably, the phenotypic resistance towards either isoniazid or rifampicin varies among the MDR-TB strains; 03M and 08M strains demonstrated high-level resistance towards rifampicin, whereas 08M, 08MB and GB2 strains demonstrated high-level resistance towards isoniazid. Target gene mutation associated with the mode of action of these drugs have been regarded as the main resistance mechanism. However, alternative mechanisms such as overexpression of efflux pump genes has shown increased resistance level in MDR-TB clinical isolates[119]. Moreover, some of the efflux pumps were found to express at higher levels in the presence of antibiotic stress[112]. A better understanding of the expression of efflux pump in the MDR-TB clinical isolates can be gained through sequencing of mycobacterial RNA. All the MDR-TB clinical isolates in this study were susceptible to the capreomycin, a second-line anti-TB agent. Capreomycin, a cyclic peptide antibiotic, targets the intracellular ribosomal subunit blocking protein synthesis in mycobacteria[294]. Capreomycin possesses multiple targets which interacts with *tlyA*-encoded methylations on riboses of both 16S and 23S rRNA, giving rise to its high potency against MDR-TB strains[123]. Another cationic cyclic AMP colistin, a powerful antibiotic against Gram-negative bacteria, has shown to have inhibitory activities towards mycobacteria[295, 296] but its clinical use is limited by the high MIC and systematic toxicity concerns. Concentration up to 512 μg/ml was reported for colistin to exert its effect on *Mtb* strain while sterilization was not achieved[297]. Colistin targets primarily the lipopolysaccharide (LPS) in bacterial outer membrane. It is an antibiotic primarily active against infection caused by Gram-negative bacteria including *Pseudomonas aeruginosa*,

Escherichia coli and *Acinetobacter baumannii*[298]. Since LPS is not present in cell envelope of *Mtb* strains[299], treatment with colistin on *Mtb* did not result in any inhibitory effect at the highest tested concentration of 86 μM in this study.

Synergy detected in combinations of first-line anti-TB drugs with D-LAK peptides

Although the D-LAK peptides were not efficient against MDR-TB clinical isolates as a single agent, it could be used to potentiate the anti-TB efficacy of conventional antibiotics. Similar strategies have been demonstrated by various groups using other AMPs[222, 261]. Thus, combinations of D-LAK peptides and rifampicin or isoniazid were evaluated for their efficacy against MDR-TB clinical isolates using chequerboard assay. It was previously shown in a CFU counting assay that D-LAK120-A and D-LAK120-HP13 could increase the potency of isoniazid against MDR-TB strain GB2 *in vitro* as compared with isoniazid when used alone[259]. The results of the present study showed the efficacy of the combinations towards three additional MDR-TB clinical isolates, 03M, 08M and 08MB strains.

The interaction between two agents in combinations fundamentally denotes by the FICI in which ≤ 1.0 is "synergy" and > 2.0 "antagonism". However, taken into account the possible dilution error, it is later defined that "synergy" is < 0.5, "antagonism" is > 4.0 and "additive" is between 0.5-4.0[300]. Strong synergistic interaction was detected in the combinations of D-LAK peptides with rifampicin against all MDR-TB strains. D-LAK peptides in combination with isoniazid also displayed similar synergistic effect against MDR-TB strains 03M and 08MB, denoted by FICI < 0.5. No antagonism was resulted in any of the combinations. Synergistic effect of AMPs and conventional antibiotics is suggested to be associated with the strong membrane-peptide interaction, leading to the increase in membrane permeability and thereby improving the accessibility of drug molecules[19]. Khara *et al.* has shown that a novel peptide $M(LLKK)_2M$ acts synergistically with rifampicin against rifampicin-resistant *Mtb* strain, possibly as a consequence of peptide-mediated action on the mycobacterial membrane[261]. Similar findings using combination treatment of AMPs, hbD-1 or PG-1, with isoniazid also resulted in the reduced growth of MDR-TB strain RM22 when compared with individual drug treatment[222]. The de-clumping effect exhibited by the D-LAK peptides against *Mtb* clinical isolates indicates that their interaction with mycobacterial cell wall might be an important mechanism which led to the reduction in bacterial load. Since MDR-TB strain can develop resistance by decreasing cell wall permeability to antibiotics, the

synergy of the present combinations suggests that the D-LAK peptides possibly exert a membrane active action on the mycobacterial cell envelope as demonstrated through its de-clumping ability, resulting in the entry of higher amount of rifampicin or isoniazid into the intracellular environment, facilitating them to reach their target sites of action.

Interestingly, combinations of D-LAK120-A or D-LAK120-HP13 with isoniazid was effective against 03M and 08MB strains but not against 08M or GB2 strains. As reference to the antibiogram (shown in Chapter 3), the MDR-TB strains 08M and GB2 strains are streptomycin-susceptible whereas 03M and 08MB strains are streptomycin-resistant. Drug resistance acquired by mycobacteria is believed to be associated with a reduction in their fitness[17]. Studies have demonstrated a marked decrease in virulence or growth yield/rate of certain mycobacterial strains harboring resistance towards rifampicin, isoniazid, aminoglycosides and fluoroquinolones[301, 302]. Mutations leading to significant effect on fitness in streptomycin-resistant strains have been reported previously[303]. It was shown that the *rpsL* gene (Lys42→Asn) mutation significantly reduced fitness and virulence in streptomycin-resistant strains *in vitro*[304, 305]. Consequently, the increase in susceptibility of 03M and 08MB strains towards D-LAK peptide and isoniazid combinations might possibly be explained by their reduced fitness due to the acquired streptomycin resistance. Furthermore, the fact that 08M and GB2 displayed high MICs towards isoniazid might suggest multiple mutations[306, 307] acquired by these strains such as abrogation of drug activation or mutation of drug target which might inactivate isoniazid molecules that have gained entry into the bacteria.

More importantly, by combining D-LAK peptides with antibiotics, the effective concentrations of both agents could be drastically reduced, as much as 40-fold. This could lead to a reduction in overall cytotoxicity and enhanced bacterial inhibitory activity. Altogether, these results suggest that D-LAK peptides effectively enhanced the action of rifampicin and isoniazid towards the resistant *Mtb* strains potentially through their membrane-active action.

Combinations of anti-TB drugs with D-LAK peptides at non-toxic concentration demonstrated in vitro *and* ex vivo *mycobactericidal effect*

Following the demonstration of inhibitory effect of the combinations on *Mtb*, their mycobactericidal efficiency was also assessed. D-LAK peptides revealed the significant

mycobactericidal effect *in vitro* on two MDR-TB clinical isolates, 03M and 08MB, at high concentrations (≥ 128 μM). *In vitro* mycobactericidal assay revealed that rifampicin and isoniazid at 1x MIC could achieve almost 1-log reduction of both MDR-TB strains. This indicated the bactericidal effect of the first-line anti-TB drugs against replicating *Mtb*[42]. D-LAK peptides in combinations with rifampicin or isoniazid demonstrated effective mycobactericidal activity against MDR-TB, 03M and 08MB strains, *in vitro*. The results provided further evidence for the assisting role of D-LAK peptides. D-LAK peptides at low, non-toxic concentrations facilitated the action of isoniazid and rifampicin to eliminate the MDR-TB strains at higher efficiency than when either drug was used alone. Moreover, the increase in concentration of D-LAK peptides enhanced the bactericidal effect of the combinations, suggested that an optimal peptide concentration is a crucial factor to obtain an effective combination. Besides, these findings demonstrated the antibiotics acts as the active agent in the combinations to target the survival of bacteria. D-LAK peptides work within a narrow window, because of its toxic effect when used at high concentration. Therefore, the concentration of isoniazid has become critical and it determines whether the combinations work efficiently and exhibit mycobactericidal effect. This suggests the positive cooperativity of D-LAK peptides to promote the action of antibiotics while reducing their effective concentration, potentially delaying the development of drug resistance.

On the other hand, as observed from the ability of D-LAK peptides to break down the clumping *Mtb*, another possible mechanism of action of the peptides may be ascribed to their interaction with the mycobacterial cell surface components such as trehalose dimycolate (TDM). *Mtb* possess cyclopropanated TDM, enables the aggregation of mycobacterial cells in a tight and definite order, forming structures known as cords[69]. This cording is considered as a virulence factor in *Mtb*. The inability to form cords impaired virulence of *Mtb* in mice[308] and increased sensitivity to rifampicin[309]. Interaction of D-LAK peptides with cell surface component might intervene with the cord structure of *Mtb*, affecting the packing of mycomembrane and in turn alters membrane permeability to antibiotics.

Also, different performances of D-LAK120-A and D-LAK120-HP13 peptides in enhancing bactericidal efficacy in combinations observed in this study suggests the association between the potency of D-LAK peptide and the distinct cell wall properties that are known to exist in different *Mtb* strains. Overall, D-LAK120-HP13 displayed a better safety profile and better bacterial inhibitory performance in combination with isoniazid against MDR-TB. This might be due to the incorporation of proline residue, as reported to reduce hemolytic potential[310] on

one hand, while on the other it increased the peptide conformation flexibility to facilitate penetration and disruption action[185]. The importance of proline hinge on cell penetration efficiency and antimicrobial potency was also shown in the structure-activity analysis of buforin II[186].

With the effective concentration obtained for both D-LAK peptides and isoniazid against MDR-TB 03M strain, *ex vivo* mycobactericidal assay was performed to assess the intracellular anti-TB capacity of the combinations. Differentiated THP-1 cells have been shown as a good model for the study of intracellular residing *Mtb*[311]. THP-1 cells infected with MDR-TB 03M strain was treated with D-LAK120-A, D-LAK120HP13 and isoniazid, either alone or in combinations. Among all the treatments, D-LAK peptides in combination with isoniazid were found to demonstrate the highest potency, achieving a much greater reduction in drug-resistant bacterial load, when compared with isoniazid used alone. This demonstrated the ability of D-LAK peptides to facilitate drug action intracellularly at non-toxic concentrations. In addition, this inefficiency of isoniazid alone can be due to the action of efflux pumps in MDR-TB clinical isolates. Jaiswal *et al.*[312] investigated the effect of efflux pumps in *Mtb* clinical isolates and reported a reduced in MIC towards isoniazid in the presence of efflux pump inhibitors (verapamil, chlorpromazine and reserpine). Further, an increased expression of efflux candidate genes such as Rv0194, Rv2688c and Rv1634 were found in XDR-TB as compared with drug-susceptible clinical isolates, indicating the contributing role of efflux pump to drug resistance[313]. Since MDR-TB strains have been shown to express efflux pump genes constitutively through chromosomal mutations[118], addition of D-LAK peptides might provide a route to overcome the efflux of isoniazid by increasing membrane permeability to promote drug influx or disrupting the electron transport chain[314] which could in turn affect the function of efflux pumps, therefore sustaining the killing action of the drug.

D-LAK peptides combination with rifampicin reveals the highest potency against Mtb *Bleupan*

Combination drug treatment, as the cornerstone of anti-TB therapy, delays the emergence of drug resistance[315] and also reduce effective concentration of each agent to lower the overall toxic effects. The combinations of D-LAK peptides with rifampicin or isoniazid demonstrated higher potency than combination with capreomycin against *Mtb* Bleupan. As reflected in the FICI, highly synergistic interaction was observed between both D-LAK

peptides and rifampicin, followed by D-LAK120-HP13 with isoniazid. Combinations of D-LAK120-A with isoniazid and the two D-LAK peptides with capreomycin were shown to have additive effect. This is primarily ascribed to the high sensitivity of H37Rv towards rifampicin and isoniazid than capreomycin. Comparing between isoniazid and rifampicin, when they were used in combination with D-LAK peptides, their effective concentration was reduced by two and four folds, respectively. Yuan *et al.*[316] reported the association of increased antibiotics susceptibility with the changes in the cell wall composition of *Mtb*. Complete replacement of keto-mycolate with methoxy-mycolate in a recombinant *Mtb* strain was found to be hypersensitive towards the hydrophobic rifampicin and the moderately hydrophobic ampicillin but not the hydrophilic isoniazid. This suggests the disturbance on mycomembrane affects the permeability of hydrophobic drugs preferably. AMPs have been demonstrated to improve the action of rifampicin through their membrane active actions, promoting entry of rifampicin and therefore their accessibility to intracellular targets[317, 318]. Anantharaman *et al.*[319] reported the synergism between rifampicin and *de novo*-designed AMPs, namely ΔFm, ΔFmscr, and Ud, promoting drug access into *E. coli* via the aid of the AMPs' membrane active action. Slama *et al.*[309] demonstrated the inhibition of the formation of a fourth cyclopropanated segment in a *Mtb* mutant leading to reduced cord forming ability and lower tolerance to rifampicin. The lipophilic nature of rifampicin enables the drug to transverse across the lipid rich mycomembrane into the intracellular environment. On the contrary, isoniazid is a hydrophilic drug which is reported to gain access into the cell through the porin channels on *Mtb*[17]. Possible membrane active action of D-LAK peptides could increase the membrane permeability, reducing the resistance for the entry of rifampicin, whereas isoniazid and capreomycin could not gain the benefit to the same extent. On the other hand, Jackson *et al.*[80] also suggested that isoniazid, with its small and non-ionized character at pH between 6-9, is plausible to diffuse through lipid membranes as shown in a liposome swelling experiment. It is however anticipated that mycolic acid layer would render higher resistance for the passive diffusion of isoniazid and therefore the synergy with D-LAK peptides was modest. Moreover, action of capreomycin was not promoted in the combination with D-LAK peptides, which might be due to its different uptake mechanism from isoniazid. Although the explicit role of each type of mycobacterial porins is yet to be verified, uptake of hydrophilic molecules of different sizes is believed to be mediated using different channels[320]. The existence of a cationic-selective porin with a main conductance of 0.7 nS was reported to have transport properties on *Mtb* and is permeable to large, hydrophilic antibiotics such as capreomycin[321]. These findings revealed that D-LAK peptides are highly likely to increase

mycomembrane permeability facilitating the diffusion of hydrophobic and possibly small hydrophilic drug into *Mtb* Bleupan whereas complete membrane disruption was not attained.

In addition, isoniazid displayed concentration-dependent rapid killing of actively growing bacteria while the residual non-replicating bacteria remain unaffected[322]. Combination of D-LAK peptide to isoniazid achieved similar killing effect at a reduced concentration of isoniazid (two-fold reduction), this suggested the action of D-LAK peptide to improve the drug performance perhaps through the enhancement of drug entry to active bacteria and also possible by interacting with the non-replicating bacteria leading to re-sensitization. Unlike isoniazid, the concentration- and time- dependent killing effect of rifampicin was reported in previous a pharmacokinetic study[323]. This effect was also demonstrated in the killing efficiency assay. The combination with D-LAK peptide at non-toxic level effectively reduced effective concentration of rifampicin by at least two-fold. Towanda *et al.*[324] studied the relationship between rifampicin exposure and microbial killing using a pharmacokinetic-pharmacodynamic model of *Mtb*. The results indicated that dosage of rifampicin higher than the current regimen (600 mg/day) could optimize the effect of rifampicin although it might not be tolerable by all patients. This reveals that D-LAK peptides have the potential to enhance the effect of rifampicin through maximizing the tolerable range of concentration. More importantly, since higher concentration of rifampicin is also likely to suppress the selection of resistance, the combination with D-LAK could possibly delay the emergence of rifampicin resistance. Delayed rifampicin resistance was also demonstrated in the synergistic AMP combination against *M. smegmatis*[324]. Future work to investigate the ability of D-LAK peptides in lowering the chance of drug resistance emergence can further unmask its potency in combating *Mtb* and MDR-TB clinical isolates.

Higher tolerance of Mtb *Bleupan towards rifampicin and isoniazid due to disparate culture conditions*

Compare with the virulent H37Rv, *Mtb* Bleupan displayed higher MICs towards rifampicin and isoniazid. This might be due to the differences in growth conditions between solid and broth medium as well as the treatment procedure to prepare for the inoculum. The use of glass beads for the de-aggregation of virulent H37Rv colonies from solid medium possibly induced mechanical disturbance to the outermost capsule layer of the bacteria, leading to the higher permeability of the drugs. Notably, the MICs of rifampicin and capreomycin against *Mtb* Bleupan are comparable to the reported *in vitro* MIC values in other studies on H37Rv[42]

while that of isoniazid was found to be much higher. This is very likely attributed to the static culture condition of *Mtb* Bleupan and the prolonged incubation time of six weeks. *Mtb* Bleupan was grown in broth medium without agitation, this might limit the availability of oxygen for a sub-population of bacteria albeit the additional aeration and vortexing performed twice-weekly throughout the incubation period. *Mtb* is known to possess numerous response and resistance mechanisms to adapt to changes or stress in the surroundings[17]. This poses the chance for a subset of bacteria to develop phenotypic-derived drug resistance conferring higher tolerance to anti-TB drugs[325]. This might explain the isoniazid tolerance demonstrated by *Mtb* Bleupan. Since isoniazid has a high efficacy towards the replicating bacteria rather than the non-replicating *Mtb*[322], the limited availability of oxygen may drive a sub-population towards persistent state[326], resulting in the increased MIC. Furthermore, peroxidase activity is significantly lowered under anaerobiosis leading to reduced isoniazid oxidation, therefore the decreased production of intracellular active isonicotinic acid[327].

The present study has shown the D-LAK peptides potentially facilitate the action of rifampicin and isoniazid against MDR-TB strains when used in combination *in vitro* and *ex vivo*. Since the current MDR-TB regimens consist of highly toxic second- and third-line drugs; the long duration of therapy brings huge impact on patients' compliance. These findings suggest the possibility of re-sensitization of MDR-TB strains towards rifampicin and isoniazid by the aid of D-LAK peptides at non-toxic level. Moreover, the reduced effective concentration of rifampicin and isoniazid through the positive cooperativity of D-LAK peptides could shorten the therapy duration thereby potentially delay the emergence of drug resistance. The remarkable ability of the D-LAK peptides in combination first-line drugs against MDR-TB indicated the prospect for clinical applications. Inhalable spray-dried powder of both D-LAK peptides have been evaluated and revealed a good aerosol performance without substantial effect on their secondary structures[328]. This shows the outstanding physiochemical properties of the peptides to be delivered via pulmonary routes. Hence, *in vivo* studies of the D-LAK peptides with rifampicin or isoniazid combinations to evaluate their bioefficacy, pharmacokinetics and host immune responses would be crucial.

Given the diverse proposed mechanisms of D-LAK peptides, the next step of this study aims to further elucidate their mode of action. *Mtb* Bleupan demonstrated similar behaviors to its parent virulent H37Rv strain in terms of responses towards antibiotic activity and combination synergy, indicating its applicability to be used as a *Mtb* model. In the following

chapters, mechanistic studies employing *Mtb* Bleupan and a fast-growing species *Mycobacterium smegmatis* are described. Using different microscopic and biophysical techniques, peptide-induced direct action on mycomembrane, changes in membrane properties and interaction with membrane components would be demonstrated. This valuable information would inform the next stage development of D-LAK peptides into formulations against MDR-TB. The continuous investigation on the D-LAK peptide and first-line drug combinations could be promising, pathing the development of a novel, safe and efficient therapeutics against MDR-TB.

Chapter 5 Mechanism of action of D-LAK peptides in combination with anti-TB drugs against *M. smegmatis*

5.1 INTRODUCTION

In the previous chapter, D-LAK peptides were found to enhance the antimicrobial activity of two first-line anti-tuberculosis (anti-TB) drugs, rifampicin and isoniazid, against MDR *Mtb* clinical isolates, suggesting that the antimicrobial peptides (AMPs) work synergistically with these two first-line anti-TB drugs. The waxy lipid-rich mycomembrane of *Mtb* is known to be one of the major barriers impeding drug entry. It is also reported to contribute to the drug resistance of *Mtb*[255]. The demonstrated synergy between AMPs and rifampicin or isoniazid may be attributed to the surface activity of the D-LAK peptides on MDR-TB clinical isolates shown in previous studies[259]. The peptides were shown to effectively break down the heavy clumping of mycobacteria and prevent bacterial cell aggregation. It is therefore hypothesized that this action of D-LAK peptides can modify the surface properties of the *Mtb* cell envelope, enhancing the efficacy of anti-TB drugs.

The first objective of this study was to investigate the surface-active action of D-LAK peptides on mycobacteria using transmission electron microscopy and confocal microscopy. The second objective of this study was to understand the effect of D-LAK peptides and various antibiotics on mycobacterial membrane properties and metabolism, thereby gaining insights to the synergy between the anti-TB agents in combinations. To investigate how *M. smegmatis* responds to the challenge of D-LAK peptides and antibiotics, three different techniques were employed. Changes in bacterial membrane properties were measured with two fluorescent probes, Laurdan and trans-1,6-diphenyl-1,3,5-hexatriene (DPH). High-resolution magic angle spinning (HR-MAS) and liquid-state nuclear magnetic resonance (NMR) metabolomics were exploited to elucidate the induced metabolic changes in the bacteria. Furthermore, D-LAK120-A and D-LAK120-HP13 exhibited different levels of synergy with rifampicin and isoniazid. The proline residue was demonstrated to enhance the antimicrobial activity of peptide against Gram-negative bacteria but this was not always the case when applied against *Mtb* H37Ra[188]. This suggests that structural differences between the proline-containing D-LAK120-HP13 and the proline-free D-LAK120-A could possibly affect their mode of action. This work also aimed to compare the mechanisms between the proline-containing and proline-free analogues against mycobacteria.

M. smegmatis has been a popular model for mycobacterial studies and it was also shown to possess the closest profile to MDR-TB strains as compared to other fast-growing mycobacterial species[329]. *M. smegmatis* is chosen as a model bacterium in this study also due to its fast-growing nature compared to *Mtb*, testing time could be reduced from two months

to a week. Besides, the non-pathogenic nature of *M. smegmatis* allows experiments to be carried out in an environment with less safety constraints, so more assays were possible.

DPH and Laurdan fluorescent probes were employed to study the changes of mycobacterial membrane in response to the challenge of D-LAK peptides and antibiotics. DPH is a rigid hydrophobic rod-like fluorescent probe, with an all-trans polyene structure that aligns along the lipid acyl chains in the phospholipid bilayer[330, 331]. DPH anisotropy allows the estimation of acyl chain mobility and is commonly used to determine structural and dynamic properties of lipid bilayers. During the measurement, vertically polarized light excites the probes embedded in the membrane, resulting in the fluorescence emission which is detected in the movable polarizer (Fig. 5.1). The measurement of the rotational diffusion of the probe in the restricted region is denoted by the anisotropy (r) (calculation as shown in Chapter 3). Since this estimation reflects the packing order of the acyl chain, the notion of anisotropy is also considered as an interpretation of membrane rigidity, in which a more rigid membrane displays a higher value of anisotropy. Laurdan is another fluorescent probe which is amphipathic in nature with a high sensitivity of excitation and emission spectra in terms of the physical state of the membrane[332]. The fluorescent moiety of Laurdan probe lies within the shallow region of the bilayer, predominantly reporting the stiffening or dehydration of the lipid carbonyls[333] (Fig. 5.2). Laurdan fluorescence at different wavelengths is quantified by general polarization (GP) in which higher value of GP represents more dehydration and reduced order of the membrane. The application of Laurdan probe was also reported in other similar studies. The effect of a cyclic hexapeptide, cWFW, was studied with Laurdan probe on the membrane of *Bacillus subtilis*[334]. Also, Laurdan was employed to measure the difference in the organization of bacterial membrane through the challenge of membrane-associated protein flotillins[335] and bacterial actin homologue MreB[336].

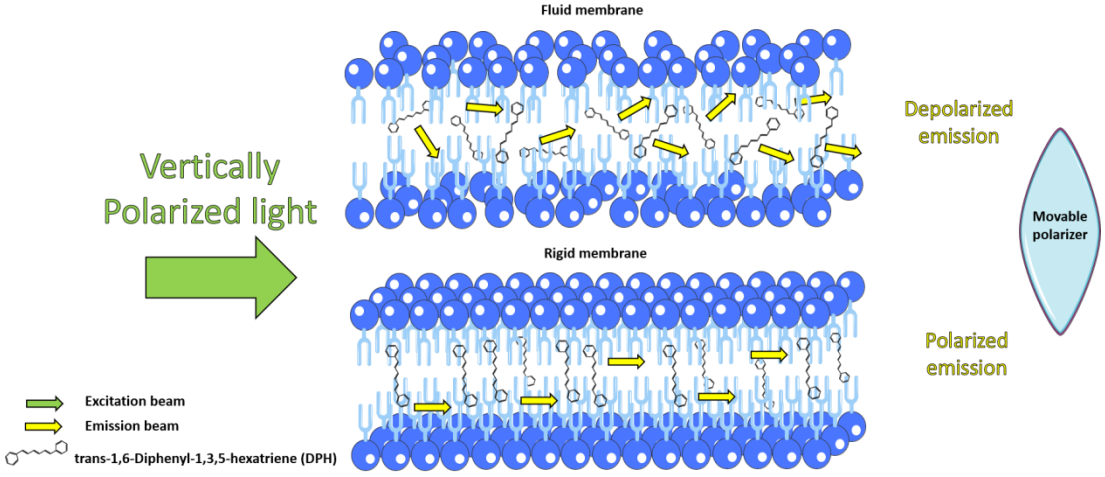

Figure 5.1 Schematic diagram of DPH anisotropy principle. Membrane fluidity can be monitored using DPH fluorescent probe. The hydrophobic probe aligned parallel to the lipid acyl chains in the bacteria membrane. Vertically polarized light is generated and excites the embedded probes resulting in the fluorescence emission detected in the movable polarizer. The intensity of vertical (I_{VV}) and horizontal (I_{VH}) polarized light are measured relative to the excitation beam. Membrane with higher fluidity allows tumbling rotation of embedded probes resulting in depolarized emission denoted by lower anisotropy (r). On the contrary, rigid membrane restricts rotation movement of DPH probes leading to polarized emission in the horizontal direction thus displaying a higher r.

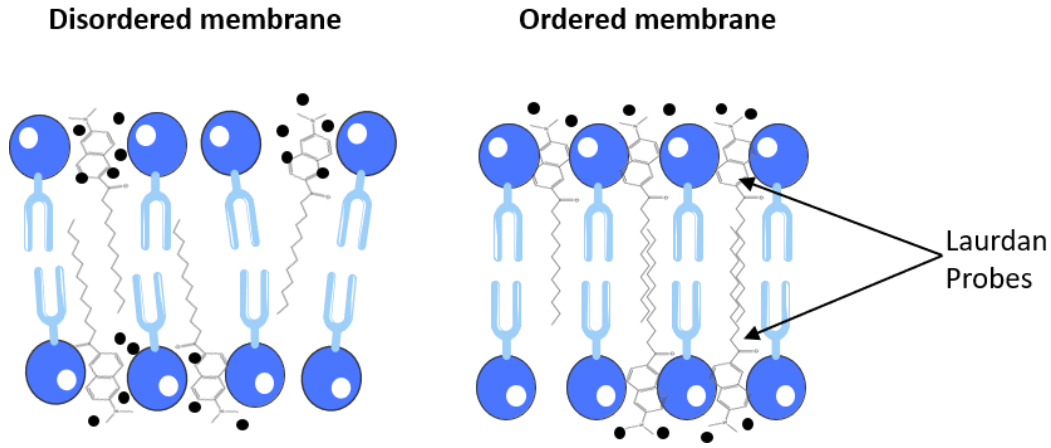

Figure 5.2 Schematic diagram of Laurdan fluorescent probes. Laurdan probes reside at the interfacial region of the membrane with the Naphthalene moiety situating towards the aqueous environment. Disordered membrane experiences more hydration by water molecules (black dot) while an ordered membrane experiences less hydration as the probes are restricted by the tight arrangement of lipid molecules. General polarization (GP) denotes the order of the membrane such that an increasing GP value corresponds to a more ordered membrane.

NMR metabolomics can be used to detect perturbations of metabolome of cell extracts to monitor disease progression and drug response. The ^{1}H NMR spectra collection is followed by multivariate data analysis. Principal component analysis (PCA) is done through reducing each NMR spectrum into a single point in a two-dimensional scores-plot. The generation of score plot allows the inspection of clusters and the identification of general trends and outliers. Further, orthogonal projections to latent structures discriminant analysis (OPLS-DA) is performed by maximizing the separation between control and each treatment condition. This provides further useful information such as the metabolic resonances that have the most discriminatory importance in the data and the reliability and predictability of statistical models. Through comparing the metabolite profile of mycobacteria subjected to different treatment conditions, it is possible to discern the respective influence of anti-TB agents, thus reasoning the synergy mechanisms of the drug combinations. In order to avoid addition effect on the erosion of bacterial capsule, the culture condition adopted in this study was employed without any detergent or agitation. This is different from usual broth culturing practice of mycobacteria[215, 261], but was essential to this study to minimize manipulation of bacterial morphology.

HR-MAS is a NMR technique that has been applied in TB studies. It is an effective means to study biological matrixes and the cell structure of intact bacteria in order to elucidate the actions of antibiotics. Hanoulle *et al.* discovered the unidentified 'ethionamide*' as the active antimycobacterial ethionamide derivative by studying ethionamide activity in *M. smegmatis* using HR-MAS[337]. Inhibition of cyclopropanation in mycolic acids of *Mycobacterium bovis* Bacillus Calmette-Guérin by another anti-TB agent, thiacetazone, was also detected by HR-MAS[338]. This demonstrated the potential of the technique to explore drug action associated with the unique lipid-rich cell envelope of mycobacteria. HR-MAS enables a non-destructive analysis which minimizes the interference to the samples as well as the possible spontaneous modification/oxidation of metabolites that may be resulted in assays which require extraction/purification processes[339]. Together with the application of DPH and Laurdan membrane probe assays, HR-MAS was demonstrated to be useful to investigate the mechanism of anti-TB agents especially for those targeting mycomembrane.

5.2 RESULTS

5.2.1 In vitro *bacterial inhibitory activity against* M. smegmatis

The antimicrobial activity of six anti-TB agents were evaluated by resazurin assay either alone or in combination with D-LAK peptides against *M. smegmatis* mc^2 155 (Table 5.1). This bacterial inhibitory assay was performed both in the presence and absence of tyloxapol. Notably, both D-LAK peptides, rifampicin and isoniazid showed a more potent anti-TB effect in the presence of tyloxapol while the activity of colistin and capreomycin were not affected. This might be the result of the capsule-shedding effect of tyloxapol which removed the outermost barrier for the passage of anti-TB agent[340].

The fractional inhibitory concentration indices (FICI) of combination of rifampicin, isoniazid, colistin or capreomycin with each of the D-LAK peptides were calculated (Table 5.2). The FICI is widely used for the interpretation of antimicrobial interaction assessment of such that FICI for "synergy" is < 0.5, "antagonism" is > 4.0 and "additive" is between 0.5-4.0[300]. Overall, the effect of the combinations was additive. Only combinations of capreomycin and the D-LAK peptides were modestly synergistic against *M. smegmatis*. In the absence of tyloxapol, the minimum inhibitory concentration (MIC) of each agent in these combinations was reduced to more than half when it was used in combination, as compared to when it was used alone. The synergistic effect was more pronounced when the combination was used in the presence of tyloxapol.

Interestingly, the two D-LAK peptides demonstrated very different behaviours when used in combination with rifampicin. Without tyloxapol, D-LAK120-A showed no synergy with rifampicin but approached an antagonistic effect, with a FICI of 2.5 which was the highest among all combinations. In contrast, though modestly, the combination of D-LAK120-HP13 with rifampicin was able to reduce MIC of both agents to half of that required when they were used alone. Similar effect was observed when D-LAK120-HP13 was used in combination with colistin but not in the combination with D-LAK120-A. The difference in assisting ability of the two D-LAK peptides towards different drugs suggests their disparate mechanism of action. The same experiments were performed with isoniazid but no synergy effect with either peptide was observed. Besides, isoniazid showed a high MIC against *M. smegmatis* which might be due to the inefficient activation of the prodrug in addition to the intrinsic resistance of the bacteria.

Based on the above observation, combinations of D-LAK peptides with rifampicin and capreomycin were chosen for the further investigation of their underlying mechanisms in the mycobacterial growth response assay.

Table 5.1 MIC_{50} of anti-TB agents alone and in combination against M. smegmatis mc^2 155. The MIC_{50} of the D-LAK peptides and antibiotics rifampicin (RIF), isoniazid (INH), capreomycin (CAP) and colistin (CST) when used alone and in combinations are listed for comparison.

Anti-TB agent	MIC_{50} alone (μM)	MIC_{50} in combination (μM)					
		D-LAK120-A	D-LAK120-HP13	RIF	INH	CST	CAP
D-LAK120-A	1.68 ± 0.43			1.56 ± 0.17	0.39 ± 0.17	1.73 ± 0.49	0.62 ± 0.07
D-LAK120-HP13	1.80 ± 0.39			0.77 ± 0.08	0.78 ± 0.01	0.66 ± 0.08	0.85 ± 0.15
RIF	38.1 ± 5.83	59.8 ± 1.39	14.6 ± 2.91				
INH	203 ± 92.3	197 ± 12.3	228 ± 18.2				
CST	4.44 ± 0.72	3.31 ± 0.90	2.96 ± 1.29				
CAP	1.35 ± 0.25	0.46 ± 0.18	0.67 ± 0.28				
D-LAK120-A*	0.82 ± 0.07			0.91 ± 0.05	0.53 ± 0.09	0.39 ± 0.12	0.09 ± 0.01
D-LAK120-HP13*	0.63 ± 0.03			0.75 ± 0.22	0.70 ± 0.10	0.19 ± 0.09	0.14 ± 0.01
RIF*	19.9 ± 3.04	9.33 ± 4.38	8.88 ± 1.44				
INH*	199 ± 46.9	228 ± 82.6	179 ± 31.0				
CST*	5.44 ± 1.66	4.25 ± 3.32	2.64 ± 0.70				
CAP*	1.72 ± 0.43	0.58 ± 0.24	0.52 ± 0.28				

*With tyloxapol

Table 5.2 FIC index of D-LAK peptides in combination with various antibiotics against M. smegmatis mc^2 155.

Anti-TB agent	RIF	INH	CST	CAP
D-LAK120-A	2.50 ± 0.14	1.19 ± 0.30	1.77 ± 0.13	0.71 ± 0.04
D-LAK120-HP13	0.81 ± 0.02	1.55 ± 0.11	1.03 ± 0.32	0.97 ± 0.20
D-LAK120-A*	1.58 ± 0.10	1.55 ± 0.18	1.26 ± 0.16	0.45 ± 0.13
D-LAK120-HP13*	1.64 ± 0.02	1.78 ± 0.11	0.79 ± 0.28	0.53 ± 0.20

*With tyloxapol

5.2.2 Assessment of action of D-LAK peptides by transmission electron microscopy

The action of D-LAK peptides on *M. smegmatis* was first investigated to verify, as suggested from their activity on *Mtb* MDR clinical isolates, their action on the mycobacterial cell wall using microscopic techniques. Transmission electron microscopy (TEM) was exploited to visualize the effect of D-LAK peptides on the ultrastructural changes of *M. smegmatis* (Fig. 5.3). Untreated cells had lipid inclusions, regular rod shape cell body with well-defined intact cell membranes and homogeneous cytoplasm (Fig. 5.3A). A distinct cell envelope was visible with the cytosol surrounded by the plasma membrane, additionally bound by an internal and an outer electron dense layer[65, 341]. Slight displacement of cell content in some untreated cells was ascribed to the sample preparation process. After the bacteria were treated with D-LAK120-A (Fig. 5.3B) and D-LAK120-HP13 (Fig. 5.3D) at 1x MIC of for 5 mins, ruffling of the membrane was observed. Detachment of inner cell membrane from the outer cell wall indicated observable cytoplasmic retraction. This phenomenon was also reported when *Escherichia coli* and *Bacillus subtilis* were exposed to a tick defensin derived AMP[342]. Ernst *et al.* presented similar findings in which granulysin demonstrated membrane active action towards *Mtb* (Erdman strain) leading to inner cell membrane detachment as observed in osmotic lysis[343]. The reduction in membrane uniformity suggests a cell penetrating action of D-LAK peptides. Notable intracellular changes including clumped cytosol and increased amount of mesosome formation were also caused by the action of D-LAK peptides. This observation is similar to other studies in which intracellular membranous mesosome structures were found in Gram-negative and Gram-positive bacteria when exposed to cationic antimicrobial peptides[170, 344]. The formation of mesosomes was suggested to be a repair mechanism adopted by bacteria to combat cell lysis[345]. Prolonged treatment by D-LAK peptides for 30 min resulted in large scale of cell lysis and cell debris could be seen (Fig. 5.3C and 5.3E). This suggests that D-LAK peptides were able to disturb cell membrane of *M. smegmatis*, leading to membrane rupture and the release of intracellular contents.

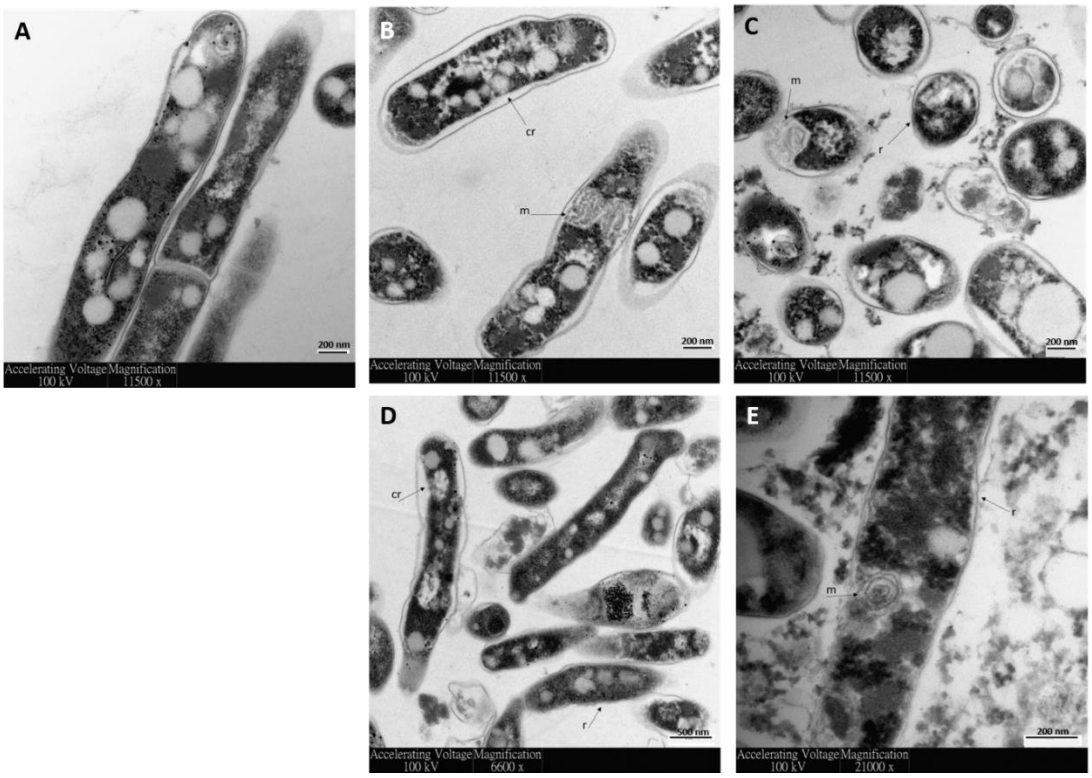

Figure 5.3 TEM images of M. smegmatis mc^2 155 exposed to D-LAK peptide treatment. As compared with control (A), ultrastructure morphological changes can be observed when M. smegmatis mc^2 155 was treated with 1x MIC D-LAK120-A (B,C) or D-LAK120-HP13(D,E) for 5 min and 30 min respectively. r – membrane ruffling, cr – cytoplasmic retraction, m – mesosome.

5.2.3 Assessment of action of D-LAK peptides by confocal microscopy

Confocal microscopy study was performed to examine the membrane activity of D-LAK peptides in the potentiation of drug entry or interaction with the bacteria. *M. smegmatis* was treated with sub- or supra- MIC of D-LAK120-A, D-LAK120-HP13, isoniazid or rifampicin (Fig. 5.4). Rifampicin and isoniazid were used as negative controls given that they do not target mycobacterial membrane directly. Only cells treated with D-LAK peptides (Fig. 5.4B-E), but not rifampicin nor isoniazid (Fig. 5.4F/G), were stained with 150 kDa fluorescein isothiocyanate (FITC) dextran. FITC-dextran has been employed to investigate the membrane permeabilization activity of different antimicrobial peptides[346, 347]. Ladokhin *et al.* [348] reported the escape of 4 kDa dextran loaded in lipid unilamellar vesicles after the exposure to antimicrobial peptide melittin while the release of the 50 kDa analogue was much less. This suggested the ability of melittin to form pores on membrane with a defined size of 25-30 Å in diameter. On the contrary, other antimicrobial peptides were found to facilitate the release of dextran at a range of different sizes, yet complete leakage was never attained[346, 347]. Due to the resolution of the image and the large size of dextran used in this study, it is difficult to distinguish whether the signal observed was inside or on the surface of the bacteria. Nonetheless, this shows that the D-LAK peptides could potentially enhance dextran adsorption on the membrane and/or increase dextran diffusion into the intracellular compartment. It is possible that the same functionality of D-LAK peptide, which caused the de-clumping of *Mtb*[259], enabled the dextran to adsorb to the surface of *M. smegmatis*. Moreover, Khara *et al.*[261] reported similar results after the exposure of *M. smegmatis* to cationic peptide $M(LLKK)_2M$ with 150 kDa FITC-dextran. They concluded that the peptide action resulted in the promotion of passive diffusion of FITC-dextran into the intracellular environment, and this uptake of FITC-dextran increases with duration of exposure. Taken together with the results from TEM, the membrane activity of D-LAK increased the permeability of the bacterial membrane thereby potentially facilitating the interaction of molecules with the bacteria. The mechanism of this peptide action was further explored in the next part of the study.

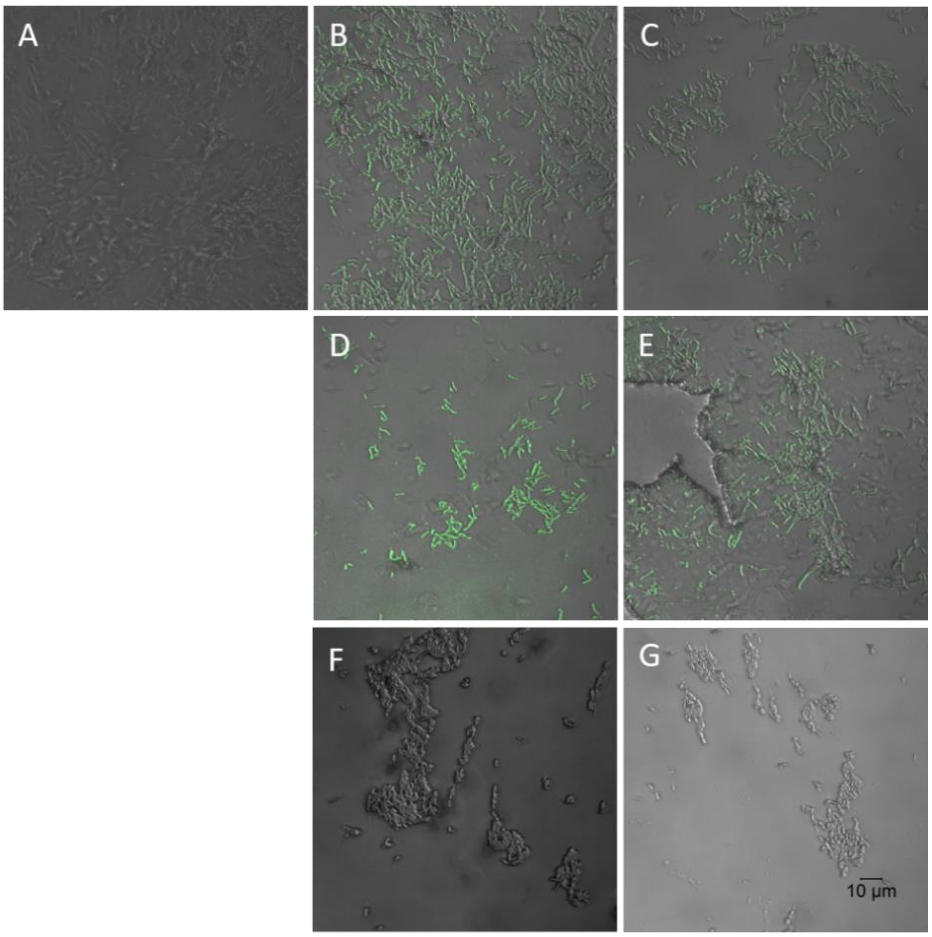

Figure 5.4 Confocal images of M. smegmatis mc^2 155 exposed to D-LAK peptide and FITC-dextran. M. smegmatis mc^2 155 either unchallenged (A) or challenged with 2x MIC isoniazid (F) or rifampicin (G), ½ MIC (B/C) or 2x MIC (D/E), D-LAK120-A (B/D) or D-LAK120-HP13 (C/E). In contrast to rifampicin and isoniazid, both peptides facilitate absorption or adsorption of the 150 kDa FITC-dextran.

5.2.4 Determination of media effect on membrane properties by Laurdan fluorescence assay

To gain better understanding of the effect of media composition on the growth of *M. smegmatis*, changes in bacterial membrane property was determined using Laurdan fluorescent probes. *M. smegmatis* grown in different media exhibited differing membrane property as detected by changes in Laurdan fluorescence, revealing the effect of media supplementation with 0.025% tyloxapol or oleic acid-albumin-dextrose-catalase (OADC) (Fig. 5.5). The general polarization (GP) value reflects the local polarity around the fluorophore and is commonly influenced by the penetration of water molecules into the lipid layer. This is taken as a proxy for membrane order in which a higher GP value denotes a higher membrane order. *M. smegmatis* grown in 7H9 broth media supplemented with OADC without tyloxapol were found to have the highest GP values. Moreover, the membrane order of mycobacteria grown in media without tyloxapol was significantly higher than those grown in 7H9 broth media with tyloxapol. Membrane order of bacteria grown in RPMI 1640 was similar to those grown in 7H9 broth media with tyloxapol. These results showed that *M. smegmatis* grown in media with tyloxapol generally demonstrate a lower membrane order which might be explained by the interaction of the detergent with membrane surface components.

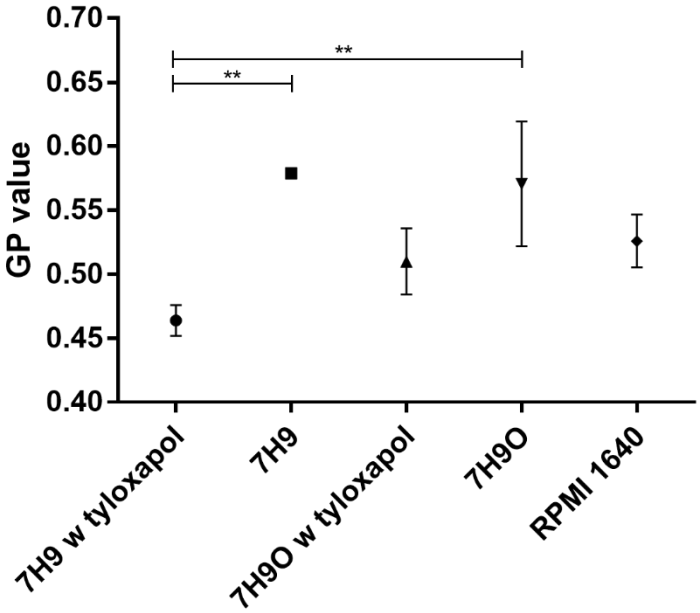

*Figure 5.5 Media effect on membrane properties of M. smegmatis mc² 155 by Laurdan fluorescence assay. 7H9 denotes the basic broth medium, 7H9 w tyloxapol denotes the additional 0.025% tyloxapol, 7H9O denotes the additional OADC supplement. Data were presented as mean ± SD (n=3). Significant difference was assessed using one-way ANOVA analysis followed by Tukey's post-hoc test, *<0.05, **<0.01, ***<0.001*

.

5.2.5 Mycobacterial growth response assays

Fluorescence assays

DPH fluorescence polarization or anisotropy is commonly employed to determine alteration in bacterial membrane fluidity in response to environmental stimulus or stress[349]. Since the DPH probes lie within the hydrophobic core aligning with the acyl chains in the membrane, increase in r represent the reduction in degree of rotation of the probes, therefore increased rigidity of the mycomembrane. Significant increases ($p < 0.01$) in fluorescence anisotropy, r, were resulted when *M. smegmatis* was challenged with D-LAK120-HP13, capreomycin or its combinations with D-LAK peptides. The same effect was also observed in the presence of 0.025 % tyloxapol (Fig. 5.6A). Small and nonsignificant increase in membrane rigidity were detected when bacteria were challenged by D-LAK120-A, colistin, isoniazid, rifampicin and D-LAK peptides with rifampicin. The change in fluorescence anisotropy indicated that

M. smegmatis responded in particular to the challenge of capreomycin and its combinations by a substantial increase in membrane rigidity.

As mentioned previously, Laurdan fluorescence polarization has been used as a measurement of membrane order in bacterial studies. Due to the nature of the Laurdan probe giving rise to its positioning in membrane interfacial region, the measurement represents the effect of solvent surrounding the probe and thereby the increase in polarity, denoted by the reduction of GP, reflecting the more disordered in regions of the membrane. As a result, any reduction of GP in the samples compared to the control indicated that the local environment around the probe become more polar, suggesting that there was a reduction of membrane order of *M. smegmatis* when they are subjected to these challenges. Significant reductions ($p < 0.001$) in Laurdan GP were observed in *M. smegmatis* when challenged with capreomycin, its combinations with D-LAK peptides or in the presence of tyloxapol (Fig. 5.6B). All the other treatments did not induce significant changes as compared to untreated control. When the bacteria were challenged with capreomycin alone, the GP reduction was significantly greater than when it was used in combination with D-LAK120-A but not that with D-LAK120-HP13.

Notably, an opposite trend was demonstrated using Laurdan fluorescent probe and DPH probe. Since the increase in DPH anisotropy is associated with the increase in membrane rigidity, this trend depicting a less-ordered (an increase of GP in Laurdan fluorescence) but more rigid membrane was surprising. Consequently, the correlation between Laurdan polarization and DPH anisotropy was assessed by the application of Spearman's rank correlation method (Fig. 5.6C). Interestingly, the result showed a strong negative correlation (Spearman's rho = -0.742) between Laurdan and DPH data which suggests the two techniques have a monotonic relationship and are reporting on the same event. Although the precise locations of where the two probes reside are yet to be determined, these results have revealed that the physical properties of the mycobacterial envelope are substantially altered in response to the challenge by capreomycin and perhaps D-LAK120-HP13 but to a lesser extent. On the contrary, other anti-TB agents and D-LAK120-A did not seem to have a significant impact on the membrane properties of *M. smegmatis*.

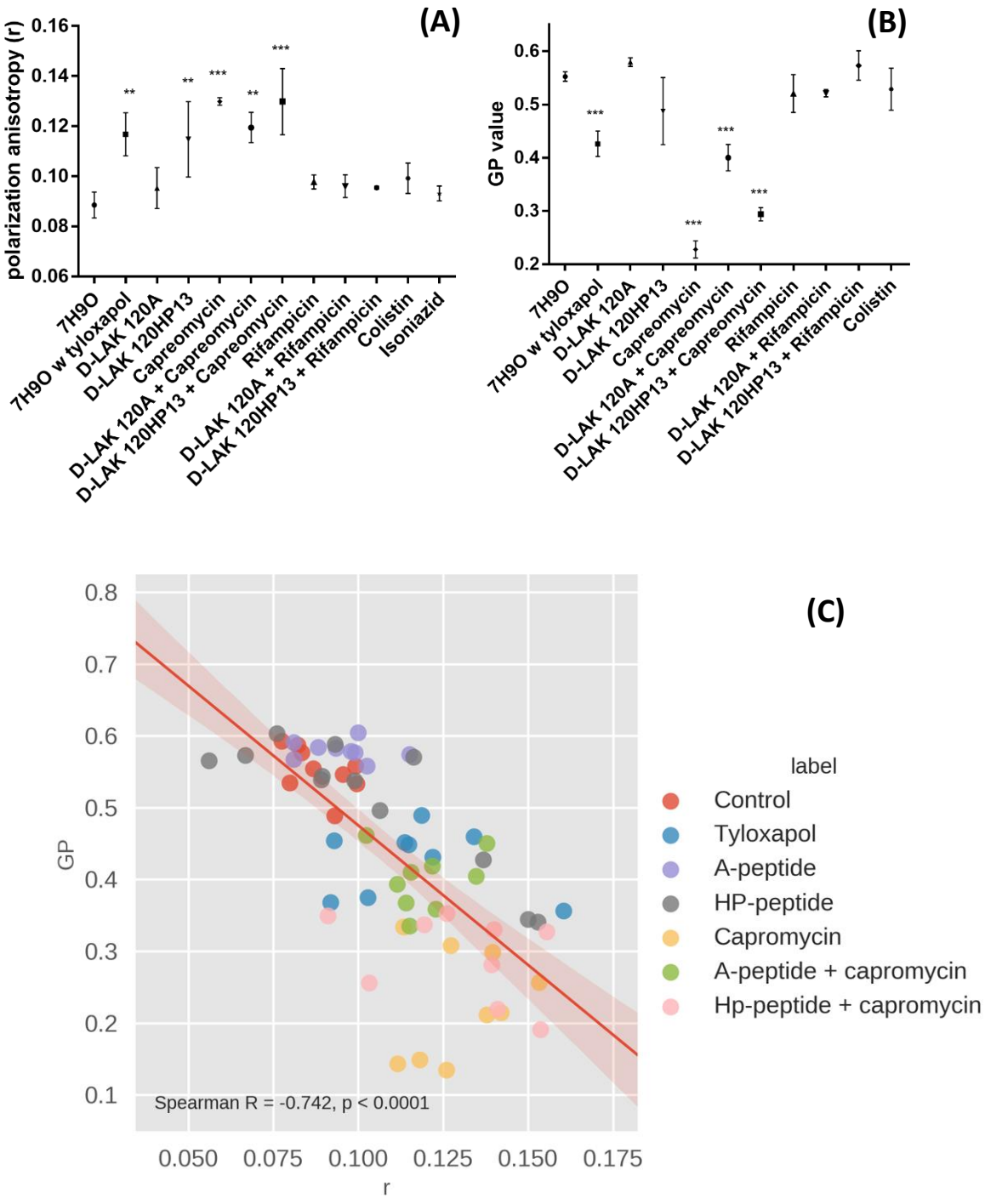

*Figure 5.6 Fluorescence spectroscopic perspective of the response of M. smegmatis mc^2 155 to challenge with antibiotics. DPH fluorescence anisotropy (A), Laurdan GP fluorescence (B) and correlation (Spearman R = -0.742, p < 0.0001) of DPH and Laurdan (C). Data were presented as mean ± SD (n=9). Significant difference was assessed using one-way ANOVA analysis followed by Dunnett's Multiple Comparison Test, *<0.05, **<0.01, ***<0.001 vs 7H9O.*

Metabolite assignment of M. smegmatis mc² 155

HR-MAS ^{1}H NMR metabolomics elucidated the metabolites in the whole cell sample of *M. smegmatis*. ^{1}H NMR spectra were obtained from HR-MAS and liquid state NMR spectrometer. Assignments of metabolites associated with peaks are shown as a reference for the backscaled loadings and NMR spectra. The unchallenged whole *M. smegmatis* cell spectrum (Fig. 5.7) was dominated by the lipid resonance including various kinds of saturated and unsaturated carbon functional groups. This could be explained by the lipid rich mycomembrane structure consisting mainly of non-oxygenated α-mycolic acids in *M. smegmatis*. Amino acids and sugars without overlapping with lipids were also identifiable, namely trehalose, sucrose, alanine, lysine, glycerate, serine, valine and glutamate. The NMR spectrum of spent media of unchallenged *M. smegmatis* (Fig. 5.8) contained sharper peaks without the influence of broad lipid resonance compared to the spectrum of the whole cell sample (Fig. 5.7). By comparing the spectra of challenged bacteria with control, spectra of HR-MAS and spent media could provide information of substantial changes in various membrane components as well as the changes in bacterial metabolism pathways.

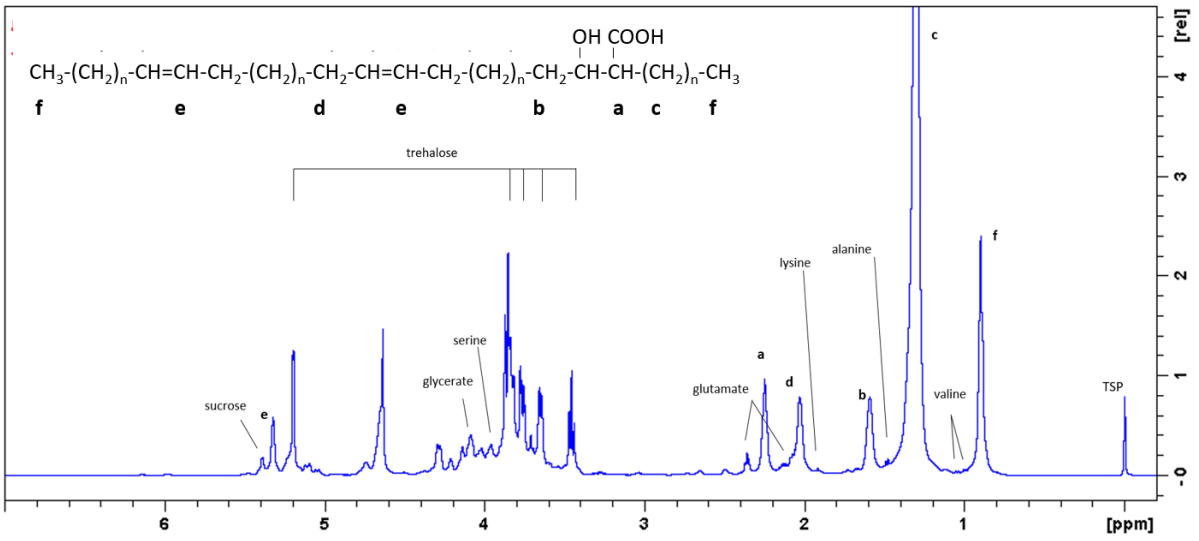

Figure 5.7 1D ^{1}H HR-MAS spectrum of whole cell M. smegmatis mc^{2} 155.

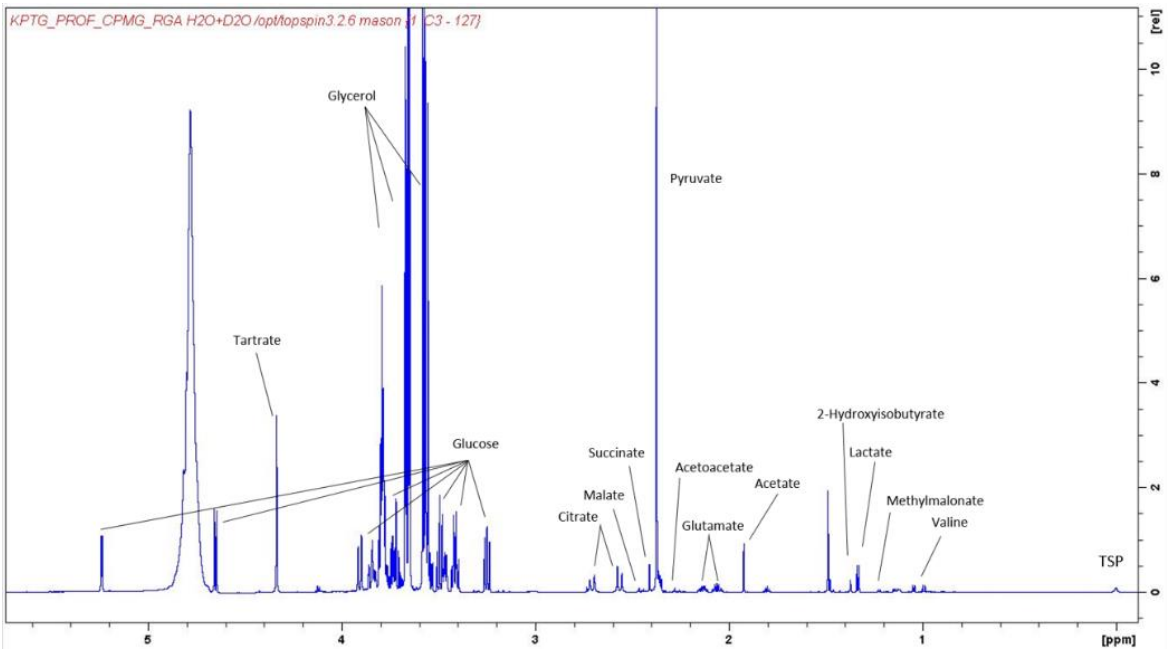

Figure 5.8 1D ^{1}H NMR spectrum of spent growth media of M. smegmatis mc^{2} 155.

Multivariate analysis

PCA is an unbiased and important preliminary evaluation of differences between different treatment groups. The PCA scores plots (Appendix B, Fig. 7.4 and 7.5) derived from the ^{1}H NMR spectra of whole cell *M. smegmatis* samples upon treatment in the presence of tyloxapol or challenges with anti-TB agents alone, D-LAK peptides alone or their combination revealed clear clustering by plotting along principle component 1 and 2 (PC 1 and 2), indicating significant changes in different challenged conditions. The challenge with D-LAK peptides (2.0 and 3.0) cluster more closely together with the unchallenged control (0.0) while capreomycin and its combinations with D-LAK peptides (7.0, 8.0 and 9.0) cluster on the other side of the coordinate plane. This marks the distinct differences in metabolic changes of *M. smegmatis* while subjected to the respective challenges.

The specific metabolites that distinguished the treatments (Appendix B, Fig. 7.4 and 7.5) indicated that the highest variance (98.1%) which was explained by PC 1 were attributed to the reduction in lipid components (1.29 ppm) and trehalose (3.86 ppm). At the same time, PC 2 accounted for the remaining variance (1.7%) found in the data set and indicated this variance was ascribed to production of trehalose.

PCA plots for spent media of *M. smegmatis* upon different challenges revealed clustering of spectra from rifampicin challenged cultures and also its combinations with D-LAK peptides while similar clustering was observed for cultures challenged with isoniazid and its combinations with D-LAK peptides. The highest variance (PC 1, 87.8%) was shown to be attributed to the reduction of glycerol (3.58 ppm) and PC 2 indicated influence by the production of pyruvate (2.38 ppm) accounting for 11.6% of the variance. This suggests that the challenged cultures grew slower than the untreated controls.

Cross-validated orthogonal projections to latent structures discriminant analysis (OPLS-DA) was done to identify significant changes in ^{1}H HR-MAS spectra acquired for *M. smegmatis* upon various challenges as indicated (Appendix B, Fig. 7.6-7.28). The key metabolites responsible for the differentiation between classes were further verified by OPLS-DA model as it can demonstrate significantly improved discrimination compared to PCA models, model predictability, as assessed by Q^2 (Table 5.3). It also indicates the level of significance in the separation between each challenge condition and the untreated control.

A hierarchical clustered heatmap was generated based on the degree of similarity of metabolite abundance profiles to give an overview of all the individual metabolite detected in

^{1}H HR-MAS (Fig. 5.9) and liquid-state (Fig. 5.10) NMR. Volcano plots allows the individual comparisons of unchallenged control with each challenged condition. Fold changes of these metabolites were generated according to their relative peak intensities compared with the pre-processed data of the ^{1}H NMR spectra. This facilitates the identification of the magnitude and significance of changes in key metabolites as compared across challenges in the univariate analysis plots to reveal individual impact.

Heatmap generated from the whole cell HR-MAS analysis gives a general trend of changes in metabolites in *M. smegmatis* subjected to different treatments (Fig. 5.9). An overall reduction in lipid resonances was induced by all treatments except for D-LAK120-A as compared with the untreated control. Production of trehalose was only resulted in treatment with capreomycin and combinations of capreomycin with D-LAK peptides. On the other hand, liquid state NMR indicated the production of tartrate and consumption of glycerol by rifampicin and its combination with D-LAK peptides or colistin alone (Fig. 5.10). Opposite changes in these two metabolites were demonstrated in all the other treatments in addition to the reduction of succinate, pyruvate and citrate. Significance of these changes are illustrated in the volcano plots in the next section.

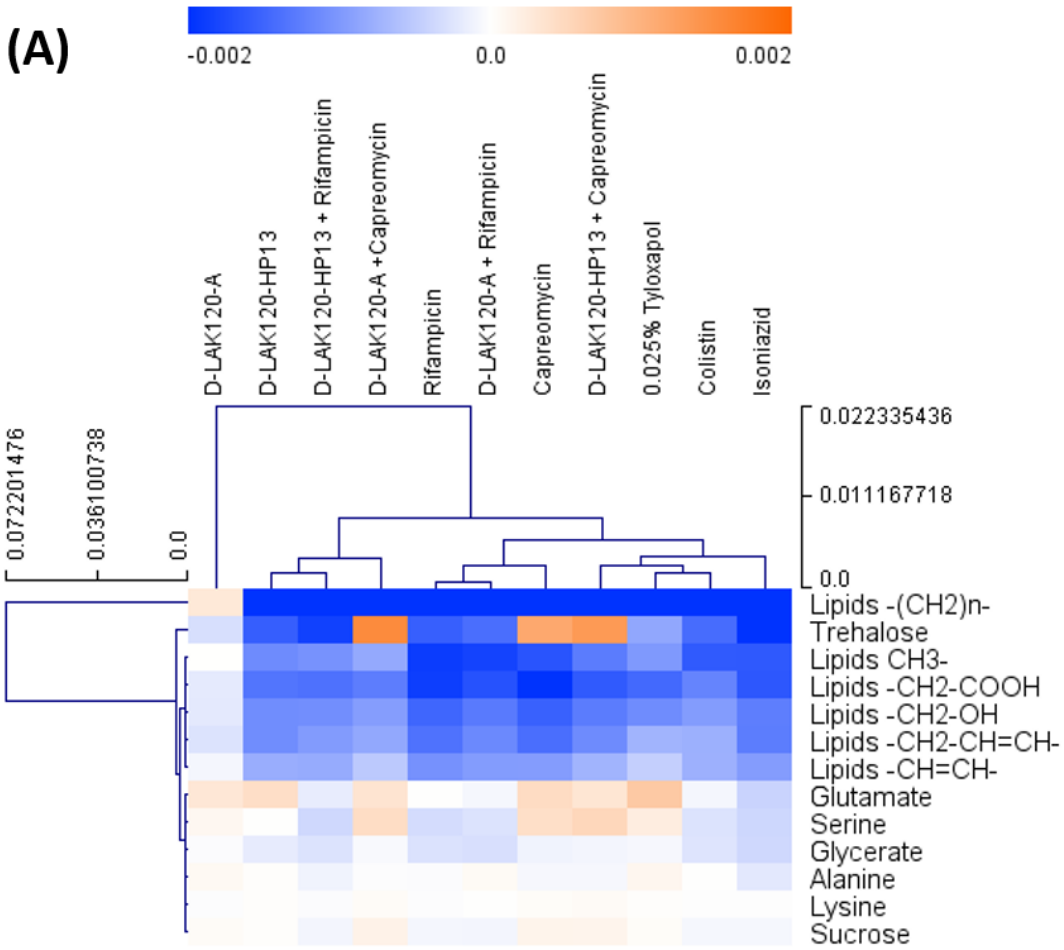

Figure 5.9 Hierarchical clustered heatmap comparing loadings obtained from cross-validated OPLS-DA of ^{1}H HR-MAS NMR spectra of M. smegmatis mc^{2} 155 challenged with indicated conditions.

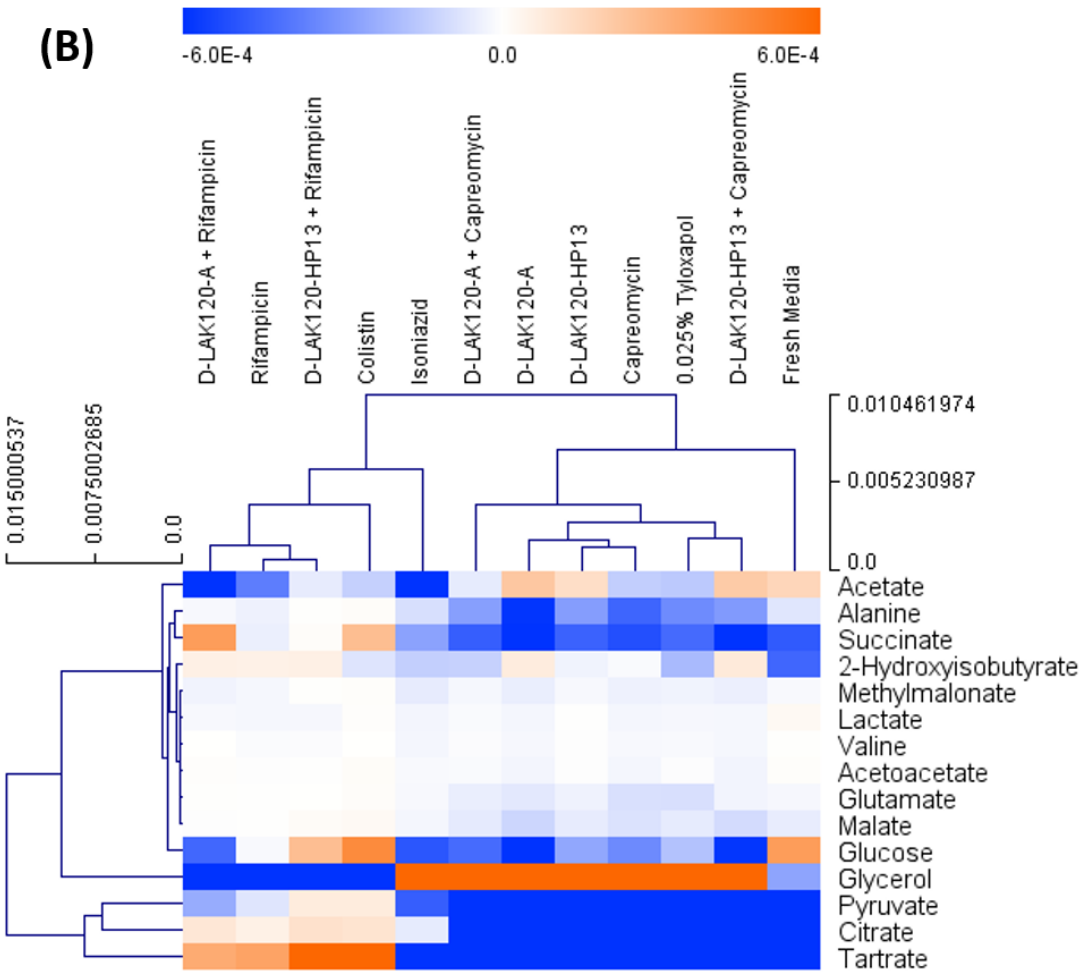

Figure 5.10 Hierarchical clustered heatmap comparing loadings obtained from cross-validated OPLS-DA of liquid-state NMR spectra of M. smegmatis mc^2 155 challenged with indicated conditions.

In the presence of 0.025% tyloxapol, *M. smegmatis* showed significant and substantial changes in a number of metabolites involving components of the mycobacterial membrane (Fig. 5.11A). The increase in the amount of glutamate was the greatest change while there was a modest increase in lysine, serine, alanine and glycerate. Highly significant reduction in lipid resonances including the R_2CH-COOH, R_2CH-OH groups as well as saturated alkyl chains -$(CH_2)_n$– were detected which are associated with mycolic acid. Notably, tyloxapol treatment did not affect the resonance of unsaturated alkyl groups –CH=CH– or -CH_2-CH=CH–. Mycolic acids of mycobacteria comprise of two branches: a short α-chain consists of saturated alkyl carbon and a long mero-chain of 40-60 carbon atoms with two functional moieties at the distal and proximal positions. Mycomembrane of *M. smegmatis*

consists of mostly non-oxygenated α' mycolic acids which possess cis-alkene functional groups in the mero-chains. In addition to the capsule-shedding effect of tyloxapol, it was also reported to reduce the amount of surface lipids of mycomembrane, especially trehalose 6,6' -dimycolate (TDM) on *M. bovis* BCG[350]. This reduction of only saturated alkyl chains might suggest the effect of tyloxapol on the short α-chains of TDM of *M. smegmatis*. It is also worth-noting that the fold changes of all the four saturated hydrocarbon lipid resonance were similar, showing the consistent reduction in the number of saturated α-chains, while the mero-chains containing unsaturated alkene were unaffected.

On the other hand, it was observed that both the saturated and unsaturated hydrocarbon lipid resonances were affected when the bacteria were challenged with rifampicin or capreomycin (Fig. 5.11D/G). Although the magnitudes of responses observed have substantial variations and qualitative differences, the common effect brought about by these challenges were the reduction of unsaturated lipid resonances. More importantly, the fold changes of all lipid resonances were similar. This might imply the reduction of the amount of intact mycolic acids instead of shortening the alkyl chains in mycolic acids. In addition to the reduction of both saturated and unsaturated lipid resonances, R_2CH-COOH and R_2CH-OH groups also followed the same trend with the similar negative fold changes, further explaining the general decrease in mycolic acid content. Mycolic acids are essential component of the mycomembrane and they play a major role in membrane permeability. With the inner leaflet covalently bonded to arabinogalactan, the outer leaflet of the mycomembrane consists of extractable free trehalose mycolates, trehalose 6-monomycolates (TMM) and TDM. In this study, an increase in signal intensity of trehalose resonance was only found when *M. smegmatis* was challenged with capreomycin (Fig. 5.11G). This increase was of similar magnitude as the decrease in mycolic acid resonances, revealing the ratio of mycolic acid to trehalose was substantially influenced when the bacteria was challenged by capreomycin. This would be consistent with a shift in the balance between TDM and TMM, leading to the predominance of the latter in mycomembrane. Significant increase in sucrose, serine and lysine also occurred as a result of the challenge by capreomycin.

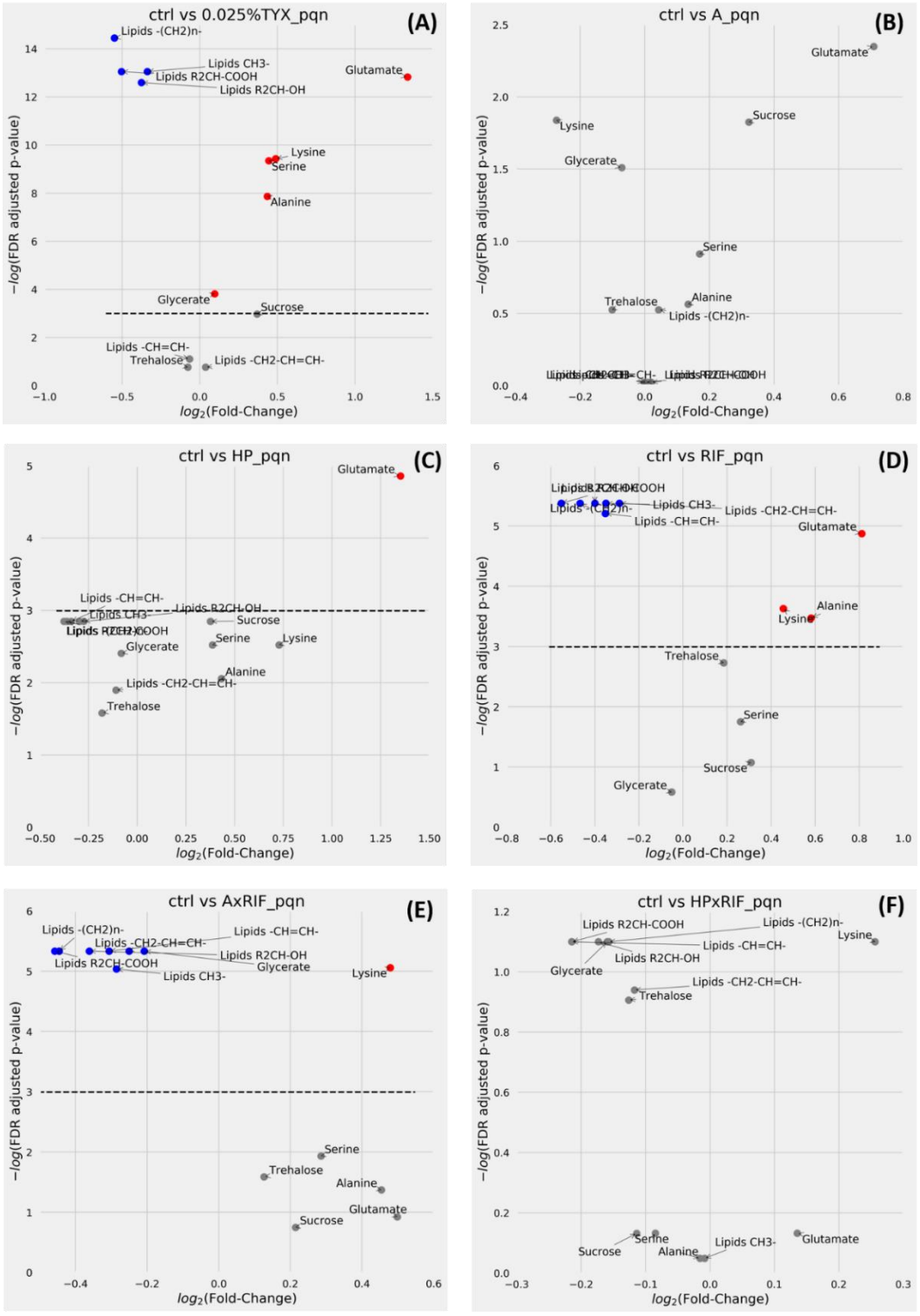

Figure 5.11A-F ¾ MIC Challenges induce changes in various metabolites in whole cell M. smegmatis mc² 155. Volcano plots are shown for individual comparisons of unchallenged bacteria and those challenged with 0.025% tyloxapol (A), D-LAK120-A (B), D-LAK120-HP13 (C), rifampicin (D), rifampicin in combination with D-LAK120-A (E) or D-LAK120-HP13 (F). Volcano plots are of PQN normalized data and allow comparison of fold changes and significance of each metabolite; blue – significant reductions, red – significant increases and grey – non-significant changes in the indicated metabolites.

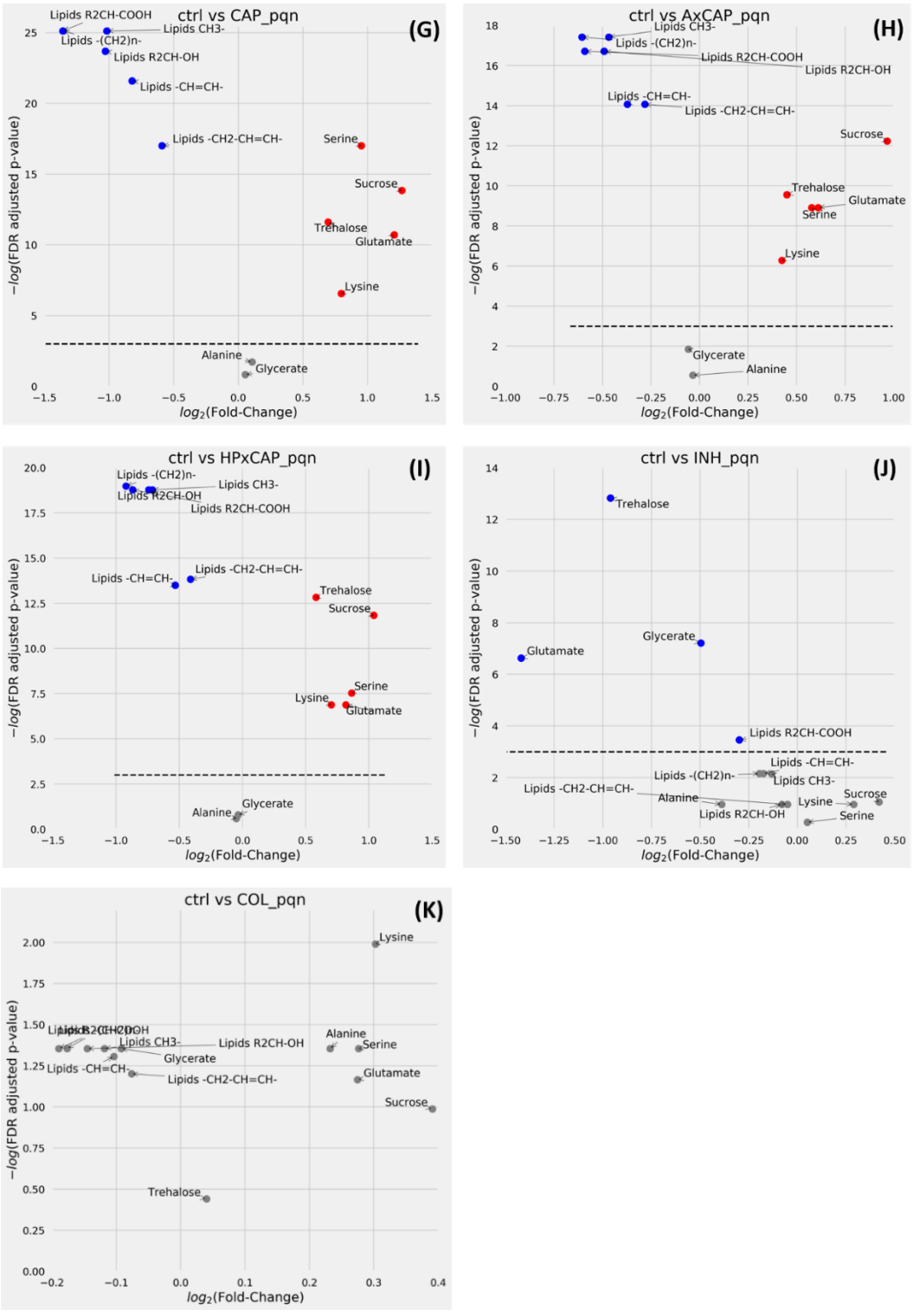

Figure 5.11G-K ¾ MIC Challenges induce changes in various metabolites in whole cell M. smegmatis mc² 155. Volcano plots are shown for individual comparisons of unchallenged bacteria and those challenged with capreomycin (G), capreomycin in combination with D-LAK120-A (H) or D-LAK120-HP13 (I), isoniazid (J) or colistin (K). Volcano plots are of PQN normalized data and allow comparison of fold changes and significance of each metabolite; blue – significant reductions, red – significant increases and grey – non-significant changes in the indicated metabolites.

The decrease in the amount of mycolic acid caused by capreomycin is much greater as compared to that of rifampicin and tyloxapol. Across different challenges, it is clear that capreomycin triggered the strongest and the most significant ($p < 0.05$) impact on both saturated and unsaturated hydrocarbons (Fig. 5.12G-L). On the contrary, rifampicin induced a modest reduction in the lipid resonances, while tyloxapol only resulted in changes in saturated hydrocarbons (Fig. 5.12G-J) but not unsaturated lipids (Fig. 5.12K-L). Again, neither rifampicin nor tyloxapol triggered significant changes in trehalose that was seen in capreomycin challenge (Fig. 5.12F). It can be concluded that the membrane remodeling effect, brought about by rifampicin, was much subtler than that induced by capreomycin which is probably the reason behind the lack of changes in membrane properties observed in the fluorescence assays. Treatment of *M. smegmatis* by isoniazid induced significant reduction in trehalose, glutamate, glycerate and lipid R_2CH-COOH. Colistin did not induce significant changes of any metabolites.

The challenge of the two D-LAK peptides resulted in quantitatively and qualitatively different responses in *M. smegmatis* as compared with rifampicin and capreomycin. The assessment of OPLS-DA models of either peptide indicated a significant response when considering all metabolites (Table 5.3). However, changes in individual metabolites were subtle and did not pass the stringent significant threshold (Fig. 5.11B/C). Volcano plots showed that D-LAK120-HP13 peptides induced a significant increase in glutamate ($p < 0.05$), which was a similar phenomenon as observed in capreomycin but not rifampicin. Unlike capreomycin, the D-LAK peptides did not cause any changes in trehalose (Fig. 5.12F). The difference in certain metabolic responses distinguishes the two D-LAK peptides which might reflect their different mechanism of actions. Significant increase ($p < 0.05$) in both saturated and unsaturated lipids was found when the bacteria were challenged with D-LAK120-HP13 but not D-LAK120-A peptide (Fig. 5.12G-L). This is consistent with the membrane manipulation activity of D-LAK120-HP13 as detected in the DPH fluorescence assay. Besides, significant increase in lysine resonance was observed in D-LAK120-HP13.

HR-MAS ^{1}H NMR data were also obtained for combinations of capreomycin and rifampicin with D-LAK peptides. Notably, concentration of capreomycin and rifampicin used in combination with D-LAK peptides were much lower than when they were used alone. Combination of D-LAK120-A with capreomycin has shown modest synergism while the combination of D-LAK120-A with rifampicin was found to be indifferent or even antagonistic. D-LAK120-A dampened the decrease in lipid resonances (Fig. 5.12G-L) and

the increase in trehalose (Fig. 5.12F) caused by capreomycin ($p < 0.05$) but had no effect on the level of glutamate (Fig. 5.12E). The responses of *M. smegmatis* on rifampicin alone or in combination with D-LAK120-A were indistinguishable.

There was modest synergism between D-LAK120-HP13 and rifampicin while only an additive effect was seen when the peptide was used in combination with capreomycin. As compared to proline-free D-LAK120-A peptide, the proline containing D-LAK120-HP13 peptide showed a weaker influence on the metabolic changes caused by rifampicin or capreomycin. Despite the lower impact on the reduction of both saturated and unsaturated hydrocarbons than capreomycin alone, the mitigation induced by the combination of D-LAK120-HP13 with capreomycin was not significant. On the other hand, combination of rifampicin with D-LAK120-HP13 did not cause great impact on changes in metabolites except -CH_3, in which a significant ($p < 0.05$) mitigation was recorded, (Fig. 5.12J).

Table 5.3 Test and permutated Q^2 scores for cross-validated OPLS-DA models from ^{1}H HR-MAS and liquid-state NMR spectra of M. smegmatis mc^2 155. Comparison of unchallenged bacteria with those obtained from bacteria treated by the indicated conditions.

^{1}H HR-MAS			**Liquid-state**		
	Q^2	permutated Q^2		Q^2	permutated Q^2
0.025% Tyloxapol	0.866	-0.377	0.025% Tyloxapol	0.820	-0.491
D-LAK120-A	0.769	-0.423	D-LAK120-A	0.222	-0.539
D-LAK120-HP13	0.729	-0.360	D-LAK120-HP13	0.632	-0.351
Rifampicin	0.571	-0.426	Rifampicin	0.767	-0.463
D-LAK120-A + Rifampicin	0.763	-0.410	D-LAK120-A + Rifampicin	0.876	-0.494
D-LAK120-HP13 + Rifampicin	0.430	-0.429	D-LAK120-HP13 + Rifampicin	0.705	-0.475
Capreomycin	0.882	-0.347	Capreomycin	0.555	-0.506
D-LAK120-A + Capreomycin	0.775	-0.367	D-LAK120-A + Capreomycin	0.577	-0.503
D-LAK120-HP13 + Capreomycin	0.823	-0.344	D-LAK120-HP13 + Capreomycin	0.625	-0.457
Colistin	0.700	-0.363	Colistin	0.526	-0.341
Isoniazid	0.859	-0.429	Isoniazid	0.900	-0.453
			Fresh media	0.846	-0.444

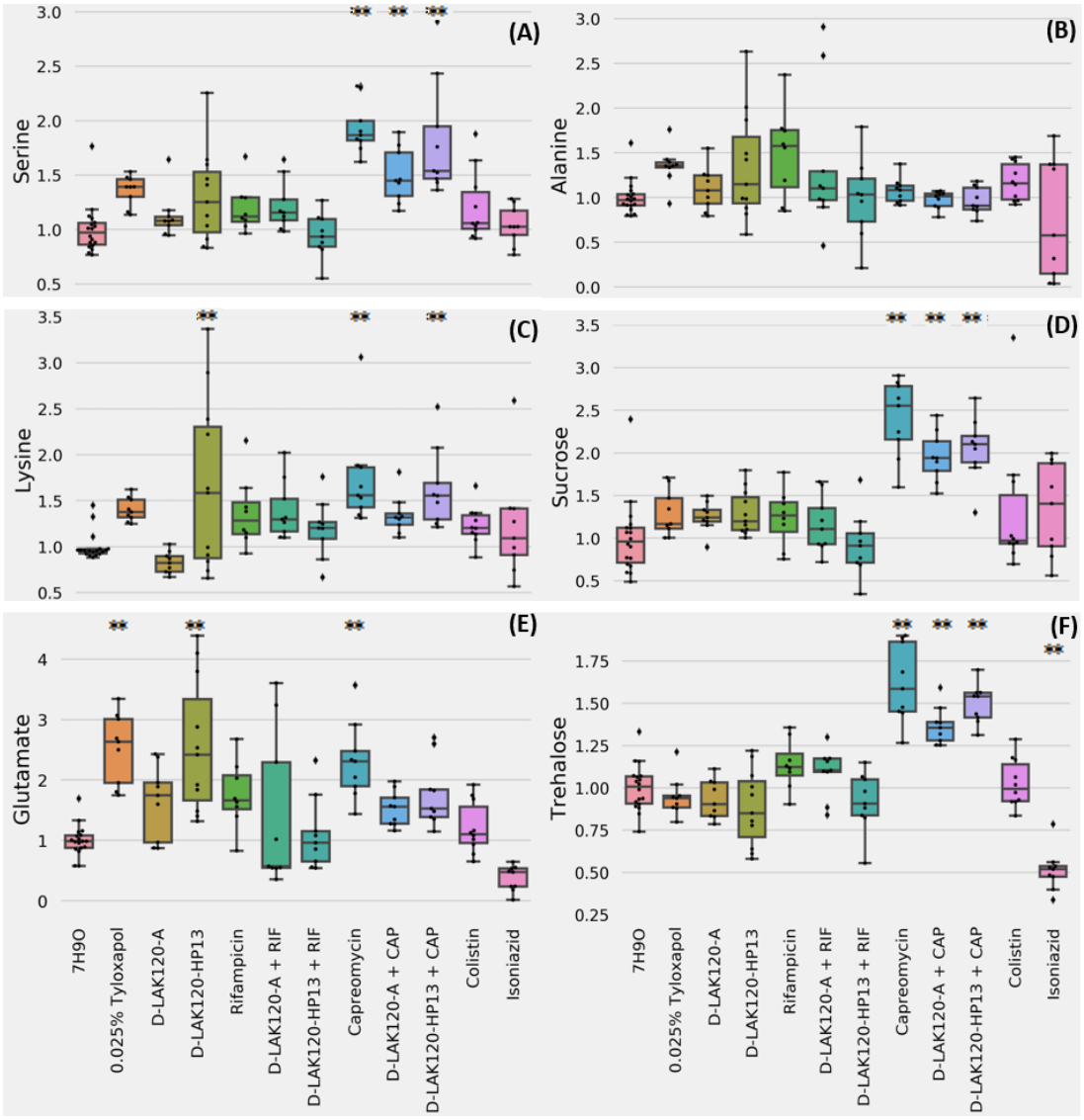

*Figure 5.12A-F Univariate analysis of relative metabolite levels in M. smegmatis mc^2 155. Significant differences with respect to unchallenged bacteria, as determined by one-way ANOVA with Tukey post-hoc test, are indicated ** (n = 9). Other significant differences are described in the text.*

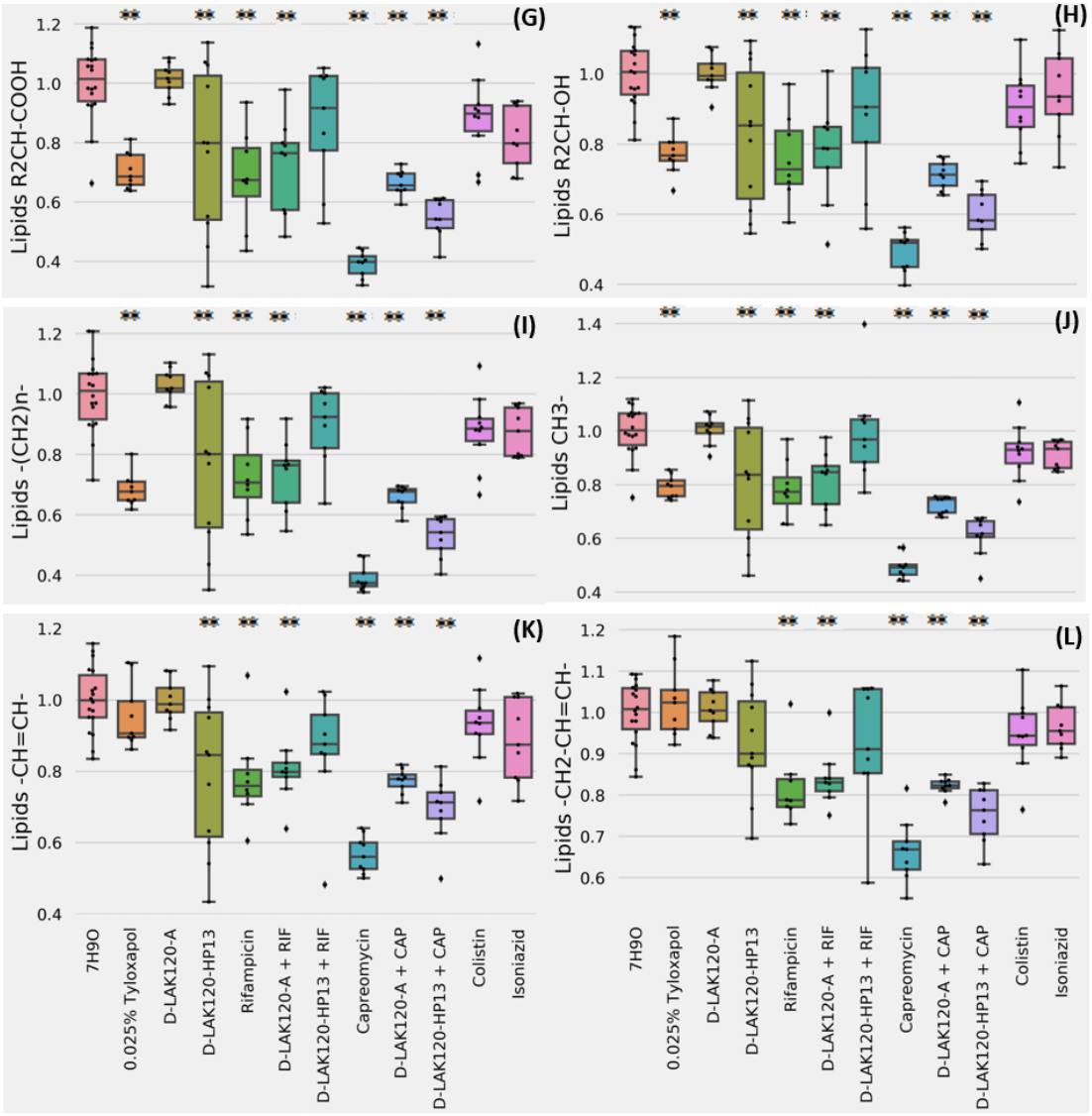

*Figure 5.12G-L Univariate analysis of relative metabolite levels in M. smegmatis mc^2 155. Significant differences with respect to unchallenged bacteria, as determined by one-way ANOVA with Tukey post-hoc test, are indicated ** (n = 9). Other significant differences are described in the text.*

To gain a better understanding of the relationship between the changes in metabolite concentration and the physical properties of mycomembrane, Spearman correlation was used to assess the samples challenged by capreomycin and/or D-LAK peptides or growth in the presence of tyloxapol. The changes of magnitude of individual metabolites and fluorescence anisotropy were evaluated using partial least square regression model (Fig. 5.13). Highly significant correlations ($p < 0.0001$) were demonstrated between the metabolites, which showed substantial changes upon aforementioned challenges, and their corresponding fluorescence anisotropy. Saturated hydrocarbons resulted in the strongest negative correlation with fluorescence anisotropy, with the Spearman constant of -0.733 for $–(CH_2)_n–$ (Fig. 5.13A) and -0.708 for $-CH_3$ (Fig. 5.13E), whereas slightly weaker correlations were found with unsaturated hydrocarbons at -0.631 for –CH=CH– (Fig. 5.13C) and -0.543 for $–CH_2$-CH=CH– (Fig. 5.13D). Positive correlation ($R = 0.564$) was detected between trehalose and fluorescence anisotropy. These correlations support the reasoning behind the observations in which capreomycin triggered responses in all lipids and trehalose, while D-LAK120-HP13 only triggered changes in most lipid resonances except $–CH_2$-CH=CH–. Tyloxapol triggered changes solely in saturated hydrocarbons. Moreover, the strength of these correlations may reveal the influence of each of these mycomembrane components on membrane rigidity. It could be deduced that the increase in rigidity of mycomembrane appears to be the direct result of the changes in membrane components, as indicated by the increase in trehalose and reduction in lipids when challenged with capreomycin and its combinations with D-LAK peptides.

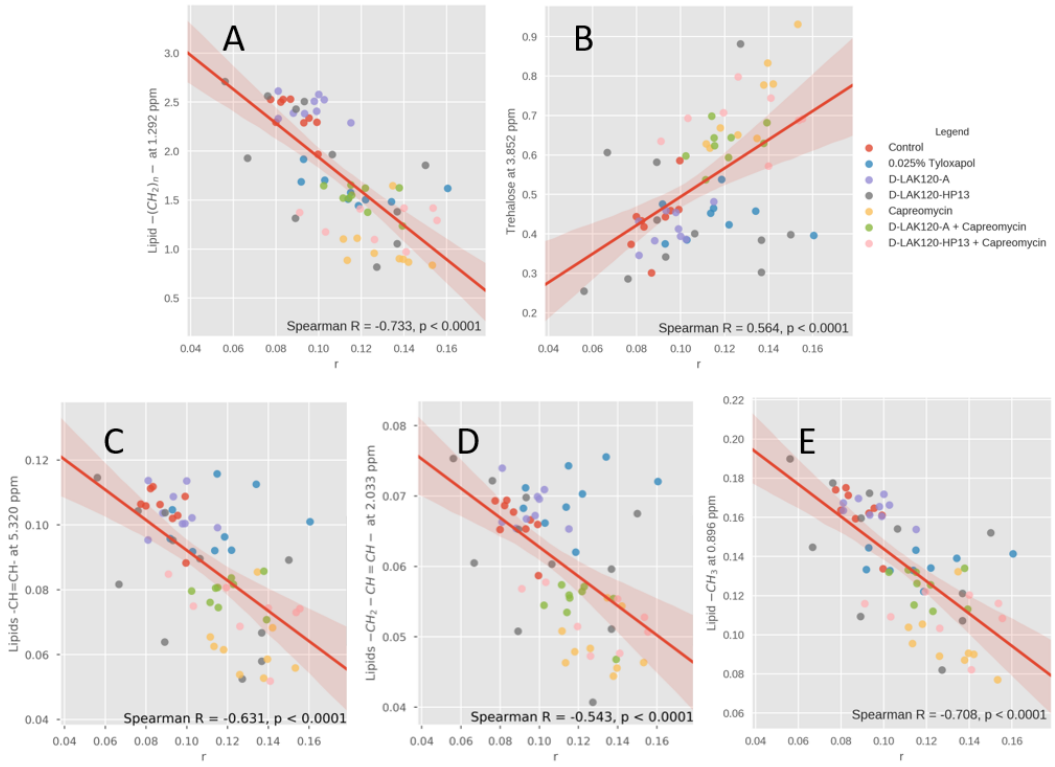

Figure 5.13 Correlation between membrane rigidity and the altered composition of the mycomembrane of M. smegmatis mc² 155. Spearman correlations are shown between DPH anisotropy (r) and ¹H HR-MAS NMR resonance intensities obtained for M. smegmatis mc² 155 grown without challenge or with 0.025% Tyloxapol or ¾ MIC of D-LAK120-A, D-LAK120-HP13, capreomycin, capreomycin with D-LAK120-A or capreomycin with D-LAK120-HP13. Data is shown for lipid –$(CH_2)_n$- (A), trehalose (B), lipid –CH=CH- (C), lipid –CH_2-CH=CH- (D) and lipid -CH_3 (E).

Changes in metabolites in spent bacterial culture media were also analyzed by OPLS-DA (Appendix B). The results illustrated that qualitative change occurred in metabolism of *M. smegmatis* only when it was challenged with rifampicin alone, its combinations with D-LAK peptides, as well as isoniazid alone (Fig. 5.14D-F/J). A binary comparison of spent media of unchallenged bacteria with fresh media indicates that *M. smegmatis* consumed glucose and produced glycerol, 2-hydroxyisobutyrate and tartrate (Fig. 5.14L). The changes in these metabolites indicate normal cell metabolism of bacteria which can denote the relative rate of bacterial growth. Upon challenging with rifampicin, there was a slight increase in consumption of citrate and glucose, and a more pronounced reduction of valine, alanine and lactate. An increase in pyruvate production and more modest decrease in malate and tartrate production were also observed (Fig. 5.14D). Since citrate and succinate are the key components of the carbon metabolic pathways, the reduction of both metabolites may be due to the increase lipid catabolism[351]. Although reduction in succinate in rifampicin treatment was just below the significant threshold, these changes in spent media together with the reduction in lipid resonances revealed in HR-MAS have demonstrated the effect of rifampicin on bacterial lipid metabolism. The changes in pyruvate, alanine, malate, tartrate, glucose and citrate were preserved when rifampicin was used in combination with D-LAK120-A but mostly muted when used in combination with D-LAK120-HP13 (Fig. 5.14E/F). Challenge with isoniazid also resulted in increased consumption of citrate in addition to the significant reduction in succinate, acetate and acetoacetate (Fig. 5.14J). De Carvalho *et al.* reported that the decrease in acetate may also be attributed to its metabolism through glyoxylate shunt[258]. This indicated the action of isoniazid on lipid biosynthesis associated with one of its mechanisms of action to inhibit anabolism of fatty acid[352]. The changes in lipid resonances in HR-MAS were found to be just below the significant threshold, possibly due to the inefficient amount of activated isoniazid to exert a significant effect on mycomembrane lipids. Apart from these conditions, no other challenges induced any significant changes in individual metabolites.

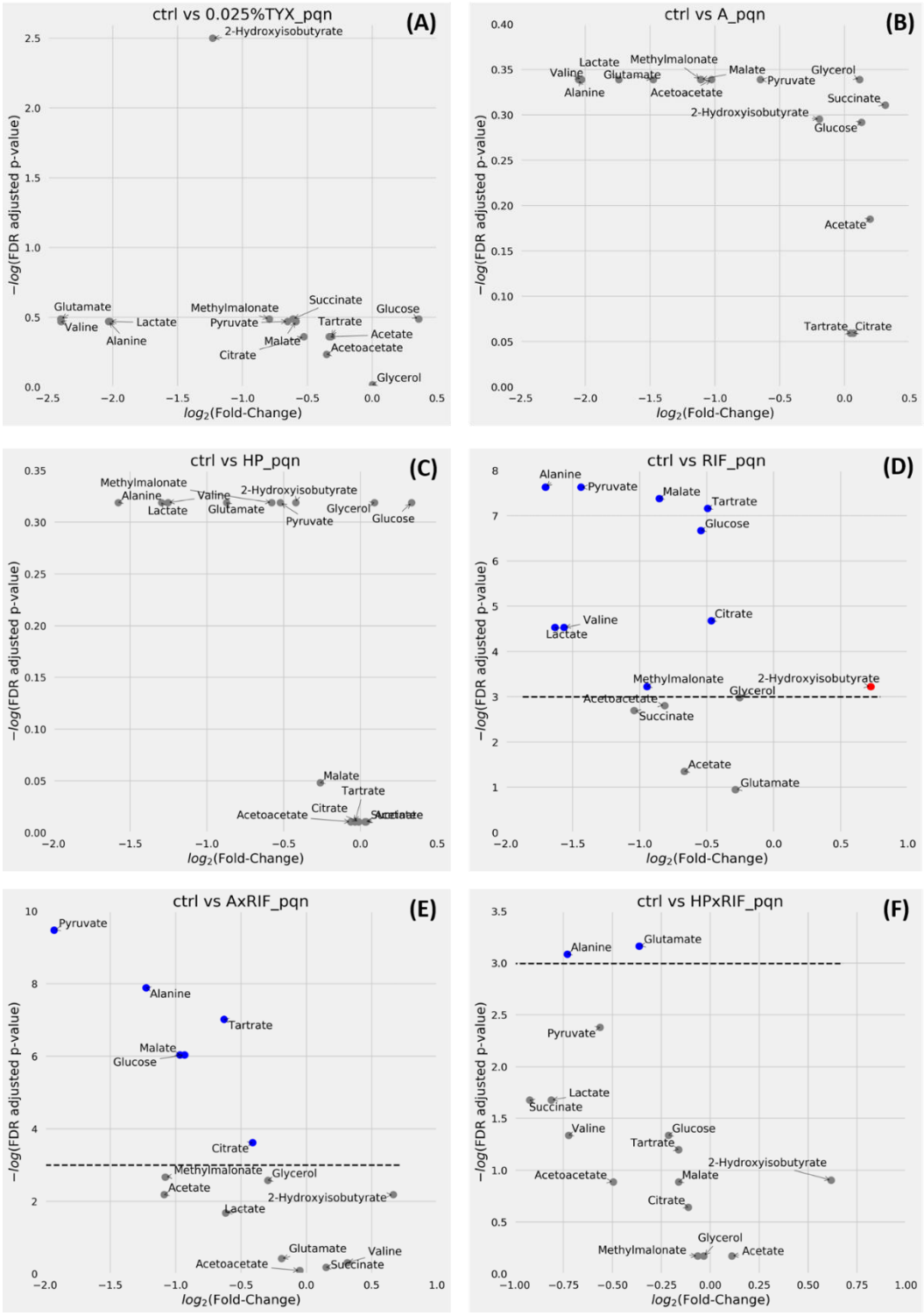

Figure 5.14A-F ¾ MIC Challenges induce changes in various metabolites in spent media of M. smegmatis mc² 155. Volcano plots are shown for individual comparisons of unchallenged bacteria and those challenged with 0.025% tyloxapol (A), D-LAK120-A (B), D-LAK120-HP13 (C), rifampicin (D), rifampicin in combination with D-LAK120-A (E) or D-LAK120-HP13 (F).Volcano plots are of PQN normalized data and allow comparison of fold changes and significance of each metabolite; blue – significant reductions, red – significant increases and grey – non-significant changes in the indicated metabolites.

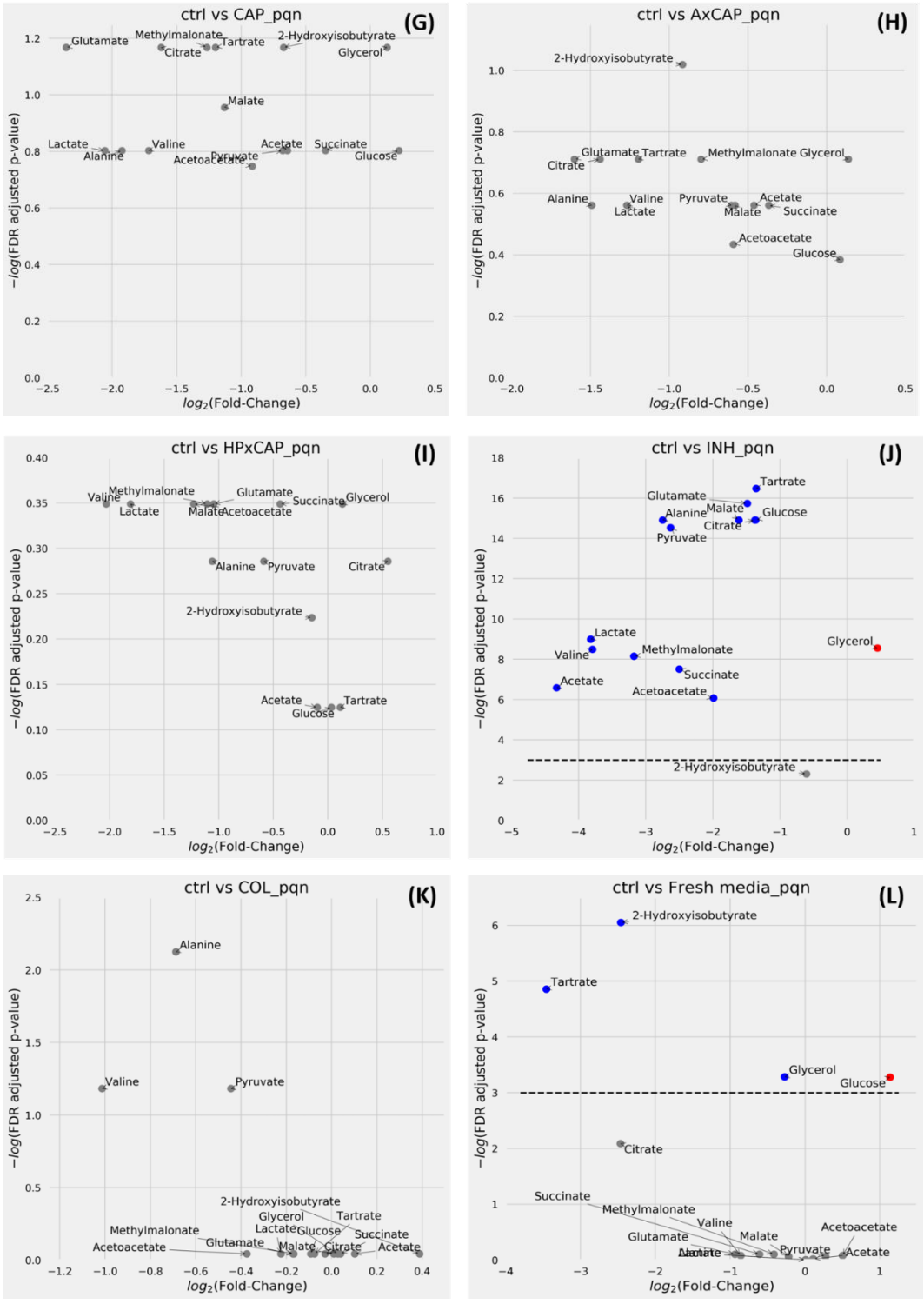

Figure 5.14G-L ¾ MIC Challenges induce changes in various metabolites in spent media of M. smegmatis mc² 155. Volcano plots are shown for individual comparisons of unchallenged bacteria and those challenged with capreomycin (G), capreomycin in combination with D-LAK120-A (H) or D-LAK120-HP13 (I), isoniazid (J), colistin (K) or Fresh Media (L). Volcano plots are of PQN normalized data and allow comparison of fold changes and significance of each metabolite; blue – significant reductions, red – significant increases and grey – non-significant changes in the indicated metabolites.

5.3 DISCUSSION

M. smegmatis mc^2 155 is a smooth morphotype strain isolated from the isogenic rough wild-type strain ATCC 607[341]. Owing to its non-pathogenic and fast-growing nature, this species is safe and practical to culture in the laboratory, making it an attractive model organism for the pathogenic *Mtb*[353]. Arguments have been raised to discuss the appropriateness of *M. smegmatis* as a *Mtb* surrogate due to its obvious differences of being a non-persistent and non-infectious saprophyte with a genome 1.7 times bigger than that of *Mtb*[354]. Surprisingly, a major portion of homologues virulence genes, and genes related to environmental sensing and response were detected in *M. smegmatis*[355]. Other similarities include the reaction to acid-fast staining, principal structure of cell wall, formation of biofilm and mycothiol synthesis. As a result, *M. smegmatis* is considered to serve as a useful system for studying stress responses[250, 356], genetic analysis[357] cell envelope characterization[63], screening of anti-TB drugs[358, 359], AMPs candidates[193, 360] and metabolomic studies[135, 253]. Given the widespread usage of *M. smegmatis* as a surrogate model to study the common biological aspects of mycobacteria, this species was employed in this study as a model to demonstrate various techniques to investigate the mode of action of anti-TB drugs and the novel D-LAK peptides, pathing the exploitation of those techniques in the study of *Mtb*.

Using the HR-MAS ^{1}H NMR metabolomic and fluorescent probes that are sensitive to membrane order and rigidity, dramatic changes in mycomembrane of *M. smegmatis* mc^2 155 were found in response to the challenge with capreomycin. In contrast, only modest changes in the mycomembrane were induced by the challenge with rifampicin, and challenge with isoniazid and colistin resulted in the least changes. D-LAK120-A and D-LAK120-HP13 peptides cannot be clearly distinguished from each other as there was not enough evidence based on the changes in physical properties of the mycomembrane. However, the different metabolic responses triggered in *M. smegmatis* have reflected distinct mechanism of action of these two peptide analogues. In the presence of tyloxapol, synergy was detected in the combinations of capreomycin with either peptide. However, this effect was attenuated in the absence of tyloxapol, leaving only modest synergy between capreomycin with D-LAK120-A but not with D-LAK120-HP13. D-LAK120-HP13 acted modestly beneficial with rifampicin in the absence of tyloxapol. These findings may provide insights to understand how the D-LAK peptides potentiate the first- and second-line anti-TB drugs against mycobacterial infections.

In vitro bacterial inhibitory assays were performed on *M. smegmatis* to evaluate the inhibitory efficacy of the anti-TB agents alone or in combinations with D-LAK peptides. *M. smegmatis* was susceptible to all the agents to a different extent. D-LAK peptides affected the growth of the bacteria with an MIC_{50} of < 2 μM in contrast to their inefficiency against *Mtb* strains shown in Chapter 4. This difference could be due to the substantial structural variations of cell wall bound mycolic acids between the two mycobacteria species, in particular the cyclopropanated mycolic acids in *Mtb* versus the olefinic ones in *M. smegmatis*[361]. On the other hand, *M. smegmatis* revealed its high tolerance towards both first-line anti-TB drugs, rifampicin and isoniazid, which is consistent with previous studies by other groups[362, 363]. Resistance to rifampicin was related to its possession of the ADP-ribosyltransferase (encoded by *arr* gene) which enables the inactivation of rifampicin through ribosylation[106]. Rifampicin susceptibility of *M. smegmatis* was reported to be similar to that of drug susceptible *Mtb* H37Rv via downregulation of the corresponding gene[364]. The alkyl hydroperoxide reductase C (*ahpC*) gene encodes the subunit C of alkyl hydroperoxide reductase, an enzyme that counteracts organic peroxides[365]. *ahpC* gene which was found in *M. smegmatis* but not in *Mtb* H37Rv[366] might partly account for the low isoniazid susceptibility. Nonetheless, the exceptionally high MIC of isoniazid displayed in this study might be reasoned by additional factors induced in the static-culturing condition. Isoniazid is a prodrug that requires the activation by the mycobacterial catalase-peroxidase in the presence of molecular oxygen[42]. Static-culturing condition reduces the availability of oxygen and therefore limits the transformation of isoniazid into the active isonicotinic acid in the mycobacterial cells. Gillespie *et al.*[367] reported that the decrease in catalase production by *M. smegmatis* grown in oxygen-depleted condition might be another factor of reduced isoniazid activation. This reduced oxygen availability might trigger dormancy responses in *M. smegmatis* similar to those of *Mtb*[356], leading to increased tolerance to isoniazid[326].

The entry pathway of capreomycin is still yet to be elucidated though it was suggested that the hydrophilic drug is likely to enter the bacteria through the porin channels[17]. Interaction of D-LAK peptides with membrane surface enhanced the permeability of capreomycin resulting in the lowest FICI among other peptides and drug combinations. Unlike the inefficacy on *Mtb* strains, colistin was effective against *M. smegmatis*. *M. smegmatis* possesses lipooligosaccharides (LOS)[368], an analogue of LPS[369], which is the target of colistin. The

effect of tyloxapol was also studied in this assay. Presence of tyloxapol reduced the MIC of D-LAK peptides and rifampicin while its effect on isoniazid, capreomycin and colistin was modest. This is mostly attributed to the capsule-shedding effect of surfactants such as Tween 80 and tyloxapol[340]. Since the D-LAK peptides act on the mycomembrane of *M. smegmatis*, the removal of bacterial capsule by tyloxapol eliminates the barrier to the peptides, thereby lowering their effective concentration. In addition to the removal of bacterial capsule, tyloxapol was also reported to reduce the amount of TDM on *M. bovis* BCG strain[350]. This potentially induces alteration in the mycomembrane permeability, reducing the resistance for the transverse of rifampicin across the cell envelope. Given the effect of morphological manipulation on mycobacteria, tyloxapol was not employed as a de-clumping agent in the culture of this study. Rather, it was included as a treatment condition for comparison with D-LAK peptides and other anti-TB drugs.

Membrane-destabilization activity of D-LAK peptides

The antimicrobial activity of AMPs was reported to be mediated by different mechanisms including targeting intracellular sites and/or cell membrane as described in Chapter 1. Cationic AMPs adopting the amphipathic structure is known to interact with bacterial membranes via a non-specific membrane-destabilization mechanism, which induces the formation of pore, membrane disruption, depolarization, and eventually disintegration following the leakage of cell content[194]. Treatment with D-LAK peptides leads to observable membrane ruffling, mesosomes formation and membrane destabilization in *M. smegmatis*. This revealed the rapid activity and direct membrane interaction of the D-LAK peptides. Similar results with the formation of mesosomes have also been shown when avirulent *Mtb* H37Ra strain was exposed to treatment by other AMPs[345].

Reflecting on the synergy demonstrated against MDR-TB strains, D-LAK peptides alone did not affect bacterial survival while combination with rifampicin or isoniazid resulted in synergy. One of the resistance mechanisms acquired by MDR-TB strain is the alteration in mycobacterial membrane. It was reported that the cell wall of MDR-TB strains is generally thicker than drug-susceptible strains[370]. This might suggest the MDR-TB strains possess mutations conferring resistance on cell envelope would be likely be affected by the action of D-LAK peptide resulted in enhanced accessibility of anti-TB drugs and consequently their intracellular action. To further investigate this argument, *M. smegmatis* incubated with

D-LAK peptides and fluorescein isothiocyanate labelled dextran was visualized by confocal microscopy. Neither rifampicin nor isoniazid treatment induced staining of *M. smegmatis*, implying the integrity of mycomembrane remained largely intact. Conversely, *M. smegmatis* treated with D-LAK peptides at various concentrations were stained with intense green signal. This revealed the ability of D-LAK peptide in altering the surface properties of bacterial membrane, potentially enhancing the access of small molecules into *M. smegmatis*. Similar study has also been done which showed the action of cationic peptide promoting passive diffusion of FITC-labelled dextran of the similar size[261]. Although the 2-dimentional images shown in this study render the impossibility to differentiate surface-absorbed from intracellular signal, provided the membrane lytic action of D-LAK peptide obtained from TEM assessment, the results clearly suggested the membrane destabilization or alteration bring forth by the action of D-LAK peptides.

Changes in membrane properties by tyloxapol and anti-TB agents

Given that D-LAK peptide act on *M. smegmatis* via membrane-active actions, the structure of mycomembrane would expect to be altered. The studies of membrane rigidity and membrane order provide additional clues to the changes in organization of the cell wall lipids brought about by the peptides' action. Rodriguez-Rivera *et al.*[371] revealed the highest membrane rigidity of mycobacteria using *M. smegmatis* as the model species as compared with the other actinobacteria included in the study. The finding suggested membrane rigidity as a function of length hydrocarbon chains and presence of functional group in mycolic acids. Fluorescence steady-state anisotropy of DPH and Laurdan general polarization were employed to measure the effect of different treatment conditions to mycomembrane. Due to the complexity of the mycobacterial cell envelope, the exact location of DPH or Laurdan probe is still yet to be elucidated. However, taken together with the HR-MAS metabolomics studies which indicated the changes in components of mycolic acids as a result of exposure to anti-TB agents, the fluorescent probe is likely to be reporting the properties of mycomembrane in the mycobacterial envelope. Also, the high correlation shown between GP and DPH anisotropy supports the findings in which membrane rigidity has an inverse relationship with membrane order on *M. smegmatis* and the changes in membrane rigidity is likely to be the result of mycomembrane remodelling in response to given challenges.

Significant difference was observed when *M. smegmatis* was grown in the presence of tyloxapol, with a higher membrane rigidity and lower membrane order when compared with the growth control without tyloxapol (7H9O). The established capsule shedding effect of tyloxapol might be one explanation. The extractable and loosely bound lipids removed from the bacterial surface might lead to the enhanced hydration of the Laurdan fluorescent moiety or facilitate the penetration of DPH probe in the mycomembrane which resulted in a lowered GP value and an increased DPH anisotropy r. Metabolic studies revealed the reduction of saturated lipid resonances in the presence of tyloxapol which suggests its effect on the mitigation of membrane surface lipid components. This further indicates the mycomembrane structure was altered in response to the action of the surfactant. In essence, tyloxapol is a lipase inhibitor which has been reported to exert metabolic effects[350].

Interestingly, capreomycin without the capsule washing action, caused the same effect of increasing rigidity whereas reducing the order of mycomembrane. Although the exact mechanism of the action of capreomycin is not fully understood, its antimicrobial activity against mycobacteria is thought to be the influence on the function of ribosomes leading to the inhibition of protein translation[110]. Specifically, it involves the *tlyA* gene coding an rRNA methyltransferase for the methylation of the ribosomal interface in 16S and 23S rRNAs[372]. A transcriptomic study on *Mtb* confirmed this essential mechanism while uncovered substantial changes in an additional range of gene classes including cell wall processes, lipid and intermediary metabolism as well as cell respiration[373]. Notably capreomycin was shown to affect the preference of carbon source, through the upregulation of *icl*, *glcB* and *acaAa* genes. The glyoxylate shunt, an anaplerotic pathway of tricarboxylic acid (TCA) cycle which utilizes fatty acid and acetate for carbohydrates biosynthesis, was stimulated. Meanwhile, the expression of a series of genes associated with electron transport chain, including those encoding for NADH dehydrogenase or NADH-ubiquinone oxidoreductase, was reduced. The present study on *M. smegmatis* is consistent with these findings in which the substantial reduction in mycolic acid corresponds to the fatty acid being diverted for use as a carbon source. Otherwise, the accumulation of glutamate and trehalose, following the challenge with capreomycin, might be a result of stress-induced response. It was reported that glutamate may serve as an energy reserve when bacteria were stressed. *M. bovis* BCG were shown to use glutamate as carbon source under acidic and nitrosative stress[374]. Cowley *et al.*[375] have also proposed the increased level in glutamate and glutamine may act as a source of amine for the synthesis of reducing buffers such as mycothiol by *Mtb* to deal with oxidative stress. Boots *et al.*[376] identified the concomitant release of free trehalose as a signal for cell envelope stress in

mycobacteria. Therefore, the action of capreomycin led to the alteration of cell wall integrity, in turn triggered the redox stress response, resulted in the increase in glutamate and trehalose production. The decrease in fatty acid and accumulation of glutamate were also shown in a *M. smegmatis* mutant with a *Mce4*- knockdown[351]. *Mce* proteins are involved in the transport of cell wall lipid and their absence alters cell wall structure and architecture. This suggests capreomycin might induce the same downstream responses through the induction of cell wall remodeling. When compared with challenge by rifampicin, no significant change was detected in individual metabolite levels in spent culture media with capreomycin. Overall, these findings indicate that a substantial shift in metabolism was initiated by the challenge of capreomycin causing a greater consumption of fatty acids, depletion of mycolic acid and mycomembrane rigidification as ratio of trehalose dimycolates to trehalose monomycolates was shifted favoring the latter. Consequently, this alteration of membrane caused by capreomycin may influence the ability of other antimicrobials to cross the barrier and reach their intracellular targets.

Alternatively, rifampicin induced a comparatively less intense reduction in saturated and unsaturated lipid resonances than capreomycin and induced modest changes in mycomembrane properties. Rifampicin targets the DNA-dependent RNA polymerase of mycobacteria, exerting a greater antimicrobial effect on *Mtb* than *M. smegmatis* due to the intrinsic resistance of the latter. Nonetheless, challenge with rifampicin against *Mtb* was reported to alter expression in genes of the same functional classes as that affected by capreomycin[377]. Moreover, activation of isocitrate lyases in *Mtb* challenged by rifampicin and isoniazid indicates the upregulation of glyoxylate shunt bypassing the TCA cycle to reduce the production of reactive oxygen species (ROS), therefore increasing the resistance towards oxidative stress[378]. The changes in mycolic acid induced by rifampicin alone or D-LAK120-A in combination with rifampicin might be an indication of oxidative stress and reflected the penetration into the bacterium. Notably, combination of rifampicin with D-LAK120-HP13 did not have the same effect. This again revealed the different mechanism of action of the two D-LAK peptides and therefore the difference in the level of potentiation when combining with various first and second-line anti-TB drugs.

Trehalose also plays a role as mycolate carrier[379]. Surprisingly, significant decrease in trehalose was shown in isoniazid treatment. This observation is unexpected as isoniazid acts by inhibiting mycolic acid synthesis and therefore accumulation of trehalose was reported as a result of the influence of isoniazid[380]. Isoniazid-treated *M. smegmatis* and *Mtb* were also

reported to accumulate free trehalose[381]. This discrepancy might be attributed to the effect of anaerobiosis as aforementioned, which reduces the amount of active isoniazid molecules rendering their ineffectiveness towards the bacteria. The absence of significance in most of the lipid resonances might also support the lack of isoniazid activity. Furthermore, it was reported that trehalose was used as a carbohydrate source by *M. smegmatis* under anaerobic conditions[367]. The dissimilar response of *M. smegmatis* to the challenge of rifampicin compared with that to capreomycin, both quantitatively in HR-MAS and also qualitatively in spent culture media proposes evidence that the bacteria resist against oxidative stress by adopting different strategies. This counteracting mechanism towards rifampicin is likely to be facilitated by the alteration in metabolism of fatty acid in *M. smegmatis* but to a lesser extent than when challenge by capreomycin.

Differing mechanism of action of D-LAK120-A and D-LAK120-HP13

The difference in response in the combinations with capreomycin and the induced changes in bacterial metabolism showed that the two D-LAK peptides have distinct mechanism of action. The presence of proline residue in D-LAK120-HP13 gives rise to its flexible conformation to facilitate its penetration into mycomembrane. Consequently, significant changes in mycomembrane rigidity and induced reduction in lipid resonances were triggered by D-LAK120-HP13 but not the proline-free D-LAK120-A. The increase in flexibility of the peptide may allow a more intimate interaction between the peptide and the anionic lipid components, leading to lipid reorganization in the mcyomembrane. Other study shows that segregation of lipids were demonstrated in model multilamellar vesicles by membrane active cationic AMPs *in vitro*[382]. The selective lipid interaction with peptide was suggested to relate to the changes in membrane fluidity. Moreover, Scheinpflug *et al.*[383] reported the membrane rigidification in live *Bacillus subtilis* induced by a synthetic cyclic hexapeptide cWFW. Adaptive response in the bacteria was also triggered on the level of membrane fatty acid composition upon cWFW stress. In addition to the changes in membrane property, stress response in *M. smegmatis* indicated by accumulation of glutamate was only observed when the bacteria were exposed to D-LAK120-HP13. This indicates D-LAK120-HP13 exert a membrane active effect inducing mycomembrane remodeling. On the contrary, D-LAK120-A inhibited the growth of *M. smegmatis* but did not induce the similar remodeling response at sub-MIC. The exact mode of action of this peptide cannot be clearly elucidated in the present study though the absence of induced membrane remodeling might shed light on other

mechanisms. For instance, the stronger synergy with capreomycin mediated by D-LAK120-A reveals its possible intracellular targeting ability. Overall, the results obtained using the combination of HR-MAS metabolomics and fluorescent probes have provided further information demonstrating distinct mechanism exhibited by the proline-free and proline-containing analogues.

Action on mycomembrane underpins synergy in combinations

In general, a synergistic combination requires two agents to work complementarily with each other by acting on different target sites or distinct effect on the same target, without counteracting each other's activities. The combination of HR-MAS ^{1}H NMR and fluorescence techniques allow the investigation of the different actions of antibiotics on the mycomembrane. This is attained by gaining the perspective of bacteria towards the exposure to antibiotics and thereby inferring the drug activity according to the corresponding bacterial responses. Using these quantitative and qualitative responses of *M. smegmatis*, the distinct membrane activity of antibiotics was proposed which underpins the synergistic effect in different combinations.

Potency of D-LAK peptides or rifampicin in isolation against *M. smegmatis* was improved in the presence of tyloxapol but the effect of their combination was indifferent. Since rifampicin and tyloxapol both triggered a certain extent of remodeling in mycomembrane, it is postulated that the membrane active effect of D-LAK peptides might be inhibited in the combination with rifampicin in the presence of tyloxapol. In the absence of tyloxapol, action of D-LAK120-HP13 was more prominent and thereby showing a better antimicrobial efficacy than D-LAK120-A when combined with rifampicin. This result may reflect the different effect on the activity of the two D-LAK peptides caused by changes in membrane properties induced by rifampicin. In contrast to the antagonistic D-LAK120-A and rifampicin combination, it could be suggested that D-LAK120-HP13, with the proline modification, is more effective in facilitating the penetration of rifampicin through the mycomembrane. On the other hand, modest synergistic interaction occurs in combination of capreomycin with either of the D-LAK peptide. Nonetheless, this interaction was promoted in the presence of tyloxapol. Since tyloxapol enhanced the action of both D-LAK peptides and rifampicin but not capreomycin against *M. smegmatis* when used alone, this promotion of synergy is more likely due to the improved access of either D-LAK peptide in the combination instead of

capreomycin. Although difference in the performance of both combinations was not significant, D-LAK120-A outperformed D-LAK120-HP13. The poorer synergy in D-LAK120-HP13 combination with capreomycin might be due to the similar mechanism of action of both agents on the mycomembrane. Also, this action of D-LAK120-HP13 could possibly affect the structure or functioning of porin channels on the mycomembrane hindering the diffusion of hydrophilic capreomycin to a certain extent. Despite the difference in magnitude of bacterial responses, the induction of changes in mycomembrane by both capreomycin and rifampicin suggest membrane interaction as one of the important determinants for synergistic interaction against *M. smegmatis*. The distinct physicochemical properties of the drugs might be a possible explanation. Capreomycin and rifampicin are both cationic molecules with the molecular weight of 668 Da and 823 Da respectively, but the net positive charge at physiological pH of capreomycin is +4, higher than +1 of rifampicin. D-LAK peptides, possessing a net charge of +9, have a high affinity for the negatively charged mycomembrane, therefore may serve as a screen for the membrane to interact with either rifampicin or capreomycin. The higher positively charged capreomycin would render it easier to overcome this screen and this may explain the observed synergy of the combinations.

In conclusion, the action of the two D-LAK peptide analogues can be distinguished based on the corresponding response of *M. smegmatis* and their different abilities in facilitating the antimicrobial activities of other antibiotics. Besides, the combination of fluorescence spectroscopy and HR-MAS ^{1}H NMR technique revealed that combining with anti-TB agent, in particular those that trigger mycomembrane remodeling, may affect the effectiveness of peptides in combinations. In addition to the mode of action of each anti-TB agents, understanding their mutual interactions would be crucial for the design of prominent antibiotic combinations. This study demonstrated the use of these techniques on *M. smegmatis*, which pathed the way to apply to the investigation on *Mtb*. In the next chapter, a severely attenuated *Mtb* Bleupan strain would be exploited to bring a step closer to the elucidation of antibiotic mechanisms on *Mtb*.

Chapter 6 Metabolic responses of *Mtb* Bleupan challenged by D-LAK peptides and/or anti-TB drugs

6.1 INTRODUCTION

In the previous chapter, a better understanding of the effect of the anti-tuberculosis (anti-TB) agents on mycobacterial membrane was gained using *Mycobacterium smegmatis* as model, HR-MAS metabolomics studies revealed the changes in the bacterial metabolites were mainly associated with the changes in the physical properties of the mycomembrane as well as an induced stress-response. The correlation of membrane rigidity with mycomembrane-dominated mycolic acids content identified the action of anti-TB agents, notably capreomycin and rifampicin, to trigger membrane remodeling in mycobacteria. These findings establish the basis for these techniques to be exploited to study the biological activity and mode of action of antibiotics on mycobacteria.

In most of the early drug screening processes, different mycobacterial models have been employed as surrogate[384] to avoid the use of slow growing, highly pathogenic *Mtb*. One of the most popular models, *Mycobacterium bovis* Bacillus Calmette-Guérin (BCG), is derived from the species *M. bovis* in the *Mtb* complex. *M. bovis* BCG was initially used for screening of 50 analogues of Para-aminosalicylic acid[385]. It has then become a popular model for TB research as it demonstrates high level of similarity to *Mtb* in terms of sensitivity towards drug candidates[386, 387]. Nonetheless, the differences between BCG and pathogenic *Mtb*, especially due to the result of region of difference 1 (RD1) deletion, rendering the use of BCG undesirable due to different host pathogen interactions. Although the doubling time of BCG (~16 hours) is shorter than that of *Mtb* (~24 hour), this remains a major limitation for efficient drug discovery studies. Instead, the fast-growing *Mycobacterium aurum*, bearing low pathogenicity but the ability to survive inside macrophage, serves as an alternative model of high throughput TB drug screening research[388]. In addition, the possession of mycolic acid analogues and similar antibiotic susceptibility profile to *Mtb* encourage the use of *M. aurum* as a surrogate to study anti-TB agents[389]. Despite the merits suggested, this non-tuberculous species also demonstrated highly deviated stress responses as compared to *Mtb* and did not show non-replicating persistence[390]. As the induced-stress response can be one of the possible mechanisms of drug action, it is necessary to take this into consideration and therefore the choice of *M. smegmatis* in the preceding study was made for its similarity to *Mtb* in this aspect[390].

Other model mycobacteria employed in TB studies include *M. fortuitum*, *M. phlei*, *M. abcessus*, *M. marinum*, all with varying strengths and weaknesses in serving as *Mtb* model[388].

The shorter doubling time and requirement of lower biosafety facility render *M. smegmatis* an attractive model for the study of TB biology[353]. However, much of the controversy involving the use of *M. smegmatis* has also stemmed from its low pathogenicity and different cell wall structure[354] while studies to verify their applicability are rare. To address this issue, the response between *Mtb* Bleupan and *M. smegmatis* were compared to deduce whether *M. smegmatis* is a reliable surrogate model. The severely attenuated *Mtb* Bleupan strain was demonstrated in Chapter 4 as a useful model for studying virulent *Mtb* strains due to their similar susceptibility towards antibiotics and D-LAK peptide combinations. Thus, corresponding drug-induced mechanistic responses of *Mtb* Bleupan were evaluated here using the combination of biophysical techniques established in the preceding chapter. Through comparison with the data generated from *Mtb* Bleupan, the level of translatability of findings in *M. smegmatis* can be deduced, allowing evaluation of the continued applicability of the latter for further antibiotic studies.

Since the high potency of combinations of D-LAK peptides with rifampicin or isoniazid against MDR-TB clinical isolates was not shown on *M. smegmatis*, a more relevant *Mtb* model was used to look for possible explanations. Therefore, this study aimed to use *Mtb* Bleupan as the model to investigate the action of anti-TB agents and the underlying mechanism of synergy between the D-LAK peptides and rifampicin or isoniazid observed in MDR-TB. This would enable a more in-depth understanding of the effect of anti-TB agents on *Mtb* metabolism and growth responses, in particular concerning components consisting the mycomembrane. More information could then be gathered to postulate the mechanism of interaction between D-LAK peptides and rifampicin or isoniazid.

In this study, the culture of *Mtb* Bleupan strain was incubated with sub-inhibitory concentration of antibiotics or D-LAK peptide combinations in liquid medium without agitation nor detergent. Owing to the slow-growth rate, two different conditions were selected for the sub-MIC challenge assay, i) six weeks challenge of 1% inoculum with ¼ MIC of anti-TB agents and ii) 72 hours challenge of six-week cultured bacteria with ½ MIC of anti-TB agents. Membrane properties were examined by DPH fluorescent probe. HR-MAS and liquid-state NMR metabolomics were performed to study metabolic changes induced by each of the challenge conditions. These experiments were designed to test how the antibiotics and their combinations with D-LAK peptides may act on *Mtb* and provide valuable insights regarding the suitability of the mycobacterial models in the study of antibiotics actions using a variety of biophysical techniques.

6.2 RESULTS

6.2.1 Determination of media effect on membrane properties by DPH and Laurdan fluorescence assays

Laurdan and DPH fluorescence assays were used to study how different culture media composition affected the membrane properties of *Mtb* Bleupan (Fig. 6.1). The aim of this preliminary experiment is to understand the effect of OADC-supplement (denoted by the "O") and tyloxapol on the growth of *Mtb* Bleupan. OADC-supplement is considered necessary for the normal growth of mycobacteria *in vitro*, whereas tyloxapol acts as an anti-clumping agent but also induced changes in mycobacterial membrane morphology as described for *M. smegmatis* in the preceding chapter. GP values and anisotropy (r) denote the membrane order and rigidity, respectively. Significant differences were found between the GP values of Laurdan dyed *Mtb* Bleupan cultured in 7H9 with tyloxapol and cultured in 7H9 alone ($p < 0.05$) as well as between *Mtb* Bleupan cultured in 7H9O with tyloxapol and 7H9O ($p < 0.01$). The membrane order, as inferred from Laurdan GP, was found to be higher in the presence of tyloxapol in both cases. The presence of OADC-supplement also resulted in significantly higher membrane order when compared with those conditions without supplement. The measurement of membrane rigidity using DPH fluorescence assay did not show any significant changes in different conditions. Albeit modestly, *Mtb* Bleupan grown in 7H9 medium with OADC supplement showed to have the highest membrane rigidity which suggests the possession of an intact mycomembrane with tight packing of mycolates. Danilchanka *et al.*[391] also demonstrated OADC maintained healthy growth and thriving of *Mtb* as compared with other carbon sources such as 1% glucose, 0.5 % glucose with glycerol or 1 % tween 80 in 7H9 medium. *Mtb* Bleupan cultured in 7H9O was then used as untreated bacterial control in this study.

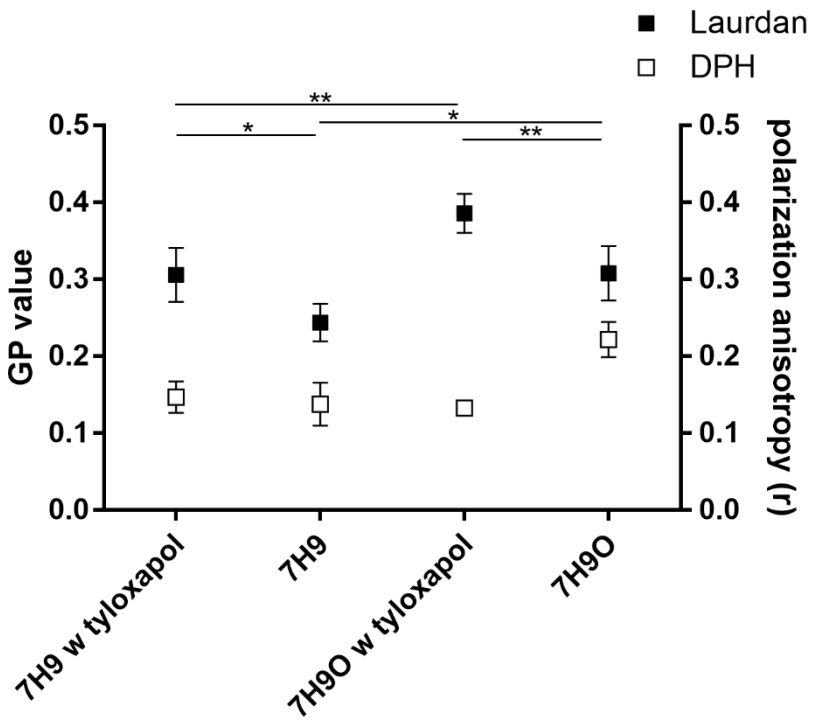

*Figure 6.1 Media effect on membrane properties of Mtb Bleupan by Laurdan and DPH fluorescence assay. The left y-axis shows the GP values from Laurdan probe; the right y-axis shows the DPH anisotropy r. Significant difference in GP values between conditions was assessed using one-way ANOVA analysis followed by Tukey's Multiple Comparisons Test, *<0.05, **<0.01, ***<0.001. No significance was detected in r between different conditions.*

6.2.2 Mycobacterial growth response assays

Fluorescence assays

In order to study the mechanism of action of different anti-TB agents and their combinations, *Mtb* Bleupan was challenged with various anti-TB agents and their combination with D-LAK peptides. Two conditions were performed in this study: i) six weeks challenge of 1% inoculum with ¼ MIC of anti-TB agents and ii) 72 hours challenge of six-week cultured bacteria with ½ MIC of anti-TB agents. Due to the complexity of *Mtb* cell envelope, the distribution of interfacial Laurdan probe would be anticipated to vary in a greater extent than DPH probes which mainly reside in the hydrophobic regions. Therefore, only DPH probe was selected to perform this study. Anisotropy of the DPH fluorescent probe was measured for bacteria grown in both conditions (Fig. 6.2). Notably, the membrane rigidity of untreated *Mtb* Bleupan was generally higher than that of *M. smegmatis* ($r < 0.1$). This might reflect the differences in the structure of mycolic acids consisting the respective mycobacterial membrane. For the six-week challenge (Fig. 6.2A), a significant decrease in membrane rigidity was observed when the bacteria were cultured in the presence of 0.025 % tyloxapol. This contrasts with the analogous experiment performed for *M. smegmatis* mc^2 155 in the previous chapter where the fluorescence anisotropy was observed to decrease for the same treatment. Growth of *Mtb* Bleupan with D-LAK peptides at ¼ MICs induced slight increase in membrane rigidity and this effect is also observed when they were used in combination with rifampicin or isoniazid while capreomycin induced similar level of changes in membrane rigidity. However, none of these changes was significant when a one-way ANOVA was performed across all samples. Since it was speculated that the modest changes in membrane property might be due to the degradation of anti-TB agents through the long incubation time, another study condition was performed in which six-week cultured bacteria were challenged with ½ MIC of anti-TB agents for 72 hours.

Challenge of *Mtb* Bleupan with ½ MIC for 72-hour resulted in slightly different observations in some of the conditions (Fig. 6.2B). Again, the general trend was that each treatment led to a modest increase in fluorescence anisotropy, and hence membrane rigidity. However, the differences were found to be non-significant when a one-way ANOVA was performed across all samples. Exceptions were treatment with isoniazid alone, which resulted in highly significant ($p < 0.001$) increase in membrane rigidity denoted by r at 0.19 ± 0.02 comparing to 0.13 ± 0.02 of untreated control (7H9O), and the combination of isoniazid with D-

LAK120-A which led to more modest increase in r. Combination with D-LAK120-HP13 was shown to mitigate the action of isoniazid itself resulting in negligible changes in membrane rigidity. These results are consistent with manipulation of the membrane physical properties by sub-inhibitory isoniazid challenge, possibly through the drug action of interfering the synthesis of mycolic acid. Neither of the D-LAK peptides induced similar responses indicating that the mechanisms of response to the D-LAK peptides are different to those found for isoniazid. This may be essential for the synergistic interaction of these different antibiotics as seen in the previous FIC studies (Chapter 4, Table 4.4). The mitigation of the isoniazid induced increase in rigidity may therefore be a hallmark of synergism but may also be related to the fact the concentration of both D-LAK peptide and isoniazid used here in the combination were much lower than when they were applied alone. Again, capreomycin challenge brought about a modest but non-significant increase in membrane rigidity. Delamanid, another anti-TB drug acts by inhibition of mycolic acid synthesis, caused an increase in membrane rigidity of the same magnitude as that induced by capreomycin but this was found to be significant ($p < 0.05$). Colistin, targeting cytoplasmic membrane of Gram-negative bacteria, on the contrary, did not induce any changes in mycobacterial membrane in both conditions.

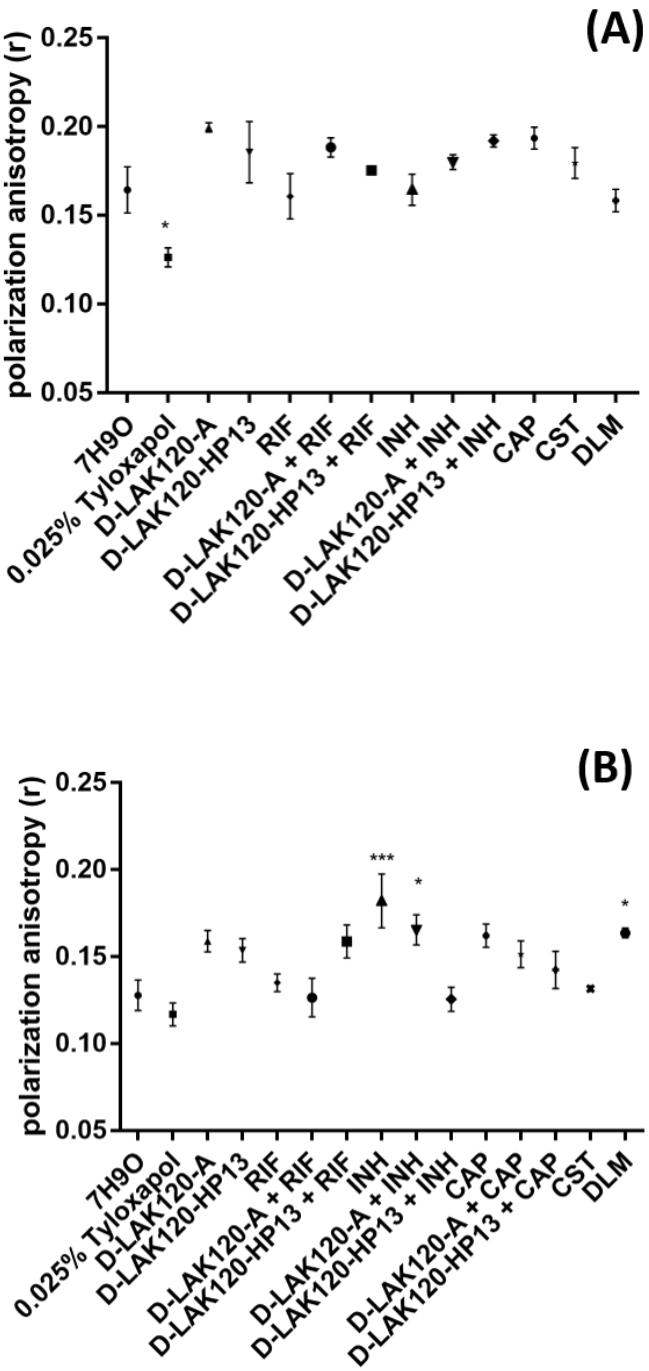

*Figure 6.2 DPH fluorescence anisotropy of Mtb Bleupan response to challenge with anti-TB agents and combinations. Mtb Bleupan subjected to challenge at ¼ MIC for 6 weeks (A) or ½ MIC for 72 hours (B). Data were presented as mean ± SD (n=9). Significant difference was assessed using one-way ANOVA analysis followed by Dunnett's Multiple Comparisons Test, *<0.05, **<0.01, ***<0.001 vs 7H9O.*

Metabolite assignment of Mycobacterium tuberculosis Bleupan

HR-MAS ^{1}H NMR metabolomics was used to elucidate the metabolites in the whole cell sample of unchallenged *Mtb* Bleupan. Comparison of the ^{1}H NMR spectra obtained from HR-MAS (Fig. 6.3) and liquid state NMR (Fig. 6.4) show the dominance of broad lipid peaks in whole cell sample of *Mtb* Bleupan in the HR-MAS spectra. As compared with spectra of *M. smegmatis*, some of the lipid resonances were less intense in the whole cell analysis whereas more metabolites were detected in the spent culture media of *Mtb* Bleupan. Assignments of metabolites associated with peaks are shown as a reference for the backscaled loadings and NMR spectra shown in this section. Lipid resonances were assigned according to the general mycolic acid structure. Distinct mycolic acid signals were identified to consist of the different saturated and unsaturated lipid resonances and trehalose. A low intensity resonance assigned to unsaturated -CH=CH- lipid (2.03 ppm) arising from the meromycolate chains of mycolic acids was detectable. Signals from the integration of cyclopropyl proton resonances (- 0.33 ppm), however, were not detected. This may be a result of the low sensitivity of HR-MAS in addition to the low diffusion rate of mycolates in the mycomembrane. Insufficient hydration by D_2O leads to very weak signals from certain protons and although the bacteria samples were allowed to hydrate for at least 2 h before being analyzed by HR-MAS, rehydration in 10 x volume of D_2O may be required[239]. Alahari *et al.* also proposed the addition of 5 µl of chloroform to disrupt the mycobacterial cell wall which allowed the observation of the protons of the cyclopropyl-ring by HR-MAS[338]. Alternatively, proton NMR analysis of lipid extract of *Mtb* enabled the detection of cyclopropane structure in mycolic acids[255]. Assignment of resonance without overlapping signal from lipids, was possible for valine, alanine, lysine, glutamate, serine, trehalose, sucrose and glycerate (Fig. 6.3). Spectra of spent culture media of *Mtb* Bleupan showed relatively higher resolution without the interference of broad peaks (Fig. 6.4). Binary comparison of metabolism of *Mtb* using spent media versus fresh media revealed the bacteria consumes pyruvate and glutamate but not glucose unlike *M. smegmatis* and, they produced mainly succinate, acetate and another metabolite cadaverine which was not detected in *M. smegmatis* culture (Fig. 6.5). Metabolites assigned with their corresponding ppm are summarized in appendix A (Table 7.1 and 7.2).

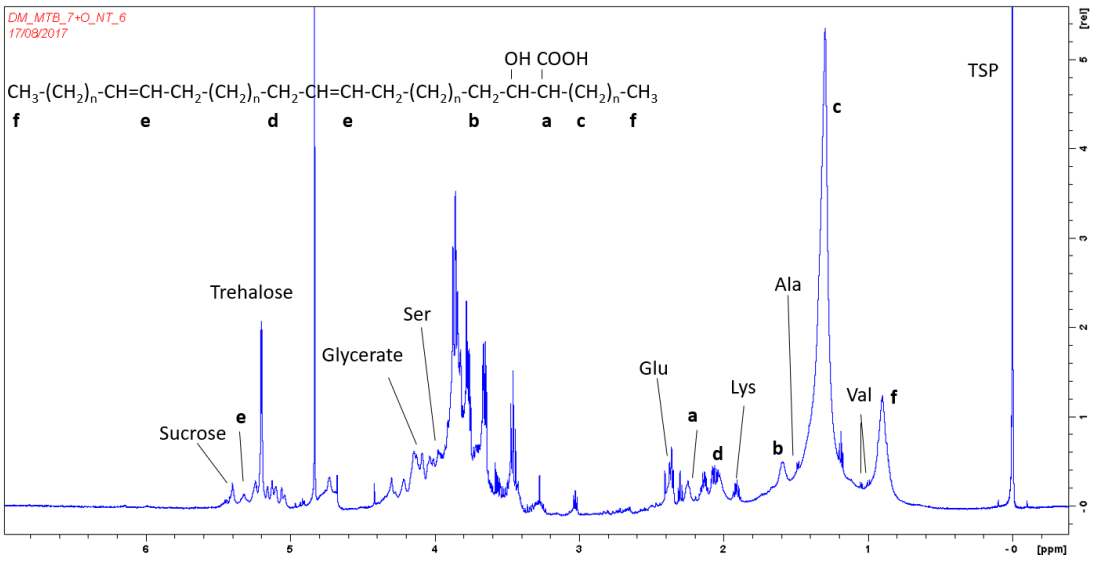

Figure 6.3 1D ^{1}H HR-MAS spectrum of whole cell Mtb Bleupan grown in 7H9O media. Spectrum was obtained at 600 MHz for ^{1}H at a sample spinning speed of 5 kHz with the sample maintained at 310 K.

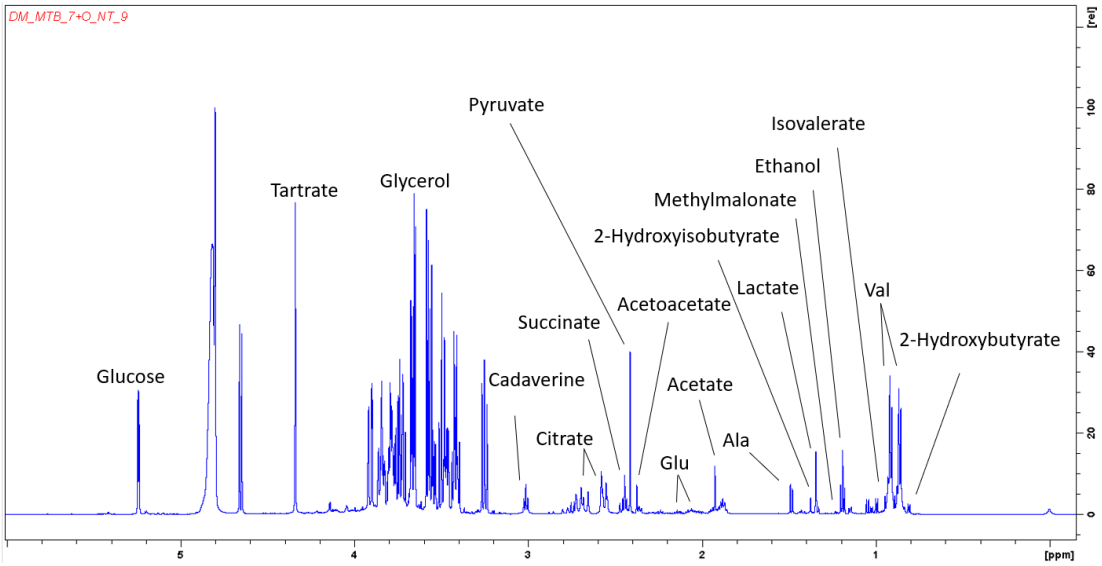

Figure 6.4 1D ^{1}H CPMG NMR spectrum of spent 7H9O culture media after 6 weeks growth of Mtb Bleupan. Spectrum was obtained at 700 MHz for ^{1}H at 298 K.

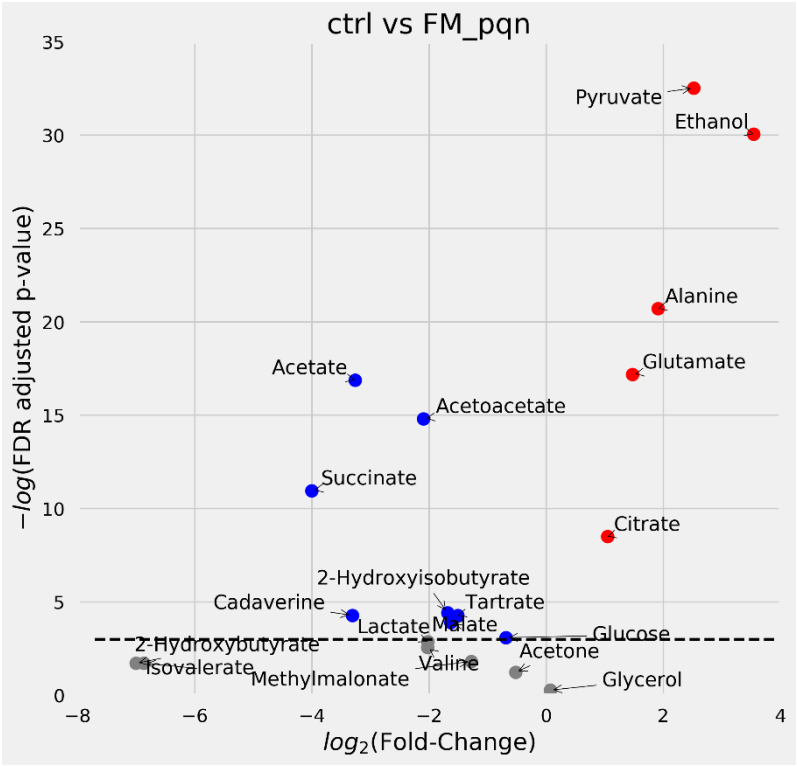

Figure 6.5 Volcano plot depicting changes in various metabolites in spent media of Mtb Bleupan incubated for 6 weeks as compared with Fresh Media 7H9O. Volcano plots are of PQN normalized data and allow comparison of fold changes and significance of each metabolite; blue – significant reductions, red – significant increases and grey – non-significant changes in the indicated metabolites. For comparison with M. smegmatis in Chapter 5, Fig. 5.14L (P. 150).

Multivariate analysis

In order to evaluate how each treatment affects the growth of *Mtb* Bleupan, the metabolic profile of whole cell bacteria and their spent media were analysed using a non-targeted NMR metabolomics approach. All reduced data matrices from ^{1}H NMR spectra after pre-processing were subjected to multivariate analysis. PCA plots were constructed initially to obtain an overview of the dataset (Appendix C, Fig. 7.30-7.33). For both six-week and 72-hour challenge, PC 1 accounted for over 90 % of the variation. The loading plots indicate that these variations are associated with the saturated lipid components at 1.29 ppm and trehalose at 3.8 ppm. PC 2 explained less than 1 % of the variation in both conditions. Nonetheless, no obvious clustering was resulted by projecting the dataset through PC1 and PC2. This phenomenon might arise as PCA is limited to a linear model which does not readily distinguish variations between within-class and between-class[392]. The most influential metabolites in sample variation were denoted, -$(CH_2)_n$- and trehalose. On the other hand, analysis of spent culture media was also similar at both conditions in which PC 1 explained the majority of the variance found in the dataset at 96.2 % and 92.9 % for six-week and 72-hour incubation, respectively. The key metabolites responsible for the variations were ethanol, pyruvate and tartrate. Fresh media samples were found to be clustering in both conditions, while samples with tyloxapol only clustered in the analysis of 72-hour challenged samples.

OPLS-DA was used to extract further information relevant to the growth response of *Mtb* Bleupan under each treatment to identify significant metabolites that contributed to their differences from the untreated control. The Q^2 and permutated Q^2 indicate the predictability of the proportion of variance in the data by machine-generated models using assigned and random class labeling respectively. (Table 6.1 and 6.2). The calculated Q^2 of assigned classes in most conditions are close to 1 or have a greater value than permutated Q^2. Value of Q^2 above zero is useful for the determination of significance of certain treatment. The greater the value of Q^2 than permutated Q^2, the more reliable the model is in illustrating the significant difference between each assigned class and the untreated control. These treatments with high Q^2 were marked in bold which resulted in significant changes illustrated by the succeeding volcano plots and univariate analysis. While in some cases such as the ^{1}H HR-MAS data of D-LAK120-A with rifampicin and D-LAK120-HP13 with rifampicin at six-week incubation, a negative Q^2 was produced. This reflects the assigned classes did not show significant difference from the untreated control, suggesting that these treatments did not trigger detectable difference in terms of metabolic responses.

Results from the 72-hour challenge reflected a generally better separation in each treatment from the untreated control where the higher drug concentration and/or shorter incubation time contribute to a more prominent effect. The best separation in the 72-hour treatment was the combination of D-LAK120-A with capreomycin and it is also the treatment that induced the most significant changes in terms of number of metabolites.

Table 6.1 Test and permutated Q^2 scores for cross-validated OPLS-DA models of ^1H HR-MAS or liquid-state NMR spectra of Mtb Bleupan challenged for 6 weeks. Comparison of unchallenged bacteria with those obtained from bacteria treated by the indicated conditions. Those conditions where significant changes are also seen in individual metabolites were highlighted in bold (univariate analysis with Mann-Whitney U test and Benjamini-Hochberg false discovery rate adjustment).

HR-MAS			**Liquid-state**		
	Q^2	permutated Q^2		Q^2	permutation Q^2
0.025%Tyloxapol	**0.788**	-0.394	0.025%Tyloxapol	**0.808**	-0.200
D-LAK120-A	0.084	-0.337	D-LAK120-A	0.361	-0.206
D-LAK120-HP13	0.162	-0.304	D-LAK120-HP13	0.407	-0.204
Rifampicin	0.319	-0.329	Rifampicin	0.457	-0.222
D-LAK120-A + RIF	-0.116	-0.282	D-LAK120-A + RIF	0.057	-0.197
D-LAK120-HP13 + RIF	-0.244	-0.236	D-LAK120-HP13 + RIF	0.103	-0.206
Isoniazid	**0.182**	-0.325	Isoniazid	**0.692**	-0.275
D-LAK120-A + INH	**0.555**	-0.357	D-LAK120-A + INH	0.562	-0.205
D-LAK120-HP13 + INH	**0.324**	-0.319	D-LAK120-HP13 + INH	-0.091	-0.203
Capreomycin	**0.594**	-0.334	Capreomycin	**0.705**	-0.211
Colistin	0.248	-0.293	Colistin	**0.832**	-0.238
Delamanid	**0.643**	-0.393	Delamanid	**0.865**	-0.306
			Fresh media	**0.931**	-0.188

Table 6.2 As above but for cross-validated OPLS-DA models of ^1H HR-MAS or liquid-state NMR spectra of Mtb Bleupan challenged for 72 hours.

HR-MAS			**Liquid-state**		
	Q^2	permutated Q^2		Q^2	permutation Q^2
0.025%Tyloxapol	0.631	-0.404	0.025%Tyloxapol	**0.886**	-0.262
D-LAK120-A	0.503	-0.271	D-LAK120-A	**0.630**	-0.267
D-LAK120-HP13	0.426	-0.337	D-LAK120-HP13	**0.824**	-0.413
Rifampicin	0.593	-0.267	Rifampicin	0.331	-0.277
D-LAK120-A + RIF	0.433	-0.313	D-LAK120-A + RIF	0.061	-0.399
D-LAK120-HP13 + RIF	0.342	-0.323	D-LAK120-HP13 + RIF	0.536	-0.380
Isoniazid	0.185	-0.275	Isoniazid	**0.497**	-0.303
D-LAK120-A + INH	0.564	-0.330	D-LAK120-A + INH	0.207	-0.319
D-LAK120-HP13 + INH	**0.405**	-0.254	D-LAK120-HP13 + INH	0.464	-0.345
Capreomycin	0.375	-0.302	Capreomycin	0.262	-0.320
D-LAK120-A + CAP	**0.736**	-0.309	D-LAK120-A + CAP	0.552	-0.329
D-LAK120-HP13 + CAP	**0.393**	-0.278	D-LAK120-HP13 + CAP	0.603	-0.305
Colistin	**0.702**	-0.348	Colistin	**0.816**	-0.399
Delamanid	0.624	-0.310	Delamanid	0.643	-0.291
			Fresh Media	**0.983**	-0.175

A hierarchical clustered heatmap compares the loadings for each model calculated from the analysis (Appendix C, Fig. 7.34 and 7.35). On a relative scale, intense changes were mostly found in saturated and unsaturated lipid resonances, trehalose and glutamate for ^{1}H HR-MAS dataset. Although the two study conditions gave quite a different response in terms of changes in these metabolites, it is probably originating from the difference in duration of drug challenges. This shows that *Mtb* Bleupan adopts alternative mechanisms when exposed to different stimuli or hostile environment as well as the length of exposure time. In the case of the changes in spent media across all treatments, accumulation and depletion of metabolites including 2-hydroxyisobutyrate, isovalerate, glycerol, ethanol, succinate, valine, pyruvate, acetate, glutamate, citrate, glucose and tartrate were more pronounced.

To further verify the magnitude and significance of changes in certain key metabolites in HR-MAS, volcano plots were constructed for individual comparison of each condition for six-week incubation (Fig. 6.6). The presence of tyloxapol induced a significant increase in both saturated and unsaturated lipid resonances: $–(CH_2)_n$-, -CH_3, -CH=CH- and R_2CH-OH, while a decrease in trehalose, glutamate, serine and lipid R_2CH-COOH were detected (Fig. 6.6A). This is markedly different from the observation in *M. smegmatis* in which a significant decrease in saturated lipid resonances was resulted whereas glutamate and serine were significantly increased without any significant changes in trehalose content. Capreomycin treated *Mtb* Bleupan was shown to reduce the level of glutamate, lysine, lipid R_2CH-COOH and both unsaturated lipids (Fig. 6.6J). This result was similar to the capreomycin-treated *M. smegmatis* in which there was a significant reduction in lipid resonances but on the contrary, a significant production of glutamate was observed. Higher amount of saturated lipid alkyl groups $–(CH_2)_n$- and -CH_3 resulted from delamanid treatment whereas a reduction in glutamate, lysine and trehalose was also observed (Fig. 6.6L). Reduction of glutamate was detected in all samples that were exposed to isoniazid, whether in combination with D-LAK peptides or not (Fig. 6.6G-I). Combining D-LAK peptides with isoniazid mitigated the reduction in glutamate but, as above, the concentration of each antibiotic used in combinations was substantially lower than when it was used alone. Changes in metabolites for other challenge conditions, including rifampicin and both D-LAK peptides, did not pass the stringent significance threshold.

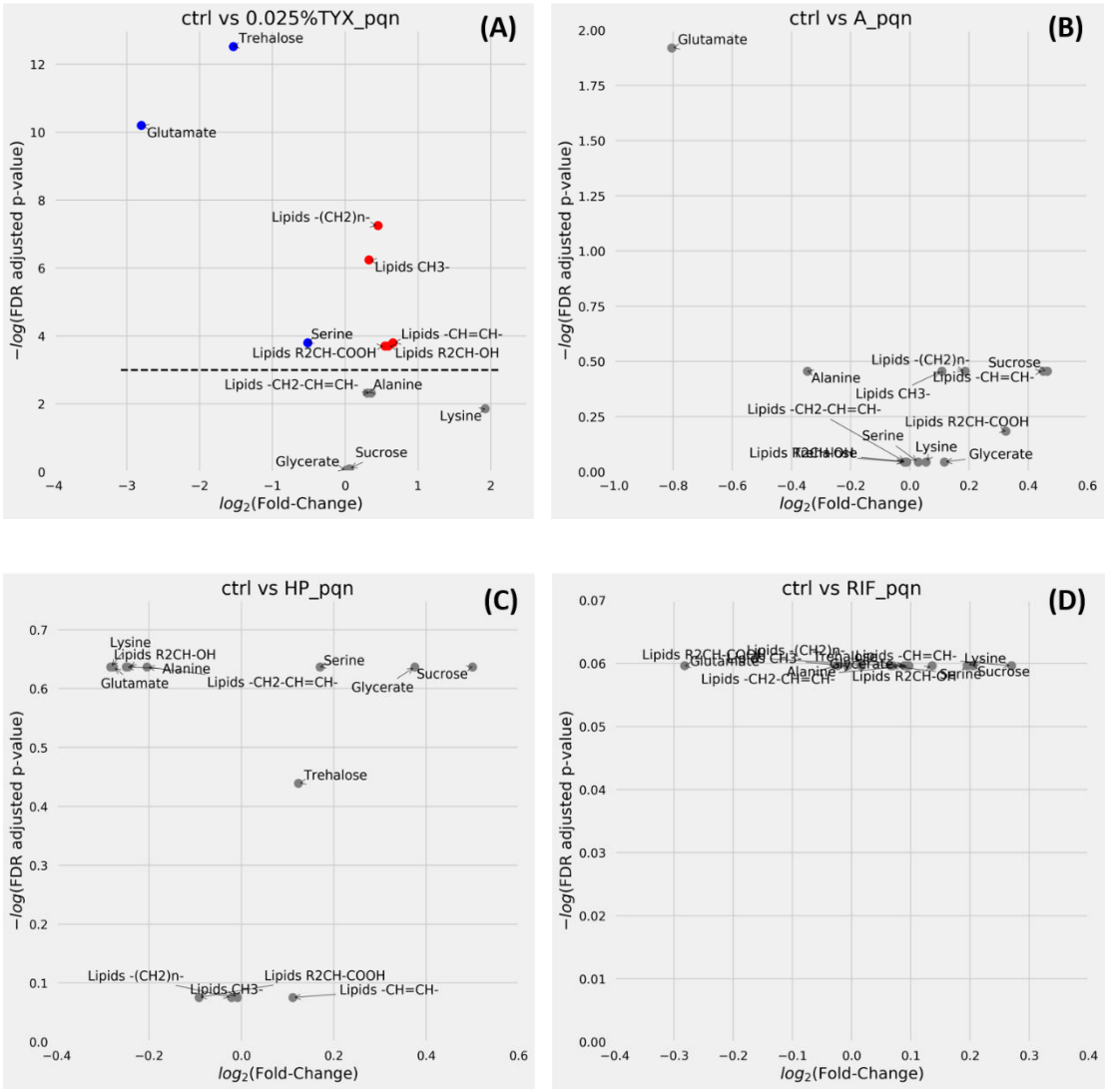

Figure 6.6A-D ¼ MIC Challenges induce changes in various metabolites in whole cell Mtb Bleupan incubated for 6 weeks. Volcano plots are shown for individual comparisons of unchallenged bacteria and those challenged with 0.025% tyloxapol (A), D-LAK120-A (B), D-LAK120-HP13 (C), rifampicin (D). Volcano plots are of PQN normalized data (n=9) and allow comparison of fold changes and significance of each metabolite; blue – significant reductions, red – significant increases and grey – non-significant changes in the indicated metabolites.

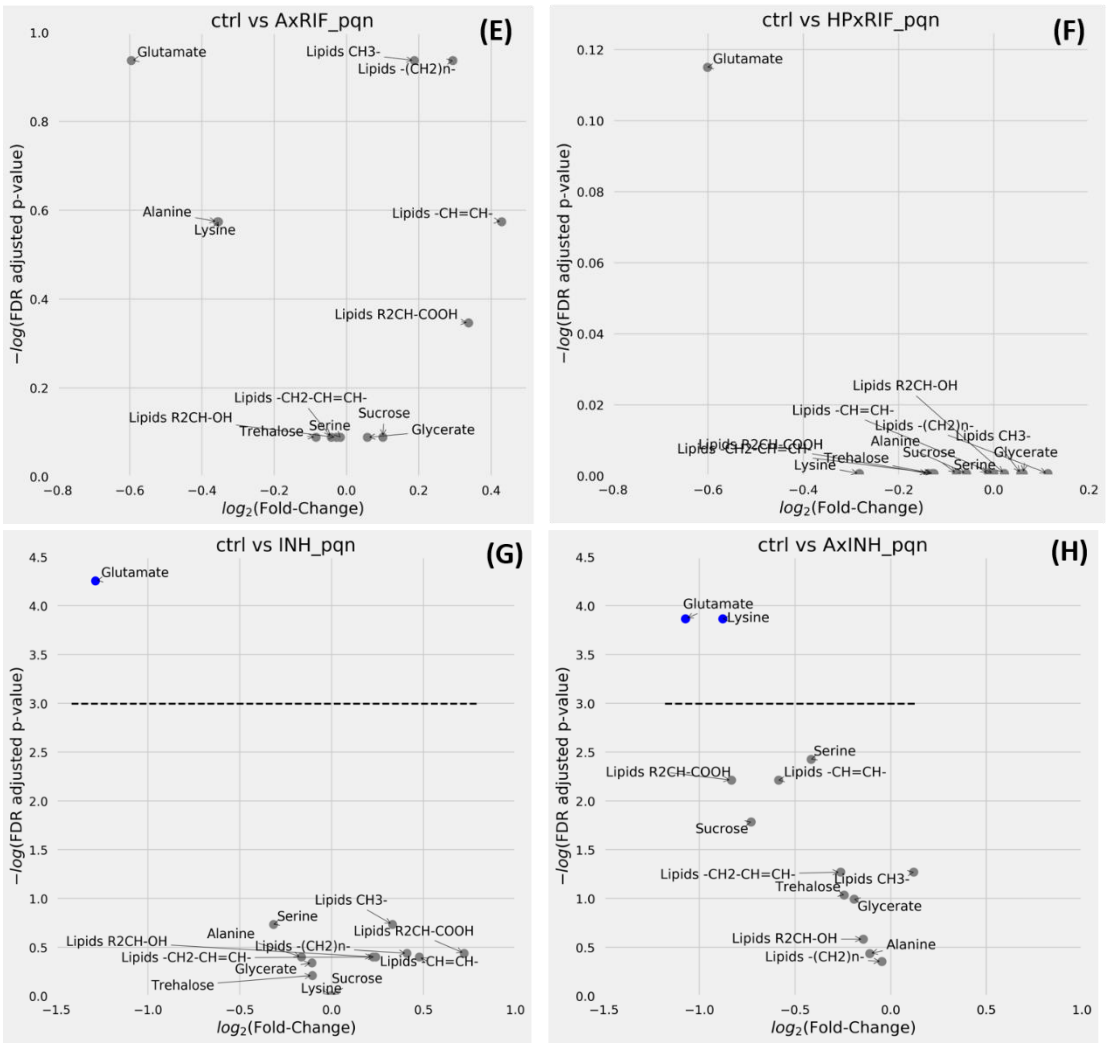

Figure 6.6E-H ¼ MIC Challenges induce changes in various metabolites in whole cell Mtb Bleupan incubated for 6 weeks. Volcano plots are shown for individual comparisons of unchallenged bacteria and those challenged with rifampicin in combination with D-LAK120-A (E) or D-LAK120-HP13 (F), isoniazid (G), isoniazid in combination with D-LAK120-A (H). Volcano plots are of PQN normalized data (n=9) and allow comparison of fold changes and significance of each metabolite; blue – significant reductions, red – significant increases and grey – non-significant changes in the indicated metabolites.

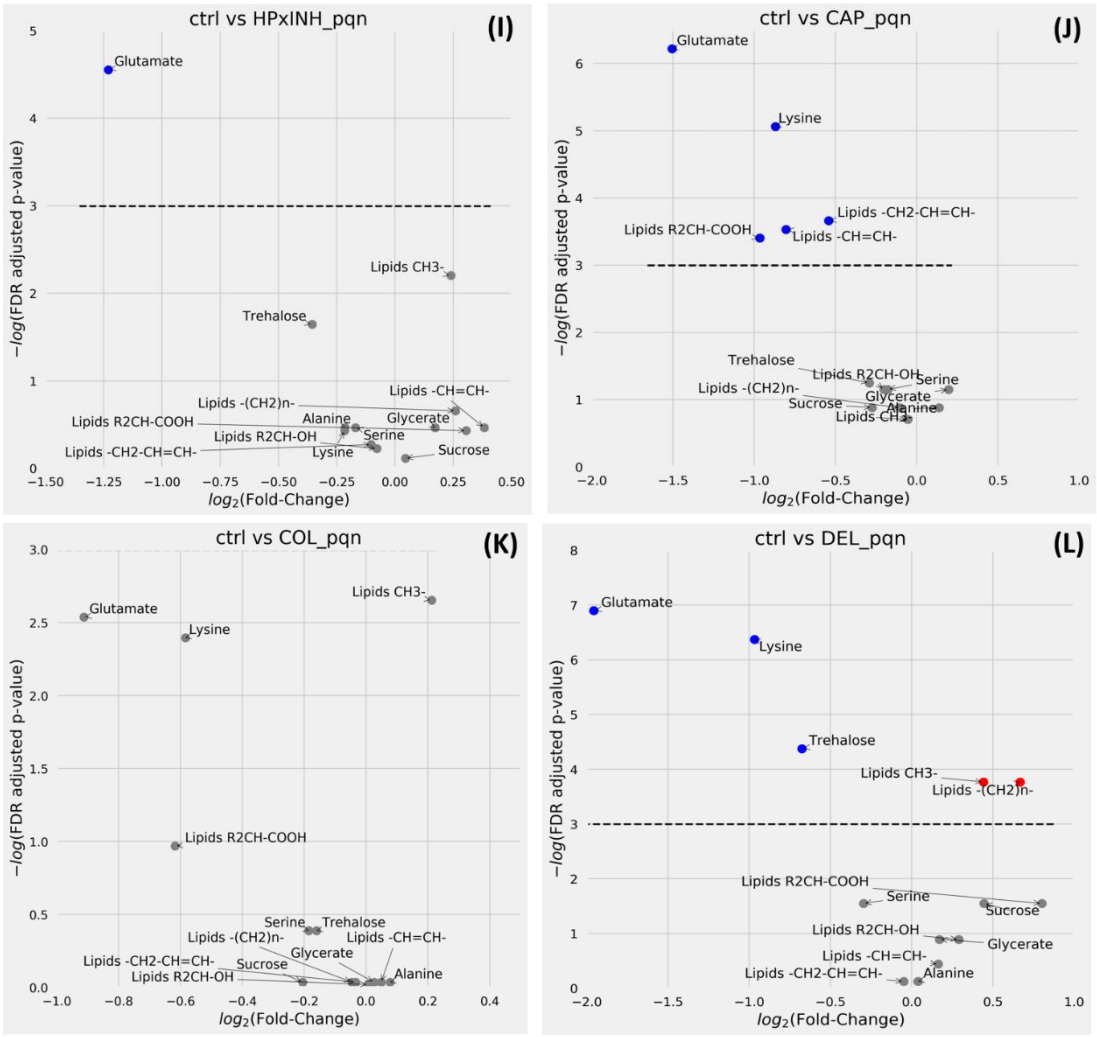

Figure 6.6I-L ¼ MIC Challenges induce changes in various metabolites in whole cell Mtb Bleupan incubated for 6 weeks. Volcano plots are shown for individual comparisons of unchallenged bacteria and those challenged with isoniazid in combination with D-LAK120-HP13 (I), capreomycin (J), colistin (K) or delamanid (L). Volcano plots are of PQN normalized data (n=9) and allow comparison of fold changes and significance of each metabolite; blue – significant reductions, red – significant increases and grey – non-significant changes in the indicated metabolites.

Univariate analysis allows the observation of significant changes in certain major metabolites across the treatments. Univariate plots (Fig. 6.7) depicting the changes in the key metabolites across treatments showed reduction in glutamate level when *Mtb* Bleupan was challenged with capreomycin and delamanid but not rifampicin (Fig. 6.7A). Delamanid also showed significant increase in saturated alkyl -CH_3 group and –$(CH_2)_n$– chains (Fig. 6.7C/D). The presence of 0.025% tyloxapol resulted in the significant reduction of trehalose and increase in saturated alkyl -CH_3 groups (Fig. 6.7B/D). Albeit modestly, increase in the saturated alkyl chains – $(CH_2)_n$– and both unsaturated alkyl groups –CH=CH– and –CH_2-CH=CH– was observed in the presence of tyloxapol as compared with the untreated control (Fig. 6.7C/E/F). Results from binary comparisons illustrated in volcano plots and univariate analysis concluded that significant changes were found in treatments with tyloxapol, capreomycin and delamanid.

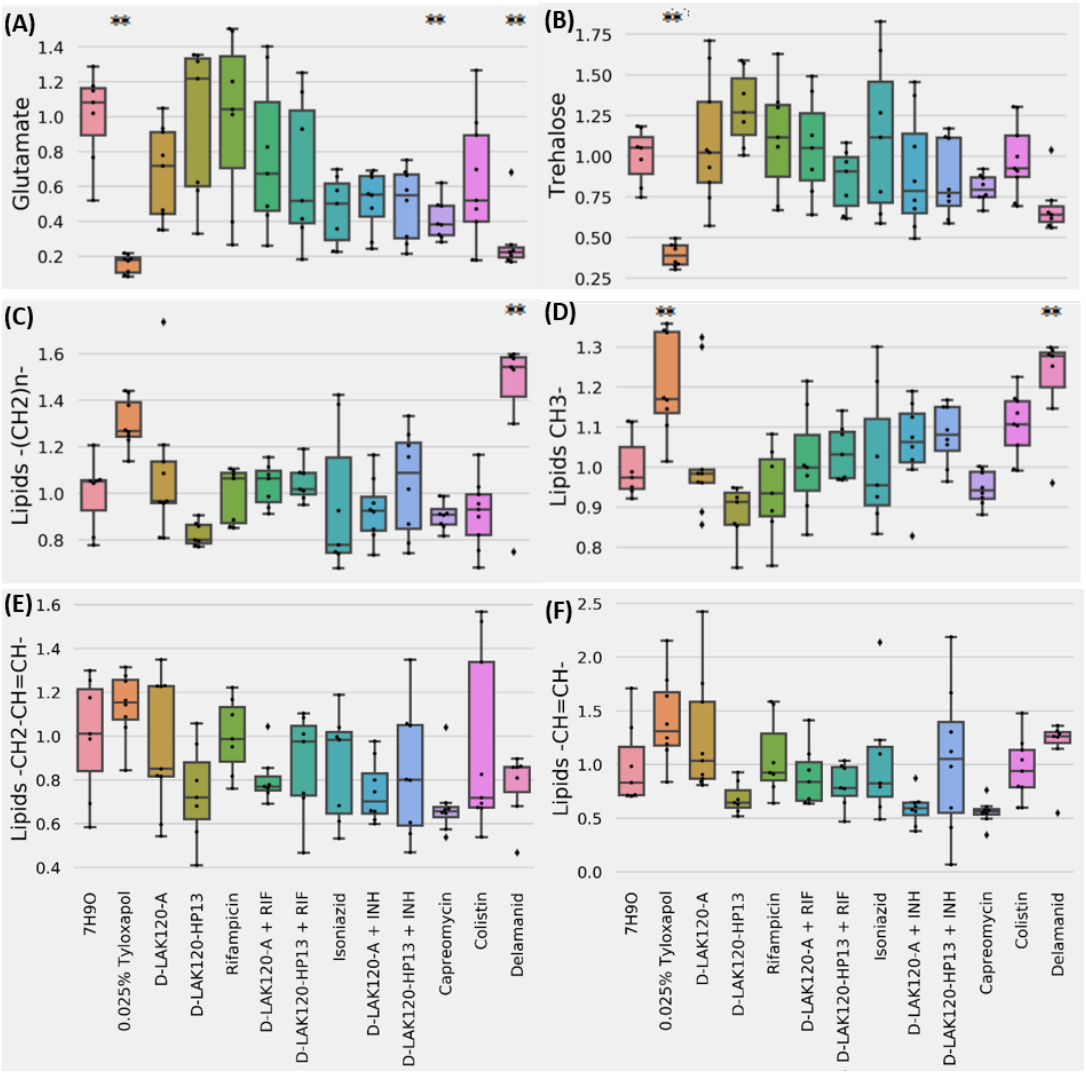

*Figure 6.7 Univariate analysis of relative metabolite levels in whole-cell Mtb Bleupan challenged with indicated conditions for 6 weeks. Data were PQN normalized and presented as mean ± SD (n=9). Significant differences with respect to unchallenged bacteria, as determined by one-way ANOVA with Tukey post-hoc test, are indicated **.*

Using partial least squares (PLS) regression model, correlation between metabolites and fluorescence anisotropy, r, were assessed (Fig. 6.8). The correlation between trehalose and DPH anisotropy was found to have the highest Spearman R correlation at 0.073. Despite the modest correlation, six-week challenge data set indicated membrane rigidity tended to increase with the increasing amount of trehalose (Fig. 6.8A) while decrease with the level of lipid resonances (Fig. 6.8C/D/E). The very modest negative correlation between membrane rigidity and lipid metabolites could also be observed from the correlations. None of the correlations was found significant therefore no trend was identified from the *Mtb* dataset. As compared with the correlation observed in anti-TB agent challenge on *M. smegmatis* in which membrane rigidity was significantly correlated with increasing trehalose content and decreasing lipid resonances, this indicated none of the anti-TB agents had any effect on *Mtb* in both challenge conditions.

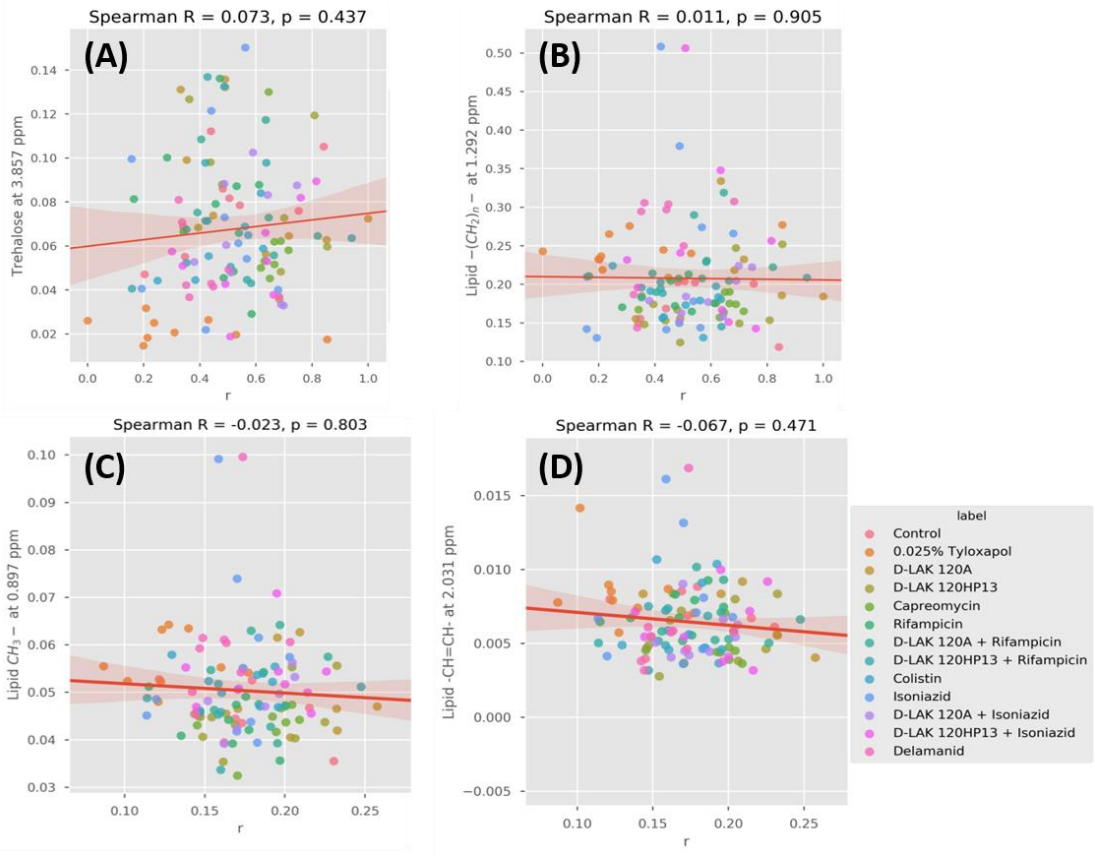

Figure 6.8 Correlation between membrane rigidity and the altered composition of the mycomembrane of Mtb Bleupan. Spearman correlations are shown between DPH anisotropy (r) and ^{1}H HR-MAS NMR resonance intensities obtained for Mtb Bleupan grown without challenge or with 0.025% Tyloxapol or

¼ MIC of indicated conditions in the legend (n=9). Data is shown for trehalose (A), lipid –$(CH_2)_n$- (B), lipid -CH_3 (C) and lipid –CH=CH- (D).

From the results of spent media at six-week challenge, changes in metabolites were found in a few conditions. Growth with 0.025% tyloxapol reduced acetoacetate, acetate and succinate production (Fig. 6.10A). Delamanid treatment reduced the production of these metabolites as well as 2-hydroxyisobutyrate. In addition, more glucose, glutamate and alanine were consumed (Fig. 6.10F). Interestingly, in contrast to delamanid, challenge with capreomycin increased production of 2-hydroxyisobutyrate, lactate, acetoacetate, acetone, valine (Fig. 6.10D) and a significant amount of glucose was found accumulated in this treatment (Fig. 6.9). Similarly, accumulation of glucose was seen in colistin treatment and there was also an increase production of citrate, methylmalonate, alanine and glutamate but not valine (Fig. 6.10E). Exposure to isoniazid caused the reduced production of acetate only. Other treatments including both D-LAK peptides and their combinations with rifampicin or isoniazid did not show significant changes in any metabolites (Appendix C, Fig. 7.48.)

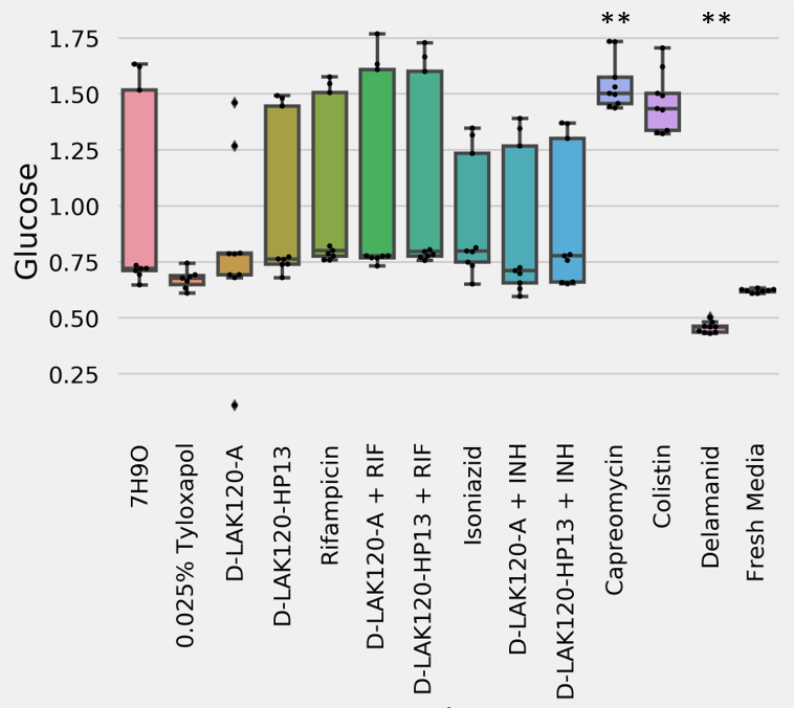

*Figure 6.9 Univariate analysis of glucose levels in spent media of Mtb Bleupan challenged with indicated conditions for 6 weeks. Data were PQN normalized and presented as mean ± SD (n=9). Significant differences with respect to unchallenged bacteria, as determined by one-way ANOVA with Tukey post-hoc test, are indicated **.*

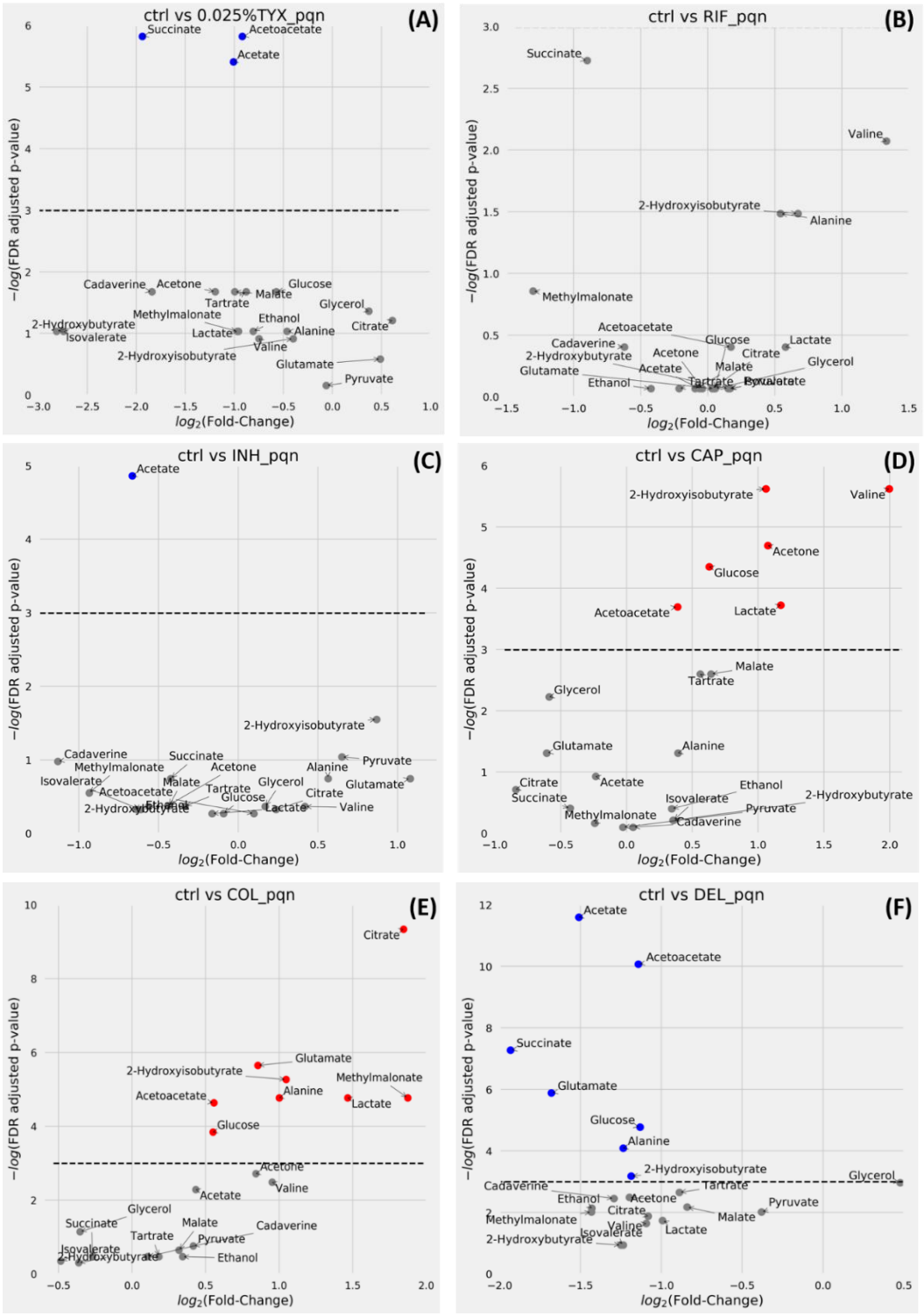

Figure 6.10A-F ¼ MIC Challenges induce changes in various metabolites in spent media of Mtb Bleupan incubated for 6 weeks. Volcano plots are shown for individual comparisons of unchallenged bacteria and those challenged with 0.025% tyloxapol (A), rifampicin (B), isoniazid (C), capreomycin (D), colistin (E), delamanid (F). Volcano plots are of PQN normalized data (n=9) and allow

comparison of fold changes and significance of each metabolite; blue – significant reductions, red – significant increases and grey – non-significant changes in the indicated metabolites.

Considering 72-hour challenge of *Mtb* Bleupan, Volcano plots of ^{1}H HR-MAS data of whole cell bacteria indicate changes in metabolites resulted in only a few conditions (Fig. 6.11). Compared with the combination of capreomycin with D-LAK120-HP13, combination with D-LAK120-A induced more changes in metabolites. Sucrose, lysine and both saturated and unsaturated lipid resonances were reduced with an increase of glycerate. Moreover, decrease in the amount of sucrose was also detected in colistin alone, and in combinations of D-LAK120-HP13 with capreomycin or D-LAK120-HP13 with isoniazid. On the other hand, significant changes were only detected in a few treatments after the analysis of spent media of *Mtb* Bleupan (Fig. 6.12). Reduction of isovalerate, 2-hydroxybutyrate, tartrate and lactate were found when the bacteria were grown in the presence of 0.025% tyloxapol. D-LAK120-HP13 challenge resulted in an increase in the level of 2-hydroxyisobutyrate, lactate and cadaverine. D-LAK120-A challenge also increased the production of cadaverine. Notably, the production of cadaverine was detected in untreated *Mtb* culture (Fig. 6.5) but the production further increased in the treatment of D-LAK peptides. The changes in this antioxidative metabolite is particular interesting as it was not detected in *M. smegmatis* samples. Besides, isoniazid induced production of succinate whereas colistin increased the amount of methylmalonate and lactate found in the spent media. Nonetheless, other treatment did not result in detectable changes in any metabolites (Appendix C, Fig. 7.50).

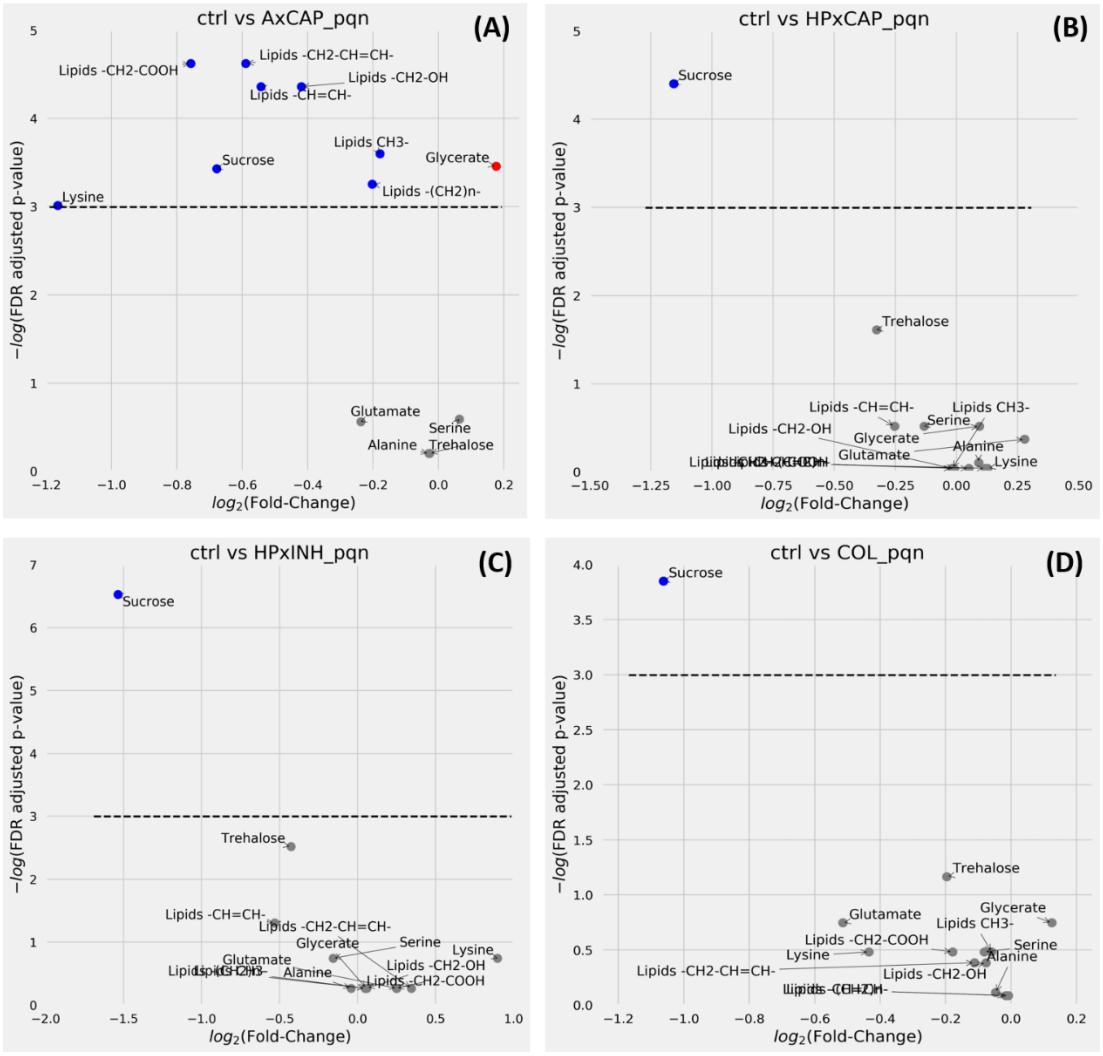

Figure 6.11A-D ½ MIC Challenges induce changes in various metabolites in whole cell Mtb Bleupan incubated for 72 hours. Volcano plots are shown for individual comparisons of unchallenged bacteria and those challenged with capreomycin in combination with D-LAK120-A (A) or D-LAK120-HP13 (B), isoniazid in combination with D-LAK120-HP13 (C), colistin (D). Volcano plots are of PQN normalized data (n=9) and allow comparison of fold changes and significance of each metabolite; blue – significant reductions, red – significant increases and grey – non-significant changes in the indicated metabolites.

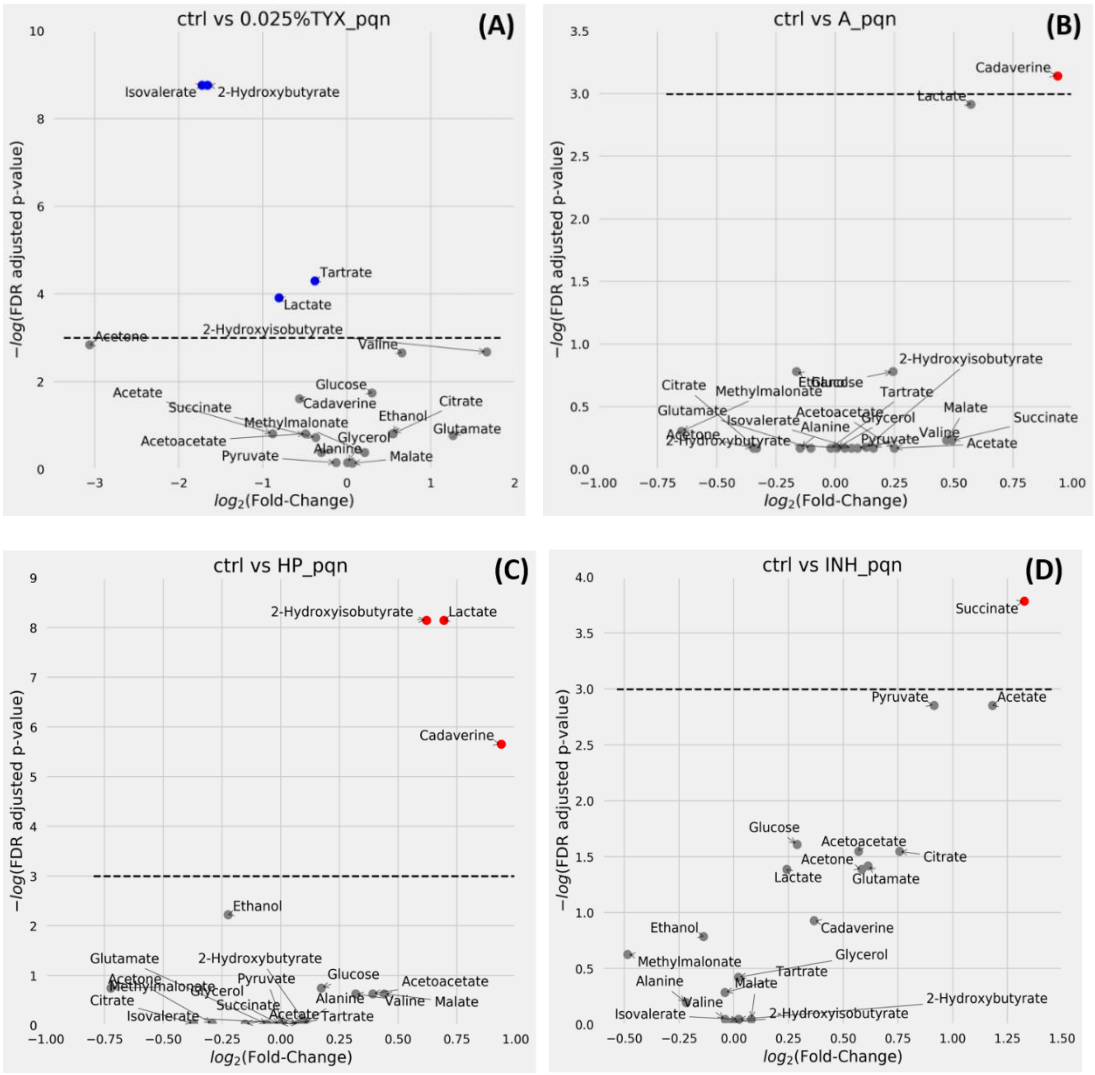

Figure 6.12A-D ½ MIC Challenges induce changes in various metabolites in spent media of Mtb Bleupan incubated for 72 hours. Volcano plots are shown for individual comparisons of unchallenged bacteria and those challenged with 0.025% tyloxapol (A), D-LAK120-A (B), D-LAK120-HP13 (C), isoniazid (D). Volcano plots are of PQN normalized data (n=9) and allow comparison of fold changes and significance of each metabolite; blue – significant reductions, red – significant increases and grey – non-significant changes in the indicated metabolites.

Re-analysis of anti-TB agent data excluding D-LAK peptides and corresponding combinations

As presented above no effect of D-LAK peptides or their combinations with anti-TB agents could be demonstrated on *Mtb* Bleupan using either the techniques of fluorescent probes and NMR metabolomics. Any observable changes were generally less significant and characterized by substantial variation when compared with the analogous study of *M. smegmatis*. Concern was raised that, in the six-week incubation the expected variable half-life of the D-LAK peptides would increase the variability of the bacterial response and this would negatively impact on the ability to discern significant differences when considering the dataset as a whole. While accepting that more work is required to optimize the treatment conditions for *Mtb,* to allow evaluation of the techniques and discussion of the information they provide on the elucidation of the mechanism of action of existing antibiotics, the analysis was performed again with the conditions involving D-LAK peptides removed.

For the six-week challenge, 0.025% tyloxapol increased membrane fluidity modestly while capreomycin triggered significant ($p < 0.01$) reduction of membrane fluidity in *Mtb* Bleupan (Fig. 6.13A). This observation was also shown in 72-hour challenge (Fig. 6.13B). In addition to capreomycin, isoniazid and delamanid both induced significant increase in membrane rigidity as compared to untreated control grown in 7H9O broth medium. Also, membrane property of *Mtb* Bleupan treated by these two agents was found to be significantly different from those grown in the presence of tyloxapol in which the latter demonstrate a higher membrane fluidity, consistent with the observation at the six-week challenge. Treatment with rifampicin did not result in any detectable changes in bacterial membrane properties as shown by a similar polarization anisotropy as the untreated control.

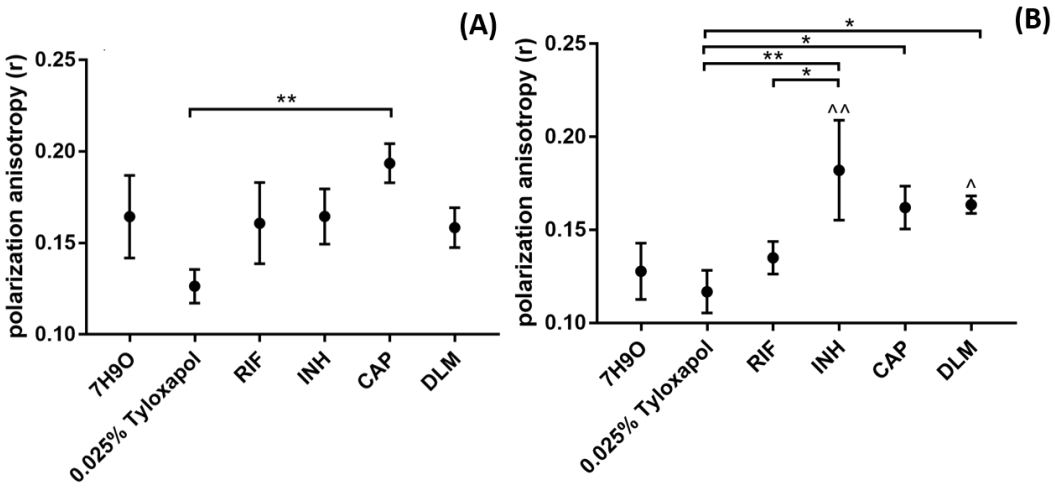

*Figure 6.13 DPH fluorescence anisotropy of Mtb Bleupan response to challenge with antibiotics. Mtb Bleupan subjected to challenge at ¼ MIC for 6 weeks (A) or ½ MIC for 72 hours (B). Data were presented as mean ± SD (n=9). Significant difference was assessed using one-way ANOVA analysis followed by Dunnett's or Tukey's Multiple Comparisons Test for comparison between conditions, *<0.05, **<0.01, ***<0.001, and by Multiple Comparisons Test to compare with untreated control (7H9O), ^ <0.05, ^^ <0.01.*

Univariate analysis shows a clearer picture of the changes triggered by each condition at six-week incubation regarding six representative metabolites (Fig. 6.14). Four treatments including isoniazid, capreomycin, delamanid and the presence of tyloxapol resulted in the same significant reduction in glutamate with respect to the unchallenged bacteria (Fig. 6.14A). *Mtb* Bleupan cultured in tyloxapol also demonstrated significant reduction of trehalose whereas capreomycin did not show an explicit effect on the level of trehalose (Fig. 6.14B). Capreomycin triggered modest reduction in lipid resonances, in particular it induced a significant reduction in -CH_2-CH=CH- which is similar to its effect on *M. smegmatis*. In contrast to delamanid and tyloxapol, none of the other three antibiotics triggered any changes in saturated carbon –$(CH_2)_n$- and CH_3- groups (Fig. 6.14C/D). The increase in saturated lipids in delamanid treatment might be the direct result of its reported mechanism to inhibit the production of keto- and methoxy-mycolic acids[393]. In terms of unsaturated lipid metabolites, significant reduction was only shown in capreomycin treatment while other conditions did not cause an apparent effect as compared with 7H9O bacterial control (Fig. 6.14E/F). The corresponding analysis for 72-hour challenge identified no significant differences between different conditions (Appendix C, Fig. 7.51).

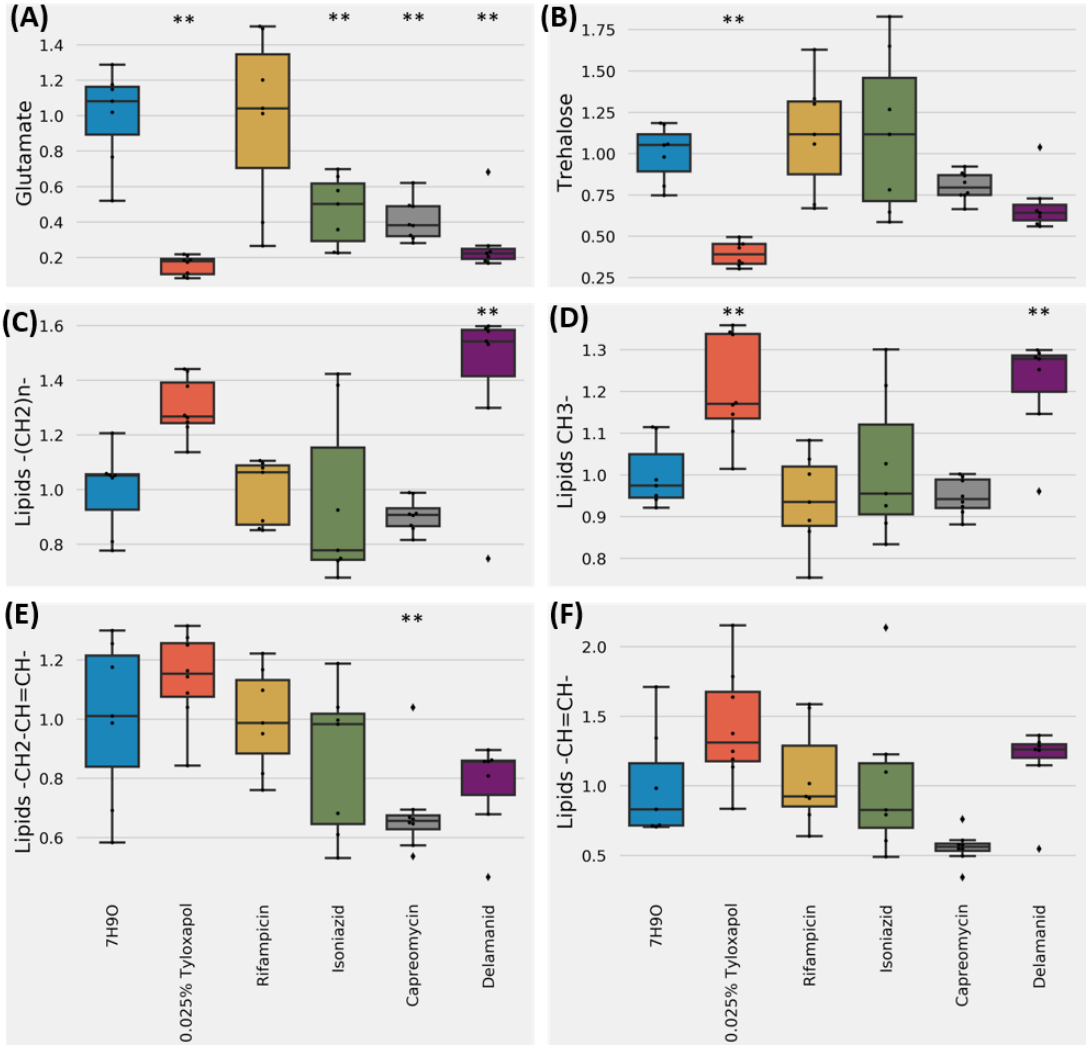

*Figure 6.14 Univariate analysis of relative metabolite levels in whole-cell Mtb Bleupan challenged for 6 weeks with ¼ MIC antibiotics or in the presence of 0.025% tyloxapol. Data were PQN normalized and presented as mean ± SD (n=9). Significant differences with respect to unchallenged bacteria, as determined by one-way ANOVA with Tukey post-hoc test, are indicated **.*

From the results of PLS regression model using the data of the five treatment conditions and the untreated control (Fig. 6.15), similar trends were observed as in Fig. 6.8 in which none of the correlations was significant.

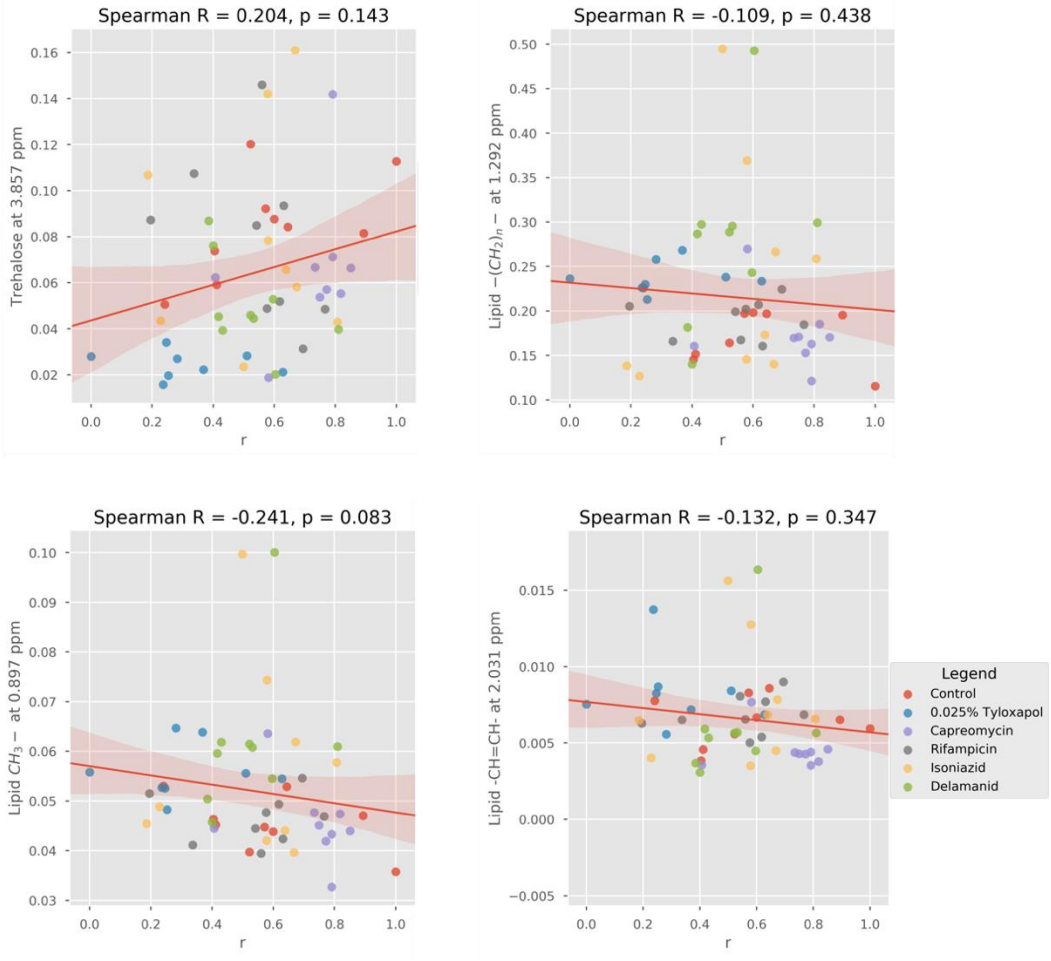

Figure 6.15 Correlation between membrane rigidity and the altered composition of the mycomembrane of Mtb Bleupan (Re-analysis). Spearman correlations are shown between DPH anisotropy (r) and ^{1}H HR-MAS NMR resonance intensities obtained for Mtb Bleupan grown without challenge or with 0.025% Tyloxapol or ¼ MIC of antibiotics. Data is shown for trehalose (A), lipid –$(CH_2)_n$- (B), lipid -CH_3 (C) and lipid –CH=CH- (D).

6.3 DISCUSSION

In the previous chapter, action of antibiotics and D-LAK peptides was shown to trigger various responses in *M. smegmatis* in terms of membrane properties and cell metabolism. Bacterial metabolism was substantially altered when challenged with tyloxapol, rifampicin and capreomycin, specifically by the remodeling of mycobacterial membrane. The changes were consistent with the increase in mycobacterial membrane rigidity detected in capreomycin and tyloxapol treatment. *M. smegmatis* is an attractive model system for the study of antibiotic mechanisms of action due to the much shorter doubling time. However, the susceptibility of *M. smegmatis* towards the combination of rifampicin or isoniazid with D-LAK peptides was quite different from that observed for the MDR-TB clinical isolates. Therefore, to better understand the extent to which *M. smegmatis* is a suitable model organism to study the mechanism of action of anti-TB agents against MDR *Mtb*, the NMR/fluorescence anisotropy approach was replicated with the severely attenuated *Mycobacterium tuberculosis* Bleupan strain here.

In the present study, fluorescence assays and NMR metabolomics studies revealed different changes induced by the anti-TB agents in *Mtb* Bleupan. As compared with *M. smegmatis*, the use of carbon sources (the preference for glucose by *M. smegmatis* but mostly pyruvate and glutamate by *Mtb* Bleupan) and disparate response to treatments such as tyloxapol suggested that the two microorganisms may adopt different biological pathways and counteracting mechanisms upon challenges. The employment of 72 hours and 6 weeks duration of challenge on *Mtb* Bleupan resulted in various levels of changes in individual metabolites and membrane properties. This indicates the greater need to understand the reason for the absence of antibiotic effect which might suggest importance of determining the *in vitro* half-life of anti-TB agents. Besides, it is essential to optimize the treatment conditions when using *Mtb* Bleupan to obtain significant understanding of action of anti-TB agents; due to its slow growing nature it is suggested that variation in the *in vitro* half-life of each antibiotic has much greater impact on the outcome of the NMR metabolomics and fluorescence anisotropy measurements than when the analogous experiment was performed in *M. smegmatis*. Notably, no impact of the D-LAK peptides, when used alone, could be detected in either treatment condition, except for an acute response at 72 hours challenge, characterized by increased production of cadaverine, detected in the spent media. Combinations of D-LAK peptides with isoniazid did induce a response but this was not significant when considered across the data set. Rifampicin and its combinations with D-LAK peptides induced no significant response.

Nevertheless, despite the generally modest responses, significant metabolic changes were consistently observed following treatment with capreomycin and delamanid, and these can be related to their reported mechanism of action. This allows a detailed comparison of the responses of the two species and is important information in understanding the relative strengths and weaknesses of the two systems for the investigation of the mechanism of anti-TB agents.

Membrane changes and NMR metabolomic responses following challenge with delamanid are consistent with its known mechanism of action

Since peptide treatments did not show a great effect on *Mtb* Bleupan but led to greater variability of the data, removing those conditions revealed responses towards other anti-TB drugs in terms of membrane manipulation and metabolic influence on *Mtb* Bleupan. Significant reduction of glutamate was found in bacteria treated with isoniazid, capreomycin, delamanid and 0.025% tyloxapol. These treatments all share the common influence on cell wall synthesis. It was proposed that glutamate and pyruvate can be converted to D-alanine and thereby the biosynthesis of peptidoglycan in mycobacteria[394]. This change in glutamate might be the result of cell wall remodeling in response to the drug action although the changes in pyruvate and alanine were not significant in most conditions. Notably, the responses triggered by delamanid correlate with its reported mode of action. Delamanid acts by inhibiting the production of keto- and methoxy- mycolic acids[393]. Therefore, the accumulation of acyl chains and reduction in trehalose as well as the significant membrane rigidification could be the direct consequences.

Differences in response observed in Mtb *Bleupan compared with* M. smegmatis *indicate appropriateness to apply for antibiotic mechanistic study*

Mtb and *M. smegmatis* differ fundamentally by their cell wall structure, virulence and rate of growth. Comparison of the two metabolomic studies reveals that *M. smegmatis* mainly consume glucose while *Mtb* Bleupan consumes pyruvate and glutamate. Utilization of difference carbon sources for the growth of *M. smegmatis* and *Mtb* was also reported[395]. The study showed that both species consumed pyruvate, glutamate and glucose but did not report the comparison of relative dependence of different carbon sources. Its non-pathogenic behaviour and fast-growing nature are the major attractions for *M. smegmatis* to be employed

over *Mtb*. The significance of this study is the elucidation of the translatability of findings of these two models for antibiotic efficacy and mechanistic study of *Mtb*. By comparing the responses of *M. smegmatis* and *Mtb* Bleupan towards different antibiotics, the strength and weakness of the corresponding models are revealed. These findings therefore facilitate the further investigation to elucidate mechanism of drug action on *Mtb*.

Delamanid was reported to show similar concentration-dependent killing effect to rifampicin against drug-susceptible *Mtb*[396]. The bacterial inhibitory studies on *Mtb* Bleupan revealed its high potency and killing efficiency resembling rifampicin. D-LAK peptides interacted synergistically with rifampicin and modestly with isoniazid against *Mtb* Bleupan. This response is similar to the action of these combinations demonstrated on MDR-TB clinical isolates. However, this synergy was not observed on *M. smegmatis* but rather when D-LAK peptides in combination with capreomycin. This may be ascribed to the intrinsic resistance of *M. smegmatis* to rifampicin and isoniazid. Agrwal *et al.*[364] generated *M. smegmatis* strains with *arr* gene deletion which was found to be susceptible to rifampicin at the same level as *Mtb*, therefore suggested its use as a surrogate for *Mtb* drug testing. Khara *et al.*[261] reported the synergy of the cationic $M(LLKK)_2M$ peptide with rifampicin on *M. smegmatis* and *M. bovis* BCG but the effect was additive on *Mtb* H37Rv. Such substantial differences in behavior suggest that variation in cell envelope composition between *Mtb* and *M. smegmatis* could serve as a critical factor on the action of AMPs especially those that interact with the mycomembrane. One of the major differences between cell wall components of the two mycobacteria is the types of structural mycolic acid. This affects the physical properties such as the packing of mycolates and rigidity of mycomembrane[397]. In terms of length, the oxygenated mycolic acids that only exist in *Mtb* contain around 84-88 carbon atoms which is four to six carbons longer than that of *M. smegmatis*[398]. In terms of structure, the occurrence of *trans*-cyclopropanes facilitates the folding of oxygenated mycolic acids into a W-conformation with the four acyl chains in parallel, forming a tight packing of mycolates in *Mtb* Bleupan[399]. These two intrinsic properties of the mycolates were shown to give rise to a high transition temperature of the cell wall of *Mtb* which could be the major factor that reduces the fluidity of the cell wall[397]. Indeed, when measured with the DPH probe, *Mtb* Bleupan exhibits a higher membrane rigidity than *M. smegmatis* as revealed by the higher fluorescence anisotropy values. In addition, the amount and nature of mycolic acids were also shown to correlate with the permeability of mycobacteria[18].

Tyloxapol treatment again demonstrated the composition difference of mycobacterial cell envelope in the two microorganisms. When *Mtb* Bleupan was grown in medium of different compositions, changes in membrane order were observed as denoted by the general polarization (GP) value. Membrane order was found to be higher in the presence of tyloxapol. An opposite trend was depicted by *M. smegmatis* on membrane GP as compared to *Mtb* Bleupan. This suggests the differences in mycolic acid structure comprising the mycomembrane confer different properties on the cell wall of mycobacterial species. Besides, 0.025 % tyloxapol led to an increase in saturated and unsaturated carbons but a reduction in trehalose content in *Mtb* Bleupan while *M. smegmatis* had an opposite response. This indicates that tyloxapol has the direct opposite effect on membrane order and lipids and trehalose in the two species. The fact that *Mtb* possesses cord-forming TDM while *M. smegmatis* does not, might give a possible explanation to this observation[255]. Tyloxapol was reported to reduce the surface TDM content of mycobacteria[350]. During the long incubation time, *Mtb* might adapt to the reduction in TDM content on the surface of cell wall and undergo remodeling by reducing TDM production, and in turns the reduction of free trehalose production and accumulation of intracellular -CH=CH- containing meromycolates. This phenomenon can also be supported by the reduced *in vitro* biofilm (formed by free MAs from TDM hydrolysis[400]) formation, in the culture with tyloxapol compared with other treatment conditions.

Furthermore, the different synergistic outcome brought about by the capreomycin combinations in the two microorganisms suggests a differing channel distribution on corresponding mycomembrane. *M. smegmatis* possesses channels mainly of > 2 nS single channel conductance[401]. Among all types of porins present in *M. smegmatis*, 70% of them are mspA porins which mediate the transport of small hydrophilic molecules while large hydrophilic substances such as aminoglycosides are thought to enter by self-promoted uptake[320]. In contrast, *Mtb* intrinsically possesses much lower amount of porin[320], apart from the existence of a few unnamed channels[321]. Other than the existence of ompA porin which is not involved in drug transport[320] and the absence of mspA homologues[44], transport systems in *Mtb* remain largely unknown. Nonetheless, these pieces of information are sufficient to conclude that the mode of entry for hydrophilic substances varies immensely between the two microorganisms.

Not only does the susceptibility and/or accessibility of *Mtb* to capreomycin differ from *M. smegmatis* but also the metabolic response, albeit with some common themes. For *Mtb*,

six-week challenge with capreomycin alone resulted in a reduction in the intensity of unsaturated lipid and lysine resonances. Meromycolate chains with double bond is the precursor of the synthesis of cyclopropanated mycolic acids in *Mtb*[255], the synthesis of meromycolate chains might be affected leading to the reduction in unsaturated carbon resonance. Also, reduction in lysine may correspond to the effect of drug treatment that affects the mycolic acid pathway[253].

Overall, the results illustrated the closer resemblance of *Mtb* Bleupan to *Mtb* and MDR-TB clinical isolate as compared with *M. smegmatis* in biological responses towards antibiotics or combinations with D-LAK peptides. The findings also deduced the higher similarity in terms of mycomembrane composition and properties of *Mtb* Bleupan to MDR-TB clinical isolates than *M. smegmatis*. This study addressed the marked differences in mycobacterial cell wall and metabolic responses between *Mtb* Bleupan and *M. smegmatis*, pointing out the important consideration when choosing to use *M. smegmatis* as model for the study of antibiotic susceptibility and/or mechanism of action.

Mtb *Bleupan as a valid model to assess antibiotic efficacy and potentially optimized for promising mechanistic study*

Modest changes in membrane rigidity of *Mtb* Bleupan were detected by the DPH probe upon challenges at various treatments and experimental conditions. A significant increase in membrane rigidity was observed in treatments with isoniazid, D-LAK120-A with isoniazid, delamanid for 72-hour incubation and with 0.025% tyloxapol but only for the six-week incubation. This insensitivity, when compared to the significant findings in *M. smegmatis*, might be attributed to the inadequate amount of drug used for challenges and the hydrolysis of drug molecules over the long incubation period; it is challenging to identify the optimum time point for assessing changes in membrane physical properties and/or metabolism. The drug concentration used in the study was determined on the basis that the growth of *Mtb* could be maintained since the initial inoculum was 1% for the six-week challenge. Further, due to the long incubation period without continuous agitation, formation of biofilm was observed in most of the treatment conditions. This biofilm is known to protect mycobacterial cells from the bactericidal activity of antibiotics[402] and related to the harboring of drug-tolerant population[403]. Vortexing was performed intermittently to impede the formation of biofilm, though this downstream effect of biofilm formation could not be completely avoided.

The drug concentration was increased at the 72-hour challenge of *Mtb* Bleupan at mid-log phase aiming to observe a more dramatic response in the membrane structure. The later challenge did induce significant membrane changes in more conditions which shows that a higher concentration could be employed to observe the immediate effects of anti-TB agents. The six-week challenge approach is easily affected by the half-life of drugs. In order to assess the growth response of *Mtb* Bleupan, additional challenges might be introduced during the six-week incubation to maintain the drug effect. One must also take into consideration the emergence of resistant population under continuous treatment of sub-MIC drug concentration[30]. Future experiments should include the evaluation of the metabolic stability and half-life of each antibiotic using quantification techniques such as liquid-chromatography mass spectrometry[404]. This will enable the challenges to be performed with optimal concentration as well as to be replenished at relevant condition, eliminating the lack of responses due to the absence of sufficient antibiotics.

Biophysical techniques and NMR metabolomics provide insight to the function of D-LAK peptides

Antimicrobial peptides such as pleurocidin and LL-37 have been reported to induce oxidative stress in *Candida albicans*[405] and *Escherichia coli*[406], respectively. There is evidence that D-LAK peptides are capable of inducing oxidative stress in mycobacteria, but this is manifested in different ways in *M. smegmatis* and *Mtb.* The significantly increased production of cadaverine in D-LAK120-A or D-LAK120-HP13 treatment after 72-hour challenge is a response observed in the metabolism of *Mtb* which was not observed in that of *M. smegmatis*; D-LAK120-HP13 but not D-LAK120-A was implicated as an enhancer of oxidative stress in *M. smegmatis* due to glyoxylate shunt associated reductions in lipids. Cadaverine is an antioxidant polyamine which is synthesized by bacteria to counter oxidative stress induced by free radicals. Loots[407] demonstrated the increase production of cadaverine in INH-resistant *Mtb* strain to compensate for the reduced catalase-peroxidase synthesis due to *katG* downregulation. Tkachenko *et al.*[408] also reported the upregulation of *katG* activity by a range of polyamine including cadaverine under the exposure to oxidative stress. This implies that the responses in *Mtb*, induced by the immediate action of D-LAK peptide, have highlighted a role for oxidative damage in the action of D-LAK peptides. Overall, these findings suggest the possible multifunctional properties of D-LAK peptides in particular against *Mtb*.

The NMR metabolomics study also provides evidence of metabolic changes in *Mtb* induced by particular treatments. D-LAK120-A in combination with capreomycin led to significant reduction of saturated and unsaturated lipid resonances after 72 hours of challenge. Since these changes were not found in either D-LAK120-A or capreomycin when they were used alone, the combination might exert an effect on the metabolism of *Mtb* Bleupan.

Overall summary

Differences in terms of membrane properties and metabolomic responses between *M. smegmatis* and *Mtb* Bleupan have highlighted the issue of applicability of the non-pathogenic model for direct extrapolation of findings. Comparing to the six-week culturing time of *Mtb*, *M. smegmatis* only needs 48-hour to attain mid-log phase. This highly desirable feature enables the acceleration of study on mycobacteria, it would therefore be recommended to employ as a preliminary model for establishment of methodology. Furthermore, this study showed that some notable differences in the biological responses, membrane physiology and metabolism of *M. smegmatis* and *Mtb* Bleupan meaning the latter is likely to more faithfully reproduce the behaviour of clinical *Mtb* strains. It can be concluded that, despite the practical challenges involved in the use of *Mtb* Bleupan, it represents as a more favorable model for *Mycobacterium tuberculosis* and can potentially generate more translatable data in the study the action of TB antibiotics. Due to the slow growth of *Mtb* Bleupan, further optimization in terms of the challenge time period and knowledge of the *in vitro* half-life for each antibiotic are essential to develop a reliable assay that can impact on tuberculosis drug discovery.

Chapter 7 Conclusions

7.1 CONCLUSIONS

Tuberculosis (TB) is a global disease that creates one of the most pressing worldwide medical emergencies; fueled by the emergence of multidrug-resistant (MDR) strains, TB is continuously endangering the gains that have already made in its control. Most of the drugs involved in TB treatment nowadays were developed four decades ago, the growing emergence of drug resistance renders these medications inefficient, creating an urgency to establish a novel, safe and effective treatments than those currently available.

Antimicrobial peptides (AMPs) are capable of rapid killing through a variety of mechanisms. They have demonstrated potent antimicrobial activity against a broad spectrum of microbes. When combined with conventional anti-TB drugs, AMPs can serve as a promising strategy for TB therapy. The novel D-LAK peptides, have displayed a detergent-like effect which affected the survival of MDR and extensively drug-resistant (XDR) TB clinical isolates *in vitro* and *ex vivo*[259]. The ability of D-LAK120-A and D-LAK120-HP13 to potentiate the activity of isoniazid against MDR *Mycobacterium tuberculosis* (*Mtb*) strain suggested the potential synergy between D-LAK peptides and first-line anti-TB agents to re-sensitize drug-resistant *Mtb* strains.

This work started with the investigation of the antimicrobial action of the combinations of D-LAK120-A or D-LAK120-HP13 with rifampicin or isoniazid and then the potential synergistic interaction of the combinations against *Mtb* strains was evaluated. The combinations were demonstrated to be effectively synergistic against MDR-TB clinical isolates 03M, 08MB, GB2 and 08M strains. Combination with either peptide re-sensitized all the four studied strains towards rifampicin, while the addition of either peptide also restored the sensitivity of 03M and 08MB towards isoniazid. *In vitro* studies revealed the mycobactericidal effect of D-LAK peptides in combination with isoniazid against 03M, and D-LAK peptides in combination with rifampicin against 08MB were comparable with rifampicin or isoniazid alone but at a reduced drug concentration. Moreover, combination of D-LAK120-HP13 with isoniazid achieved a log reduction of 03M in THP-1 macrophages as compared with isoniazid used alone. This synergy demonstrated by the combinations with D-LAK peptides achieved at least two-fold reduction of rifampicin or isoniazid concentration, reflecting the possibility of these combinations to delay the emergence of drug resistance. Incorporation of D-LAK peptides at non-toxic concentration enhanced the efficacy of rifampicin and isoniazid, overcoming the resistant phenotype of MDR *Mtb* strains. This

indicates the potential of these combinations to be further developed as new therapeutics against drug-resistant TB.

Based on the de-clumping action demonstrated by the D-LAK peptides in the previous studies[259, 310], further investigation on the interaction of D-LAK peptides with mycobacterial membrane was performed using transmission electron microscopy and confocal microscopy. Treatment with D-LAK120-A and D-LAK120-HP13 revealed their instant influence leading to obvious morphological changes in *Mycobacterium smegmatis* while prolonged treatment led to bacterial lysis as indicated by the formation of mesosomes, cell content leakage and cell death. Besides, treatment by D-LAK peptides promoted the interaction of 150 kDa FTIC-dextran with the mycobacteria. These results suggested the D-LAK peptides interact with the bacteria to potentially manipulate or modify their membrane properties.

After establishing the surface-active action of D-LAK peptides, the mechanism underlying the synergistic effect on MDR-TB clinical isolates was studied using a bacterial growth response assay. The growth response of *M. smegmatis* after incubating with subinhibitory concentrations of different treatments was determined. Significant increase in membrane rigidity and decrease in membrane order was resulted after treatment with tyloxapol, capreomycin or its combinations with D-LAK peptides. The study of whole cell metabolism by HR-MAS revealed the significant decrease in both saturated and unsaturated lipid resonances while an increase in trehalose content was caused by capreomycin and its combinations with D-LAK peptides. A much subtler reduction in saturated and unsaturated lipid resonances was induced by rifampicin while the presence of tyloxapol only induced reduction in saturated lipid resonances. Neither of the treatment caused changes in trehalose. This indicated the effect of capreomycin in triggering membrane remodeling in *M. smegmatis,* leading to a shift in ratio between mycomembrane components, trehalose monomycolate and trehalose dimycolates. The remodeling effect by rifampicin or tyloxapol was much subtler which is presumably the origin of the lower significance in membrane properties changes as detected by fluorescence techniques.

Liquid state nuclear magnetic resonance (NMR) metabolomics identified induced oxidative stress in treatment with capreomycin or rifampicin. Using *M. smegmatis* as a model, the combination of fluorescence spectroscopy and NMR metabolomics is established as a useful tool for the elucidation of mode of actions of antibiotics against mycobacteria. Consequently, these techniques were further exploited to evaluate the action of first-line anti-TB drugs and their combinations against *Mtb* Bleupan. Two challenge conditions were performed to assess

the growth response of *Mtb* Bleupan in the presence of subinhibitory concentration of antibiotics and their combinations with D-LAK peptides. Significant increase in membrane rigidity was resulted in treatment with isoniazid, D-LAK120-A with isoniazid and delamanid at 72-hour incubation and only in the presence of tyloxapol at 6-week incubation. Only modest changes in individual metabolite and bacterial membrane rigidity were observed by other treatments at either condition. Despite subtle changes in *Mtb* metabolism or membrane properties, this study marked the first use of HR-MAS on the investigation of direct action of antibiotics on a *Mtb* strain. The modest changes induced by certain antibiotics, such as isoniazid and delamanid, is likely to resemble their known mechanisms.

Due to the complication of sample preparation of virulent *Mtb* species, previous studies of drug action using HR-MAS were only demonstrated on surrogate models such as *Mycobacterium bovis* Bacillus Calmette-Guérin and *M. smegmatis*. Using this attenuated *Mtb* Bleupan strain, drug action studies can be performed on a more reliable basis and generate more translatable findings. Although two different challenge conditions were included in this study, the slow-growing nature of *Mtb* is still rendered a main constraint for the detection of significant changes. Further optimizations on concentration and challenge duration could likely increase the significance of growth responses, enriching the basis for the elucidation of antimicrobial action on *Mtb*.

Finally, this study addressed the translatability of findings using one of the most commonly employed *M. smegmatis* model to compare with the results of *Mtb* strains. The findings revealed apparent differences in terms of the responses to antibiotics by *M. smegmatis* as compared to *Mtb*. In contrast to *M. smegmatis*, synergy of D-LAK peptides combinations with rifampicin or isoniazid was observed when used against the severely attenuated *Mtb* Bleupan and MDR *Mtb* strains. However, the synergy between D-LAK peptides and capreomycin against *M. smegmatis* was not observed against *Mtb* Bleupan. Fluorescence spectroscopy revealed that generally, *Mtb* Bleupan has a higher membrane rigidity than *M. smegmatis* due to their possession of differing mycolic acids. Besides, culturing in the presence of tyloxapol showed a completely opposite effect on the membrane rigidity between *M. smegmatis* and *Mtb* Bleupan. Furthermore, significant membrane remodeling action triggered by capreomycin treatments in *M. smegmatis* was not observed in *Mtb* Bleupan. Thus, it may be concluded that cautious interpretation should be carried out when using *M. smegmatis* to study and develop anti-TB therapy. Nonetheless, the fast-growing nature of *M. smegmatis* makes it a highly desirable organism for the establishment of TB studying

techniques. Finally, this study also demonstrated the higher resemblance of *Mtb* Bleupan to *Mtb* clinical isolates, suggesting that this category 2 *Mtb* strain is applicable and useful for the production of translatable findings on TB antibiotic studies.

7.2 LIMITATIONS

The study of MDR-TB strain poses various limitations. The doubling time of a drug susceptible *Mtb* strain is around 24 hours and takes three to four weeks to reach mid-log phase. Due to the fitness-cost of mutant strains, MDR-TB takes an even longer period for optimal growth. All experiments are confined to a containment level 3 laboratory, rendering restricted use in times of emergencies such as malfunctioning of controlled pressure system and spillage accidents leading to laboratory suspension for disinfection. These unpredictable scenarios occurred randomly, leading to delay of data collection and unretrievable experimental data.

On the other hand, due to safety concerns, experiments with *Mtb* strains may only be performed within the area of the cabinet. In this circumstance, no measurement involving external instruments, such as fluorescence reading of resazurin dye, was possible and largely limited the studies that could be performed on the bacteria. Moreover, resazurin is also used as a redox indicator[409] which might affect the interpretation of results as some antibiotics induces the production of reactive oxygen species. Alternatively, measurement of metabolic activity via ATP level with the BacTiter-Glo™ Microbial Cell Viability Assay[410] or quenched-fluorescence oxygen sensing[411] are two methods that can provide informative insights of cell viability in *in vitro* assays.

Using as a surrogate, the findings from *M. smegmatis* must be interpreted carefully and should not be directly extrapolate to *Mtb*. The differences in the action of D-LAK peptides on *M. smegmatis* and MDR-TB strains have demonstrated a good example in this regard. *M. smegmatis* is undoubtedly a convenient and useful model for the preliminary study of experimental assays and techniques, nevertheless, *Mtb* strains would be the best choice to aim for translatable findings. Concerning the use of fluorescent probe, uneven nature of annular labelling observed in mycobacteria introduces obscurity in data interpretation[412]. The substantial differences in mycomembrane composition or in the physical state of lipid components lead to possible uneven distribution, exclusion or differing affinities of fluorescent probes, resulting in uneven annular labelling. This poses further challenges in

data interpretation, as fluorescent probe assay only provides an average value for the lipid order but does not indicate by scale whether a more rigid region is segregated from a more fluid region on the same membrane. Therefore, future investigation in the labelling characteristics on mycobacteria would be beneficial to further TB research.

Studies on *Mtb* has been a challenge owing to the physiology of the bacteria; on one hand the slow growth rate implies long incubation time, and therefore, unpredictable morphological changes and induced metabolomic adaptations. On the other hand, disease complexity increases the difficulty of interpreting clinical outcome based on results of *in vitro* assays. As a result, a consensus regarding culture conditions such as medium composition and pH, carbon source and time of incubation has to be reached within the field.

7.3 FUTURE WORK

This study has further demonstrated the synergy of D-LAK peptides and rifampicin or isoniazid combinations on MDR *Mtb* clinical isolates. It has also established biophysical and membrane sensitive techniques for detecting the action of antibiotics and addressed the applicability of *M. smegmatis* model while proposed a *Mtb* Bleupan model with higher translatability. Study findings creates a foundation for subsequent questions which initiate the need of more research work.

The combination of fluorescence spectroscopy and NMR metabolomics techniques was demonstrated to be useful in elucidating the mode of action of antibiotics on *M. smegmatis*. However, no definitive mechanistic explanations of antibiotics or synergy of D-LAK peptide combinations against *Mtb* strains were determined in this work. Thus, further work could focus on the optimization of the mechanistic studies of anti-TB agents on *Mtb* Bleupan. Challenges at various conditions with different concentrations can trigger disparate growth responses in *Mtb*, enabling the determination of suitable protocol for the observation of action of anti-TB agents as demonstrated in *M. smegmatis*.

The fluorescent probes used in this work were deduced to label predominantly the mycomembrane layer of the mycobacteria. Nonetheless, due to the complexity of mycobacterial cell envelope, the distribution or location of membrane fluorescent probes can be more precisely determined. Some preliminary work has been attempted to observe the distribution of Laurdan probe on *M. bovis* BCG using fluorescence microscopy (Fig. 7.1). The resolution of the images, however, was insufficient for the determination of their exact

locations. Thus, future work would exploit confocal microscopy to obtain higher resolution images and to produce Z-stack images to visualize the exact location of probes in the mycobacteria. On the other hand, to further evaluate peptide internalization in mycobacteria, studies can be performed by treating mycobacteria with fluorescence-labelled D-LAK peptides and observe the localization using fluorescence microscopy[215] or making use of radiolabeled peptides[413].

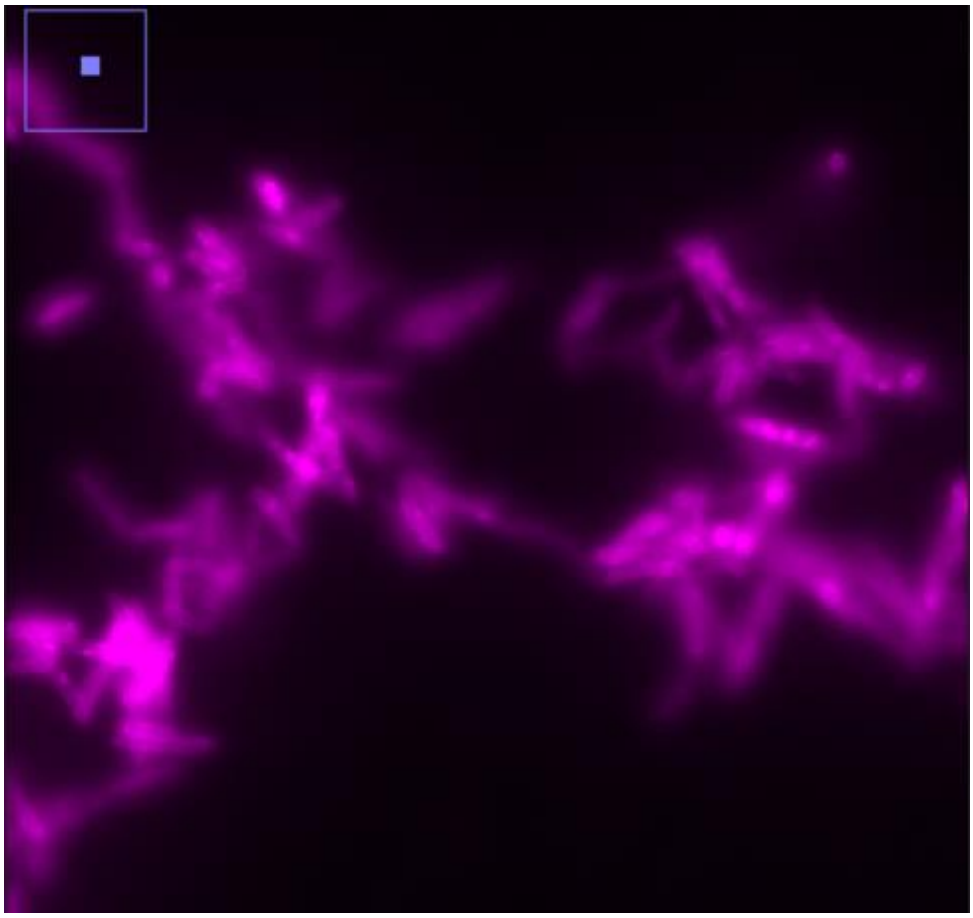

Figure 7.1 M. bovis BCG labelled with Laurdan fluorescent probes. Fixed bacteria were re-suspended in PBS and stained by 2.5 μM Laurdan fluorescent probe. Samples were imaged with a 65x oil-immersion objective lens using a Zeiss LSM-510 inverted confocal microscope (Carl Zeiss Inc., Germany).

Synergistic studies were conducted to evaluate the mycobactericidal activity of D-LAK peptides and rifampicin against 03M and D-LAK peptides and isoniazid against 08MB *in vitro* and *ex vivo*. However, the assay was irretrievable due to an unexpected BSL 3 laboratory incident occurred simultaneous to the present studies. Since 03M and 08MB displayed resistance towards rifampicin and isoniazid respectively when the drug was used

alone, potential synergistic interaction in the combinations with D-LAK peptide would be anticipated to be more beneficial in terms of overcoming the resistant phenotype. It would therefore, be essential to obtain these results again. In addition to RIF and INH, synergy between D-LAK peptides and fluoroquinolones or current second-line anti-TB agents could also be investigated as the combinations might be beneficial to reduce the effective concentration of these highly toxic agents. Besides, conducting cell viability assay using a wider range of macrophage models for *Mtb* such as murine J744 and primary human or murine macrophages would be beneficial to obtain a more comprehensive picture of the biocompatibility of the combinations.[414]

Moreover, this study revealed the potential of combination with D-LAK peptides to reduce the effective dosage of rifampicin and isoniazid by at least two-fold, indicating the positive cooperativity of the peptides to potentiate the action of the drug. More importantly, this synergy may also prevent or delay the development of drug resistance in bacteria[261, 415]. It will be interesting to decipher the capability of D-LAK peptide combinations in supressing the selection of resistant *Mtb* mutants through conducting the drug resistance stimulation study.

Synergy was demonstrated in D-LAK peptides in combination with rifampicin against all the four MDR isolates, while combinations with isoniazid only showed synergistic effect against particular strains. This indicates that there might be possible sequence specificity exhibited by the D-LAK peptides combinations, and therefore, genomic sequencing of the MDR-TB clinical isolates is a logical step to gain better understanding of this aspect. Genome-wide techniques are useful to identify drug target, mode of action and resistance mechanism[416, 417]. Through sequencing the MDR-TB isolates, corresponding genes that are biochemically or physiologically relevant to the peptides' mode of action can be unveiled, therefore enriching our knowledge on potential genome-specific drug targets.

Appendix

Appendix A: Notes on metabolite assignment

Table 7.1 Assignments used for liquid-state NMR experiments.

Metabolite	ppm
2-Hydroxybutyrate	0.86
2-Hydroxyisobutyrate	1.37
Acetate	1.92
Acetoacetate	2.27
Acetone	2.23
Alanine	1.48
Citrate	2.57
Dimethylamine	2.73
Ethanol	1.19
Glucose	3.24
Glutamate	2.06
Glycerol	3.65
Isovalerate	0.91
Lactate	1.33
Malate	2.46
Methylmalonate	1.22
Pyruvate	2.37
Succinate	2.41
Tartrate	4.33
Valine	0.98

Table 7.2 Assignments used for ^{1}H HR-MAS NMR experiments.

Metabolite	ppm
Lipids CH_3-	0.89
Lipids -$(CH_2)_n$-	1.29
Alanine	1.47
Lipids -CH_2-OH	1.59
Lysine	1.91
Lipids -CH_2-CH=CH-	2.03
Lipids -CH_2-COOH	2.24
Glutamate	2.36
Trehalose	3.84
Serine	3.95
Glycerate	4.07
Lipids -CH=CH-	5.32
Sucrose	5.38

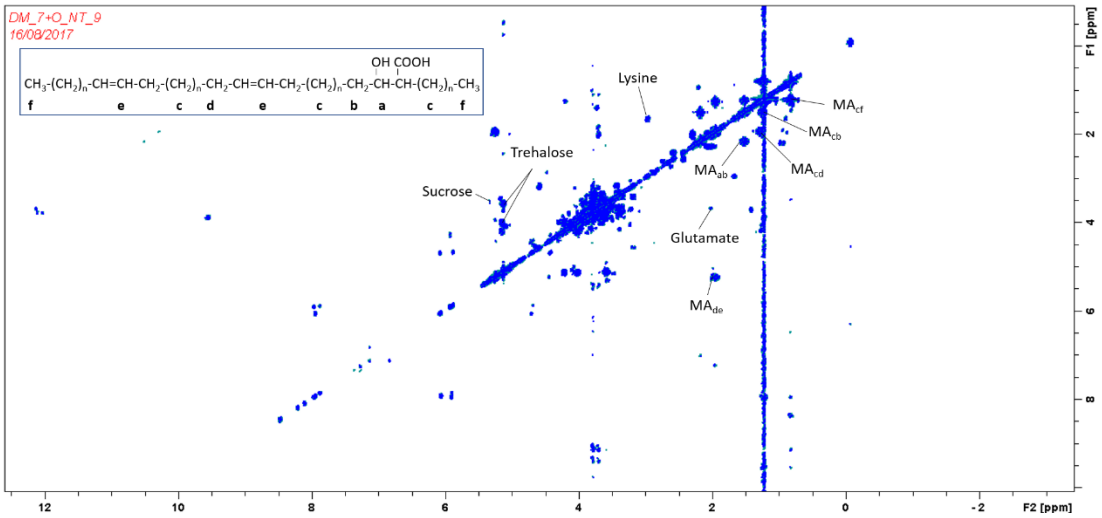

Figure 7.2 Representative 2D COSY ^{1}H HR-MAS NMR spectrum of M. smegmatis mc^{2} 155. A partial assignment is shown of identified metabolites. the spectrum was obtained on a 600 MHz Bruker spectrometer. General formula of mycolic acid (MA) is shown for the identification of cross-peaks between carbon groups.

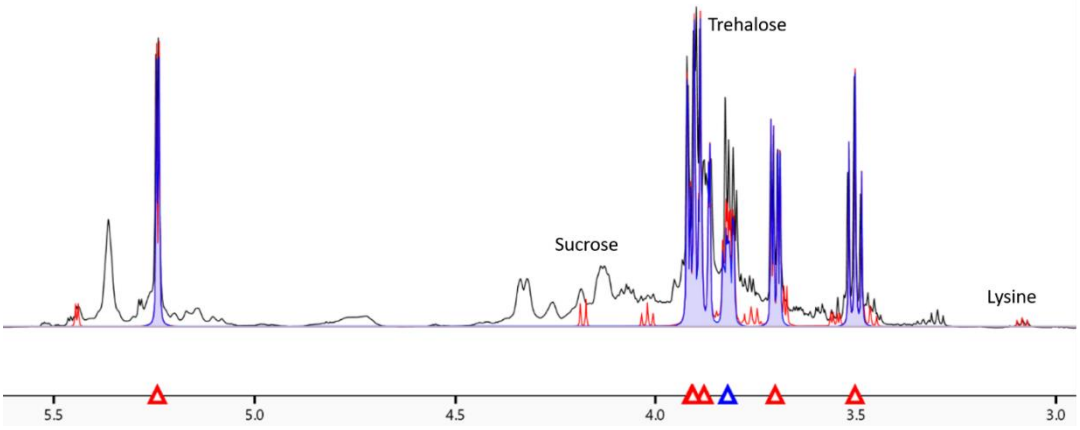

Figure 7.3 Representative metabolite assignment of a 1D ^{1}H HR-MAS NMR spectrum of M. smegmatis mc^{2} 155 with Chenomx software. Chenomx allows the overlaying of standard NMR spectra of compounds (coloured) with the NMR spectrum of sample under study (black).

Appendix B: Supplementary figures for multivariate analysis of mycobacterial growth response assay on *M. smegmatis*

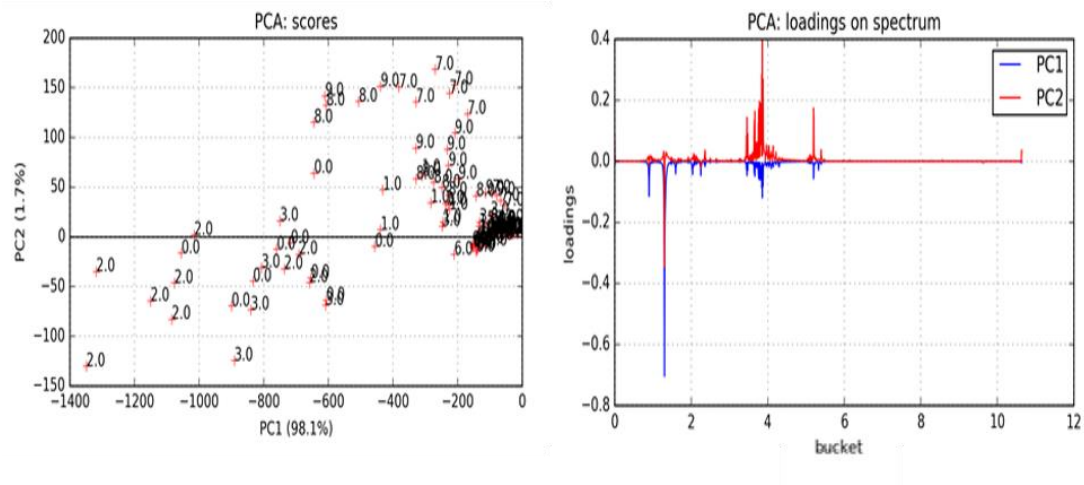

Figure 7.4 PCA of whole cell M. smegmatis mc^2 155 subjected to different challenges. PCA score plot (Left) as shown for unchallenged bacteria (1.0), in the presence of 0.025% tyloxapol (1.0) or those challenged with ¾ MIC of D-LAK120-A (2.0), D-LAK120-HP13 (3.0), rifampicin (4.0), rifampicin in combination with D-LAK120-A (5.0) or D-LAK120-HP13 (6.0), capreomycin (7.0), capreomycin in combination with D-LAK120-A (8.0) or D-LAK120-HP13 (9.0), colistin (10.0), isoniazid (11.0). PCA loadings (Right) denoted the major metabolite responsible for the clustering in the score plot.

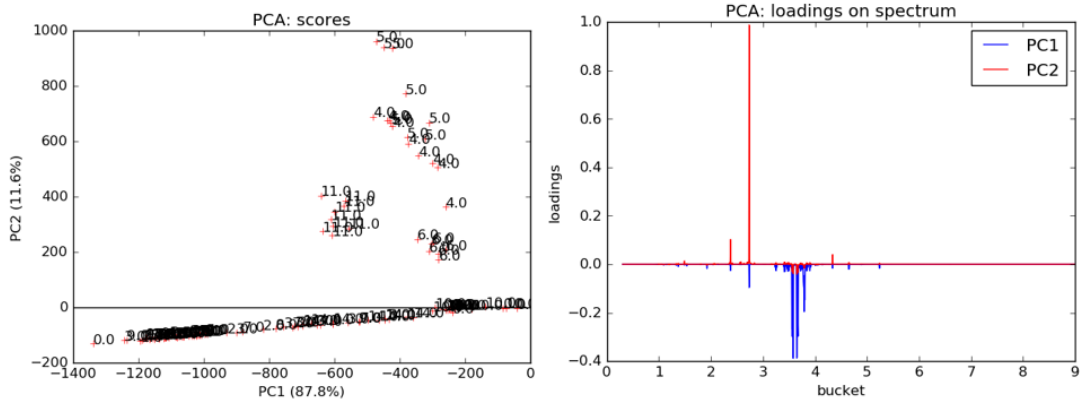

Figure 7.5 PCA of spent culture media of M. smegmatis mc^2 155 subjected to different challenges. PCA score plot (Left) as shown for unchallenged bacteria (1.0), in the presence of 0.025% tyloxapol (1.0) or those challenged with ¾ MIC of D-LAK120-A (2.0), D-LAK120-HP13 (3.0), rifampicin (4.0), rifampicin in combination with D-LAK120-A (5.0) or D-LAK120-HP13 (6.0), capreomycin (7.0), capreomycin in combination with D-LAK120-A (8.0) or D-LAK120-HP13 (9.0), colistin (10.0), isoniazid (11.0). PCA loadings (Right) denoted the major metabolite responsible for the clustering in the score plot.

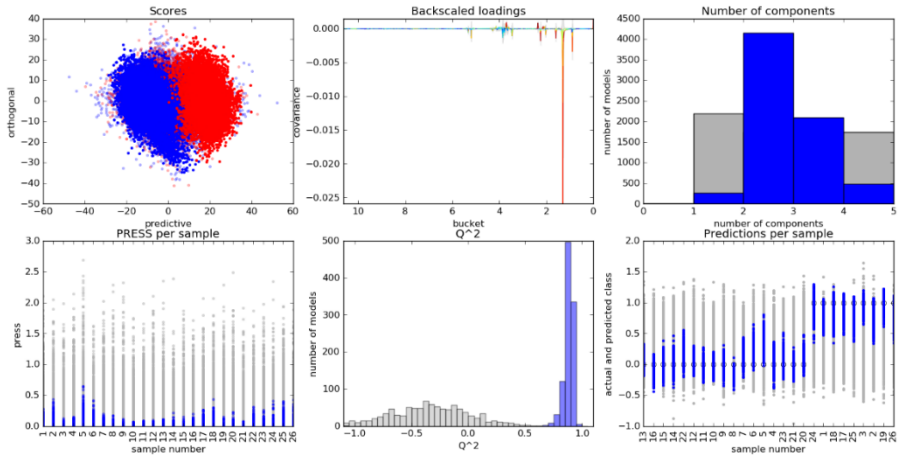

Figure 7.6 OPLS-DA cross-validation data of whole cell M. smegmatis mc^2 155 in the presence of 0.025% tyloxapol as compared with unchallenged bacteria.

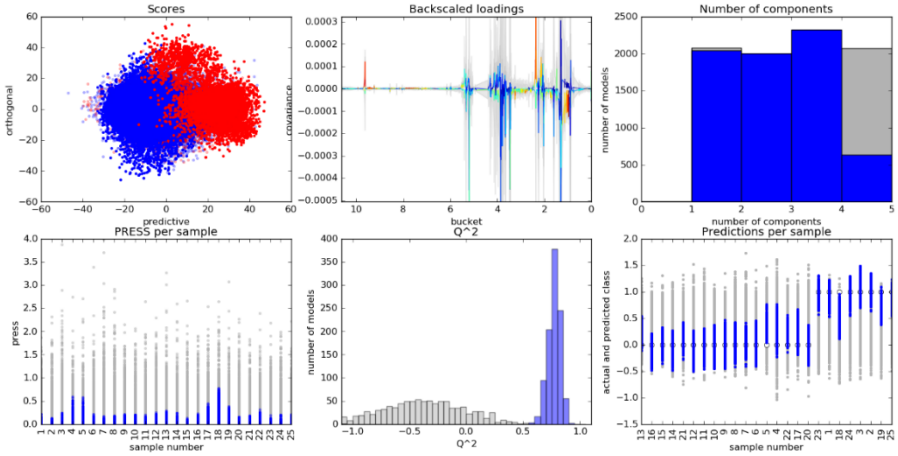

Figure 7.7 OPLS-DA cross-validation data of whole cell M. smegmatis mc^2 155 in the presence of ¾ MIC of D-LAK120-A as compared with unchallenged bacteria.

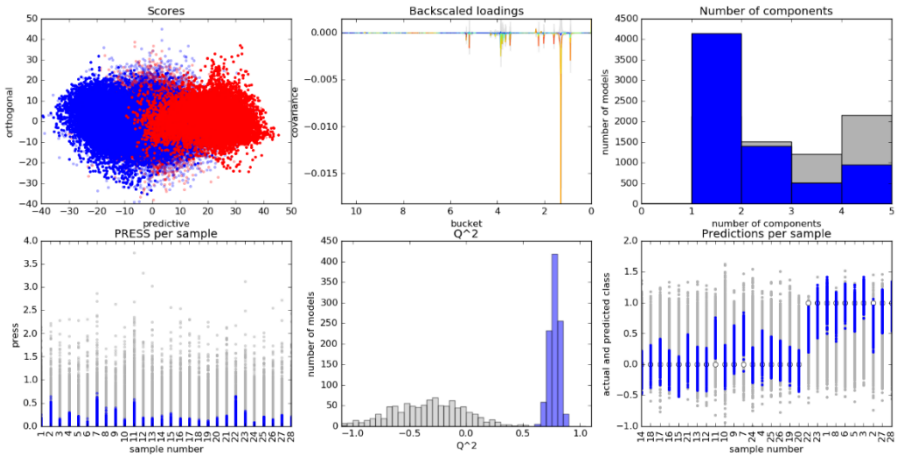

Figure 7.8 OPLS-DA cross-validation data of whole cell M. smegmatis mc^2 155 in the presence of ¾ MIC of D-LAK120-HP13 as compared with unchallenged bacteria.

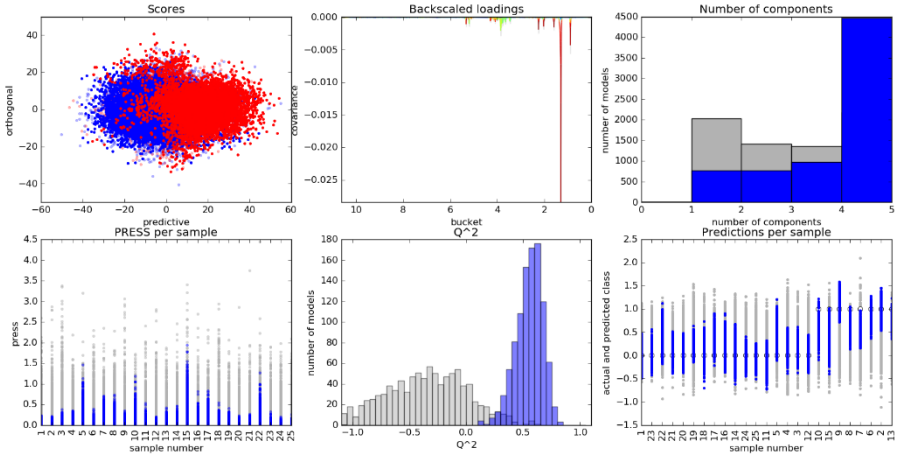

Figure 7.9 OPLS-DA cross-validation data of whole cell M. smegmatis mc^2 155 in the presence of ¾ MIC of rifampicin as compared with unchallenged bacteria.

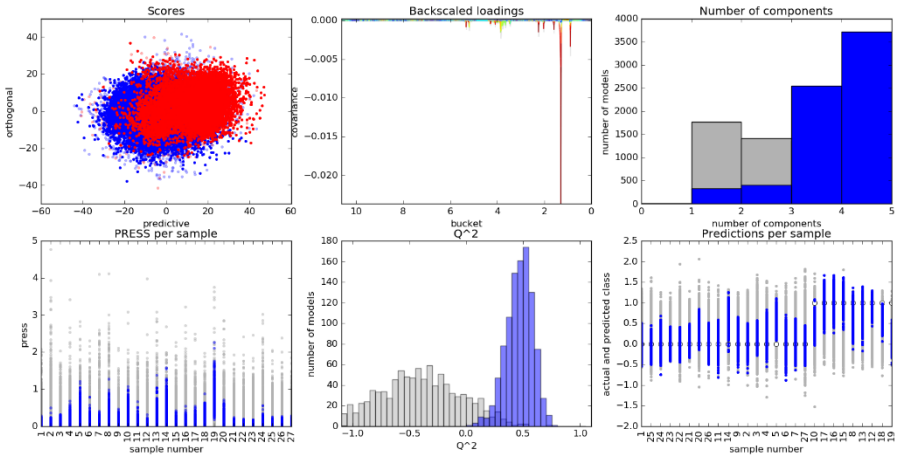

Figure 7.10 OPLS-DA cross-validation data of whole cell M. smegmatis mc^2 155 in the presence of ¾ MIC of D-LAK120-A with rifampicin in combination as compared with unchallenged bacteria.

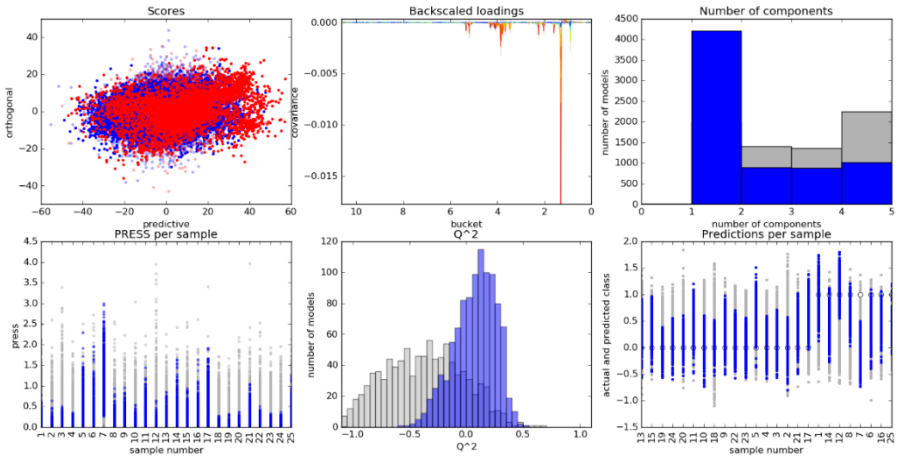

Figure 7.11 OPLS-DA cross-validation data of whole cell M. smegmatis mc^2 155 in the presence of ¾ MIC of D-LAK120-HP13 with rifampicin in combination as compared with unchallenged bacteria.

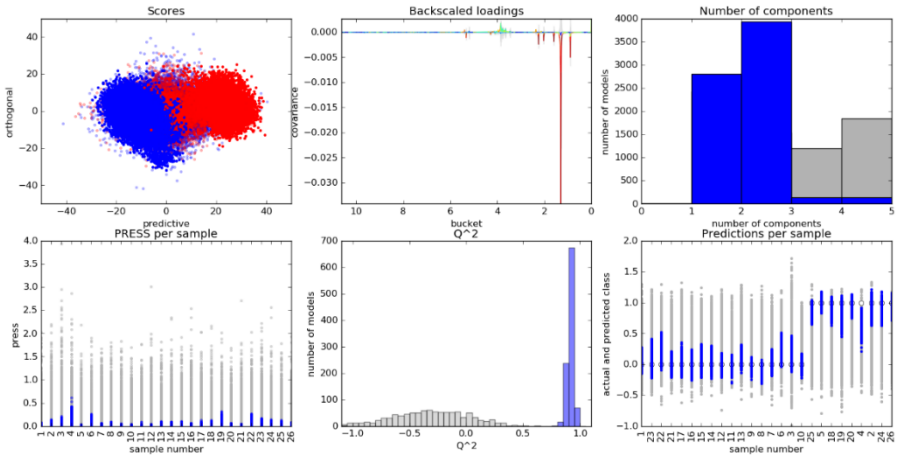

Figure 7.12 OPLS-DA cross-validation data of whole cell M. smegmatis mc^2 155 in the presence of ¾ MIC of capreomycin as compared with unchallenged bacteria.

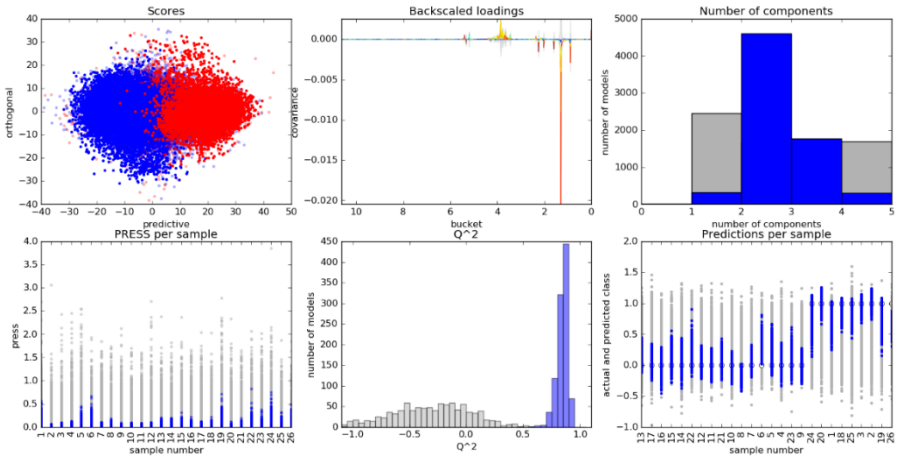

Figure 7.13 OPLS-DA cross-validation data of whole cell M. smegmatis mc^2 155 in the presence of ¾ MIC of D-LAK120-A with capreomycin in combination as compared with unchallenged bacteria.

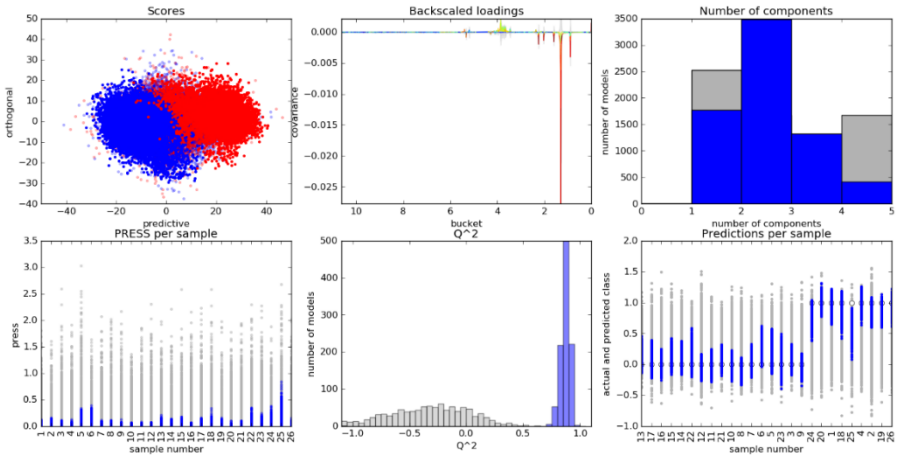

Figure 7.14 OPLS-DA cross-validation data of whole cell M. smegmatis mc^2 155 in the presence of ¾ MIC of D-LAK120-HP13 with capreomycin in combination as compared with unchallenged bacteria.

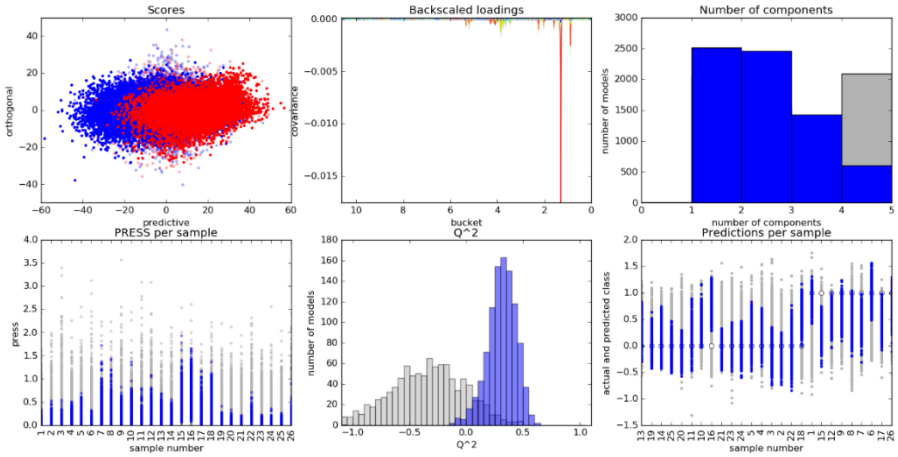

Figure 7.15 OPLS-DA cross-validation data of whole cell M. smegmatis mc^2 155 in the presence of ¾ MIC of colistin as compared with unchallenged bacteria.

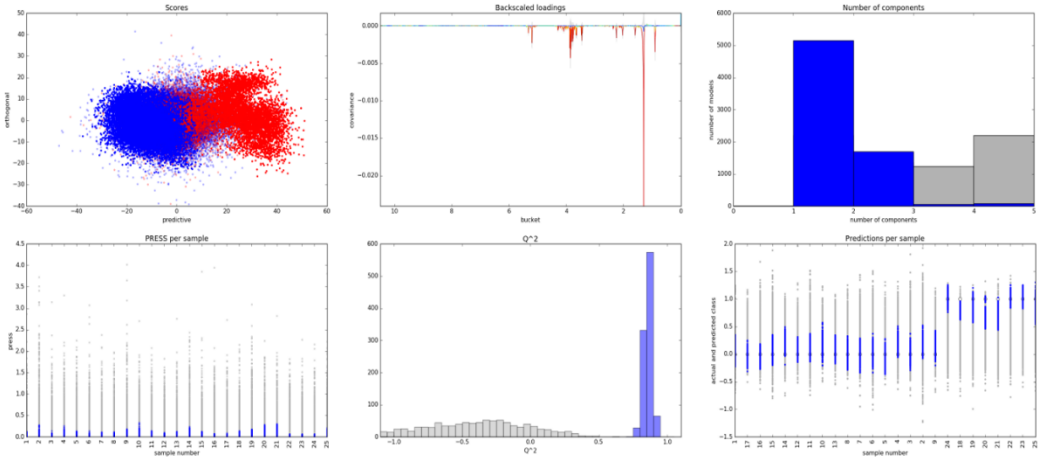

Figure 7.16 OPLS-DA cross-validation data of whole cell M. smegmatis mc^2 155 in the presence of ¾ MIC of isoniazid as compared with unchallenged bacteria.

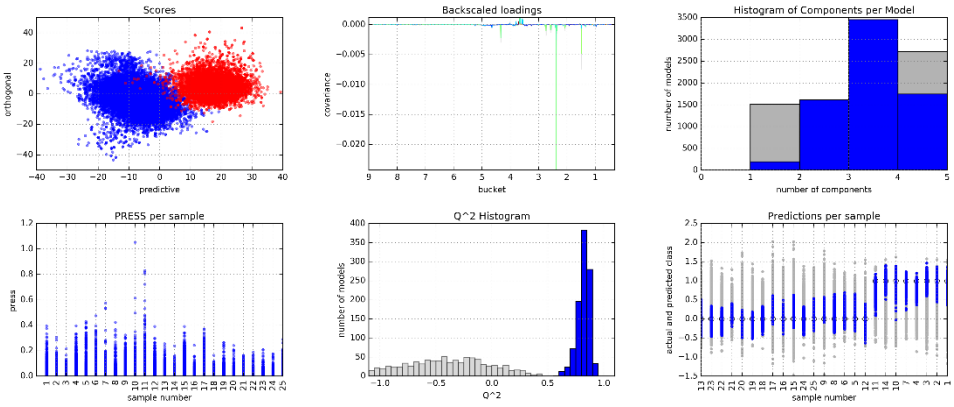

Figure 7.17 OPLS-DA cross-validation data of spent culture media of M. smegmatis mc^2 155 in the presence of 0.025% tyloxapol as compared with unchallenged bacteria.

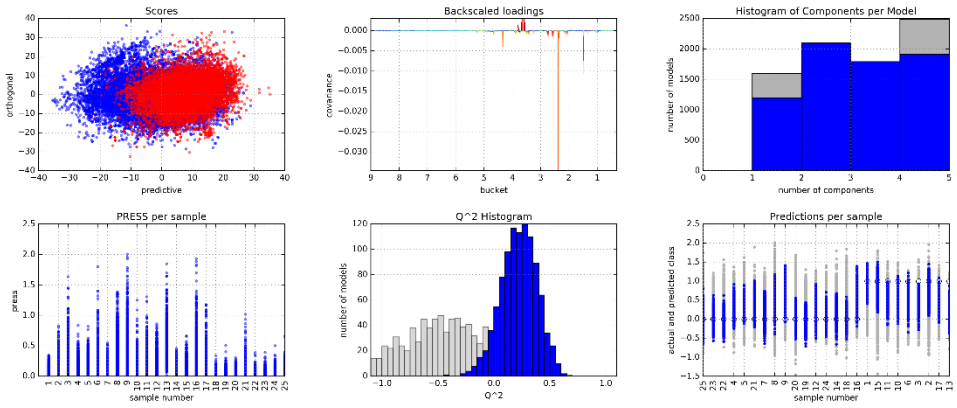

Figure 7.18 OPLS-DA cross-validation data of spent culture media M. smegmatis mc^2 155in the presence of ¾ MIC of D-LAK120-A as compared with unchallenged bacteria.

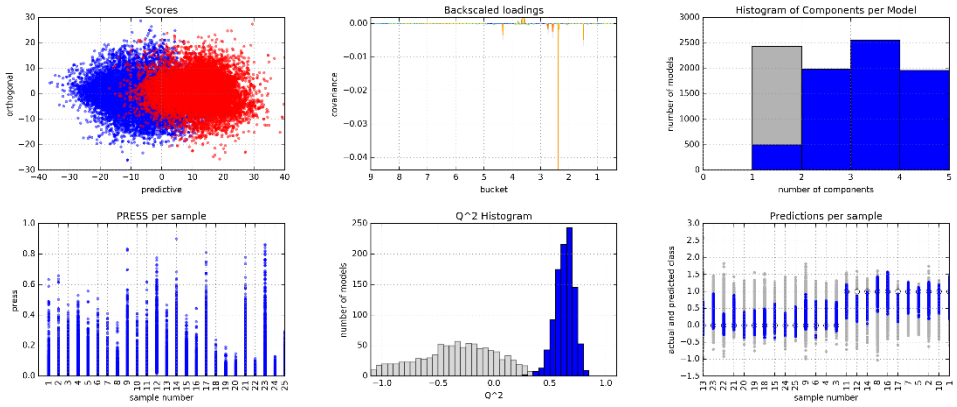

Figure 7.19 OPLS-DA cross-validation data of spent culture media M. smegmatis mc^2 155 in the presence of ¾ MIC of D-LAK120-HP13 as compared with unchallenged bacteria.

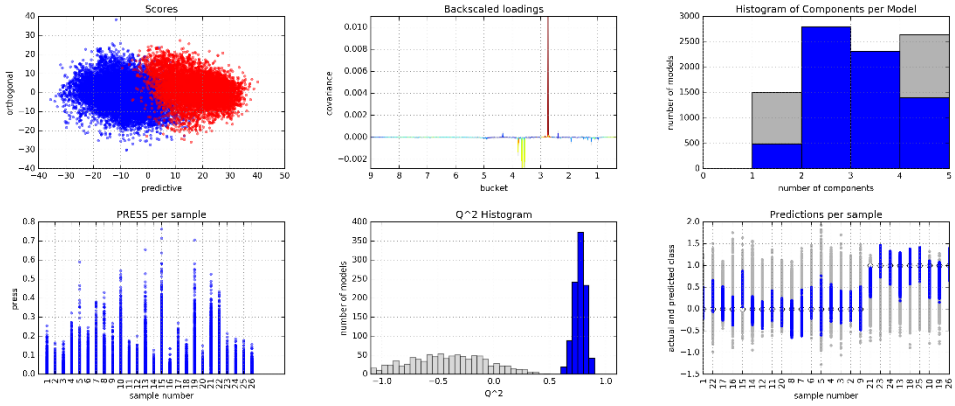

Figure 7.20 OPLS-DA cross-validation data of spent culture media M. smegmatis mc^2 155in the presence of ¾ MIC of rifampicin as compared with unchallenged bacteria.

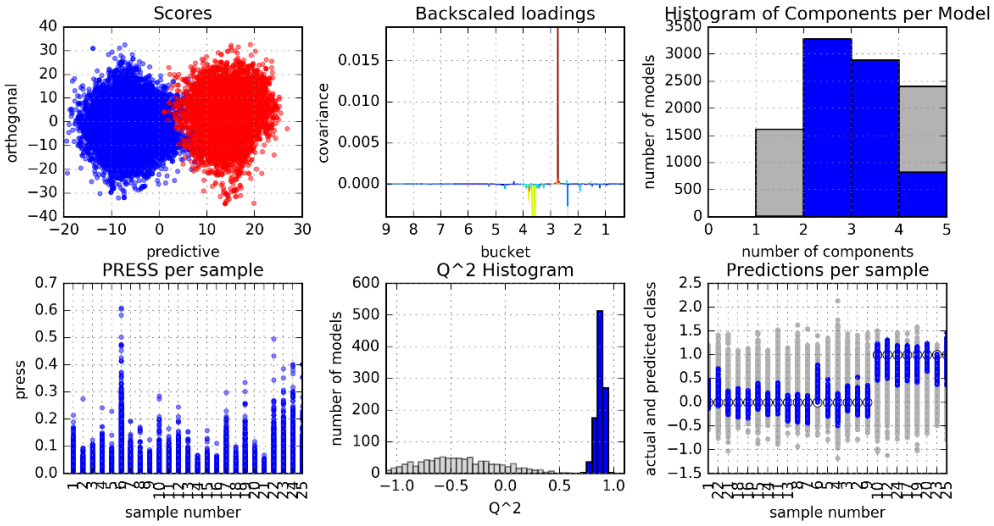

Figure 7.21 OPLS-DA cross-validation data of spent culture media of M. smegmatis mc^2 155 in the presence of ¾ MIC of D-LAK120-A with rifampicin in combination as compared with unchallenged bacteria.

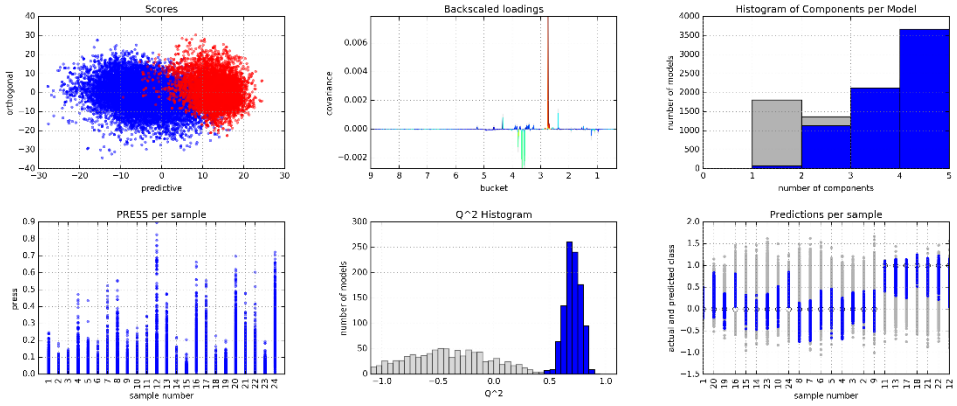

Figure 7.22 OPLS-DA cross-validation data of spent culture media of M. smegmatis mc^2 155 in the presence of ¾ MIC of D-LAK120-HP13 with rifampicin in combination as compared with unchallenged bacteria.

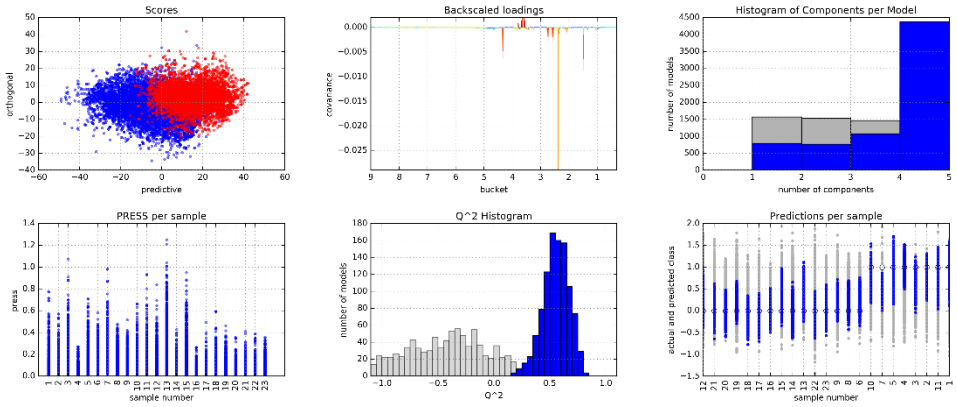

Figure 7.23 OPLS-DA cross-validation data of spent culture media of M. smegmatis mc^2 155 in the presence of ¾ MIC of capreomycin as compared with unchallenged bacteria.

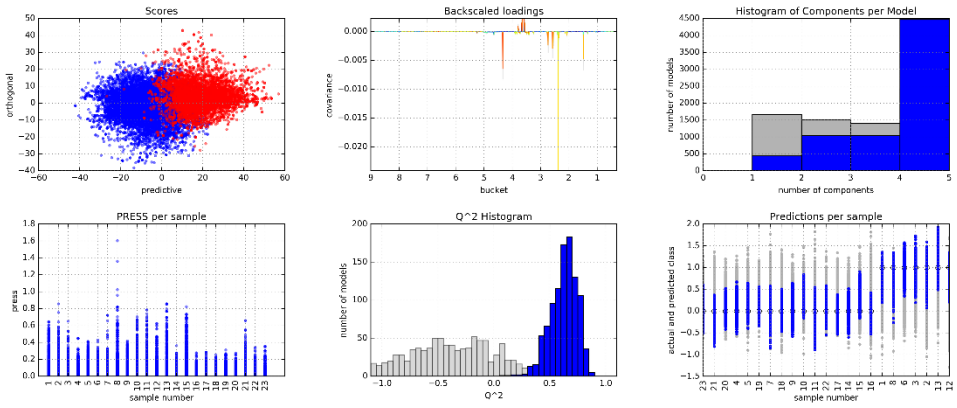

Figure 7.24 OPLS-DA cross-validation data of spent culture media of M. smegmatis mc^2 155 in the presence of ¾ MIC of D-LAK120-A with capreomycin in combination as compared with unchallenged bacteria.

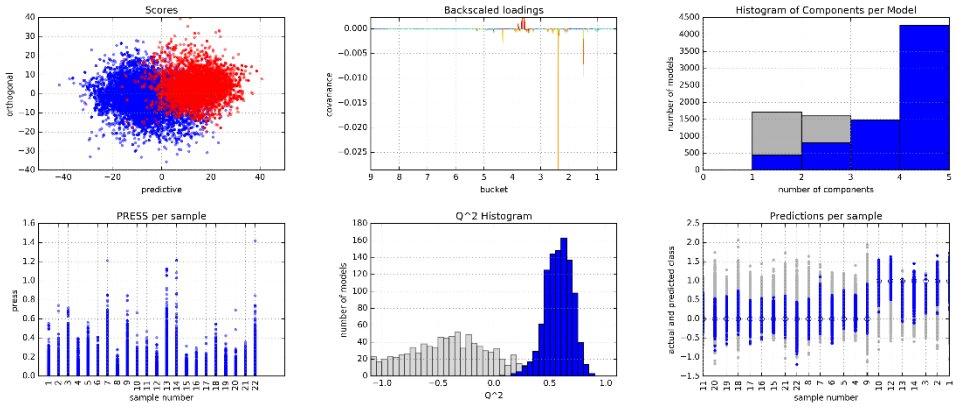

Figure 7.25 OPLS-DA cross-validation data of spent culture media of M. smegmatis mc^2 155 in the presence of ¾ MIC of D-LAK120-HP13 with capreomycin in combination as compared with unchallenged bacteria.

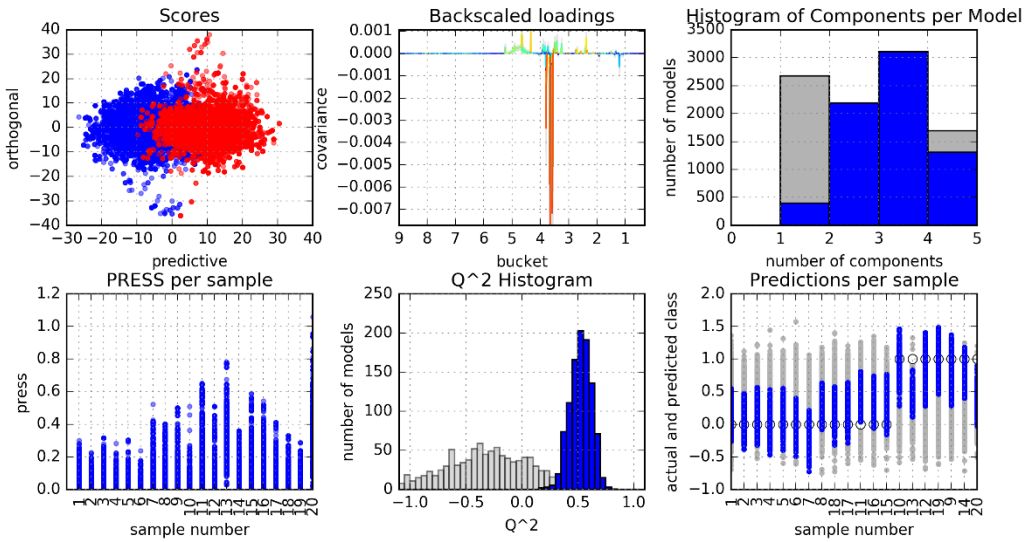

Figure 7.26 OPLS-DA cross-validation data of spent culture media of M. smegmatis mc^2 155 in the presence of ¾ MIC of colistin as compared with unchallenged bacteria.

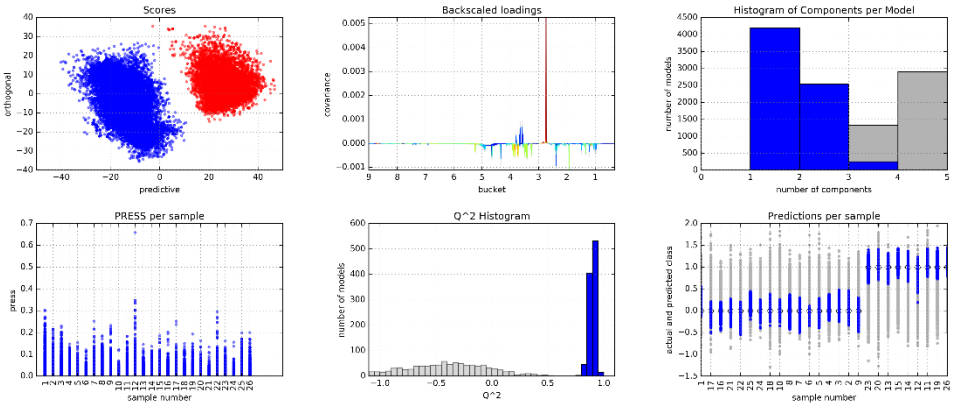

Figure 7.27 OPLS-DA cross-validation data of spent culture media of M. smegmatis mc^2 155 in the presence of ¾ MIC of isoniazid as compared with unchallenged bacteria.

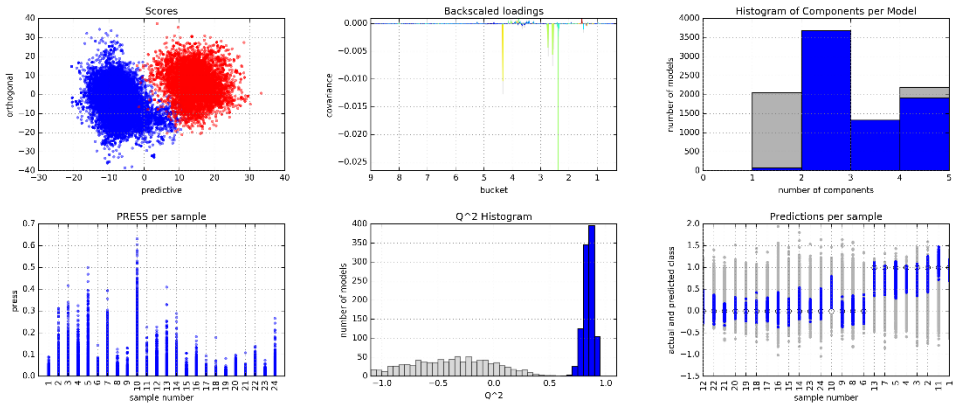

Figure 7.28 OPLS-DA cross-validation data of fresh media as compared with spent culture media of unchallenged M. smegmatis mc^2 155.

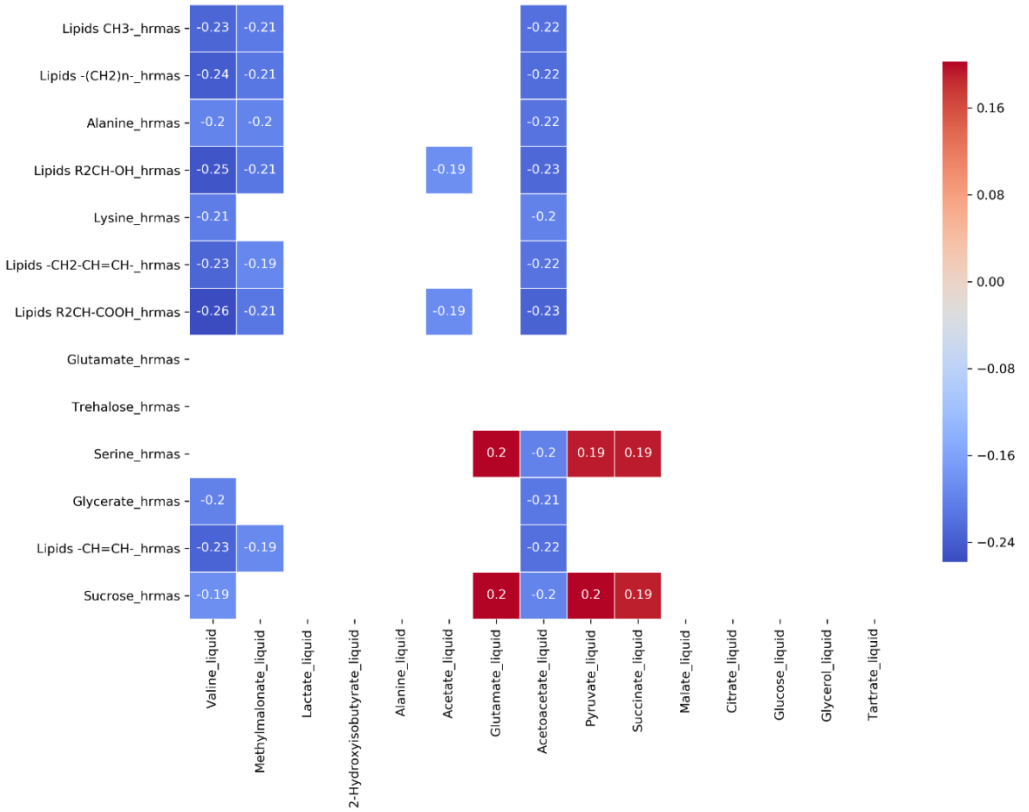

Figure 7.29 Heatmap illustrating the correlation between metabolites identified in HR-MAS and liquid-state NMR spectra of M. smegmatis mc^2 155. The correlation constant did not pass the significant threshold of 0.3 indicating there is no correlation between any of the metabolites detected in HR-MAS and those in liquid-NMR.

Appendix C: Supplementary figures for multivariate analysis of mycobacterial growth response assay on *Mtb* Bleupan

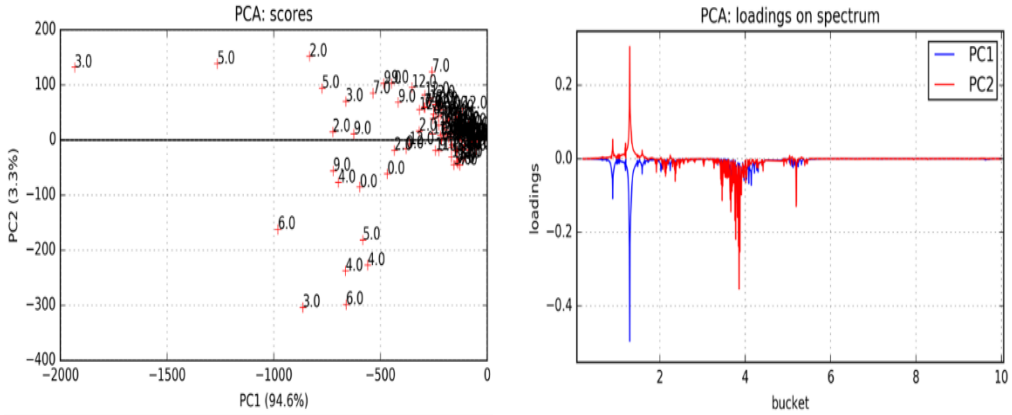

Figure 7.30 PCA of whole cell Mtb Bleupan subjected to different challenges for 6-week. PCA score plot (Left) as shown for unchallenged bacteria (1.0), in the presence of 0.025% tyloxapol (1.0) or those challenged with ¼ MIC of D-LAK120-A (2.0), D-LAK120-HP13 (3.0), rifampicin (4.0), rifampicin in combination with D-LAK120-A (5.0) or D-LAK120-HP13 (6.0), isoniazid (7.0), isoniazid in combination with D-LAK120-A (8.0) or D-LAK120-HP13 (9.0), capreomycin (10.0), colistin (11.0), delamanid (12.0). PCA loadings (Right) denoted the major metabolite responsible for the clustering in the score plot.

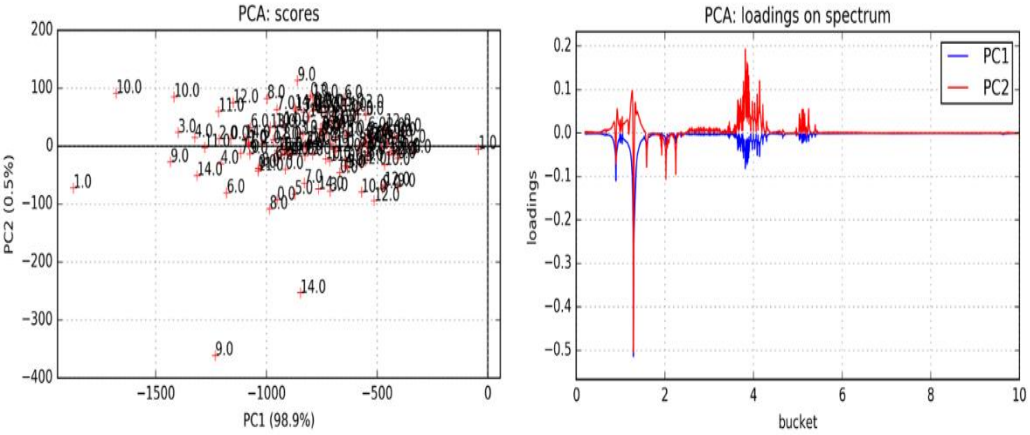

Figure 7.31 PCA of whole cell Mtb Bleupan subjected to different challenges for 72-hour. PCA score plot (Left) as shown for unchallenged bacteria (1.0), in the presence of 0.025% tyloxapol (1.0) or those challenged with ½ MIC of D-LAK120-A (2.0), D-LAK120-HP13 (3.0), rifampicin (4.0), rifampicin in combination with D-LAK120-A (5.0) or D-LAK120-HP13 (6.0), isoniazid (7.0), isoniazid in combination with D-LAK120-A (8.0) or D-LAK120-HP13 (9.0), capreomycin (10.0), capreomycin in combination with D-LAK120-A (11.0) or D-LAK120-HP13 (12.0), colistin (13.0), delamanid (14.0). PCA loadings (Right) denoted the major metabolite responsible for the clustering in the score plot

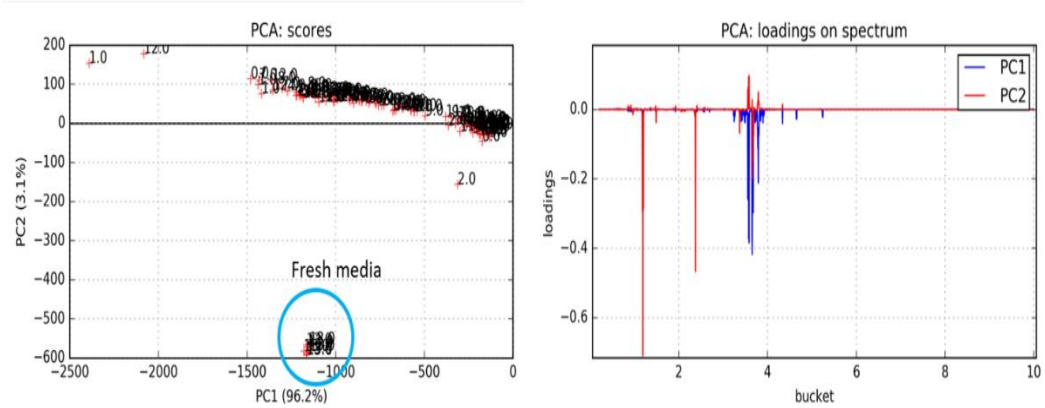

Figure 7.32 PCA of spent media of Mtb Bleupan subjected to different challenges for 6-week. PCA score plot (Left) as shown for unchallenged bacteria (1.0), in the presence of 0.025% tyloxapol (1.0) or those challenged with ¼ MIC of D-LAK120-A (2.0), D-LAK120-HP13 (3.0), rifampicin (4.0), rifampicin in combination with D-LAK120-A (5.0) or D-LAK120-HP13 (6.0), isoniazid (7.0), isoniazid in combination with D-LAK120-A (8.0) or D-LAK120-HP13 (9.0), capreomycin (10.0), colistin (11.0), delamanid (12.0). PCA loadings (Right) denoted the major metabolite responsible for the clustering in the score plot

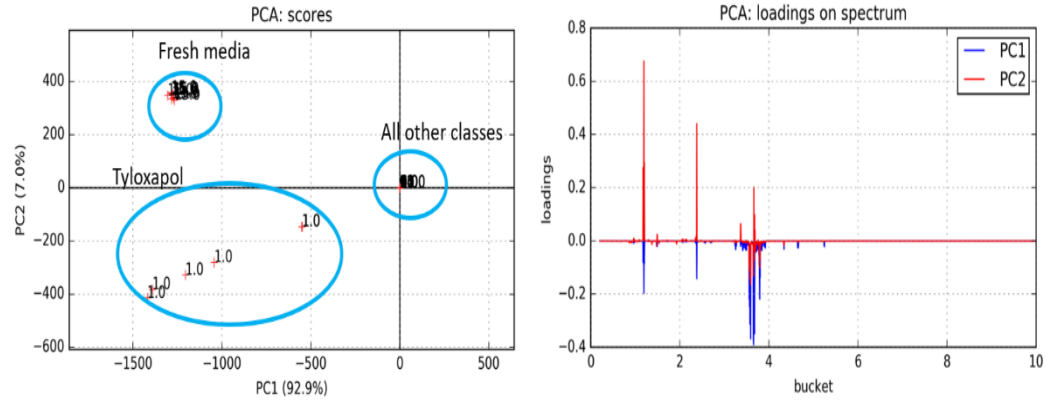

Figure 7.33 PCA of spent media of Mtb Bleupan subjected to different challenges for 72-hour. PCA score plot (Left) as shown for unchallenged bacteria (1.0), in the presence of 0.025% tyloxapol (1.0) or those challenged with ½ MIC of D-LAK120-A (2.0), D-LAK120-HP13 (3.0), rifampicin (4.0), rifampicin in combination with D-LAK120-A (5.0) or D-LAK120-HP13 (6.0), isoniazid (7.0), isoniazid in combination with D-LAK120-A (8.0) or D-LAK120-HP13 (9.0), capreomycin (10.0), capreomycin in combination with D-LAK120-A (11.0) or D-LAK120-HP13 (12.0),, colistin (13.0), delamanid (14.0). PCA loadings (Right) denoted the major metabolite responsible for the clustering in the score plot

(A)

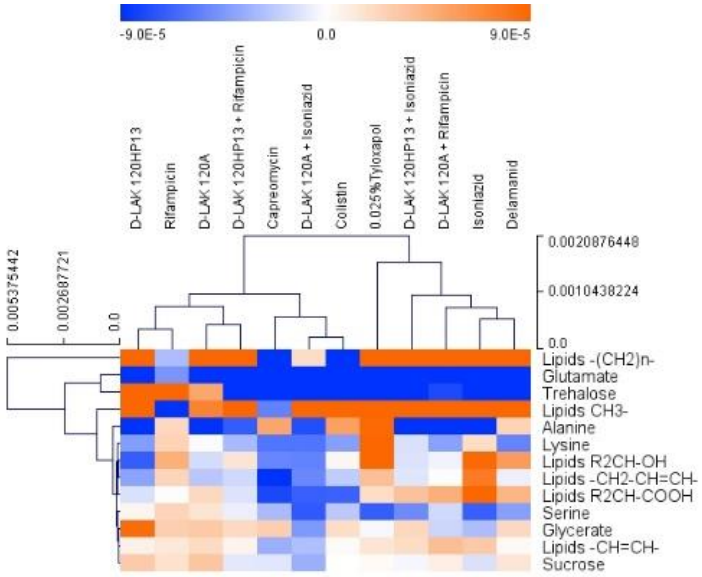

(B)

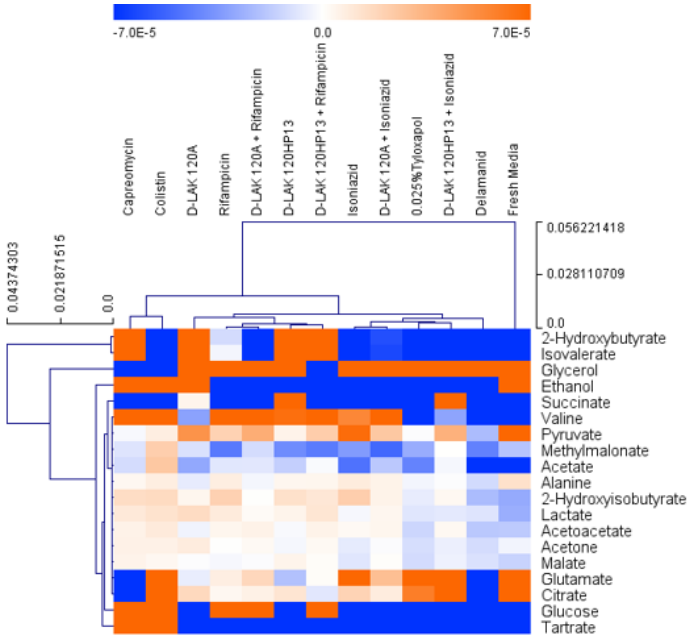

Figure 7.34 Hierarchical clustered heatmap comparing loadings obtained from cross-validated OPLS-DA of ^{1}H HR-MAS (A) and liquid-state (B) NMR spectra of Mtb Bleupan challenged with indicated conditions for 6 weeks.

(A)

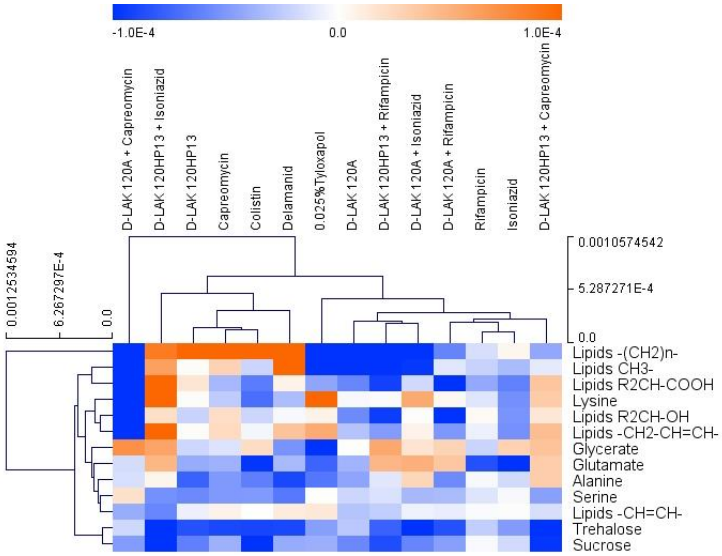

(B)

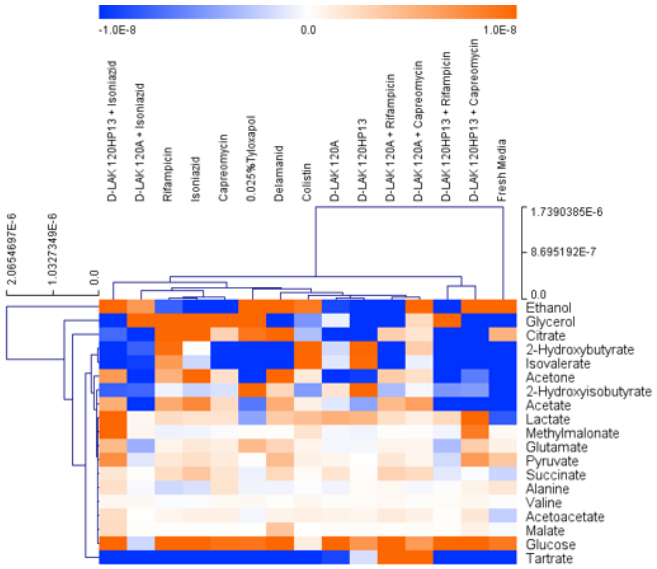

Figure 7.35 Hierarchical clustered heatmap comparing loadings obtained from cross-validated OPLS-DA of ^{1}H HR-MAS (A) and liquid-state (B) NMR spectra of Mtb Bleupan challenged with indicated conditions for 72 hours.

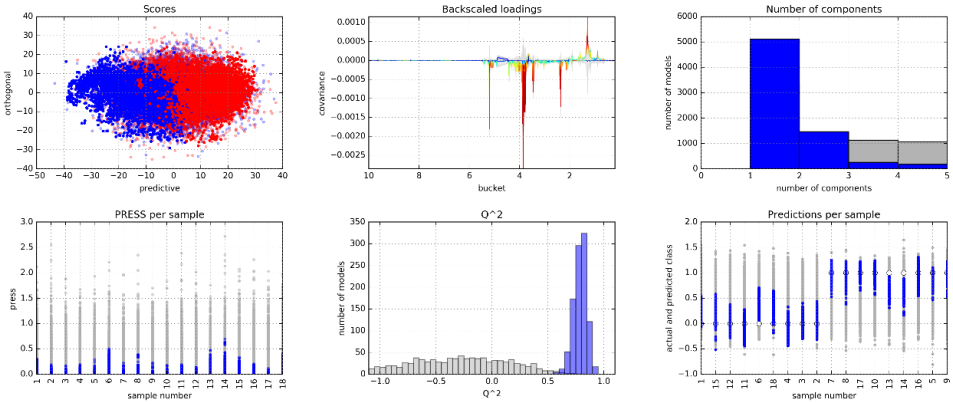

Figure 7.36 OPLS-DA cross-validation data whole cell Mtb Bleupan in the presence of 0.025% tyloxapol as compared with unchallenged bacteria.

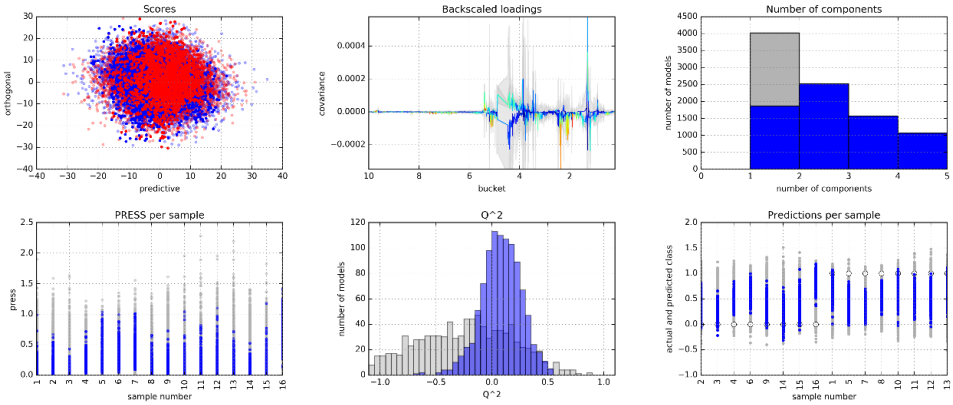

Figure 7.37 OPLS-DA cross-validation data of whole cell Mtb Bleupan in the presence of ¼ MIC of D-LAK120-A as compared with unchallenged bacteria.

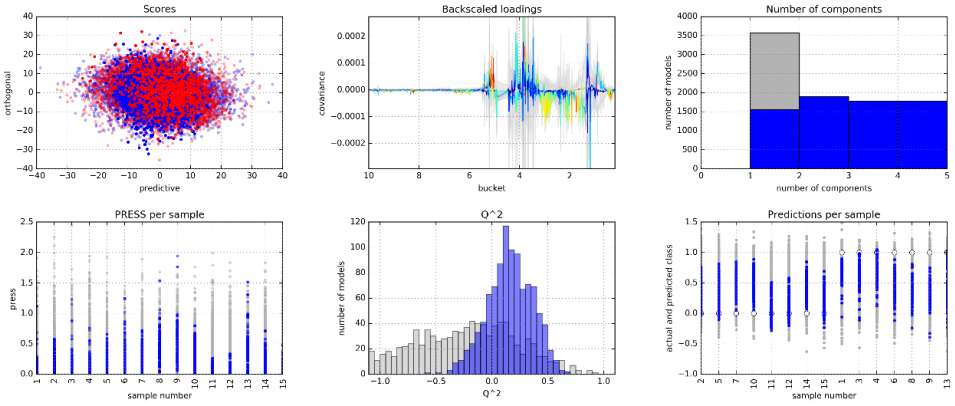

Figure 7.38 OPLS-DA cross-validation data of whole cell Mtb Bleupan in the presence of ¼ MIC of D-LAK120HP13 as compared with unchallenged bacteria.

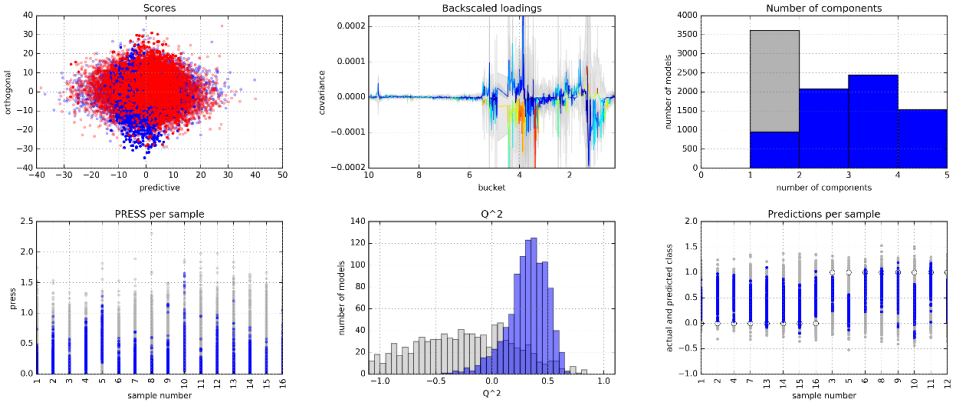

Figure 7.39 OPLS-DA cross-validation data of whole cell Mtb Bleupan in the presence of ¼ MIC of rifampicin as compared with unchallenged bacteria.

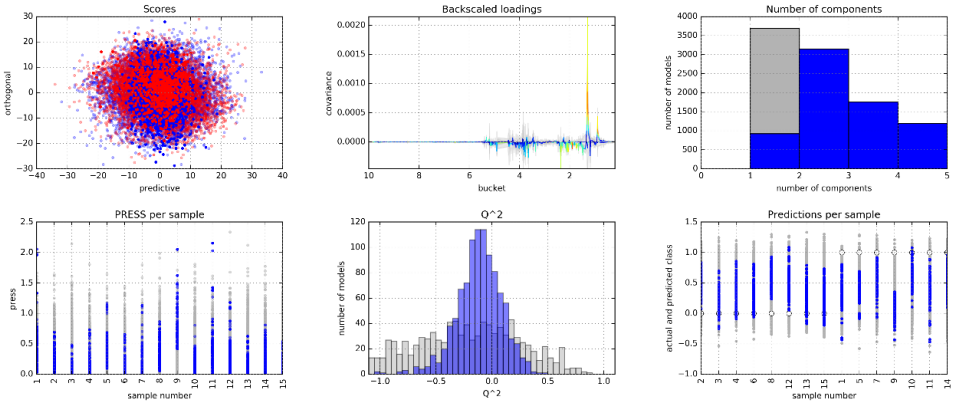

Figure 7.40 OPLS-DA cross-validation data of whole cell Mtb Bleupan in the presence of ¼ MIC of D-LAK120-A with rifampicin in combination as compared with unchallenged bacteria.

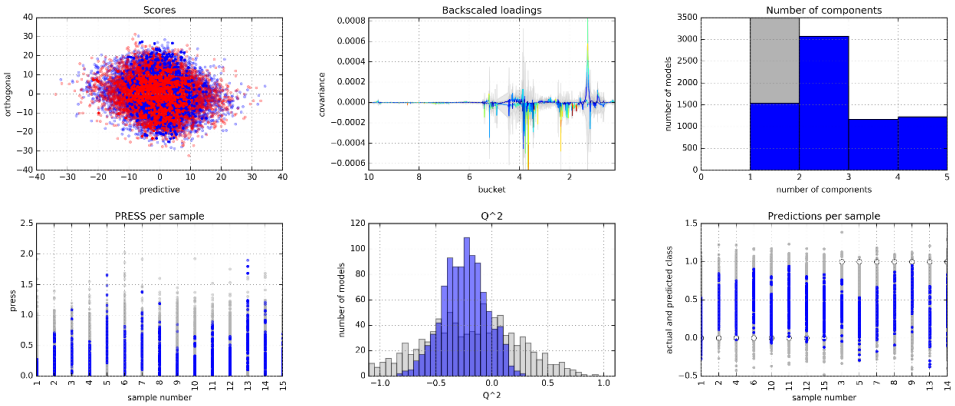

Figure 7.41 OPLS-DA cross-validation data of whole cell Mtb Bleupan in the presence of ¼ MIC of D-LAK120-HP13 with rifampicin in combination as compared with unchallenged bacteria.

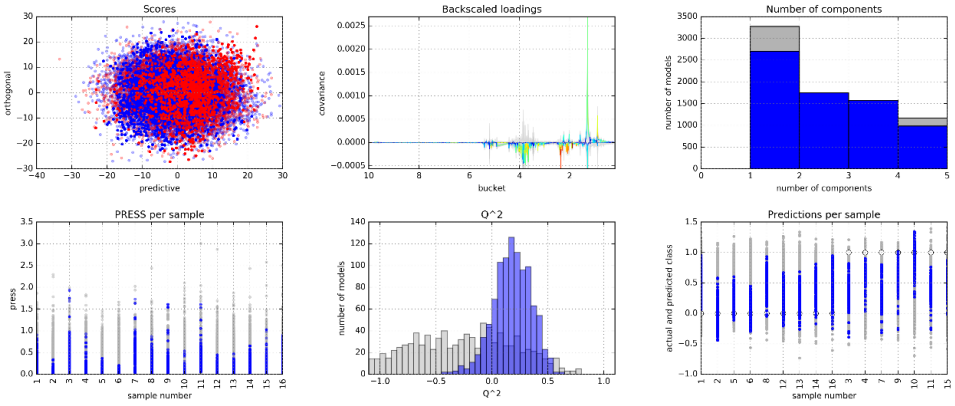

Figure 7.42 OPLS-DA cross-validation data of whole cell Mtb Bleupan in the presence of ¼ MIC of isoniazid as compared with unchallenged bacteria.

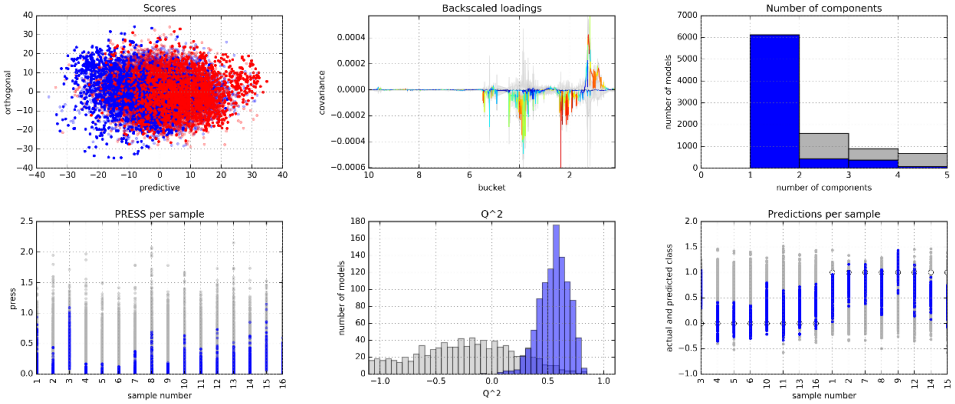

Figure 7.43 OPLS-DA cross-validation data of whole cell Mtb Bleupan in the presence of ¼ MIC of D-LAK120-A with isoniazid in combination as compared with unchallenged bacteria.

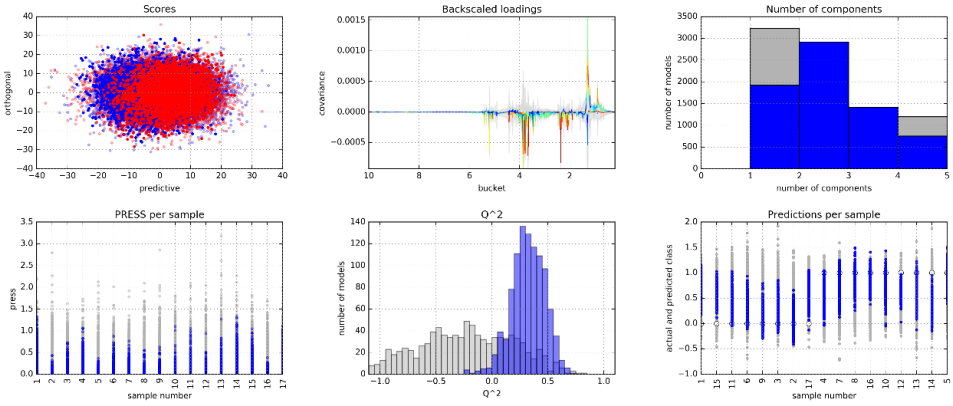

Figure 7.44 OPLS-DA cross-validation data of whole cell Mtb Bleupan in the presence of ¼ MIC of D-LAK120-HP13 with isoniazid in combination as compared with unchallenged bacteria.

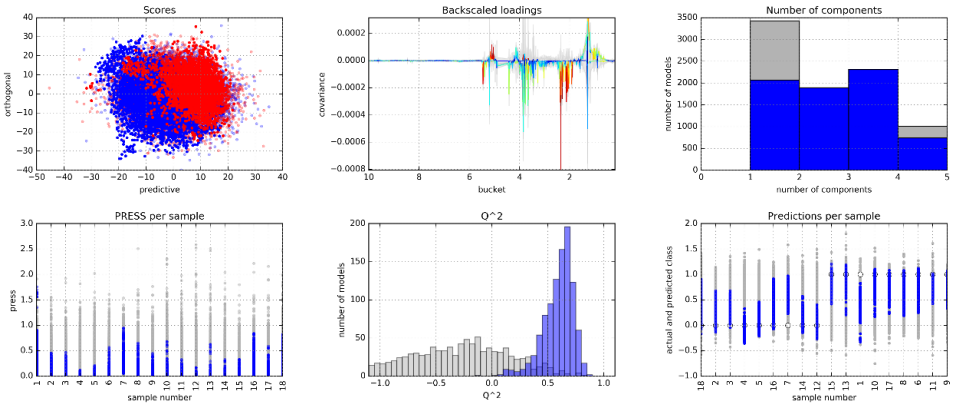

Figure 7.45 OPLS-DA cross-validation data of whole cell Mtb Bleupan in the presence of ¼ MIC of capreomycin as compared with unchallenged bacteria.

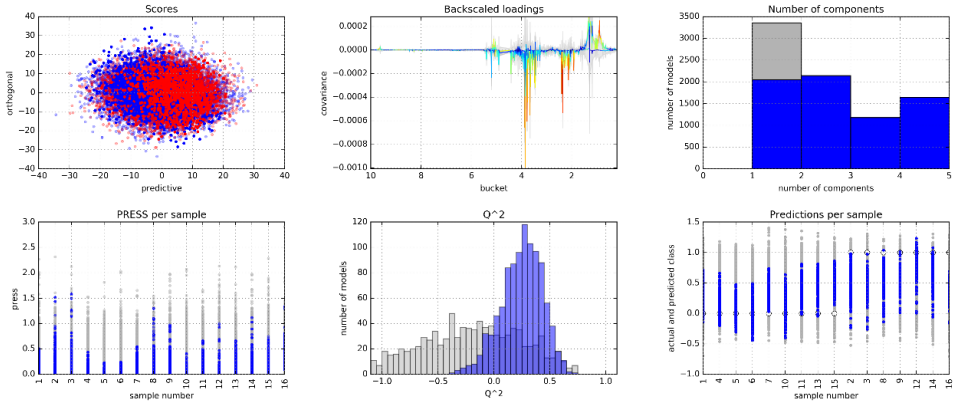

Figure 7.46 OPLS-DA cross-validation data of whole cell Mtb Bleupan in the presence of ¼ MIC of colistin as compared with unchallenged bacteria.

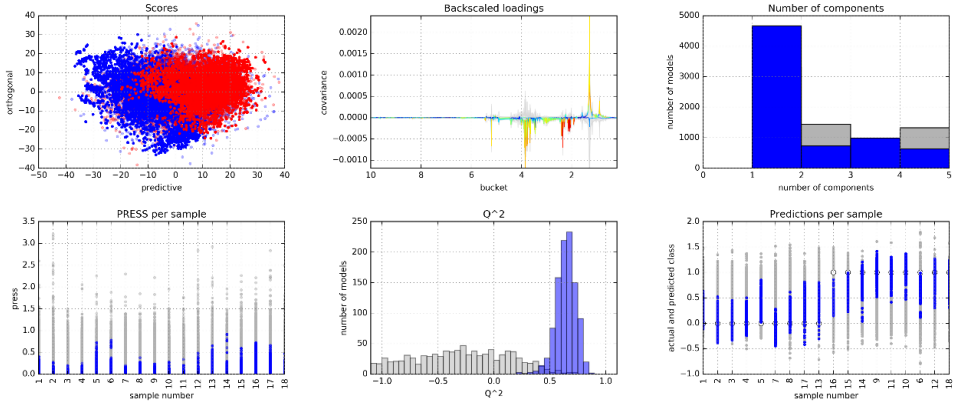

Figure 7.47 OPLS-DA cross-validation data of whole cell Mtb Bleupan in the presence of ¼ MIC of delamanid as compared with unchallenged bacteria.

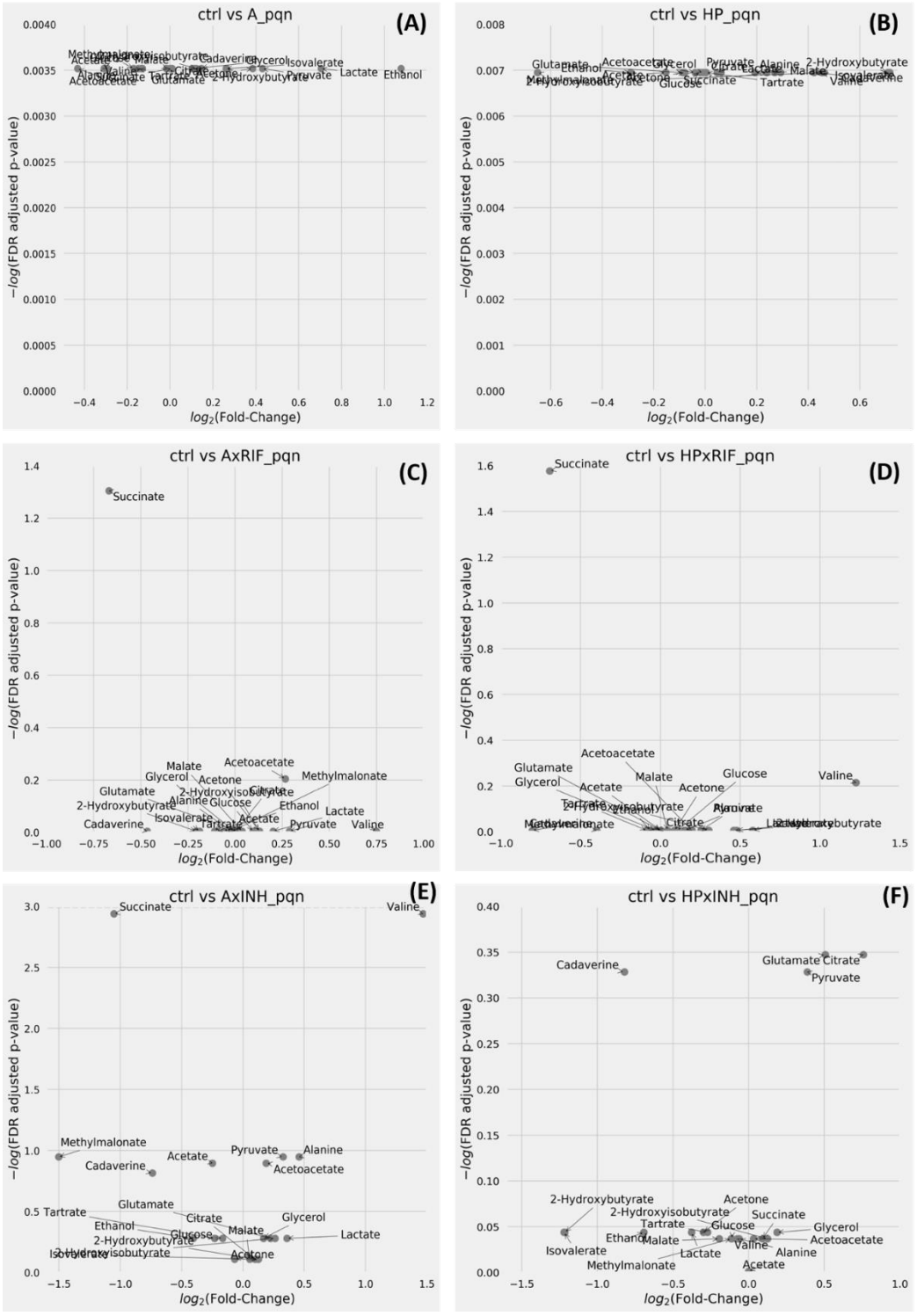

Figure 7.48A-F ¼ MIC Challenges induce changes in various metabolites in spent media of Mtb Bleupan incubated for 6 weeks. Volcano plots are shown for individual comparisons of unchallenged bacteria and those challenged with D-LAK120-A (A), D-LAK120-HP13 (B), rifampicin in combination with D-LAK120-A (C) or D-LAK120-HP13 (D), isoniazid in combination with D-LAK120-A (E) or D-LAK120-HP13 (F). Volcano plots are of PQN normalized data and allow comparison of fold changes and significance of each metabolite; blue – significant reductions, red – significant increases and grey – non-significant changes in the indicated metabolites.

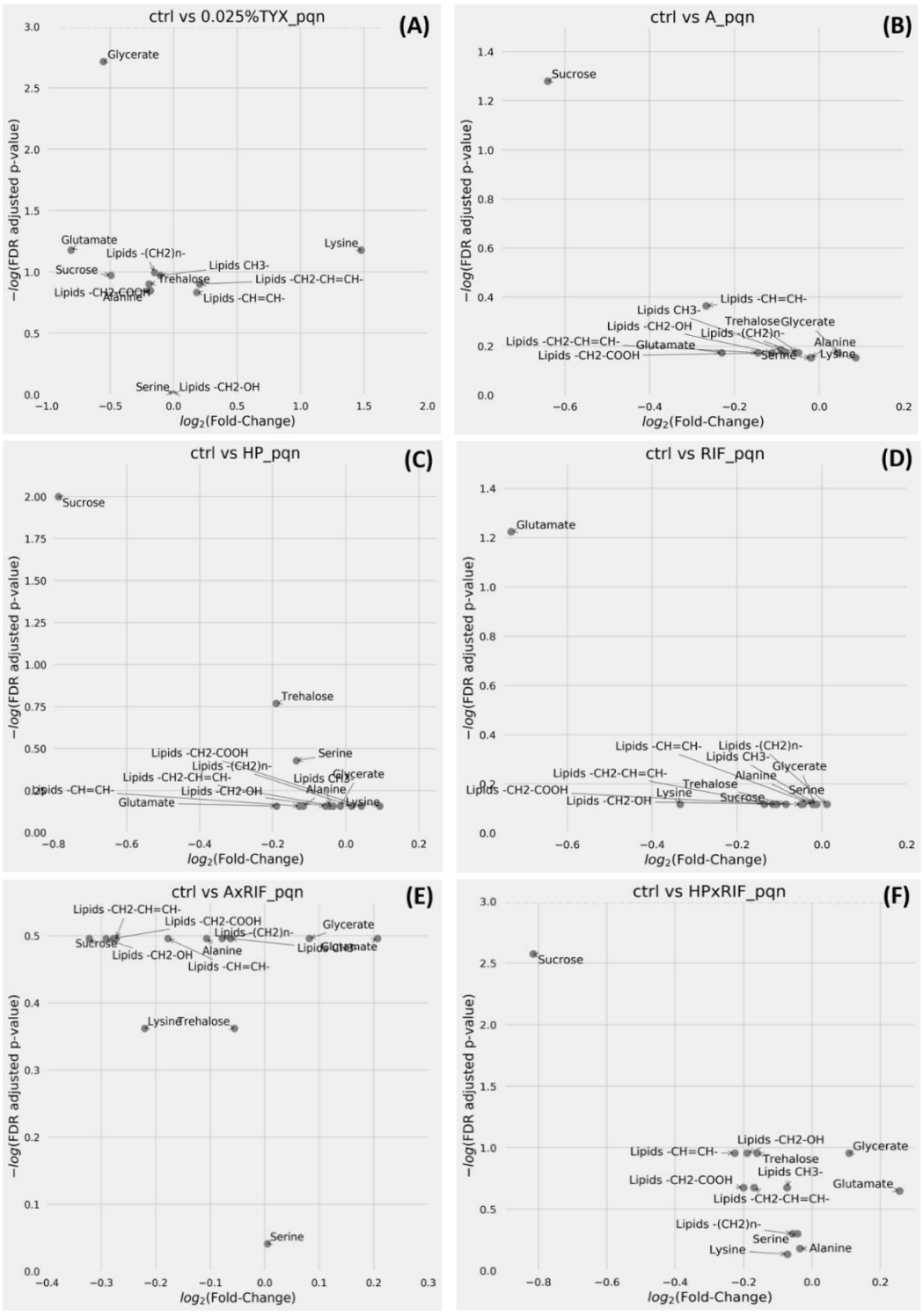

Figure 7.49A-F ½ MIC Challenges induce changes in various metabolites in whole cell Mtb Bleupan incubated for 72 hours. Volcano plots are shown for individual comparisons of unchallenged bacteria and those challenged with 0.025% tyloxapol (A), D-LAK120-A (B), D-LAK120-HP13 (C), rifampicin (D), rifampicin in combination with D-LAK120-A (E) or D-LAK120-HP13 (F). Volcano plots are of PQN normalized data and allow comparison of fold changes and significance of each metabolite; blue – significant reductions, red – significant increases and grey – non-significant changes in the indicated metabolites.

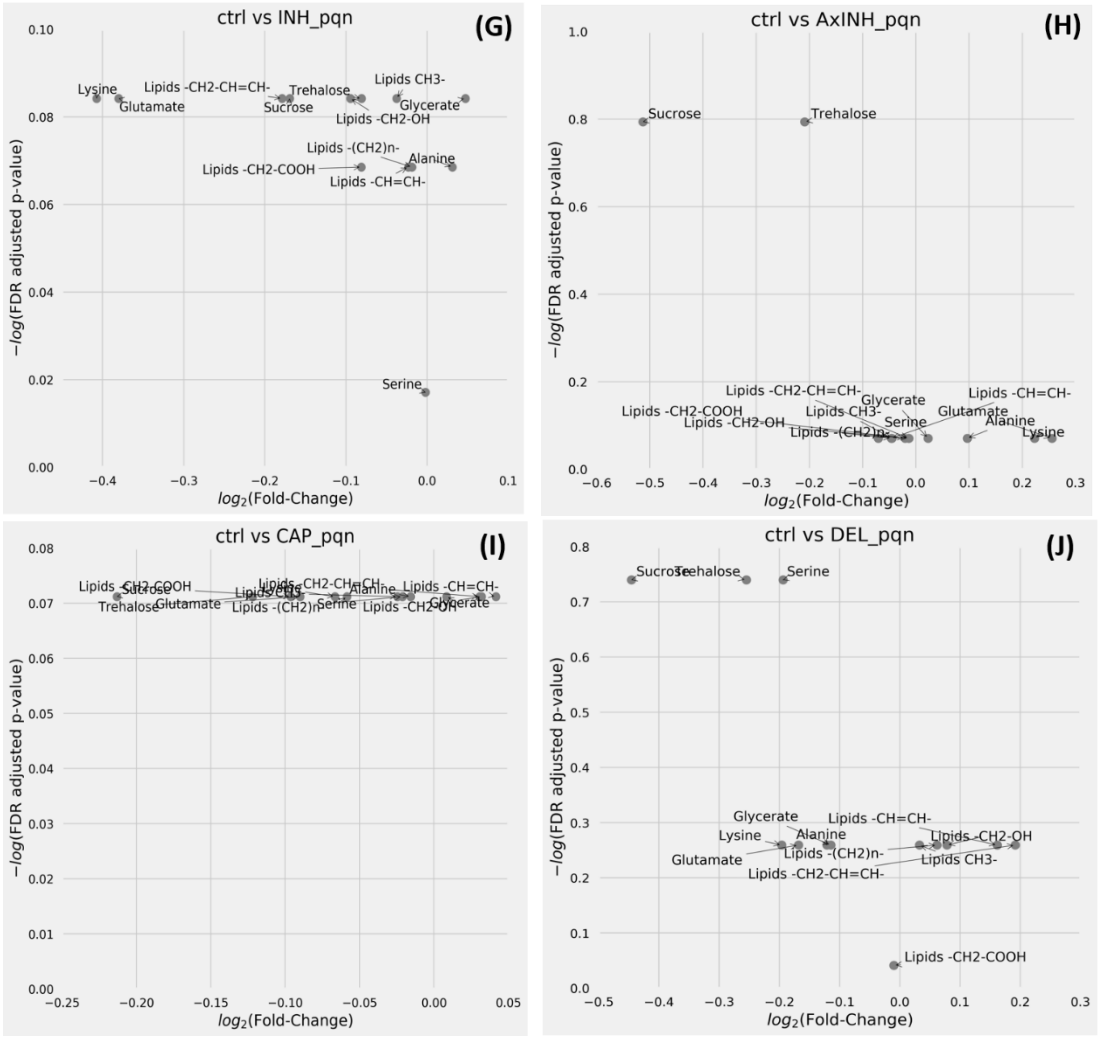

Figure 7.49G-J ½ MIC Challenges induce changes in various metabolites in whole cell Mtb Bleupan incubated for 72 hours. Volcano plots are shown for individual comparisons of unchallenged bacteria and those challenged with isoniazid (G), isoniazid in combination with D-LAK120-A (H), capreomycin (I), delamanid (J). Volcano plots are of PQN normalized data and allow comparison of fold changes and significance of each metabolite; blue – significant reductions, red – significant increases and grey – non-significant changes in the indicated metabolites.

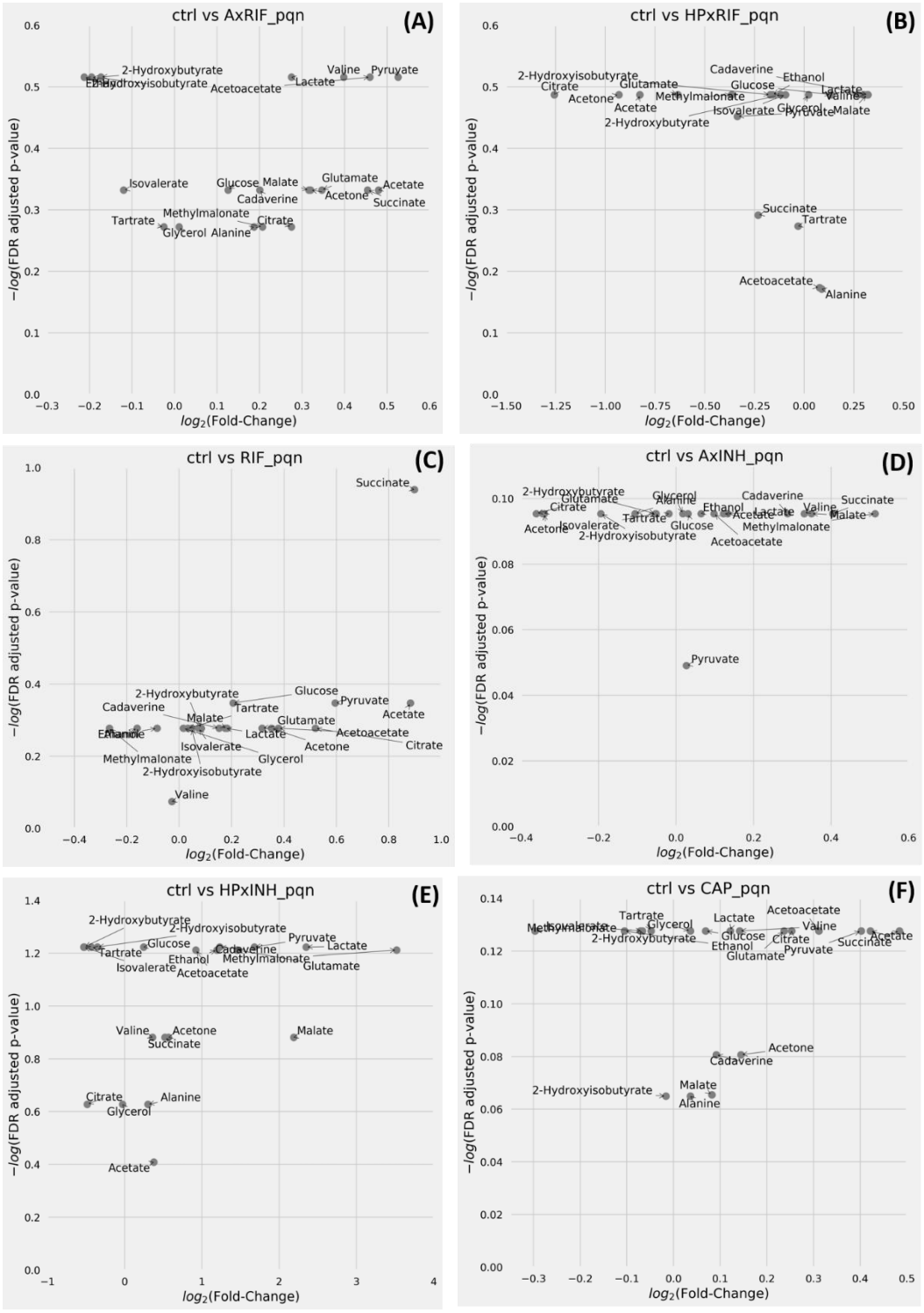

Figure 7.50A-F ½ MIC Challenges induce changes in various metabolites in spent media of Mtb Bleupan incubated for 72 hours. Volcano plots are shown for individual comparisons of unchallenged bacteria and those challenged with rifampicin in combination with D-LAK120-A (A) or D-LAK120-HP13 (B), rifampicin (C), isoniazid in combination with D-LAK120-A (D) or D-LAK120-HP13 (E), capreomycin (F). Volcano plots are of PQN normalized data (n=9) and allow comparison of fold changes and significance of each metabolite; blue – significant reductions, red – significant increases and grey – non-significant changes in the indicated metabolites.

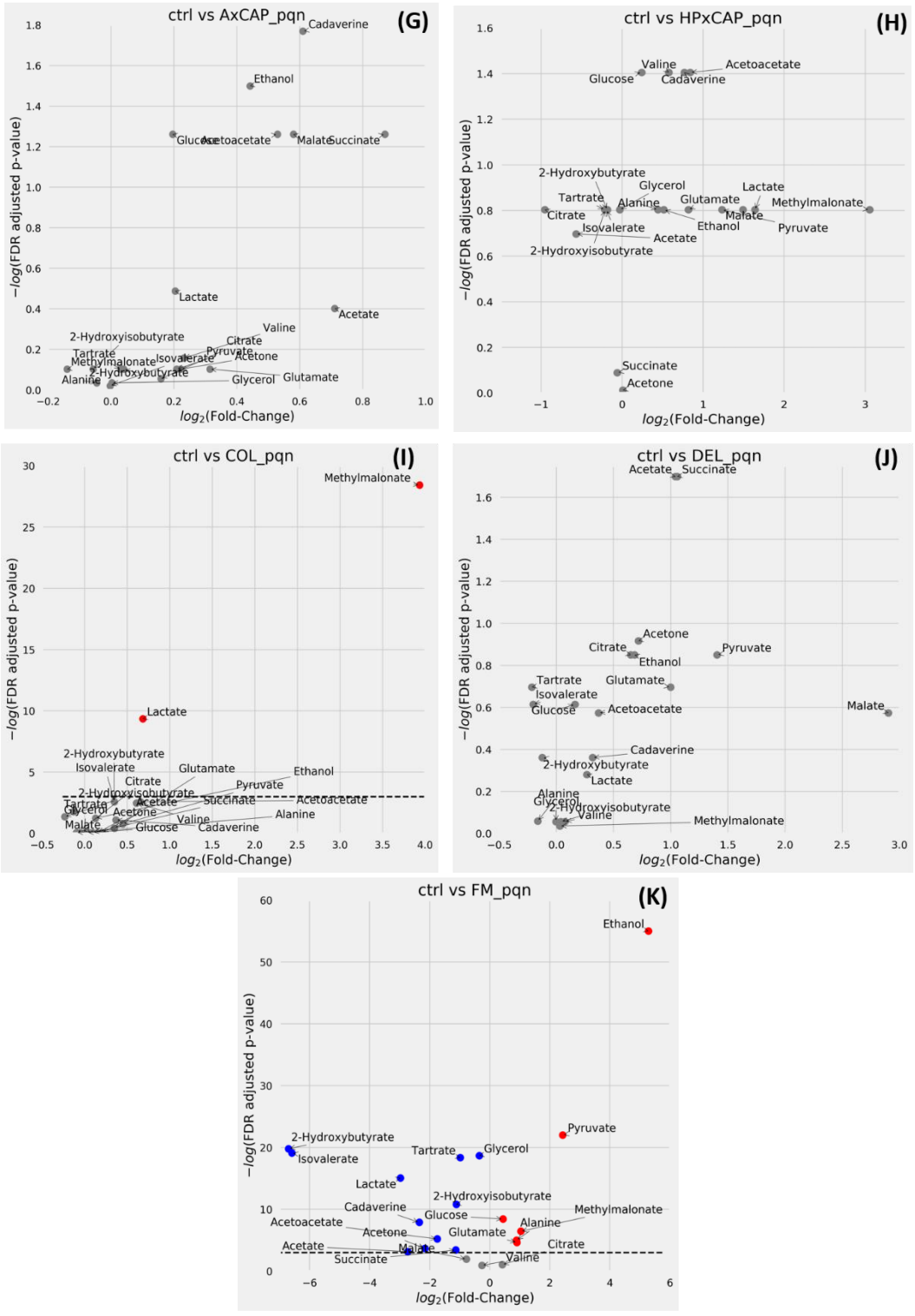

Figure 7.50 G-K ½ MIC Challenges induce changes in various metabolites in spent media of Mtb Bleupan incubated for 72 hours. Volcano plots are shown for individual comparisons of unchallenged bacteria and those challenged with capreomycin in combination with D-LAK120-A (G) or D-LAK120-HP13 (H), colistin (H), delamanid (J) or Fresh Media (K). Volcano plots are of PQN normalized data (n=9) and allow comparison of fold changes and significance of each metabolite; blue – significant reductions, red – significant increases and grey – non-significant changes in the

indicated *metabolites.*

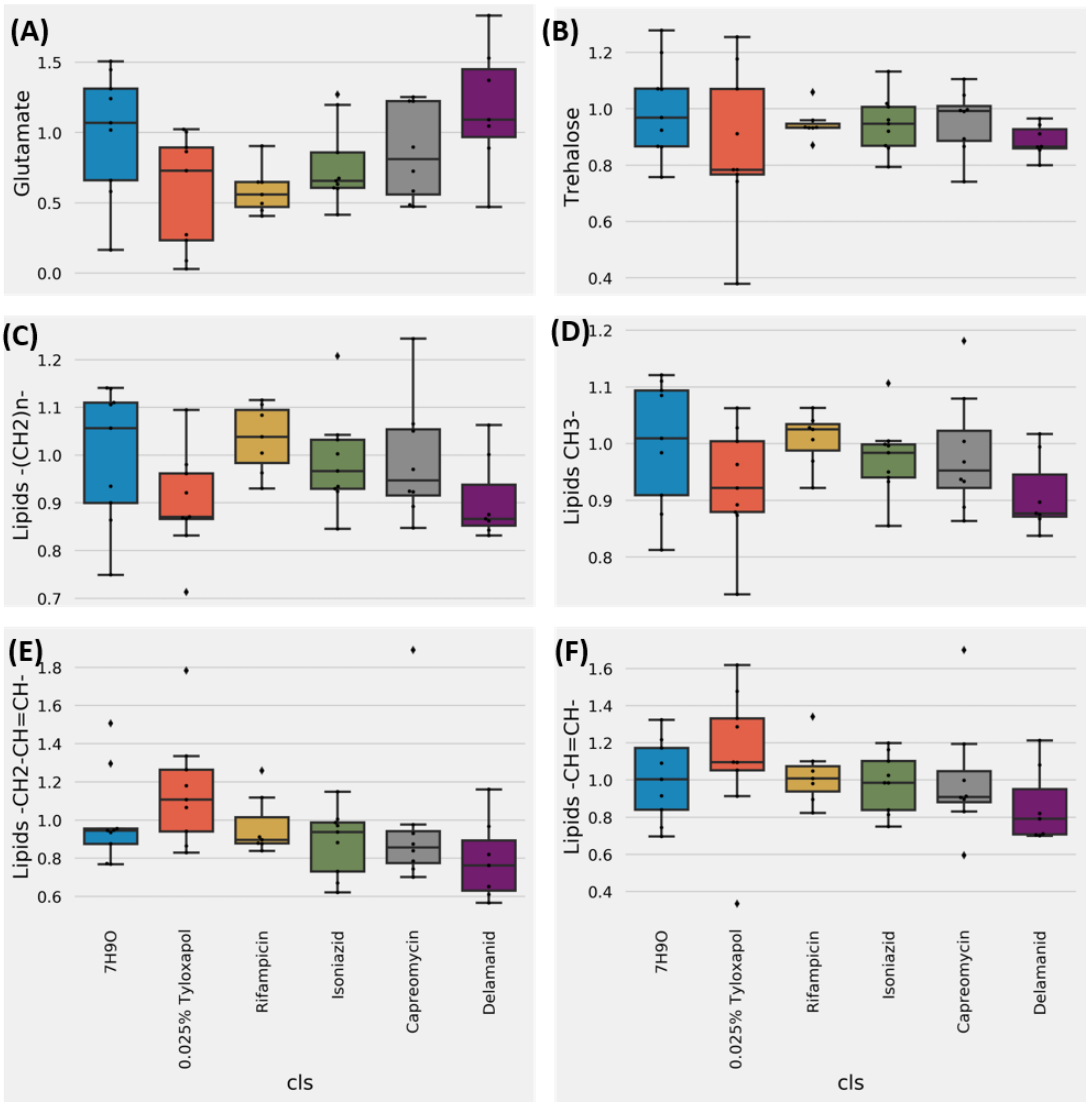

*Figure 7.51 Univariate analysis of relative metabolite levels in whole-cell Mtb Bleupan challenged for 72 hours with ½ MIC antibiotics or in the presence of 0.025% tyloxapol. Significant differences with respect to unchallenged bacteria, as determined by one-way ANOVA with Tukey post-hoc test, are indicated **.*

References

1. Rothschild BM, Martin LD, Lev G, Bercovier H, Bar-Gal GK, Greenblatt C, et al. Mycobacterium tuberculosis complex DNA from an extinct bison dated 17,000 years before the present. Clinical infectious diseases : an official publication of the Infectious Diseases Society of America. 2001;33(3):305-11.
2. Zink AR, Sola C, Reischl U, Grabner W, Rastogi N, Wolf H, et al. Characterization of Mycobacterium tuberculosis complex DNAs from Egyptian mummies by spoligotyping. J Clin Microbiol. 2003;41(1):359-67.
3. Konomi N, Lebwohl E, Mowbray K, Tattersall I, Zhang D. Detection of mycobacterial DNA in Andean mummies. J Clin Microbiol. 2002;40(12):4738-40.
4. Gawad J, Bonde C. Current Affairs, Future Perspectives of Tuberculosis and Antitubercular Agents. The Indian journal of tuberculosis. 2018;65(1):15-22.
5. Al-Humadi HW, Al-Saigh RJ, Al-Humadi AW. Addressing the Challenges of Tuberculosis: A Brief Historical Account. Frontiers in Pharmacology. 2017;8:689.
6. Brites D, Gagneux S. Co-evolution of Mycobacterium tuberculosis and Homo sapiens. Immunological reviews. 2015;264(1):6-24.
7. Gutierrez MC, Brisse S, Brosch R, Fabre M, Omais B, Marmiesse M, et al. Ancient origin and gene mosaicism of the progenitor of Mycobacterium tuberculosis. PLoS Pathog. 2005;1(1):e5.
8. Khusro A, Aarti C, Barbabosa-Pliego A, Salem AZM. Neoteric advancement in TB drugs and an overview on the anti-tubercular role of peptides through computational approaches. Microbial pathogenesis. 2017;114:80-9.
9. Organization WH. Global Tuberculosis Report 2017. Geneva: World Health Organization 2017.
10. Velayati AA, Farnia P, Hoffner S. Drug-resistant Mycobacterium tuberculosis: Epidemiology and role of morphological alterations. Journal of global antimicrobial resistance. 2018;12:192-6.
11. Caminero JA, Sotgiu G, Zumla A, Migliori GB. Best drug treatment for multidrug-resistant and extensively drug-resistant tuberculosis. The Lancet Infectious diseases. 2010;10(9):621-9.
12. Gunther G. Multidrug-resistant and extensively drug-resistant tuberculosis: a review of current concepts and future challenges. Clinical medicine (London, England). 2014;14(3):279-85.
13. Barry CE, 3rd, Boshoff HI, Dartois V, Dick T, Ehrt S, Flynn J, et al. The spectrum of latent tuberculosis: rethinking the biology and intervention strategies. Nature reviews Microbiology. 2009;7(12):845-55.
14. Kerantzas CA, Jacobs WR, Jr. Origins of Combination Therapy for Tuberculosis: Lessons for Future Antimicrobial Development and Application. MBio. 2017;8(2).
15. Daffe M, Draper P. The envelope layers of mycobacteria with reference to their pathogenicity. Advances in microbial physiology. 1998;39:131-203.
16. Brennan PJ, Goren MB. Structural studies on the type-specific antigens and lipids of the mycobacterium avium. Mycobacterium intracellulare. Mycobacterium scrofulaceum serocomplex. Mycobacterium intracellulare serotype 9. The Journal of biological chemistry. 1979;254(10):4205-11.
17. Gygli SM, Borrell S, Trauner A, Gagneux S. Antimicrobial resistance in Mycobacterium tuberculosis: mechanistic and evolutionary perspectives. FEMS microbiology reviews. 2017;41(3):354-73.
18. Brennan PJ, Nikaido H. The envelope of mycobacteria. Annual review of biochemistry. 1995;64:29-63.

19. AlMatar M, Makky EA, Yakici G, Var I, Kayar B, Koksal F. Antimicrobial peptides as an alternative to anti-tuberculosis drugs. Pharmacological research. 2018;128:288-305.
20. Gupta A, Kaul A, Tsolaki AG, Kishore U, Bhakta S. Mycobacterium tuberculosis: immune evasion, latency and reactivation. Immunobiology. 2012;217(3):363-74.
21. Cambier CJ, Takaki KK, Larson RP, Hernandez RE, Tobin DM, Urdahl KB, et al. Mycobacteria manipulate macrophage recruitment through coordinated use of membrane lipids. Nature. 2013;505:218.
22. Arbues A, Lugo-Villarino G, Neyrolles O, Guilhot C, Astarie-Dequeker C. Playing hide-and-seek with host macrophages through the use of mycobacterial cell envelope phthiocerol dimycocerosates and phenolic glycolipids. Frontiers in Cellular and Infection Microbiology. 2014;4:173.
23. van der Wel N, Hava D, Houben D, Fluitsma D, van Zon M, Pierson J, et al. M. tuberculosis and M. leprae Translocate from the Phagolysosome to the Cytosol in Myeloid Cells. Cell. 2007;129(7):1287-98.
24. Simeone R, Sayes F, Song O, Groschel MI, Brodin P, Brosch R, et al. Cytosolic access of Mycobacterium tuberculosis: critical impact of phagosomal acidification control and demonstration of occurrence in vivo. PLoS Pathog. 2015;11(2):e1004650.
25. Gomez JE, McKinney JD. M. tuberculosis persistence, latency, and drug tolerance. Tuberculosis (Edinburgh, Scotland). 2004;84(1-2):29-44.
26. Houben RM, Dodd PJ. The Global Burden of Latent Tuberculosis Infection: A Re-estimation Using Mathematical Modelling. PLoS medicine. 2016;13(10):e1002152.
27. Zaman SB, Hussain MA, Nye R, Mehta V, Mamun KT, Hossain N. A Review on Antibiotic Resistance: Alarm Bells are Ringing. Cureus. 2017;9(6):e1403.
28. Goossens H, Ferech M, Vander Stichele R, Elseviers M. Outpatient antibiotic use in Europe and association with resistance: a cross-national database study. Lancet (London, England). 2005;365(9459):579-87.
29. Dooley KE, Chaisson RE. Tuberculosis and diabetes mellitus: convergence of two epidemics. The Lancet Infectious diseases. 2009;9(12):737-46.
30. Al-Saeedi M, Al-Hajoj S. Diversity and evolution of drug resistance mechanisms in Mycobacterium tuberculosis. Infection and drug resistance. 2017;10:333-42.
31. Boritsch EC, Khanna V, Pawlik A, Honoré N, Navas VH, Ma L, et al. Key experimental evidence of chromosomal DNA transfer among selected tuberculosis-causing mycobacteria. Proceedings of the National Academy of Sciences. 2016;113(35):9876-81.
32. Marshall DD, Halouska S, Zinniel DK, Fenton RJ, Kenealy K, Chahal HK, et al. Assessment of Metabolic Changes in Mycobacterium smegmatis Wild-Type and alr Mutant Strains: Evidence of a New Pathway of d-Alanine Biosynthesis. Journal of proteome research. 2017;16(3):1270-9.
33. Igarashi M, Ishizaki Y, Takahashi Y. New antituberculous drugs derived from natural products: current perspectives and issues in antituberculous drug development. The Journal of antibiotics. 2017.
34. Herrmann J, Rybniker J, Muller R. Novel and revisited approaches in antituberculosis drug discovery. Current opinion in biotechnology. 2017;48:94-101.
35. Crofton J, Mitchison DA. Streptomycin Resistance in Pulmonary Tuberculosis. British Medical Journal. 1948;2(4588):1009-15.
36. TREATMENT of pulmonary tuberculosis with streptomycin and para-aminosalicylic acid; a Medical Research Council investigation. Br Med J. 1950;2(4688):1073-85.
37. Sensi P. History of the development of rifampin. Reviews of infectious diseases. 1983;5 Suppl 3:S402-6.
38. SHORT-COURSE CHEMOTHERAPY IN PULMONARY TUBERCULOSIS. The Lancet. 1975;305(7899):119-24.

39. Boeree MJ, Heinrich N, Aarnoutse R, Diacon AH, Dawson R, Rehal S, et al. High-dose rifampicin, moxifloxacin, and SQ109 for treating tuberculosis: a multi-arm, multi-stage randomised controlled trial. The Lancet Infectious diseases. 2017;17(1):39-49.
40. Blumberg HM, Burman WJ, Chaisson RE, Daley CL, Etkind SC, Friedman LN, et al. American Thoracic Society/Centers for Disease Control and Prevention/Infectious Diseases Society of America: treatment of tuberculosis. American journal of respiratory and critical care medicine. 2003;167(4):603-62.
41. Organization WH. Global Tuberculosis Report 1997. Geneva: World Health Organization 1997.
42. Handbook of anti TB agents. Tuberculosis. 2008;88(2):85-170.
43. Ma Z, Ginsberg AM, Spigelman M. 7.24 - Antimycobacterium Agents A2 - Taylor, John B. In: Triggle DJ, editor. Comprehensive Medicinal Chemistry II. Oxford: Elsevier; 2007. p. 699-730.
44. Mailaender C, Reiling N, Engelhardt H, Bossmann S, Ehlers S, Niederweis M. The MspA porin promotes growth and increases antibiotic susceptibility of both Mycobacterium bovis BCG and Mycobacterium tuberculosis. Microbiology (Reading, England). 2004;150(Pt 4):853-64.
45. AlMatar M, AlMandeal H, Var I, Kayar B, Köksal F. New drugs for the treatment of Mycobacterium tuberculosis infection. Biomedicine & Pharmacotherapy. 2017;91:546-58.
46. Organization WH. Guidelines for establishing DOTS-PLUS pilot projects for the management of multidrug-resistant tuberculosis (MDR-TB). 2000.
47. Organization WH. WHO treatment guidelines for drug-resistant tuberculosis (2016 update). Geneva: World Health Organization 2017.
48. Shringarpure KS, Isaakidis P, Sagili KD, Baxi RK, Das M, Daftary A. "When Treatment Is More Challenging than the Disease": A Qualitative Study of MDR-TB Patient Retention. PLoS One. 2016;11(3):e0150849.
49. Zhang X, Falagas ME, Vardakas KZ, Wang R, Qin R, Wang J, et al. Systematic review and meta-analysis of the efficacy and safety of therapy with linezolid containing regimens in the treatment of multidrug-resistant and extensively drug-resistant tuberculosis. Journal of thoracic disease. 2015;7(4):603-15.
50. Modongo C, Sobota RS, Kesenogile B, Ncube R, Sirugo G, Williams SM, et al. Successful MDR-TB treatment regimens including amikacin are associated with high rates of hearing loss. BMC infectious diseases. 2014;14:542.
51. Hopkins AL. Network pharmacology: the next paradigm in drug discovery. Nature chemical biology. 2008;4(11):682-90.
52. Kwon Y-S, Jeong B-H, Koh W-J. Tuberculosis: clinical trials and new drug regimens. Current Opinion in Pulmonary Medicine. 2014;20(3):280-6.
53. Zumla A, Chakaya J, Centis R, D'Ambrosio L, Mwaba P, Bates M, et al. Tuberculosis treatment and management--an update on treatment regimens, trials, new drugs, and adjunct therapies. The Lancet Respiratory medicine. 2015;3(3):220-34.
54. Van Deun A, Maug AK, Salim MA, Das PK, Sarker MR, Daru P, et al. Short, highly effective, and inexpensive standardized treatment of multidrug-resistant tuberculosis. American journal of respiratory and critical care medicine. 2010;182(5):684-92.
55. Venkatesh KK, Swaminathan S, Andrews JR, Mayer KH. Tuberculosis and HIV Co-Infection. Drugs. 2011;71(9):1133-52.
56. Kaufmann SH, Lange C, Rao M, Balaji KN, Lotze M, Schito M, et al. Progress in tuberculosis vaccine development and host-directed therapies--a state of the art review. The Lancet Respiratory medicine. 2014;2(4):301-20.
57. Lawn SD, Zumla AI. Tuberculosis. Lancet (London, England). 2011;378(9785):57-72.

58. Gumbo T. New susceptibility breakpoints for first-line antituberculosis drugs based on antimicrobial pharmacokinetic/pharmacodynamic science and population pharmacokinetic variability. Antimicrob Agents Chemother. 2010;54(4):1484-91.
59. Prideaux B, Via LE, Zimmerman MD, Eum S, Sarathy J, O'Brien P, et al. The association between sterilizing activity and drug distribution into tuberculosis lesions. Nature medicine. 2015;21(10):1223-7.
60. Cambau E, Viveiros M, Machado D, Raskine L, Ritter C, Tortoli E, et al. Revisiting susceptibility testing in MDR-TB by a standardized quantitative phenotypic assessment in a European multicentre study. Journal of Antimicrobial Chemotherapy. 2015;70(3):686-96.
61. Brennan PJ. Structure, function, and biogenesis of the cell wall of Mycobacterium tuberculosis. Tuberculosis (Edinburgh, Scotland). 2003;83(1-3):91-7.
62. Silva JP, Appelberg R, Gama FM. Antimicrobial peptides as novel anti-tuberculosis therapeutics. Biotechnology advances. 2016;34(5):924-40.
63. Sani M, Houben ENG, Geurtsen J, Pierson J, de Punder K, van Zon M, et al. Direct Visualization by Cryo-EM of the Mycobacterial Capsular Layer: A Labile Structure Containing ESX-1-Secreted Proteins. PLOS Pathogens. 2010;6(3):e1000794.
64. Chiaradia L, Lefebvre C, Parra J, Marcoux J, Burlet-Schiltz O, Etienne G, et al. Dissecting the mycobacterial cell envelope and defining the composition of the native mycomembrane. Scientific Reports. 2017;7(1):12807.
65. Hoffmann C, Leis A, Niederweis M, Plitzko JM, Engelhardt H. Disclosure of the mycobacterial outer membrane: Cryo-electron tomography and vitreous sections reveal the lipid bilayer structure. Proceedings of the National Academy of Sciences of the United States of America. 2008;105(10):3963-7.
66. Minnikin DE. Chemical principles in the organization of lipid components in the mycobacterial cell envelope. Research in Microbiology. 1991;142(4):423-7.
67. Gutsmann T. Interaction between antimicrobial peptides and mycobacteria. Biochimica et biophysica acta. 2016;1858(5):1034-43.
68. Boritsch EC, Frigui W, Cascioferro A, Malaga W, Etienne G, Laval F, et al. pks5-recombination-mediated surface remodelling in Mycobacterium tuberculosis emergence. Nat Microbiol. 2016;1:15019.
69. Daffé M, Quémard A, Marrakchi H. Mycolic Acids: From Chemistry to Biology. In: Geiger O, editor. Biogenesis of Fatty Acids, Lipids and Membranes. Cham: Springer International Publishing; 2017. p. 1-36.
70. Chapman GB, Hanks JH, Wallace JH. An electron microscope study of the disposition and fine structure of Mycobacterium lepraemurium in mouse spleen. Journal of bacteriology. 1959;77(2):205-11.
71. Daffé M, Etienne G. The capsule of Mycobacterium tuberculosis and its implications for pathogenicity. Tubercle and Lung Disease. 1999;79(3):153-69.
72. Stokes RW, Norris-Jones R, Brooks DE, Beveridge TJ, Doxsee D, Thorson LM. The Glycan-Rich Outer Layer of the Cell Wall of Mycobacterium tuberculosis Acts as an Antiphagocytic Capsule Limiting the Association of the Bacterium with Macrophages. Infection and immunity. 2004;72(10):5676-86.
73. Raynaud C, Etienne G, Peyron P, Laneelle MA, Daffe M. Extracellular enzyme activities potentially involved in the pathogenicity of Mycobacterium tuberculosis. Microbiology (Reading, England). 1998;144 (Pt 2):577-87.
74. Ortalo-Magne A, Lemassu A, Laneelle MA, Bardou F, Silve G, Gounon P, et al. Identification of the surface-exposed lipids on the cell envelopes of Mycobacterium tuberculosis and other mycobacterial species. Journal of bacteriology. 1996;178(2):456-61.
75. Verschoor JA, Baird MS, Grooten J. Towards understanding the functional diversity of cell wall mycolic acids of Mycobacterium tuberculosis. Progress in lipid research. 2012;51(4):325-39.

76. Portevin D, de Sousa-D'Auria C, Houssin C, Grimaldi C, Chami M, Daffé M, et al. A polyketide synthase catalyzes the last condensation step of mycolic acid biosynthesis in mycobacteria and related organisms. Proceedings of the National Academy of Sciences. 2004;101(1):314-9.
77. Vilcheze C, Morbidoni HR, Weisbrod TR, Iwamoto H, Kuo M, Sacchettini JC, et al. Inactivation of the inhA-encoded fatty acid synthase II (FASII) enoyl-acyl carrier protein reductase induces accumulation of the FASI end products and cell lysis of Mycobacterium smegmatis. Journal of bacteriology. 2000;182(14):4059-67.
78. Marrakchi H, Lanéelle M-A, Daffé M. Mycolic Acids: Structures, Biosynthesis, and Beyond. Chemistry & biology. 2014;21(1):67-85.
79. Rao V, Gao F, Chen B, Jacobs WR, Glickman MS. Trans -cyclopropanation of mycolic acids on trehalose dimycolate suppresses Mycobacterium tuberculosis –induced inflammation and virulence. The Journal of Clinical Investigation. 2006;116(6):1660-7.
80. Jackson M, Raynaud C, Laneelle MA, Guilhot C, Laurent-Winter C, Ensergueix D, et al. Inactivation of the antigen 85C gene profoundly affects the mycolate content and alters the permeability of the Mycobacterium tuberculosis cell envelope. Molecular microbiology. 1999;31(5):1573-87.
81. George KM, Yuan Y, Sherman DR, Barry CE, 3rd. The biosynthesis of cyclopropanated mycolic acids in Mycobacterium tuberculosis. Identification and functional analysis of CMAS-2. The Journal of biological chemistry. 1995;270(45):27292-8.
82. Yuan Y, Crane DC, Musser JM, Sreevatsan S, Barry CE, 3rd. MMAS-1, the branch point between cis- and trans-cyclopropane-containing oxygenated mycolates in Mycobacterium tuberculosis. The Journal of biological chemistry. 1997;272(15):10041-9.
83. Dubnau E, Chan J, Raynaud C, Mohan VP, Laneelle MA, Yu K, et al. Oxygenated mycolic acids are necessary for virulence of Mycobacterium tuberculosis in mice. Molecular microbiology. 2000;36(3):630-7.
84. Ishikawa E, Ishikawa T, Morita YS, Toyonaga K, Yamada H, Takeuchi O, et al. Direct recognition of the mycobacterial glycolipid, trehalose dimycolate, by C-type lectin Mincle. The Journal of experimental medicine. 2009;206(13):2879-88.
85. Bloch H. Studies on the virulence of tubercle bacilli; isolation and biological properties of a constituent of virulent organisms. Journal of Experimental Medicine. 1950;91(2):197-218.
86. Patin EC, Geffken AC, Willcocks S, Leschczyk C, Haas A, Nimmerjahn F, et al. Trehalose dimycolate interferes with FcγR-mediated phagosome maturation through Mincle, SHP-1 and FcγRIIB signalling. PLOS ONE. 2017;12(4):e0174973.
87. Hunter RL, Armitige L, Jagannath C, Actor JK. TB Research at UT-Houston – A review of cord factor: new approaches to drugs, vaccines and the pathogenesis of tuberculosis. Tuberculosis. 2009;89:S18-S25.
88. Astarie-Dequeker C, Le Guyader L, Malaga W, Seaphanh FK, Chalut C, Lopez A, et al. Phthiocerol dimycocerosates of M. tuberculosis participate in macrophage invasion by inducing changes in the organization of plasma membrane lipids. PLoS Pathog. 2009;5(2):e1000289.
89. Sturgill-Koszycki S, Schlesinger PH, Chakraborty P, Haddix PL, Collins HL, Fok AK, et al. Lack of acidification in Mycobacterium phagosomes produced by exclusion of the vesicular proton-ATPase. Science (New York, NY). 1994;263(5147):678-81.
90. F. QC, Dani H, M. JF. Developing a Conceptual Model of STEAM Teaching Practices. School Science and Mathematics. 2017;117(1-2):1-12.
91. Groschel MI, Sayes F, Simeone R, Majlessi L, Brosch R. ESX secretion systems: mycobacterial evolution to counter host immunity. Nature reviews Microbiology. 2016;14(11):677-91.

92. Diane H, Caroline D, Jakko vI, Jorge P, Lucy B, M. AA, et al. ESX - 1 - mediated translocation to the cytosol controls virulence of mycobacteria. Cellular Microbiology. 2012;14(8):1287-98.
93. Augenstreich J, Arbues A, Simeone R, Haanappel E, Wegener A, Sayes F, et al. ESX-1 and phthiocerol dimycocerosates of Mycobacterium tuberculosis act in concert to cause phagosomal rupture and host cell apoptosis. Cell Microbiol. 2017;19(7).
94. Kang PB, Azad AK, Torrelles JB, Kaufman TM, Beharka A, Tibesar E, et al. The human macrophage mannose receptor directs Mycobacterium tuberculosis lipoarabinomannan-mediated phagosome biogenesis. The Journal of experimental medicine. 2005;202(7):987-99.
95. K. OA, D. BA, Dhinakaran S, Tsungda H, Xavier T, Yann G, et al. Growth of Mycobacterium tuberculosis biofilms containing free mycolic acids and harbouring drug - tolerant bacteria. Molecular microbiology. 2008;69(1):164-74.
96. Blanc L, Gilleron M, Prandi J, Song O-r, Jang M-S, Gicquel B, et al. Mycobacterium tuberculosis inhibits human innate immune responses via the production of TLR2 antagonist glycolipids. Proceedings of the National Academy of Sciences. 2017;114(42):11205-10.
97. Nasiri MJ, Haeili M, Ghazi M, Goudarzi H, Pormohammad A, Imani Fooladi AA, et al. New Insights in to the Intrinsic and Acquired Drug Resistance Mechanisms in Mycobacteria. Frontiers in microbiology. 2017;8:681.
98. Favrot L, Ronning DR. Targeting the mycobacterial envelope for tuberculosis drug development. Expert review of anti-infective therapy. 2012;10(9):1023-36.
99. Jackson M, McNeil MR, Brennan PJ. Progress in targeting cell envelope biogenesis in Mycobacterium tuberculosis. Future microbiology. 2013;8(7):855-75.
100. Jankute M, Cox JA, Harrison J, Besra GS. Assembly of the Mycobacterial Cell Wall. Annual review of microbiology. 2015;69:405-23.
101. Singh A, Gupta R, Vishwakarma RA, Narayanan PR, Paramasivan CN, Ramanathan VD, et al. Requirement of the mymA operon for appropriate cell wall ultrastructure and persistence of Mycobacterium tuberculosis in the spleens of guinea pigs. Journal of bacteriology. 2005;187(12):4173-86.
102. Singh P, Rao RN, Reddy JR, Prasad RB, Kotturu SK, Ghosh S, et al. PE11, a PE/PPE family protein of Mycobacterium tuberculosis is involved in cell wall remodeling and virulence. Sci Rep. 2016;6:21624.
103. Abraham EP, Chain E, Fletcher CM, Gardner AD, Heatley NG, Jennings MA, et al. Further observations on penicillin. The Lancet. 1941;238(6155):177-89.
104. Maurer FP, Bruderer VL, Castelberg C, Ritter C, Scherbakov D, Bloemberg GV, et al. Aminoglycoside-modifying enzymes determine the innate susceptibility to aminoglycoside antibiotics in rapidly growing mycobacteria. The Journal of antimicrobial chemotherapy. 2015;70(5):1412-9.
105. Vetting MW, Hegde SS, Javid-Majd F, Blanchard JS, Roderick SL. Aminoglycoside 2'-N-acetyltransferase from Mycobacterium tuberculosis in complex with coenzyme A and aminoglycoside substrates. Nature structural biology. 2002;9(9):653-8.
106. Baysarowich J, Koteva K, Hughes DW, Ejim L, Griffiths E, Zhang K, et al. Rifamycin antibiotic resistance by ADP-ribosylation: Structure and diversity of Arr. Proc Natl Acad Sci U S A. 2008;105(12):4886-91.
107. Buriankova K, Doucet-Populaire F, Dorson O, Gondran A, Ghnassia JC, Weiser J, et al. Molecular basis of intrinsic macrolide resistance in the Mycobacterium tuberculosis complex. Antimicrob Agents Chemother. 2004;48(1):143-50.
108. Vetting MW, Hegde SS, Fajardo JE, Fiser A, Roderick SL, Takiff HE, et al. Pentapeptide repeat proteins. Biochemistry. 2006;45(1):1-10.

109. Hegde SS, Vetting MW, Roderick SL, Mitchenall LA, Maxwell A, Takiff HE, et al. A fluoroquinolone resistance protein from Mycobacterium tuberculosis that mimics DNA. Science (New York, NY). 2005;308(5727):1480-3.
110. Maus CE, Plikaytis BB, Shinnick TM. Mutation of tlyA confers capreomycin resistance in Mycobacterium tuberculosis. Antimicrob Agents Chemother. 2005;49(2):571-7.
111. Dey A, Verma AK, Chatterji D. Role of an RNA polymerase interacting protein, MsRbpA, from Mycobacterium smegmatis in phenotypic tolerance to rifampicin. Microbiology (Reading, England). 2010;156(Pt 3):873-83.
112. Gupta AK, Reddy VP, Lavania M, Chauhan DS, Venkatesan K, Sharma VD, et al. jefA (Rv2459), a drug efflux gene in Mycobacterium tuberculosis confers resistance to isoniazid & ethambutol. The Indian journal of medical research. 2010;132:176-88.
113. Hu YM, Butcher PD, Sole K, Mitchison DA, Coates AR. Protein synthesis is shutdown in dormant Mycobacterium tuberculosis and is reversed by oxygen or heat shock. FEMS microbiology letters. 1998;158(1):139-45.
114. Smith T, Wolff KA, Nguyen L. Molecular Biology of Drug Resistance in Mycobacterium tuberculosis. Current topics in microbiology and immunology. 2013;374:53-80.
115. Nguyen L, Chinnapapagari S, Thompson CJ. FbpA-Dependent Biosynthesis of Trehalose Dimycolate Is Required for the Intrinsic Multidrug Resistance, Cell Wall Structure, and Colonial Morphology of Mycobacterium smegmatis. Journal of bacteriology. 2005;187(19):6603-11.
116. Warrier T, Kapilashrami K, Argyrou A, Ioerger TR, Little D, Murphy KC, et al. N-methylation of a bactericidal compound as a resistance mechanism in Mycobacterium tuberculosis. Proc Natl Acad Sci U S A. 2016;113(31):E4523-30.
117. Rodrigues L, Machado D, Couto I, Amaral L, Viveiros M. Contribution of efflux activity to isoniazid resistance in the Mycobacterium tuberculosis complex. Infection, genetics and evolution : journal of molecular epidemiology and evolutionary genetics in infectious diseases. 2012;12(4):695-700.
118. Milano A, Pasca MR, Provvedi R, Lucarelli AP, Manina G, Ribeiro AL, et al. Azole resistance in Mycobacterium tuberculosis is mediated by the MmpS5-MmpL5 efflux system. Tuberculosis (Edinburgh, Scotland). 2009;89(1):84-90.
119. Li G, Zhang J, Guo Q, Jiang Y, Wei J, Zhao LL, et al. Efflux pump gene expression in multidrug-resistant Mycobacterium tuberculosis clinical isolates. PLoS One. 2015;10(2):e0119013.
120. Li XZ, Zhang L, Nikaido H. Efflux pump-mediated intrinsic drug resistance in Mycobacterium smegmatis. Antimicrob Agents Chemother. 2004;48(7):2415-23.
121. Nasiri MJ, Darban-Sarokhalil D, Fooladi AA, Feizabadi MM. katG Ser315 and rpoB 81-bp hotspot region substitutions: Reliability for detection of drug-resistant strains of Mycobacterium tuberculosis. Journal of global antimicrobial resistance. 2016;5:92-3.
122. Redgrave LS, Sutton SB, Webber MA, Piddock LJV. Fluoroquinolone resistance: mechanisms, impact on bacteria, and role in evolutionary success. Trends in microbiology. 2014;22(8):438-45.
123. Johansen SK, Maus CE, Plikaytis BB, Douthwaite S. Capreomycin Binds across the Ribosomal Subunit Interface Using tlyA-Encoded 2′-O-Methylations in 16S and 23S rRNAs. Molecular cell. 2006;23(2):173-82.
124. Miesel L, Rozwarski DA, Sacchettini JC, Jacobs WR, Jr. Mechanisms for isoniazid action and resistance. Novartis Foundation symposium. 1998;217:209-20; discussion 20-1.
125. Gu Y, Yu X, Jiang G, Wang X, Ma Y, Li Y, et al. Pyrazinamide resistance among multidrug-resistant tuberculosis clinical isolates in a national referral center of China and its correlations with pncA, rpsA, and panD gene mutations. Diagn Microbiol Infect Dis. 2016;84(3):207-11.

126. Telenti A, Philipp WJ, Sreevatsan S, Bernasconi C, Stockbauer KE, Wieles B, et al. The emb operon, a gene cluster of Mycobacterium tuberculosis involved in resistance to ethambutol. Nature medicine. 1997;3(5):567-70.
127. Safi H, Lingaraju S, Amin A, Kim S, Jones M, Holmes M, et al. Evolution of high-level ethambutol-resistant tuberculosis through interacting mutations in decaprenylphosphoryl-beta-D-arabinose biosynthetic and utilization pathway genes. Nature genetics. 2013;45(10):1190-7.
128. da Silva PE, Von Groll A, Martin A, Palomino JC. Efflux as a mechanism for drug resistance in Mycobacterium tuberculosis. FEMS immunology and medical microbiology. 2011;63(1):1-9.
129. Hartkoorn RC, Uplekar S, Cole ST. Cross-resistance between clofazimine and bedaquiline through upregulation of MmpL5 in Mycobacterium tuberculosis. Antimicrob Agents Chemother. 2014;58(5):2979-81.
130. Campbell EA, Korzheva N, Mustaev A, Murakami K, Nair S, Goldfarb A, et al. Structural mechanism for rifampicin inhibition of bacterial rna polymerase. Cell. 2001;104(6):901-12.
131. Maus CE, Plikaytis BB, Shinnick TM. Molecular analysis of cross-resistance to capreomycin, kanamycin, amikacin, and viomycin in Mycobacterium tuberculosis. Antimicrob Agents Chemother. 2005;49(8):3192-7.
132. Kambli P, Ajbani K, Nikam C, Sadani M, Shetty A, Udwadia Z, et al. Correlating rrs and eis promoter mutations in clinical isolates of Mycobacterium tuberculosis with phenotypic susceptibility levels to the second-line injectables. International journal of mycobacteriology. 2016;5(1):1-6.
133. Meier A, Kirschner P, Bange FC, Vogel U, Bottger EC. Genetic alterations in streptomycin-resistant Mycobacterium tuberculosis: mapping of mutations conferring resistance. Antimicrob Agents Chemother. 1994;38(2):228-33.
134. Morlock GP, Metchock B, Sikes D, Crawford JT, Cooksey RC. ethA, inhA, and katG loci of ethionamide-resistant clinical Mycobacterium tuberculosis isolates. Antimicrob Agents Chemother. 2003;47(12):3799-805.
135. Halouska S, Chacon O, Fenton RJ, Zinniel DK, Barletta RG, Powers R. Use of NMR metabolomics to analyze the targets of D-cycloserine in mycobacteria: role of D-alanine racemase. Journal of proteome research. 2007;6(12):4608-14.
136. Minato Y, Thiede JM, Kordus SL, McKlveen EJ, Turman BJ, Baughn AD. Mycobacterium tuberculosis folate metabolism and the mechanistic basis for para-aminosalicylic acid susceptibility and resistance. Antimicrob Agents Chemother. 2015;59(9):5097-106.
137. Hillemann D, Rusch-Gerdes S, Richter E. In vitro-selected linezolid-resistant Mycobacterium tuberculosis mutants. Antimicrob Agents Chemother. 2008;52(2):800-1.
138. Beckert P, Hillemann D, Kohl TA, Kalinowski J, Richter E, Niemann S, et al. rplC T460C identified as a dominant mutation in linezolid-resistant Mycobacterium tuberculosis strains. Antimicrob Agents Chemother. 2012;56(5):2743-5.
139. Haver HL, Chua A, Ghode P, Lakshminarayana SB, Singhal A, Mathema B, et al. Mutations in genes for the F420 biosynthetic pathway and a nitroreductase enzyme are the primary resistance determinants in spontaneous in vitro-selected PA-824-resistant mutants of Mycobacterium tuberculosis. Antimicrob Agents Chemother. 2015;59(9):5316-23.
140. Huitric E, Verhasselt P, Koul A, Andries K, Hoffner S, Andersson DI. Rates and mechanisms of resistance development in Mycobacterium tuberculosis to a novel diarylquinoline ATP synthase inhibitor. Antimicrob Agents Chemother. 2010;54(3):1022-8.
141. Sloan DJ, Davies GR, Khoo SH. Recent advances in tuberculosis: New drugs and treatment regimens. Current respiratory medicine reviews. 2013;9(3):200-10.

142. Matsumoto M, Hashizume H, Tomishige T, Kawasaki M, Tsubouchi H, Sasaki H, et al. OPC-67683, a Nitro-Dihydro-Imidazooxazole Derivative with Promising Action against Tuberculosis In Vitro and In Mice. PLoS medicine. 2006;3(11):e466.
143. Saliu OY, Crismale C, Schwander SK, Wallis RS. Bactericidal activity of OPC-67683 against drug-tolerant Mycobacterium tuberculosis. Journal of Antimicrobial Chemotherapy. 2007;60(5):994-8.
144. Gopalan N, Chandrasekaran P, Swaminathan S, Tripathy S. Current trends and intricacies in the management of HIV-associated pulmonary tuberculosis. AIDS research and therapy. 2016;13:34.
145. Haagsma AC, Abdillahi-Ibrahim R, Wagner MJ, Krab K, Vergauwen K, Guillemont J, et al. Selectivity of TMC207 towards Mycobacterial ATP Synthase Compared with That towards the Eukaryotic Homologue. Antimicrobial Agents and Chemotherapy. 2009;53(3):1290-2.
146. Field SK. Bedaquiline for the treatment of multidrug-resistant tuberculosis: great promise or disappointment? Therapeutic Advances in Chronic Disease. 2015;6(4):170-84.
147. Hards K, Robson JR, Berney M, Shaw L, Bald D, Koul A, et al. Bactericidal mode of action of bedaquiline. The Journal of antimicrobial chemotherapy. 2015;70(7):2028-37.
148. Andries K, Verhasselt P, Guillemont J, Göhlmann HWH, Neefs J-M, Winkler H, et al. A Diarylquinoline Drug Active on the ATP Synthase of Mycobacterium tuberculosis. Science (New York, NY). 2005;307(5707):223-7.
149. Ibrahim M, Andries K, Lounis N, Chauffour A, Truffot-Pernot C, Jarlier V, et al. Synergistic activity of R207910 combined with pyrazinamide against murine tuberculosis. Antimicrob Agents Chemother. 2007;51(3):1011-5.
150. Williams KN, Stover CK, Zhu T, Tasneen R, Tyagi S, Grosset JH, et al. Promising antituberculosis activity of the oxazolidinone PNU-100480 relative to that of linezolid in a murine model. Antimicrob Agents Chemother. 2009;53(4):1314-9.
151. Wallis RS, Jakubiec W, Kumar V, Bedarida G, Silvia A, Paige D, et al. Biomarker-assisted dose selection for safety and efficacy in early development of PNU-100480 for tuberculosis. Antimicrob Agents Chemother. 2011;55(2):567-74.
152. Sacksteder KA, Protopopova M, Barry CE, Andries K, Nacy CA. Discovery and development of SQ109: a new antitubercular drug with a novel mechanism of action. Future microbiology. 2012;7(7):823-37.
153. Li K, Schurig-Briccio LA, Feng X, Upadhyay A, Pujari V, Lechartier B, et al. Multitarget drug discovery for tuberculosis and other infectious diseases. Journal of medicinal chemistry. 2014;57(7):3126-39.
154. Pethe K, Bifani P, Jang J, Kang S, Park S, Ahn S, et al. Discovery of Q203, a potent clinical candidate for the treatment of tuberculosis. Nature medicine. 2013;19(9):1157-60.
155. Makarov V, Manina G, Mikusova K, Mollmann U, Ryabova O, Saint-Joanis B, et al. Benzothiazinones kill Mycobacterium tuberculosis by blocking arabinan synthesis. Science (New York, NY). 2009;324(5928):801-4.
156. Hoagland DT, Liu J, Lee RB, Lee RE. New agents for the treatment of drug-resistant Mycobacterium tuberculosis. Advanced drug delivery reviews. 2016;102:55-72.
157. Reddy VM, O' Sullivan JF, Gangadharam PRJ. Antimycobacterial activities of riminophenazines. Journal of Antimicrobial Chemotherapy. 1999;43(5):615-23.
158. Van Deun A, Salim MA, Das AP, Bastian I, Portaels F. Results of a standardised regimen for multidrug-resistant tuberculosis in Bangladesh. The international journal of tuberculosis and lung disease : the official journal of the International Union against Tuberculosis and Lung Disease. 2004;8(5):560-7.
159. Hwang TJ, Dotsenko S, Jafarov A, Weyer K, Falzon D, Lunte K, et al. Safety and availability of clofazimine in the treatment of multidrug and extensively drug-resistant

tuberculosis: analysis of published guidance and meta-analysis of cohort studies. BMJ open. 2014;4(1):e004143.
160. Yoo JW, Lyu J, Lee SD, Kim WS, Kim DS, Shim TS. Clinical experience of using clofazimine to treat multidrug-resistant tuberculosis [Correspondence]. The international journal of tuberculosis and lung disease : the official journal of the International Union against Tuberculosis and Lung Disease. 2013;17(9):1243-4.
161. Freilich EB, Coe GC, Wien NA. THe use of sulfanilamide in pulmonary tuberculosis; preliminary report*. Annals of Internal Medicine. 1939;13(6):1042-5.
162. Hasse B, Walker AS, Fehr J, Furrer H, Hoffmann M, Battegay M, et al. Co-trimoxazole prophylaxis is associated with reduced risk of incident tuberculosis in participants in the Swiss HIV Cohort Study. Antimicrob Agents Chemother. 2014;58(4):2363-8.
163. Oladimeji O, Isaakidis P, Obasanya OJ, Eltayeb O, Khogali M, Van den Bergh R, et al. Intensive-phase treatment outcomes among hospitalized multidrug-resistant tuberculosis patients: results from a nationwide cohort in Nigeria. PLoS One. 2014;9(4):e94393.
164. Alsaad N, van Altena R, Pranger AD, van Soolingen D, de Lange WC, van der Werf TS, et al. Evaluation of co-trimoxazole in the treatment of multidrug-resistant tuberculosis. The European respiratory journal. 2013;42(2):504-12.
165. Tsukamura M. In-vitro antimycobacterial activity of minocycline. Tubercle. 1980;61(1):37-8.
166. Bouzid F, Astier H, Osman DA, Javelle E, Hassan MO, Simon F, et al. Extended spectrum of antibiotic susceptibility for tuberculosis, Djibouti. International journal of antimicrobial agents. 2018;51(2):235-8.
167. Dubos RJ. Studies on a bactericidal agent extracted from a soil bacillus. Journal of Experimental Medicine. 1939;70(1):11-7.
168. Nakatsuji T, Gallo RL. Antimicrobial Peptides: Old Molecules with New Ideas. Journal of Investigative Dermatology. 2012;132(3):887-95.
169. Rivas-Santiago B, Rivas Santiago CE, Castaneda-Delgado JE, Leon-Contreras JC, Hancock RE, Hernandez-Pando R. Activity of LL-37, CRAMP and antimicrobial peptide-derived compounds E2, E6 and CP26 against Mycobacterium tuberculosis. International journal of antimicrobial agents. 2013;41(2):143-8.
170. Friedrich CL, Moyles D, Beveridge TJ, Hancock RE. Antibacterial action of structurally diverse cationic peptides on gram-positive bacteria. Antimicrob Agents Chemother. 2000;44(8):2086-92.
171. Ramón-García S, Mikut R, Ng C, Ruden S, Volkmer R, Reischl M, et al. Targeting Mycobacterium tuberculosis and Other Microbial Pathogens Using Improved Synthetic Antibacterial Peptides. Antimicrobial Agents and Chemotherapy. 2013;57(5):2295-303.
172. Kumar P, Kizhakkedathu J, Straus S. Antimicrobial Peptides: Diversity, Mechanism of Action and Strategies to Improve the Activity and Biocompatibility In Vivo. Biomolecules. 2018;8(1):4.
173. Baxter AA, Lay FT, Poon IKH, Kvansakul M, Hulett MD. Tumor cell membrane-targeting cationic antimicrobial peptides: novel insights into mechanisms of action and therapeutic prospects. Cellular and molecular life sciences : CMLS. 2017;74(20):3809-25.
174. Sachdeva S. Peptides as 'Drugs': The Journey so Far. International Journal of Peptide Research and Therapeutics. 2017;23(1):49-60.
175. Westerhoff HV, Juretić D, Hendler RW, Zasloff M. Magainins and the disruption of membrane-linked free-energy transduction. Proceedings of the National Academy of Sciences. 1989;86(17):6597-601.
176. Subbalakshmi C, Nagaraj R, Sitaram N. Biological activities of C-terminal 15-residue synthetic fragment of melittin: design of an analog with improved antibacterial activity. FEBS Lett. 1999;448(1):62-6.

177. Park Y, Park SC, Park HK, Shin SY, Kim Y, Hahm KS. Structure-activity relationship of HP (2-20) analog peptide: enhanced antimicrobial activity by N-terminal random coil region deletion. Biopolymers. 2007;88(2):199-207.
178. Juba ML, Porter DK, Williams EH, Rodriguez CA, Barksdale SM, Bishop BM. Helical cationic antimicrobial peptide length and its impact on membrane disruption. Biochimica et Biophysica Acta (BBA) - Biomembranes. 2015;1848(5):1081-91.
179. Giangaspero A, Sandri L, Tossi A. Amphipathic α helical antimicrobial peptides. . European journal of biochemistry. 2001;268(21):5589-600.
180. Dathe M, Nikolenko H, Meyer J, Beyermann M, Bienert M. Optimization of the antimicrobial activity of magainin peptides by modification of charge. FEBS Letters. 2001;501(2):146-50.
181. Ziqing J, I. VA, D. HJ, W. HRE, L. VM, S. HR. Effects of net charge and the number of positively charged residues on the biological activity of amphipathic α - helical cationic antimicrobial peptides. Peptide Science. 2008;90(3):369-83.
182. Wieprecht T, Dathe M, Epand RM, Beyermann M, Krause E, Maloy WL, et al. Influence of the Angle Subtended by the Positively Charged Helix Face on the Membrane Activity of Amphipathic, Antibacterial Peptides. Biochemistry. 1997;36(42):12869-80.
183. Giuliani A, Pirri G, Nicoletto S. Antimicrobial peptides: an overview of a promising class of therapeutics. Open Life Sciences2007. p. 1.
184. Wang W, Smith DK, Moulding K, Chen HM. The Dependence of Membrane Permeability by the Antibacterial Peptide Cecropin B and Its Analogs, CB-1 and CB-3, on Liposomes of Different Composition. Journal of Biological Chemistry. 1998;273(42):27438-48.
185. Xie Y, Fleming E, Chen JL, Elmore DE. Effect of proline position on the antimicrobial mechanism of buforin II. Peptides. 2011;32(4):677-82.
186. Park CB, Yi KS, Matsuzaki K, Kim MS, Kim SC. Structure-activity analysis of buforin II, a histone H2A-derived antimicrobial peptide: the proline hinge is responsible for the cell-penetrating ability of buforin II. Proc Natl Acad Sci U S A. 2000;97(15):8245-50.
187. Lee S-A, Kim YK, Lim SS, Zhu WL, Ko H, Shin SY, et al. Solution Structure and Cell Selectivity of Piscidin 1 and Its Analogues. Biochemistry. 2007;46(12):3653-63.
188. Vermeer LS, Lan Y, Abbate V, Ruh E, Bui TT, Wilkinson LJ, et al. Conformational Flexibility Determines Selectivity and Antibacterial, Antiplasmodial, and Anticancer Potency of Cationic α-Helical Peptides. Journal of Biological Chemistry. 2012;287(41):34120-33.
189. Avrahami D, Shai Y. Conjugation of a magainin analogue with lipophilic acids controls hydrophobicity, solution assembly, and cell selectivity. Biochemistry. 2002;41(7):2254-63.
190. Huang Y, Huang J, Chen Y. Alpha-helical cationic antimicrobial peptides: relationships of structure and function. Protein & cell. 2010;1(2):143-52.
191. Binu J, Il - Seon P, Jeong - Kyu B, Yub SS. Short KR - 12 analogs designed from human cathelicidin LL - 37 possessing both antimicrobial and antiendotoxic activities without mammalian cell toxicity. Journal of Peptide Science. 2013;19(11):700-7.
192. Ziqing J, Jan KB, Hein VDL, I. VA, D. HJ, T. MC, et al. Effects of Hydrophobicity on the Antifungal Activity of α - Helical Antimicrobial Peptides. Chemical Biology & Drug Design. 2008;72(6):483-95.
193. Khara JS, Lim FK, Wang Y, Ke XY, Voo ZX, Yang YY, et al. Designing alpha-helical peptides with enhanced synergism and selectivity against Mycobacterium smegmatis: Discerning the role of hydrophobicity and helicity. Acta biomaterialia. 2015;28:99-108.
194. Arranz-Trullen J, Lu L, Pulido D, Bhakta S, Boix E. Host Antimicrobial Peptides: The Promise of New Treatment Strategies against Tuberculosis. Frontiers in immunology. 2017;8:1499.

195. Torrent M, Andreu D, Nogues VM, Boix E. Connecting peptide physicochemical and antimicrobial properties by a rational prediction model. PLoS One. 2011;6(2):e16968.
196. Li JWH, Vederas JC. Drug Discovery and Natural Products: End of an Era or an Endless Frontier? Science (New York, NY). 2009;325(5937):161.
197. Cullen TW, Schofield WB, Barry NA, Putnam EE, Rundell EA, Trent MS, et al. Antimicrobial peptide resistance mediates resilience of prominent gut commensals during inflammation. Science (New York, NY). 2015;347(6218):170-5.
198. Diamond G, Beckloff N, Weinberg A, Kisich KO. The Roles of Antimicrobial Peptides in Innate Host Defense. Current pharmaceutical design. 2009;15(21):2377-92.
199. Ziqing J, Michael PH, James W, Kevin OK, Martin IV, Robert SH. Anti-Tuberculosis Activity of α-Helical Antimicrobial Peptides: De Novo Designed L- and D-Enantiomers Versus L- and D-LL37. Protein & Peptide Letters. 2011;18(3):241-52.
200. Rao M, Streur TL, Aldwell FE, Cook GM. Intracellular pH regulation by Mycobacterium smegmatis and Mycobacterium bovis BCG. Microbiology (Reading, England). 2001;147(Pt 4):1017-24.
201. Santos P, Gordillo A, Osses L, Salazar LM, Soto CY. Effect of antimicrobial peptides on ATPase activity and proton pumping in plasma membrane vesicles obtained from mycobacteria. Peptides. 2012;36(1):121-8.
202. Chingaté S, Delgado G, Salazar LM, Soto C-Y. The ATPase activity of the mycobacterial plasma membrane is inhibited by the LL37-analogous peptide LLAP. Peptides. 2015;71:222-8.
203. Carroll J, Draper LA, O'Connor PM, Coffey A, Hill C, Ross RP, et al. Comparison of the activities of the lantibiotics nisin and lacticin 3147 against clinically significant mycobacteria. International journal of antimicrobial agents. 2010;36(2):132-6.
204. Sharma S, Verma I, Khuller GK. Antibacterial activity of human neutrophil peptide-1 against Mycobacterium tuberculosis H37Rv: in vitro and ex vivo study. The European respiratory journal. 2000;16(1):112-7.
205. Sharma A, Pohane AA, Bansal S, Bajaj A, Jain V, Srivastava A. Cell penetrating synthetic antimicrobial peptides (SAMPs) exhibiting potent and selective killing of mycobacterium by targeting its DNA. Chemistry (Weinheim an der Bergstrasse, Germany). 2015;21(9):3540-5.
206. Otvos L, Jr., O I, Rogers ME, Consolvo PJ, Condie BA, Lovas S, et al. Interaction between heat shock proteins and antimicrobial peptides. Biochemistry. 2000;39(46):14150-9.
207. Torres-Juarez F, Cardenas-Vargas A, Montoya-Rosales A, González-Curiel I, Garcia-Hernandez MH, Enciso-Moreno JA, et al. LL-37 Immunomodulatory Activity during Mycobacterium tuberculosis Infection in Macrophages. Infection and immunity. 2015;83(12):4495-503.
208. Hwang SA, Kruzel ML, Actor JK. Oral recombinant human or mouse lactoferrin reduces Mycobacterium tuberculosis TDM induced granulomatous lung pathology. Biochemistry and cell biology = Biochimie et biologie cellulaire. 2017;95(1):148-54.
209. Rekha RS, Rao Muvva SS, Wan M, Raqib R, Bergman P, Brighenti S, et al. Phenylbutyrate induces LL-37-dependent autophagy and intracellular killing of Mycobacterium tuberculosis in human macrophages. Autophagy. 2015;11(9):1688-99.
210. Yuk JM, Shin DM, Lee HM, Yang CS, Jin HS, Kim KK, et al. Vitamin D3 induces autophagy in human monocytes/macrophages via cathelicidin. Cell Host Microbe. 2009;6(3):231-43.
211. Rivas-Santiago B, Castaneda-Delgado JE, Rivas Santiago CE, Waldbrook M, Gonzalez-Curiel I, Leon-Contreras JC, et al. Ability of innate defence regulator peptides IDR-1002, IDR-HH2 and IDR-1018 to protect against Mycobacterium tuberculosis infections in animal models. PLoS One. 2013;8(3):e59119.

212. Rivas-Santiago CE, Hernández-Pando R, Rivas-Santiago B. Immunotherapy for pulmonary TB: antimicrobial peptides and their inducers. Immunotherapy. 2013;5(10):1117-26.
213. Salditt T, Li C, Spaar A. Structure of antimicrobial peptides and lipid membranes probed by interface-sensitive X-ray scattering. Biochimica et Biophysica Acta (BBA) - Biomembranes. 2006;1758(9):1483-98.
214. Banerjee DI, Gohil TP. Interaction of antimicrobial peptide with mycolyl transferase in Mycobacterium tuberculosis. International journal of mycobacteriology. 2016;5(1):83-8.
215. Khara JS, Priestman M, Uhía I, Hamilton MS, Krishnan N, Wang Y, et al. Unnatural amino acid analogues of membrane-active helical peptides with anti-mycobacterial activity and improved stability. Journal of Antimicrobial Chemotherapy. 2016;71(8):2181-91.
216. Rodriguez A, Villegas E, Montoya-Rosales A, Rivas-Santiago B, Corzo G. Characterization of antibacterial and hemolytic activity of synthetic pandinin 2 variants and their inhibition against Mycobacterium tuberculosis. PLoS One. 2014;9(7):e101742.
217. Corrales-Garcia L, Ortiz E, Castañeda-Delgado J, Rivas-Santiago B, Corzo G. Bacterial expression and antibiotic activities of recombinant variants of human β-defensins on pathogenic bacteria and M. tuberculosis. Protein Expression and Purification. 2013;89(1):33-43.
218. Fehlbaum P, Rao M, Zasloff M, Anderson GM. An essential amino acid induces epithelial beta -defensin expression. Proc Natl Acad Sci U S A. 2000;97(23):12723-8.
219. Rivas - Santiago CE, Rivas - Santiago B, León DA, Castañeda - Delgado J, Pando RH. Induction of β - defensins by l - isoleucine as novel immunotherapy in experimental murine tuberculosis. Clinical & Experimental Immunology. 2011;164(1):80-9.
220. Gupta K, Singh S, van Hoek M. Short, Synthetic Cationic Peptides Have Antibacterial Activity against Mycobacterium smegmatis by Forming Pores in Membrane and Synergizing with Antibiotics. Antibiotics. 2015;4(3):358.
221. Kalita A, Verma I, Khuller GK. Role of human neutrophil peptide-1 as a possible adjunct to antituberculosis chemotherapy. The Journal of infectious diseases. 2004;190(8):1476-80.
222. Fattorini L, Gennaro R, Zanetti M, Tan D, Brunori L, Giannoni F, et al. In vitro activity of protegrin-1 and beta-defensin-1, alone and in combination with isoniazid, against Mycobacterium tuberculosis. Peptides. 2004;25(7):1075-7.
223. Mirsaeidi M, Banoei MM, Winston BW, Schraufnagel DE. Metabolomics: Applications and Promise in Mycobacterial Disease. Annals of the American Thoracic Society. 2015;12(9):1278-87.
224. Fiehn O. Metabolomics--the link between genotypes and phenotypes. Plant molecular biology. 2002;48(1-2):155-71.
225. Guo Y, Xiao P, Lei S, Deng F, Xiao GG, Liu Y, et al. How is mRNA expression predictive for protein expression? A correlation study on human circulating monocytes. Acta biochimica et biophysica Sinica. 2008;40(5):426-36.
226. Lindon JC, Holmes E, Nicholson JK. So what's the deal with metabonomics? Anal Chem. 2003;75(17):384a-91a.
227. Villas-Boas SG, Mas S, Akesson M, Smedsgaard J, Nielsen J. Mass spectrometry in metabolome analysis. Mass spectrometry reviews. 2005;24(5):613-46.
228. Banoei MM, Donnelly SJ, Mickiewicz B, Weljie A, Vogel HJ, Winston BW. Metabolomics in critical care medicine: a new approach to biomarker discovery. Clinical and investigative medicine Medecine clinique et experimentale. 2014;37(6):E363-76.
229. Li F, Miao Y, Zhang L, Neuenswander SA, Douglas JT, Ma X. Metabolomic analysis reveals novel isoniazid metabolites and hydrazones in human urine. Drug metabolism and pharmacokinetics. 2011;26(6):569-76.

230. Loots DT, Wiid IJ, Page BJ, Mienie LJ, van Helden PD. Melatonin prevents the free radical and MADD metabolic profiles induced by antituberculosis drugs in an animal model. Journal of pineal research. 2005;38(2):100-6.
231. du Preez I, Loots du T. Altered fatty acid metabolism due to rifampicin-resistance conferring mutations in the rpoB Gene of Mycobacterium tuberculosis: mapping the potential of pharmaco-metabolomics for global health and personalized medicine. Omics : a journal of integrative biology. 2012;16(11):596-603.
232. Cai G, Pauli GF, Wang Y, Jaki BU, Franzblau SG. Rapid determination of growth inhibition of Mycobacterium tuberculosis by GC-MS/MS quantitation of tuberculostearic acid. Tuberculosis (Edinburgh, Scotland). 2013;93(3):322-9.
233. Chow ED, Cox JS. TB lipidomics--the final frontier. Chemistry & biology. 2011;18(12):1517-8.
234. Chen J-H, Singer S. Chapter 4 - High-Resolution Magic Angle Spinning NMR Spectroscopy. The Handbook of Metabonomics and Metabolomics. Amsterdam: Elsevier Science B.V.; 2007. p. 113-47.
235. Bond L, W. Griffin J, V. Harris R, M. Denslow K, L. Moran T. Evaluation of Non-Nuclear Techniques for Well Logging: Final Report2011.
236. Macomber RS. A complete introduction to modern NMR spectroscopy: Wiley; 1998.
237. Ross A, Schlotterbeck G, Dieterle F, Senn H. Chapter 3 - NMR Spectroscopy Techniques for Application to Metabonomics. The Handbook of Metabonomics and Metabolomics. Amsterdam: Elsevier Science B.V.; 2007. p. 55-112.
238. Renault M, Shintu L, Piotto M, Caldarelli S. Slow-spinning low-sideband HR-MAS NMR spectroscopy: delicate analysis of biological samples. Scientific Reports. 2013;3:3349.
239. Li W, Lee RE, Lee RE, Li J. Methods for acquisition and assignment of multidimensional high-resolution magic angle spinning NMR of whole cell bacteria. Anal Chem. 2005;77(18):5785-92.
240. Somashekar BS, Amin AG, Rithner CD, Troudt J, Basaraba R, Izzo A, et al. Metabolic profiling of lung granuloma in Mycobacterium tuberculosis infected guinea pigs: ex vivo 1H magic angle spinning NMR studies. Journal of proteome research. 2011;10(9):4186-95.
241. Cheng LL, Burns MA, Lean CL. High Resolution Magic Angle Spinning (HRMAS) Proton MRS of Surgical Specimens. In: Webb GA, editor. Modern Magnetic Resonance. Dordrecht: Springer Netherlands; 2006. p. 1051-64.
242. Matsuoka S, Inoue M. Application of REDORNMR in natural product chemistry. Chemical Communications. 2009(38):5664-75.
243. Craig A, Cloarec O, Holmes E, Nicholson JK, Lindon JC. Scaling and normalization effects in NMR spectroscopic metabonomic data sets. Anal Chem. 2006;78(7):2262-7.
244. Worley B, Powers R. Multivariate Analysis in Metabolomics. Current Metabolomics. 2013;1(1):92-107.
245. Ebbels T, Cavill R. Bioinformatic methods in NMR-based metabolic profiling2009. 361-74 p.
246. JOLLIFFE IT. Principal Component Analysis. 2 ed. New York: Springer-Verlag New York, Inc; 2002.
247. Westerhuis JA, Hoefsloot HCJ, Smit S, Vis DJ, Smilde AK, van Velzen EJJ, et al. Assessment of PLSDA cross validation. Metabolomics : Official journal of the Metabolomic Society. 2008;4(1):81-9.
248. Anderssen E, Dyrstad K, Westad F, Martens H. Reducing over-optimism in variable selection by cross-model validation. Chemometrics and Intelligent Laboratory Systems. 2006;84(1):69-74.

249. Halouska S, Fenton RJ, Zinniel DK, Marshall DD, Barletta RG, Powers R. Metabolomics Analysis Identifies D-Alanine-D-alanine Ligase as the Primary Lethal Target of D-cycloserine in Mycobacteria. Journal of proteome research. 2014;13(2):1065-76.
250. Behrends V, Williams KJ, Jenkins VA, Robertson BD, Bundy JG. Free glucosylglycerate is a novel marker of nitrogen stress in Mycobacterium smegmatis. Journal of proteome research. 2012;11(7):3888-96.
251. De Buck J, Shaykhutdinov R, Barkema HW, Vogel HJ. Metabolomic Profiling in Cattle Experimentally Infected with Mycobacterium avium subsp. paratuberculosis. PLoS ONE. 2014;9(11):e111872.
252. Mahrous EA, Lee RB, Lee RE. A rapid approach to lipid profiling of mycobacteria using 2D HSQC NMR maps. Journal of lipid research. 2008;49(2):455-63.
253. Halouska S, Fenton RJ, Barletta RG, Powers R. Predicting the in vivo mechanism of action for drug leads using NMR metabolomics. ACS chemical biology. 2012;7(1):166-71.
254. Takahashi M, Nagai T, Okamura N, Takahashi H, Okano A. Promoting effect of beta-mercaptoethanol on in vitro development under oxidative stress and cystine uptake of bovine embryos. Biology of reproduction. 2002;66(3):562-7.
255. Glickman MS, Cox JS, Jacobs WR, Jr. A novel mycolic acid cyclopropane synthetase is required for cording, persistence, and virulence of Mycobacterium tuberculosis. Molecular cell. 2000;5(4):717-27.
256. Sampson SL, Dascher CC, Sambandamurthy VK, Russell RG, Jacobs WR, Jr., Bloom BR, et al. Protection elicited by a double leucine and pantothenate auxotroph of Mycobacterium tuberculosis in guinea pigs. Infection and immunity. 2004;72(5):3031-7.
257. Caleffi-Ferracioli KR, Maltempe FG, Siqueira VL, Cardoso RF. Fast detection of drug interaction in Mycobacterium tuberculosis by a checkerboard resazurin method. Tuberculosis (Edinburgh, Scotland). 2013;93(6):660-3.
258. de Carvalho LP, Fischer SM, Marrero J, Nathan C, Ehrt S, Rhee KY. Metabolomics of Mycobacterium tuberculosis reveals compartmentalized co-catabolism of carbon substrates. Chemistry & biology. 2010;17(10):1122-31.
259. Lan Y, Lam JT, Siu GK, Yam WC, Mason AJ, Lam JK. Cationic amphipathic D-enantiomeric antimicrobial peptides with in vitro and ex vivo activity against drug-resistant Mycobacterium tuberculosis. Tuberculosis (Edinburgh, Scotland). 2014;94(6):678-89.
260. Andreu N, Fletcher T, Krishnan N, Wiles S, Robertson BD. Rapid measurement of antituberculosis drug activity in vitro and in macrophages using bioluminescence. The Journal of antimicrobial chemotherapy. 2012;67(2):404-14.
261. Khara JS, Wang Y, Ke XY, Liu S, Newton SM, Langford PR, et al. Anti-mycobacterial activities of synthetic cationic alpha-helical peptides and their synergism with rifampicin. Biomaterials. 2014;35(6):2032-8.
262. Worley B, Powers R. MVAPACK: a complete data handling package for NMR metabolomics. ACS chemical biology. 2014;9(5):1138-44.
263. Vermeer LS, Fruhwirth GO, Pandya P, Ng T, Mason AJ. NMR metabolomics of MTLn3E breast cancer cells identifies a role for CXCR4 in lipid and choline regulation. Journal of proteome research. 2012;11(5):2996-3003.
264. Dieterle F, Ross A, Schlotterbeck G, Senn H. Probabilistic quotient normalization as robust method to account for dilution of complex biological mixtures. Application in 1H NMR metabonomics. Anal Chem. 2006;78(13):4281-90.
265. Kozlowska J, Rivett DW, Vermeer LS, Carroll MP, Bruce KD, Mason AJ, et al. A relationship between Pseudomonal growth behaviour and cystic fibrosis patient lung function identified in a metabolomic investigation. Metabolomics : Official journal of the Metabolomic Society. 2013;9(6).
266. Olivier I, Loots du T. A metabolomics approach to characterise and identify various Mycobacterium species. Journal of microbiological methods. 2012;88(3):419-26.

267. Shin JH, Yang JY, Jeon BY, Yoon YJ, Cho SN, Kang YH, et al. (1)H NMR-based metabolomic profiling in mice infected with Mycobacterium tuberculosis. Journal of proteome research. 2011;10(5):2238-47.
268. Chen Y, Wu J, Tu L, Xiong X, Hu X, Huang J, et al. 1H-NMR Spectroscopy Revealed Mycobacterium tuberculosis Caused Abnormal Serum Metabolic Profile of Cattle. PLOS ONE. 2013;8(9):e74507.
269. Liu J, Nikaido H. A mutant of Mycobacterium smegmatis defective in the biosynthesis of mycolic acids accumulates meromycolates. Proc Natl Acad Sci U S A. 1999;96(7):4011-6.
270. Yuan Y, Barry CE. A common mechanism for the biosynthesis of methoxy and cyclopropyl mycolic acids in Mycobacterium tuberculosis. Proceedings of the National Academy of Sciences of the United States of America. 1996;93(23):12828-33.
271. Ulrich EL, Akutsu H, Doreleijers JF, Harano Y, Ioannidis YE, Lin J, et al. BioMagResBank. Nucleic Acids Research. 2008;36(suppl_1):D402-D8.
272. Saeed AI, Sharov V, White J, Li J, Liang W, Bhagabati N, et al. TM4: a free, open-source system for microarray data management and analysis. BioTechniques. 2003;34(2):374-8.
273. Hong SY, Oh JE, Lee K-H. Effect of d-amino acid substitution on the stability, the secondary structure, and the activity of membrane-active peptide. Biochemical Pharmacology. 1999;58(11):1775-80.
274. Kozlowska J, Vermeer LS, Rogers GB, Rehnnuma N, Amos S-BTA, Koller G, et al. Combined Systems Approaches Reveal Highly Plastic Responses to Antimicrobial Peptide Challenge in Escherichia coli. PLOS Pathogens. 2014;10(5):e1004104.
275. Vilcheze C, Copeland J, Keiser TL, Weisbrod T, Washington J, Jain P, et al. Rational Design of Biosafety Level 2-Approved, Multidrug-Resistant Strains of Mycobacterium tuberculosis through Nutrient Auxotrophy. MBio. 2018;9(3).
276. Andreu N, Zelmer A, Fletcher T, Elkington PT, Ward TH, Ripoll J, et al. Optimisation of bioluminescent reporters for use with mycobacteria. PLoS One. 2010;5(5):e10777.
277. Sharma S, Gelman E, Narayan C, Bhattacharjee D, Achar V, Humnabadkar V, et al. Simple and Rapid Method To Determine Antimycobacterial Potency of Compounds by Using Autoluminescent Mycobacterium tuberculosis. Antimicrobial Agents and Chemotherapy. 2014;58(10):5801-8.
278. Meighen EA. Molecular biology of bacterial bioluminescence. Microbiological reviews. 1991;55(1):123-42.
279. Andreu N, Zelmer A, Sampson SL, Ikeh M, Bancroft GJ, Schaible UE, et al. Rapid in vivo assessment of drug efficacy against Mycobacterium tuberculosis using an improved firefly luciferase. The Journal of antimicrobial chemotherapy. 2013;68(9):2118-27.
280. Andrew PW, Roberts IS. Construction of a bioluminescent mycobacterium and its use for assay of antimycobacterial agents. Journal of Clinical Microbiology. 1993;31(9):2251-4.
281. Kong Y, Yang D, Cirillo SL, Li S, Akin A, Francis KP, et al. Application of Fluorescent Protein Expressing Strains to Evaluation of Anti-Tuberculosis Therapeutic Efficacy In Vitro and In Vivo. PLoS One. 2016;11(3):e0149972.
282. B. AR. Mycobacterium tuberculosis Reporter Strains as Tools for Drug Discovery and Development. IUBMB Life.0(0).
283. Naran K, Moosa A, Barry CE, Boshoff HIM, Mizrahi V, Warner DF. Bioluminescent Reporters for Rapid Mechanism of Action Assessment in Tuberculosis Drug Discovery. Antimicrobial Agents and Chemotherapy. 2016;60(11):6748-57.

284. John OB, Ian W, Terry O, François P. Investigation of the Alamar Blue (resazurin) fluorescent dye for the assessment of mammalian cell cytotoxicity. European journal of biochemistry. 2000;267(17):5421-6.
285. Aguila EMD, LPG, Cyntia S. Freitas, Patricia R., Paschoalin PaVF. Chapter 3 - Natural Antimicrobials in Food Processing: Bacteriocins, Peptides and Chitooligosaccharides. In: Choudhary A-uRaMI, editor. Frontiers in Anti-Infective Drug Discovery. 5: Bentham Science Publishers; 2017. p. 55-108.
286. Rifampin. Tuberculosis. 2008;88(2):151-4.
287. Isoniazid. Tuberculosis. 2008;88(2):112-6.
288. Ramaswamy S, Musser JM. Molecular genetic basis of antimicrobial agent resistance in Mycobacterium tuberculosis: 1998 update. Tubercle and lung disease : the official journal of the International Union against Tuberculosis and Lung Disease. 1998;79(1):3-29.
289. Bahar AA, Ren D. Antimicrobial Peptides. Pharmaceuticals. 2013;6(12):1543-75.
290. V. Eldem SO, Y. Bakir, T. Unver. Chapter 6 - Antimicrobial Polypeptides in the control of plant pathogenic bacteria. In: V. Rajesh Kannan KKB, editor. Sustainable Approaches to Controlling Plant Pathogenic Bacteria. 1 ed: CRC Press; 2015. p. 123-50.
291. Bansal S, Singh M, Kidwai S, Bhargava P, Singh A, Sreekanth V, et al. Bile acid amphiphiles with tunable head groups as highly selective antitubercular agents. MedChemComm. 2014;5(11):1761-8.
292. Nuti R, Goud NS, Saraswati AP, Alvala R, Alvala M. Antimicrobial Peptides: A Promising Therapeutic Strategy in Tackling Antimicrobial Resistance. Current medicinal chemistry. 2017;24(38):4303-14.
293. Khandelia H, Ipsen JH, Mouritsen OG. The impact of peptides on lipid membranes. Biochimica et Biophysica Acta (BBA) - Biomembranes. 2008;1778(7):1528-36.
294. Lin Y, Li Y, Zhu N, Han Y, Jiang W, Wang Y, et al. The antituberculosis antibiotic capreomycin inhibits protein synthesis by disrupting interaction between ribosomal proteins L12 and L10. Antimicrob Agents Chemother. 2014;58(4):2038-44.
295. David HL, Rastogi N. Antibacterial action of colistin (polymyxin E) against Mycobacterium aurum. Antimicrob Agents Chemother. 1985;27(5):701-7.
296. Rastogi N, Potar MC, David HL. Antimycobacterial spectrum of colistin (polymixin E). Annales de l'Institut Pasteur Microbiologie. 1986;137a(1):45-53.
297. Bax HI, de Steenwinkel JE, Ten Kate MT, van der Meijden A, Verbon A, Bakker-Woudenberg IA. Colistin as a potentiator of anti-TB drug activity against Mycobacterium tuberculosis. The Journal of antimicrobial chemotherapy. 2015;70(10):2828-37.
298. Loho T, Dharmayanti A. Colistin: an antibiotic and its role in multiresistant Gram-negative infections. Acta medica Indonesiana. 2015;47(2):157-68.
299. Orgeur M, Brosch R. Evolution of virulence in the Mycobacterium tuberculosis complex. Curr Opin Microbiol. 2017;41:68-75.
300. Odds FC. Synergy, antagonism, and what the chequerboard puts between them. Journal of Antimicrobial Chemotherapy. 2003;52(1):1-.
301. Gagneux S, Long CD, Small PM, Van T, Schoolnik GK, Bohannan BJM. The Competitive Cost of Antibiotic Resistance in Mycobacterium tuberculosis. Science (New York, NY). 2006;312(5782):1944-6.
302. Borrell S, Teo Y, Giardina F, Streicher EM, Klopper M, Feldmann J, et al. Epistasis between antibiotic resistance mutations drives the evolution of extensively drug-resistant tuberculosis. Evolution, Medicine, and Public Health. 2013;2013(1):65-74.
303. Sander P, Springer B, Prammananan T, Sturmfels A, Kappler M, Pletschette M, et al. Fitness cost of chromosomal drug resistance-conferring mutations. Antimicrob Agents Chemother. 2002;46(5):1204-11.

304. Sander P, Springer B, Prammananan T, Sturmfels A, Kappler M, Pletschette M, et al. Fitness Cost of Chromosomal Drug Resistance-Conferring Mutations. Antimicrobial Agents and Chemotherapy. 2002;46(5):1204-11.
305. Björkman J, Hughes D, Andersson DI. Virulence of antibiotic-resistant Salmonella typhimurium. Proceedings of the National Academy of Sciences of the United States of America. 1998;95(7):3949-53.
306. Seifert M, Catanzaro D, Catanzaro A, Rodwell TC. Genetic Mutations Associated with Isoniazid Resistance in Mycobacterium tuberculosis: A Systematic Review. PLoS ONE. 2015;10(3):e0119628.
307. Khadka DK, Eampokalap B, Panitchakorn J, Ramasoota P, Khusmith S. Multiple mutations in katG and inhA identified in Thai isoniazid-resistant Mycobacterium tuberculosis isolates. The Southeast Asian journal of tropical medicine and public health. 2007;38(2):376-82.
308. Glickman MS, Cox JS, Jacobs WR. A Novel Mycolic Acid Cyclopropane Synthetase Is Required for Cording, Persistence, and Virulence of Mycobacterium tuberculosis. Molecular cell. 2000;5(4):717-27.
309. Slama N, Jamet S, Frigui W, Pawlik A, Bottai D, Laval F, et al. The changes in mycolic acid structures caused by hadC mutation have a dramatic effect on the virulence of Mycobacterium tuberculosis. Molecular microbiology. 2016;99(4):794-807.
310. Vermeer LS, Lan Y, Abbate V, Ruh E, Bui TT, Wilkinson LJ, et al. Conformational Flexibility Determines Selectivity and Antibacterial, Antiplasmodial and Anticancer Potency of Cationic α-Helical Peptides. The Journal of biological chemistry. 2012;287(41):34120-33.
311. Rivera-Marrero CA, Stewart J, Shafer WM, Roman J. The down-regulation of cathepsin G in THP-1 monocytes after infection with Mycobacterium tuberculosis is associated with increased intracellular survival of bacilli. Infection and immunity. 2004;72(10):5712-21.
312. Jaiswal I, Jain A, Verma SK, Singh P, Kant S, Singh M. Effect of efflux pump inhibitors on the susceptibility of Mycobacterium tuberculosis to isoniazid. Lung India. 2017;34(6):499-505.
313. Kanji A, Hasan R, Zhang Y, Shi W, Imtiaz K, Iqbal K, et al. Increased expression of efflux pump genes in extensively drug-resistant isolates of Mycobacterium tuberculosis. International journal of mycobacteriology. 2016;5 Suppl 1:S150.
314. Spindler E, D F Hale J, Giddings T, E W Hancock R, Gill R. Deciphering the Mode of Action of the Synthetic Antimicrobial Peptide Bac8c2011. 1706-16 p.
315. Loddenkemper R, Sagebiel D, Brendel A. Strategies against multidrug-resistant tuberculosis. European Respiratory Journal. 2002;20(36 suppl):66s-77s.
316. Yuan Y, Zhu Y, Crane DD, Barry CE, 3rd. The effect of oxygenated mycolic acid composition on cell wall function and macrophage growth in Mycobacterium tuberculosis. Molecular microbiology. 1998;29(6):1449-58.
317. Luisa MM, C. RA, Antonio DG, Giuseppina M, Argante B, Donatella B, et al. Structure–function relationships of temporins, small antimicrobialpeptides from amphibian skin. European journal of biochemistry. 2000;267(5):1447-54.
318. Cirioni O, Silvestri C, Ghiselli R, Orlando F, Riva A, Mocchegiani F, et al. Protective effects of the combination of α-helical antimicrobial peptides and rifampicin in three rat models of Pseudomonas aeruginosa infection. Journal of Antimicrobial Chemotherapy. 2008;62(6):1332-8.
319. Anantharaman A, Rizvi MS, Sahal D. Synergy with rifampin and kanamycin enhances potency, kill kinetics, and selectivity of de novo-designed antimicrobial peptides. Antimicrob Agents Chemother. 2010;54(5):1693-9.

320. Danilchanka O, Pavlenok M, Niederweis M. Role of Porins for Uptake of Antibiotics by Mycobacterium smegmatis. Antimicrobial Agents and Chemotherapy. 2008;52(9):3127-34.
321. Kartmann B, Stenger S, Niederweis M, Stengler S. Porins in the Cell Wall of Mycobacterium tuberculosis1999. 6543-6 p.
322. Jayaram R, Shandil RK, Gaonkar S, Kaur P, Suresh BL, Mahesh BN, et al. Isoniazid pharmacokinetics-pharmacodynamics in an aerosol infection model of tuberculosis. Antimicrob Agents Chemother. 2004;48(8):2951-7.
323. Jayaram R, Gaonkar S, Kaur P, Suresh BL, Mahesh BN, Jayashree R, et al. Pharmacokinetics-pharmacodynamics of rifampin in an aerosol infection model of tuberculosis. Antimicrob Agents Chemother. 2003;47(7):2118-24.
324. Gumbo T, Louie A, Deziel MR, Liu W, Parsons LM, Salfinger M, et al. Concentration-dependent Mycobacterium tuberculosis killing and prevention of resistance by rifampin. Antimicrob Agents Chemother. 2007;51(11):3781-8.
325. Zhang Y, Yew WW. Mechanisms of drug resistance in Mycobacterium tuberculosis: update 2015. The international journal of tuberculosis and lung disease : the official journal of the International Union against Tuberculosis and Lung Disease. 2015;19(11):1276-89.
326. Vilcheze C, Hartman T, Weinrick B, Jain P, Weisbrod TR, Leung LW, et al. Enhanced respiration prevents drug tolerance and drug resistance in Mycobacterium tuberculosis. Proc Natl Acad Sci U S A. 2017;114(17):4495-500.
327. Bardou F, Raynaud C, Ramos C, Laneelle MA, Laneelle G. Mechanism of isoniazid uptake in Mycobacterium tuberculosis. Microbiology (Reading, England). 1998;144 (Pt 9):2539-44.
328. Kwok PC, Grabarek A, Chow MY, Lan Y, Li JC, Casettari L, et al. Inhalable spray-dried formulation of D-LAK antimicrobial peptides targeting tuberculosis. International journal of pharmaceutics. 2015;491(1-2):367-74.
329. Chaturvedi V, Dwivedi N, Tripathi RP, Sinha S. Evaluation of Mycobacterium smegmatis as a possible surrogate screen for selecting molecules active against multi-drug resistant Mycobacterium tuberculosis. The Journal of general and applied microbiology. 2007;53(6):333-7.
330. do Canto AMTM, Robalo JR, Santos PD, Carvalho AJP, Ramalho JPP, Loura LMS. Diphenylhexatriene membrane probes DPH and TMA-DPH: A comparative molecular dynamics simulation study. Biochimica et Biophysica Acta (BBA) - Biomembranes. 2016;1858(11):2647-61.
331. Grebowski J, Krokosz A, Puchala M. Membrane fluidity and activity of membrane ATPases in human erythrocytes under the influence of polyhydroxylated fullerene. Biochimica et Biophysica Acta (BBA) - Biomembranes. 2013;1828(2):241-8.
332. Suwalsky M, Villena F, Bagnara M, Sotomayor CP. Interaction of the antiarrhythmic drug procainamide with phospholipid bilayers. Zeitschrift fur Naturforschung C, Journal of biosciences. 1995;50(3-4):248-56.
333. Kulig W, Jurkiewicz P, Olżyńska A, Tynkkynen J, Javanainen M, Manna M, et al. Experimental determination and computational interpretation of biophysical properties of lipid bilayers enriched by cholesteryl hemisuccinate. Biochimica et Biophysica Acta (BBA) - Biomembranes. 2015;1848(2):422-32.
334. Scheinpflug K, Wenzel M, Krylova O, Bandow JE, Dathe M, Strahl H. Antimicrobial peptide cWFW kills by combining lipid phase separation with autolysis. Sci Rep. 2017;7:44332.
335. Bach JN, Bramkamp M. Flotillins functionally organize the bacterial membrane. Molecular microbiology. 2013;88(6):1205-17.
336. Strahl H, Burmann F, Hamoen LW. The actin homologue MreB organizes the bacterial cell membrane. Nature communications. 2014;5:3442.

337. Hanoulle X, Wieruszeski JM, Rousselot-Pailley P, Landrieu I, Baulard AR, Lippens G. Monitoring of the ethionamide pro-drug activation in mycobacteria by (1)H high resolution magic angle spinning NMR. Biochemical and biophysical research communications. 2005;331(2):452-8.
338. Alahari A, Trivelli X, Guerardel Y, Dover LG, Besra GS, Sacchettini JC, et al. Thiacetazone, an antitubercular drug that inhibits cyclopropanation of cell wall mycolic acids in mycobacteria. PLoS One. 2007;2(12):e1343.
339. Hanoulle X, Wieruszeski JM, Rousselot-Pailley P, Landrieu I, Locht C, Lippens G, et al. Selective intracellular accumulation of the major metabolite issued from the activation of the prodrug ethionamide in mycobacteria. The Journal of antimicrobial chemotherapy. 2006;58(4):768-72.
340. Prados-Rosales R, Carreño LJ, Weinrick B, Batista-Gonzalez A, Glatman-Freedman A, Xu J, et al. The Type of Growth Medium Affects the Presence of a Mycobacterial Capsule and Is Associated With Differences in Protective Efficacy of BCG Vaccination Against Mycobacterium tuberculosis. The Journal of infectious diseases. 2016;214(3):426-37.
341. Etienne G, Laval F, Villeneuve C, Dinadayala P, Abouwarda A, Zerbib D, et al. The cell envelope structure and properties of Mycobacterium smegmatis mc(2)155: is there a clue for the unique transformability of the strain? Microbiology (Reading, England). 2005;151(Pt 6):2075-86.
342. Taute H, Bester MJ, Neitz AWH, Gaspar ARM. Investigation into the mechanism of action of the antimicrobial peptides Os and Os-C derived from a tick defensin. Peptides. 2015;71:179-87.
343. Ernst WA, Thoma-Uszynski S, Teitelbaum R, Ko C, Hanson DA, Clayberger C, et al. Granulysin, a T cell product, kills bacteria by altering membrane permeability. Journal of immunology (Baltimore, Md : 1950). 2000;165(12):7102-8.
344. Hartmann M, Berditsch M, Hawecker J, Ardakani MF, Gerthsen D, Ulrich AS. Damage of the bacterial cell envelope by antimicrobial peptides gramicidin S and PGLa as revealed by transmission and scanning electron microscopy. Antimicrob Agents Chemother. 2010;54(8):3132-42.
345. van Breda SV, Buys A, Apostolides Z, Nardell EA, Stoltz AC. The antimicrobial effect of colistin methanesulfonate on Mycobacterium tuberculosis in vitro. Tuberculosis. 2015;95(4):440-6.
346. Hristova K, Selsted ME, White SH. Critical role of lipid composition in membrane permeabilization by rabbit neutrophil defensins. The Journal of biological chemistry. 1997;272(39):24224-33.
347. Marcellini L, Borro M, Gentile G, Rinaldi AC, Stella L, Aimola P, et al. Esculentin-1b(1-18)--a membrane-active antimicrobial peptide that synergizes with antibiotics and modifies the expression level of a limited number of proteins in Escherichia coli. The FEBS journal. 2009;276(19):5647-64.
348. Ladokhin AS, Selsted ME, White SH. Sizing membrane pores in lipid vesicles by leakage of co-encapsulated markers: pore formation by melittin. Biophys J. 1997;72(4):1762-6.
349. Mykytczuk NC, Trevors JT, Leduc LG, Ferroni GD. Fluorescence polarization in studies of bacterial cytoplasmic membrane fluidity under environmental stress. Progress in biophysics and molecular biology. 2007;95(1-3):60-82.
350. Behling C, Nolte FS, Tinkley A, Hunter R. Effect of tyloxapol on surface lipids and biological activities of BCG1994. 1-14 p.
351. Santangelo MP, Heuberger A, Blanco F, Forrellad M, Taibo C, Klepp L, et al. Metabolic profile of Mycobacterium smegmatis reveals Mce4 proteins are relevant for cell wall lipid homeostasis. Metabolomics : Official journal of the Metabolomic Society. 2016;12(6):1-11.

352. A. SR, E. LR, E. BC. Isoniazid affects multiple components of the type II fatty acid synthase system of Mycobacterium tuberculosis. Molecular microbiology. 2000;38(3):514-25.
353. Shiloh MU, DiGiuseppe Champion PA. To catch a killer. What can mycobacterial models teach us about Mycobacterium tuberculosis pathogenesis? Current opinion in microbiology. 2010;13(1):86-92.
354. Reyrat JM, Kahn D. Mycobacterium smegmatis: an absurd model for tuberculosis? Trends in microbiology. 2001;9(10):472-4.
355. Tyagi JS, Sharma D. Mycobacterium smegmatis and tuberculosis. Trends in microbiology. 2002;10(2):68-9.
356. Dick T, Lee BH, Murugasu-Oei B. Oxygen depletion induced dormancy in Mycobacterium smegmatis. FEMS microbiology letters. 1998;163(2):159-64.
357. Jacobs WR. Mycobacterium tuberculosis: a once genetically intractable organism. ASM Press. 2000:1–16.
358. Lu T, Drlica K. In vitro activity of C-8-methoxy fluoroquinolones against mycobacteria when combined with anti-tuberculosis agents. The Journal of antimicrobial chemotherapy. 2003;52(6):1025-8.
359. Andries K, Verhasselt P, Guillemont J, Gohlmann HW, Neefs JM, Winkler H, et al. A diarylquinoline drug active on the ATP synthase of Mycobacterium tuberculosis. Science (New York, NY). 2005;307(5707):223-7.
360. Gupta K, Singh S, van Hoek ML. Short, Synthetic Cationic Peptides Have Antibacterial Activity against Mycobacterium smegmatis by Forming Pores in Membrane and Synergizing with Antibiotics. Antibiotics (Basel, Switzerland). 2015;4(3):358-78.
361. Wang L, Slayden RA, Barry CE, 3rd, Liu J. Cell wall structure of a mutant of Mycobacterium smegmatis defective in the biosynthesis of mycolic acids. The Journal of biological chemistry. 2000;275(10):7224-9.
362. Quan S, Venter H, Dabbs ER. Ribosylative inactivation of rifampin by Mycobacterium smegmatis is a principal contributor to its low susceptibility to this antibiotic. Antimicrob Agents Chemother. 1997;41(11):2456-60.
363. Chung GA, Aktar Z, Jackson S, Duncan K. High-throughput screen for detecting antimycobacterial agents. Antimicrob Agents Chemother. 1995;39(10):2235-8.
364. Agrawal P, Miryala S, Varshney U. Use of Mycobacterium smegmatis deficient in ADP-ribosyltransferase as surrogate for Mycobacterium tuberculosis in drug testing and mutation analysis. PLoS One. 2015;10(4):e0122076.
365. Chen L, Xie QW, Nathan C. Alkyl hydroperoxide reductase subunit C (AhpC) protects bacterial and human cells against reactive nitrogen intermediates. Molecular cell. 1998;1(6):795-805.
366. Dhandayuthapani S, Zhang Y, Mudd MH, Deretic V. Oxidative stress response and its role in sensitivity to isoniazid in mycobacteria: characterization and inducibility of ahpC by peroxides in Mycobacterium smegmatis and lack of expression in M. aurum and M. tuberculosis. Journal of bacteriology. 1996;178(12):3641-9.
367. Gillespie J, Barton LL, Rypka EW. Phenotypic changes in mycobacteria grown in oxygen-limited conditions. Journal of Medical Microbiology. 1986;21(3):251-5.
368. Etienne G, Malaga W, Laval F, Lemassu A, Guilhot C, Daffe M. Identification of the polyketide synthase involved in the biosynthesis of the surface-exposed lipooligosaccharides in mycobacteria. Journal of bacteriology. 2009;191(8):2613-21.
369. Boll JM, Crofts AA, Peters K, Cattoir V, Vollmer W, Davies BW, et al. A penicillin-binding protein inhibits selection of colistin-resistant, lipooligosaccharide-deficient Acinetobacter baumannii. Proceedings of the National Academy of Sciences of the United States of America. 2016;113(41):E6228-E37.
370. Velayati AA, Farnia P, Ibrahim TA, Haroun RZ, Kuan HO, Ghanavi J, et al. Differences in cell wall thickness between resistant and nonresistant strains of

Mycobacterium tuberculosis: using transmission electron microscopy. Chemotherapy. 2009;55(5):303-7.
371. Rodriguez-Rivera FP, Zhou X, Theriot JA, Bertozzi CR. Visualization of mycobacterial membrane dynamics in live cells. J Am Chem Soc. 2017;139(9):3488-95.
372. Johansen SK, Maus CE, Plikaytis BB, Douthwaite S. Capreomycin binds across the ribosomal subunit interface using tlyA-encoded 2'-O-methylations in 16S and 23S rRNAs. Molecular cell. 2006;23(2):173-82.
373. Fu LM, Shinnick TM. Genome-wide exploration of the drug action of capreomycin on Mycobacterium tuberculosis using Affymetrix oligonucleotide GeneChips. The Journal of infection. 2007;54(3):277-84.
374. Gallant JL, Viljoen AJ, van Helden PD, Wiid IJ. Glutamate Dehydrogenase Is Required by Mycobacterium bovis BCG for Resistance to Cellular Stress. PLoS One. 2016;11(1):e0147706.
375. Cowley S, Ko M, Pick N, Chow R, Downing KJ, Gordhan BG, et al. The Mycobacterium tuberculosis protein serine/threonine kinase PknG is linked to cellular glutamate/glutamine levels and is important for growth in vivo. Molecular microbiology. 2004;52(6):1691-702.
376. Boot M, van Winden VJC, Sparrius M, van de Weerd R, Speer A, Ummels R, et al. Cell envelope stress in mycobacteria is regulated by the novel signal transduction ATPase IniR in response to trehalose. PLoS Genetics. 2017;13(12):e1007131.
377. de Knegt GJ, Bruning O, ten Kate MT, de Jong M, van Belkum A, Endtz HP, et al. Rifampicin-induced transcriptome response in rifampicin-resistant Mycobacterium tuberculosis. Tuberculosis (Edinburgh, Scotland). 2013;93(1):96-101.
378. Moreira AS, Lourenço AB, Sá-Correia I. 1H-NMR-Based Endometabolome Profiles of Burkholderia cenocepacia Clonal Variants Retrieved from a Cystic Fibrosis Patient during Chronic Infection. Frontiers in microbiology. 2016;7(2024).
379. Murphy HN, Stewart GR, Mischenko VV, Apt AS, Harris R, McAlister MS, et al. The OtsAB pathway is essential for trehalose biosynthesis in Mycobacterium tuberculosis. The Journal of biological chemistry. 2005;280(15):14524-9.
380. Winder FG, Brennan PJ, McDonnell I. Effects of isoniazid on the composition of mycobacteria, with particular reference to soluble carbohydrates and related substances. Biochemical Journal. 1967;104(2):385-93.
381. Winder F, Brennan P. The accumulation of free trehalose by mycobacteria exposed to isoniazid. Biochimica et biophysica acta. 1964;90:442-4.
382. Joanne P, Galanth C, Goasdoué N, Nicolas P, Sagan S, Lavielle S, et al. Lipid reorganization induced by membrane-active peptides probed using differential scanning calorimetry. Biochimica et Biophysica Acta (BBA) - Biomembranes. 2009;1788(9):1772-81.
383. Scheinpflug K, Wenzel M, Krylova O, Bandow JE, Dathe M, Strahl H. Antimicrobial peptide cWFW kills by combining lipid phase separation with autolysis. Scientific Reports. 2017;7:44332.
384. Franzblau SG, DeGroote MA, Cho SH, Andries K, Nuermberger E, Orme IM, et al. Comprehensive analysis of methods used for the evaluation of compounds against Mycobacterium tuberculosis. Tuberculosis. 2012;92(6):453-88.
385. Lehmann J. Para-aminosalicylic acid in the treatment of tuberculosis. Lancet (London, England). 1946;1(6384):15.
386. Khan A, Sarkar D. A simple whole cell based high throughput screening protocol using Mycobacterium bovis BCG for inhibitors against dormant and active tubercle bacilli. Journal of microbiological methods. 2008;73(1):62-8.
387. Altaf M, Miller CH, Bellows DS, O'Toole R. Evaluation of the Mycobacterium smegmatis and BCG models for the discovery of Mycobacterium tuberculosis inhibitors. Tuberculosis (Edinburgh, Scotland). 2010;90(6):333-7.

388. Gupta A, Bhakta S. An integrated surrogate model for screening of drugs against Mycobacterium tuberculosis. Journal of Antimicrobial Chemotherapy. 2012;67(6):1380-91.
389. Phelan J, Maitra A, McNerney R, Nair M, Gupta A, Coll F, et al. The draft genome of Mycobacterium aurum, a potential model organism for investigating drugs against Mycobacterium tuberculosis and Mycobacterium leprae. International journal of mycobacteriology. 2015;4(3):207-16.
390. Sood S, Yadav A, Shrivastava R. Mycobacterium aurum is Unable to Survive Mycobacterium tuberculosis Latency Associated Stress Conditions: Implications as Non-suitable Model Organism. Indian journal of microbiology. 2016;56(2):198-204.
391. Danilchanka O, Sun J, Pavlenok M, Maueröder C, Speer A, Siroy A, et al. An outer membrane channel protein of Mycobacterium tuberculosis with exotoxin activity. Proceedings of the National Academy of Sciences of the United States of America. 2014;111(18):6750-5.
392. Max B, Mattias R, Olivier C, K. NJ, Elaine H, Johan T. OPLS discriminant analysis: combining the strengths of PLS - DA and SIMCA classification. Journal of Chemometrics. 2006;20(8 - 10):341-51.
393. Xavier AS, Lakshmanan M. Delamanid: A new armor in combating drug-resistant tuberculosis. Journal of Pharmacology & Pharmacotherapeutics. 2014;5(3):222-4.
394. Marshall DD, Halouska S, Zinniel DK, Fenton RJ, Kenealy K, Chahal HK, et al. Assessment of Metabolic Changes in Mycobacterium smegmatis Wild-Type and alr Mutant Strains: Evidence of a New Pathway of d-Alanine Biosynthesis. Journal of proteome research. 2017;16(3):1270-9.
395. Baloni P, Padiadpu J, Singh A, Gupta KR, Chandra N. Identifying feasible metabolic routes in Mycobacterium smegmatis and possible alterations under diverse nutrient conditions. BMC microbiology. 2014;14:276.
396. Saliu OY, Crismale C, Schwander SK, Wallis RS. Bactericidal activity of OPC-67683 against drug-tolerant Mycobacterium tuberculosis. The Journal of antimicrobial chemotherapy. 2007;60(5):994-8.
397. Liu J, Barry CE, Besra GS, Nikaido H. Mycolic Acid Structure Determines the Fluidity of the Mycobacterial Cell Wall. Journal of Biological Chemistry. 1996;271(47):29545-51.
398. Watanabe M, Aoyagi Y, Ridell M, Minnikin DE. Separation and characterization of individual mycolic acids in representative mycobacteria. Microbiology (Reading, England). 2001;147(Pt 7):1825-37.
399. Villeneuve M, Kawai M, Horiuchi K, Watanabe M, Aoyagi Y, Hitotsuyanagi Y, et al. Conformational folding of mycobacterial methoxy- and ketomycolic acids facilitated by alpha-methyl trans-cyclopropane groups rather than cis-cyclopropane units. Microbiology (Reading, England). 2013;159(Pt 11):2405-15.
400. Ojha AK, Trivelli X, Guerardel Y, Kremer L, Hatfull GF. Enzymatic hydrolysis of trehalose dimycolate releases free mycolic acids during mycobacterial growth in biofilms. The Journal of biological chemistry. 2010;285(23):17380-9.
401. Joaquim T, Roland B. Permeability of the cell wall of Mycobacterium smegmatis. Molecular microbiology. 1994;14(2):283-90.
402. Sambandan D, Dao DN, Weinrick BC, Vilcheze C, Gurcha SS, Ojha A, et al. Keto-mycolic acid-dependent pellicle formation confers tolerance to drug-sensitive Mycobacterium tuberculosis. MBio. 2013;4(3):e00222-13.
403. Ojha AK, Baughn AD, Sambandan D, Hsu T, Trivelli X, Guerardel Y, et al. Growth of Mycobacterium tuberculosis biofilms containing free mycolic acids and harbouring drug-tolerant bacteria. Molecular microbiology. 2008;69(1):164-74.
404. McNaney CA, Drexler DM, Hnatyshyn SY, Zvyaga TA, Knipe JO, Belcastro JV, et al. An automated liquid chromatography-mass spectrometry process to determine metabolic

stability half-life and intrinsic clearance of drug candidates by substrate depletion. Assay and drug development technologies. 2008;6(1):121-9.
405. Cho J, Lee DG. Oxidative stress by antimicrobial peptide pleurocidin triggers apoptosis in Candida albicans. Biochimie. 2011;93(10):1873-9.
406. Choi H, Yang Z, Weisshaar JC. Oxidative stress induced in E. coli by the human antimicrobial peptide LL-37. PLOS Pathogens. 2017;13(6):e1006481.
407. Loots DT. An Altered Mycobacterium tuberculosis Metabolome Induced by katG Mutations Resulting in Isoniazid Resistance. Antimicrobial Agents and Chemotherapy. 2014;58(4):2144-9.
408. Tkachenko A, Nesterova L, Pshenichnov M. The role of the natural polyamine putrescine in defense against oxidative stress in Escherichia coli. Arch Microbiol. 2001;176(1-2):155-7.
409. Nakai M, Mori A, Watanabe A, Mitsumoto Y. 1-methyl-4-phenylpyridinium (MPP+) decreases mitochondrial oxidation-reduction (REDOX) activity and membrane potential (Deltapsi(m)) in rat striatum. Experimental neurology. 2003;179(1):103-10.
410. Ballell L, Bates RH, Young RJ, Alvarez-Gomez D, Alvarez-Ruiz E, Barroso V, et al. Fueling Open-Source Drug Discovery: 177 Small-Molecule Leads against Tuberculosis. Chemmedchem. 2013;8(2):313-21.
411. Reisner BS, Gatson AM, Woods GL. Evaluation of mycobacteria growth indicator tubes for susceptibility testing of Mycobacterium tuberculosis to isoniazid and rifampin. Diagn Microbiol Infect Dis. 1995;22(4):325-9.
412. Christensen H, Garton NJ, Horobin RW, Minnikin DE, Barer MR. Lipid domains of mycobacteria studied with fluorescent molecular probes. Molecular microbiology. 1999;31(5):1561-72.
413. Castle M, Nazarian A, Yi SS, Tempst P. Lethal effects of apidaecin on Escherichia coli involve sequential molecular interactions with diverse targets. The Journal of biological chemistry. 1999;274(46):32555-64.
414. Johnson BK, Abramovitch RB. Macrophage Infection Models for Mycobacterium tuberculosis. In: Parish T, Roberts DM, editors. Mycobacteria Protocols. New York, NY: Springer New York; 2015. p. 329-41.
415. Wu YL, Scott EM, Po AL, Tariq VN. Ability of azlocillin and tobramycin in combination to delay or prevent resistance development in Pseudomonas aeruginosa. The Journal of antimicrobial chemotherapy. 1999;44(3):389-92.
416. Arnoldo A, Kittanakom S, Heisler LE, Mak AB, Shukalyuk AI, Torti D, et al. A genome scale overexpression screen to reveal drug activity in human cells. Genome Medicine. 2014;6(4):32-.
417. Fu LM, Shinnick TM. Genome-wide exploration of the drug action of capreomycin on Mycobacterium tuberculosis using Affymetrix oligonucleotide GeneChips. Journal of Infection. 2007;54(3):277-84.